BUCCAL TRANSMUCOSAL DELIVERY OF LARGE MOLECULE THERAPEUTICS USING ORALLY DISINTEGRATING TABLET TECHNOLOGY

AFFIONG RAPHAEL IYIRE

Doctor of Philosophy

ASTON UNIVERSITY

March 2016

Aston University

Buccal transmucosal delivery of large molecule therapeutics using orally disintegrating tablet technology

Affiong Raphael Iyire

Doctor of Philosophy

Thesis Summary

Buccal drug delivery combines the advantage of enhanced patient acceptance/ compliance of oral delivery, with overcoming drug degradation and poor absorption in the gastro intestinal tract (GIT), especially for large molecule therapeutics, such as insulin. Orally disintegrating tablets (ODTs) that dissolve rapidly in the mouth, are gaining widespread popularity, especially with extreme populations, including children and the elderly. This project unifies the advantages of buccal drug delivery with that of ODTs, with the view to developing a non-invasive delivery system for proteins like insulin.

This work was carried out in three parallel streams: A Quality by Design (QbD) based characterisation of excipients to identify and predict multi-functional behaviours as binder/ disintegrant/ mucoadhesive agent in ODT formulations; the investigation of a cost effective and easily reproducible cell culture based *in vitro* method for assessment of buccal delivery; and protein characterisation followed by an *in vitro* investigation of the effect of basic and acidic amino acids on the solubility, permeability, mechanism and transport route of insulin through TR146 buccal cell culture layers as safe and effective alternative permeation enhancers for proteins.

D-mannitol based tablets containing 7% low-substituted hydroxypropyl cellulose (LHPC) with 1.3 % Polyox™ polymers compacted at 30 kN were able to maintain high mechanical properties with fast disaggregation of tablets and mucoadhesive properties. Addition of 1.2 to 1.5 mM Ca^{2+} to cell culture media was found to increase culture stratification, forming a tighter barrier to paracellular transport of macromolecules, to mimic *in vivo* barriers. Amino acids were able to significantly enhance insulin solubility in water, and exhibited a concentration-dependent enhancement of insulin permeability (over 400% enhancement) *in vitro*. Interestingly, results revealed that insulin was transported by an active transcellular process, probably provided by the presence of insulin receptors and amino acid nutrient transporters on the cell membrane.

This result obtained for insulin is the first indication of a possible amino acid mediated transport of insulin via formation of insulin-amino acid neutral complexes by ion pairing.

Keywords: Buccal drug delivery, insulin, amino acid, facilitated transport, ion pairs, permeability

Acknowledgements

First and foremost, I will like to use this opportunity to thank God Almighty for the grace to complete this work.

I am extremely grateful to my supervisor Dr Afzal Mohammed for his kind direction, motivation, encouragement and transfer of in-depth knowledge - I could not have asked for a better supervisor. I appreciate my associate supervisor Professor Clifford Bailey for his timely advice and support throughout the duration of this program.

I am thankful to the University of Uyo Nigeria for providing the opportunity, and the Commonwealth Scholarships Commission in the UK for providing the funding, for me to undertake this PhD.

My appreciation goes to members of my research group Dr Ali Alkhattawi, Dr Craig Russel, Mrs Eman Dahmash, Mr Tom Dennison, Mr Hamad Alyami, Mr Jasdip Koner and Mr Annsar Warraich who make such a good team to work with and have co-authored some papers with me. Heartfelt thanks go to the technical staff particularly Mr Jiteen Ahmed and Ms Christine Jakeman; and the staff and fellow students in the medicines research unit (MRU) at Aston University for making my work easier.

My appreciation goes to Ms Charlie Bland and the Aston Research Centre for Healthy Ageing (ARCHA) for support with confocal studies. I acknowledge Rajith Rajoli from Liverpool John Moores University for validating the HPLC method in an independent laboratory; and Miss Maryam Alaayedi for carrying out some of the insulin transport studies.

Finally I appreciate all my friends that have become family and family that have become friends; my Full Life Christian Centre Nigeria and El-shaddai Birmingham church families that have created a home away from home for me at every stage of my life. May God bless you all.

Dedication

I dedicate this thesis to my family. First to my husband Mr Aniedi Ralph Iyire who has stood by me, supporting me tirelessly and continuously sacrificing so that I can achieve my dreams; and to my children Eldora and Beulah for bearing with me all the way.

To my parents Dr & Pharm (Mrs) F. E. U. Isangedighi, for instilling in me a drive for exceptional achievements and the moral attitude to balance my life.

To my sisters Arit, Edak, Atim, Henrietta, Nkoyo and Awo; thank you for forming a support base for me throughout my life.

Words cannot express my sincere gratitude to you, but I pray that the Lord Almighty bless you exceedingly.

List of contents

Acknowledgements 3

Dedication 4

List of contents 5

List of tables 12

List of figures 15

Abbreviations list 25

Chapter 1: Introduction and literature review 28

1.1 Introduction 29

1.2 Overview of the oral cavity 30

1.2.1 Physiological opportunities for drug delivery via the oral cavity 32

1.2.2 Physiological barriers to oral transmucosal drug delivery and possible solutions 33

1.2.3 Routes of drug transport via the buccal mucosa 36

1.3 Considerations for therapeutic peptides and proteins 37

1.3.1 Protein structure 38

1.3.2 Physicochemical properties of proteins 40

1.3.3 Enzymatic degradation and intracellular metabolism 41

1.4 Formulation strategies for buccal delivery of GIT-sensitive agents 42

1.4.1 Permeation enhancers 43

1.4.1.1 Use of amino acids as permeation enhancers 45

1.4.2 Enzyme inhibitors 46

1.4.3 Mucoadhesive polymeric systems 47

1.5 Methods for assessing buccal drug transport 48

1.5.1 *In vivo* methods for assessing buccal drug permeation 48

1.5.2 *In vitro* methods for assessing buccal drug permeation 49

1.5.2.1 Excised animal tissue 49

1.5.2.2 Theory of cell culture (Mather and Roberts 1998, Butler 2003) 50

1.5.2.3 Buccal cell cultures 52

1.6 Model Protein – Insulin 54

1.6.1 Previous work done on oral transmucosal delivery of insulin 55

1.6.2 Non-invasive buccal insulin formulations on the market or under development 56

1.7 Orally Disintegrating Tablets (ODTs) 59

1.7.1 Characteristic Limitations/ Possible Solutions of ODTs 60
1.7.2 ODT formulation 61
1.8 Research aims and objectives 61
Chapter 2: Investigation of the role of low substituted hydroxypropyl cellulose (LHPC) and HPC in the formulation of orally disintegrating tablests by direct compression 64
2.1 Introduction 65
2.2 Materials and methods 68
2.2.1 Materials 68
2.2.2 Methods 69
2.2.2.1 Bulk/ pre-formulation characteristics of powders 69
2.2.2.1.1 Particle size analysis (Diffractometry) 69
2.2.2.1.2 Angle of repose (ɵ) 69
2.2.2.1.3 Bulk and tapped density 70
2.2.2.1.4 True density and porosity of powders 70
2.2.2.1.5 Powder moisture content 71
2.2.2.1.6 Scanning electron microscopy (SEM) 71
2.2.2.1.7 Fourier transform infrared (FTIR) spectroscopy 71
2.2.2.1.8 X-ray diffractometry (XRD) 72
2.2.2.2 Tablet preparation and characterisation 72
2.2.2.2.1 Tabletting behaviour of pure polymer tablets 73
2.2.2.2.1 Tablet hardness 73
2.2.2.2.2 Tablet porosity 73
2.2.2.2.3 Tablet friability 74
2.2.2.2.4 Tablet disintegration time 74
2.2.2.2.5 Formulation optimisation 74
2.2.2.6 Statistical analysis 75
2.3 Results and discussion 75
2.3.1 Pre-formulation characterisation 75
2.3.1.1 Effect of morphology on power characteristics 75
2.3.1.2 Effect of degree of substitution on powder properties 79
2.3.2 Compaction characteristics of polymers 82
2.3.2.1 Compaction mechanisms 82
2.3.2.2 Compressibility, compactability & tabletability 89
2.3.3 Placebo tablet characterisation 91
2.3.3.1 Tablet hardness 91

2.3.3.2 Tablet disintegration time 93
2.3.3.3 Tablet friability 94
2.3.4 Formulation optimisation 95
2.4 Conclusion 97
Chapter 3: Effect of polymer viscosity, concentration and compaction pressure on ODT characteristics – a quality by design (QbD) approach 98
3.1 Introduction 99
3.2 Materials and methods 101
3.2.1 Materials 101
3.2.2 Methods 101
3.2.2.1 Pre-formulation characterisation of polymers 101
3.2.2.1.1 Angle of repose (ɵ) 101
3.2.2.1.2 Bulk and tapped density 102
3.2.2.1.3 True density and porosity 102
3.2.2.1.4 Powder moisture content 103
3.2.2.2 Elements of quality by design (QbD) 103
3.2.2.2.1 Design of experiments (DoE) 104
3.2.2.2.2 Regression model verification & interpretation 104
3.2.2.3 Tablet preparation & characterisation 106
3.2.2.3.1 Tablet disintegration time 106
3.2.2.3.2 Tablet friability 106
3.2.2.3.3 Tablet hardness 106
3.2.2.3.4 Tablet porosity 107
3.2.2.3.5 Mucoadhesive efficiency 107
3.2.2.4 Statistical analysis 108
3.3 Results and discussion 108
3.3.1 Bulk characteristics of polyox 108
3.3.2 Elements of quality by design (QbD) 109
3.3.2.1 Model verification 111
3.3.2.1.1 PLS model summary fit plot 111
3.3.2.1.2 Analysis of variance (ANOVA) 114
3.3.2.1.3 Observed vs predicted plot 115
3.3.2.2 Effect of factor variation on responses 117
3.3.2.2.1 Regression models for all CQA 118
3.3.2.2.2 Effect on disintegration time (Y_1) 118

3.3.2.2.3 Effect on tablet friability (Y_2) 121
3.3.2.2.4 Effect on tablet hardness (Y_3) and porosity (Y_4) 122
3.3.2.3 Prediction of design space/ formulation optimisation 125
3.3.3 Mucoadhesive efficiency 126
3.4 Conclusion 129
Chapter 4: A systematic investigation of the role of extracellular calcium ion in promoting stratification of buccal cell layers 130
4.1 Introduction 131
4.2 Materials and methods 134
4.2.1 Materials 134
4.2.2 Methods 134
4.2.2.1 TR146 Cell culture procedure 134
4.2.2.2 Passaging of cells 134
4.2.2.3 Cell storage and revival 135
4.2.2.4 Seeding of cells 135
4.2.2.5 Cell quantification (haemocytometry) 136
4.2.2.6 Effect of extracellular calcium on cell viability, proliferation and stratification 136
4.2.2.6.1 Preparation of calcium solutions 136
4.2.2.6.2 Qualitative analysis 137
4.2.2.6.2.1 Light microscopy 137
4.2.2.6.2.2 Confocal Laser Scanning Microscopy (CLSM) 137
4.2.2.6.3 Quantitative analysis 138
4.2.2.6.3.1 Cell proliferation using haemocytometry 138
4.2.2.6.3.2 Cell proliferation/ viability by MTT assay 138
4.2.2.6.3.3 Transepithelial electrical resistance (TEER) 139
4.2.2.6.3.4 Permeability studies using transport markers 139
4.2.2.6.3.4.1 Transport studies 139
4.2.2.6.3.4.2 High performance liquid chromatography (HPLC) 140
4.2.2.7 Statistical analysis 141
4.3 Results and discussion 141
4.3.1 Cell proliferation of TR146 cells using light microscopy 141
4.3.2 Effect of extracellular Ca^{2+} concentration on cell proliferation, viability, stratification and permeability 142
4.3.2.1 Light microscopy 142
4.3.2.2 Confocal Laser Scanning Microscopy (CLSM) 145

4.3.2.3 MTT assay 148
4.3.2.4 Haemocytometry 150
4.3.2.5 Transepthelial electrical resistance (TEER) 151
4.3.2.6 Permeability of paracellular and transcellular markers 153
4.4 Conclusion 157
Chapter 5: Protein quantification and characterisation 158
5.1 Introduction 159
5.1.1 Protein structure and aggregation 159
5.1.2 Insulin 159
5.1.3 Circular dichroism (CD) 160
5.1.4 High performance liquid chromatography (HPLC) 162
5.2 Materials and methods 166
5.2.1 Materials 166
5.2.2 Methods 166
5.2.2.1 High performance liquid chromatography (HPLC) assay 166
5.2.2.2 HPLC assay validation 166
5.2.2.2.1 Specificity (identification and assay) 167
5.2.2.2.2 Linearity 167
5.2.2.2.3 Accuracy 167
5.2.2.2.4 Precision 167
5.2.2.2.5 Limit of detection (LOD) & limit of quantification (LOQ) 167
5.2.2.2.6 Inter-laboratory method validation 168
5.2.2.3 Stability of insulin solutions 168
5.2.2.4 Circular dichroism (CD) 168
5.2.2.5 Fourier transform infra-red (FTIR) spectroscopy 169
5.3 Results and discussion 169
5.3.1 HPLC method development for quantification of insulin 169
5.3.2 HPLC assay validation 175
5.3.2.1 Specificity 175
5.3.2.2 Linearity 176
5.3.2.3 Repeatability (instrument and operator precision) 177
5.3.2.4 Limit of detection & limit of quantification 179
5.3.2.5 Inter-laboratory method validation 179
5.3.3 Stability of insulin solutions 180
5.3.4 Effect of compaction pressure on the secondary structure of insulin 181

5.3.4.1 Circular dichroism (CD) 181
5.3.4.1.1 CD data verification 181
5.3.4.1.2 CD data interpretation 182
5.3.4.2 Fourier-transform infra-red (FTIR) 184
5.4 Conclusion 185
Chapter 6: Pre-formulation and systematic evaluation of amino acid assisted permeability of insulin across buccal cell layers in vitro 187
6.1 Introduction 188
6.2 Materials and methods 192
6.2.1 Materials 192
6.2.2 Methods 192
6.2.2.1 High performance liquid chromatography (HPLC) assay 192
6.2.2.2 Insulin solubility in water & HBSS 193
6.2.2.3 Insulin distribution coefficient in 1-octanol/ water 194
6.2.2.4 TR146 cell culture procedures 194
6.2.2.5 Trans-epithelium electric resistance (TEER) 194
6.2.2.6 Cytotoxicity testing via MTT assay 195
6.2.2.7 *In vitro* transbuccal permeation studies 195
6.2.2.8 Route of insulin transport 197
6.2.2.9 Mechanism of insulin transport 197
6.2.2.10 Statistical analysis 198
6.3 Results & discussion 198
6.3.1 Insulin solubility in water 198
6.3.2 Insulin solubility in HBSS 201
6.3.3 Insulin octanol/ water distribution 205
6.3.4 Insulin permeability across TR146 cell layers 207
6.3.4.1 Basic amino acids 208
6.3.4.1.1 Arginine 208
6.3.4.1.2 Lysine 215
6.3.4.1.3 Histidine 218
6.3.4.2 Acidic amino acids 221
6.3.4.2.1 Glutamic acid 221
6.3.4.2.2 Aspartic acid 223
6.3.4.3 Sodium deoxycholate 226
6.3.5 Route of insulin transport 229

6.3.6 Mechanism of insulin transport through TR146 cell culture model 233
6.4 Conclusion 236
Chapter 7: Characterisation of insulin buccal tablets 237
7.1 Introduction 238
7.2 Materials and methods 240
7.2.1 Materials 240
7.2.2 Methods 240
7.2.2.1 Preparation of insulin buccal tablets 240
7.2.2.2 Tablet disintegration/ disaggregation 241
7.2.2.3 Tablet friability 241
7.2.2.4 Tablet hardness 241
7.2.2.5 Drug release from buccal tablets 242
7.2.2.6 Determination of insulin release mechanism from buccal tablets 242
7.2.2.6 Statistical analysis 243
7.3 Results and discussion 243
7.3.1 Insulin buccal tablet characteristics 243
7.3.2 *In vitro* insulin release from buccal tablets 245
7.4 Conclusion 247
Chapter 8: General Discussion 248
8.1 General discussion 249
Future work 252
List of References 254
Appendices 277

List of tables

Table 1.1 Table highlighting pros and cons of buccal drug delivery and possible strategies to overcome these disadvantages, including considerations for each strategy (Salamat-Miller *et al* 2005, Khafagy *et al* 2007, Park *et al* 2011, Patel *et al* 2011, Caon *et al* 2014) 34

Table 1.2 Table highlighting some enzymes identified in the buccal mucosa of various species and their peptide substrates (Veuillez *et al* 2001, Walker *et al* 2002) 41

Table 1.3 Classes and examples of absorption enhancers in common use and their proposed mechanisms of action (Bernkop-Schnürch and Kast 2001, Aungst 2012, Behra *et al* 2012, Caon *et al* 2014) 44

Table 1.4 Classes of polymers used to develop buccal mucoadhesive systems with examples (Khafagy *et al* 2007, Roy *et al* 2009b, Behra *et al* 2012) 48

Table 1.5 Comparing the characteristics of available animal tissues used to model buccal drug delivery. Porcine buccal mucosa most closely resembles that of humans in thickness, morphology and biochemical composition. (Lesch *et al* 1989, Shojaei 1998, Patel *et al* 2012)..... 51

Table 1.6 Comparing the use of excised animal tissues against buccal cell culture for modelling buccal drug delivery (Balimane et al 2000, Reichl et al 2004) 54

Table 1.7 Summary of insulin buccal transport studies employing bile salts and surfactants as permeation enhancers (Caon *et al* 2014); adapted 57

Table 1.8 Oral insulin formulations in development; adapted from (Heinemann and Jacques 2009) 58

Table 2.1 Composition of placebo tablets 72

Table 2.2 Particle size analysis of powders using difractometry (n=3). HPC exhibited significantly smaller particle size than LHPC..... 76

Table 2.3 Summary of pre-formulation characteristics of HPC and LHPC powders (n=3)..... 78

Table 2.4 AOR and Carr's index as indicators of powder flowability (Aulton, 2002, adapted)... 78

Table 2.5 Characteristics of pure HPC and LHPC tablets compacted at various pressures (n=3) 84

Table 3.1 List of independent variables (factors/ CPP) with their feasible investigational ranges that were employed in the optimisation DoE 105

Table 3.2 Preformulation characterisation of different viscosity grades of polyox polymers. No significant difference was observed for all characteristics tested, except that of true density. ... 109

Table 3.3 QTPP and CQAs of the final ODTs used for risk assessment..... 109

Table 3.4 Risk assessment of the process parameters against the CQAs including justification for assigning these risk values. 110

Table 3.5 Summary of results obtained from ANOVA of four responses to test model validity. P is the probability and R^2 is the regression coefficient. 116

Table 3.6 Quantitative factor effects on the responses and their corresponding p values. A (+) sign indicates a direct proportionality while a (-) sign indicates a reverse proportionality. 118

Table 3.7. Table highlighting CPP levels chosen by the MODDE optimiser to yield ODTs with favourable characteristics, and results obtained after testing the ODTs (n=3). ODTs prepared without polyox were used as control**.**..... 127

Table 4.1 Characteristics of solid supports for cell culture: dimensions and media volumes used 136

Table 4.2 Volumes of calcium chloride solution required to prepare 50 mL of calcium fortified media..... 137

Table 4.3 HPLC conditions for test substances..... 141

Table 4.4 Four hour permeability parameters of transport markers through TR146 cells grown in media fortified with increasing Ca^{2+} concentrations, normal media used as control (n=3). (*) represents the level of significant difference from the control ($p<0.05$)..... 154

Table 5.1 Some HPLC methods for insulin quantification in literature..... 165

Table 5.2 Specificity of insulin HPLC method 176

Table 5.3 Factors of the regression equation linking insulin concentration to the analytical response (area under the peak)..... 177

Table 5.4 Table highlighting intra-day accuracy and precision parameters of the HPLC method due to high %recovery and low RSD (n=3)..... 178

Table 5.5 Inter-day precision and accuracy parameters for HPLC method (n=6)..... 178

Table 5.6 Intra-day HPLC validation parameters for insulin method carried out in a different laboratory, with a different operator and different HPLC system on the same day, to assess method reproducibility (n=3) 180

Table 5.7 Inter-day precision and accuracy parameters carried out in a different laboratory with a different operator and HPLC system on three different days, to assess method reproducibility (n=9) 180

Table 5.8 Stability of 1000 µg/mL insulin solutions after storage at 2 - 8 °C for 72 hours (n=3). Results show that insulin solutions are stable for 3 days when stored in the fridge. 181

Table 5.9 Parameters of CD analysis of insulin powder and insulin tablets compacted at 10 and 30 kN respectively (n=3). Normalised root mean square deviation (NRMSD) values close to zero depict the validity of the data generated. 182

Table 5.10 Summary of CD data for insulin before and after compaction at 10 and 30 kN respectively (n=3). One-way ANOVA results (P>0.99) showed no significant difference in quantitation of secondary structures in all samples..... 184

Table 6.1 Properties of amino acids used in this study, highlighting the pKa of their ionisable side chains (Silen and Forte 1975, Hames and Hooper 2005)..... 201

Table 6.2 Effect of penetration enhancers on permeability of insulin through TR146 cell layers (n=3)..... 209

Table 6.3 Transepithelial electrical resistance (TEER) measurements for enhancers before and after permeability experiments through TR146 cell layers (n=9). 213

Table 7.1 Table highlighting the overall mechanism of drug release from cylindrically shaped systems such as tablets derived from the release exponent of the Korsmeyer-peppas model (Jacques *et al* 1974, Shoaib *et al* 2006, Dash *et al* 2010) 239

Table 7.2 Composition of insulin buccal tablets developed from the critical process parameters (CPP) determined from results from chapters 3 and 6. 241

Table 7.3 Results of tablet characteristics and drug release parameters for insulin buccal tablets (n=3)..... 244

Table 7.4 Release parameters for insulin buccal tablets containing LHPC (7%) and various viscosity grades of polyox polymer (n=3) 247

List of figures

Figure 1.1 Schematic diagram highlighting the anatomical locations of the lining, masticatory and specialised mucosa that cover the oral cavity (Squier and Kremer 2000, Patel *et al* 2011) 30

Figure 1.2 A schematic diagram of the human buccal epithelium highlighting possible barriers to drug delivery (Hao and Heng, 2003)..... 31

Figure 1.3 A schematic representation of the possible routes of drug transport across the buccal mucosa (Patel *et al* 2011)..... 37

Figure 1.4 Mechanism of cell adhesion to a solid support. Proteins necessary for cell attachment and spreading: cell surface glycoproteins (v), (o) conditioning factors secreted by cells, ( ) serum-derived glycoproteins (Butler 2003). 52

Figure 1.5 Primary structure of insulin showing A and B polypeptide chains, with inter- and intra-molecular di-sulphide bridges (Snyder et al 2012) 55

Figure 2.1 Molecular structure of cellulose showing repeating anhydrous glucose molecules linked by β(1,4)-glycosidic linkages (Roy *et al* 2009a)..... 65

Figure 2.2 Intra-molecular hydrogen bonding in cellulose (Roy *et al* 2009a)..... 66

Figure 2.3 Inter-molecular hydrogen bonding in cellulose (Roy *et al* 2009a)..... 66

Figure 2.4 Idealised structure of hydroxypropyl cellulose portraying hydroxypropylation occurring either on the hydroxyl group of glucose, or on previously hydroxypropylated side chains (Werbowyj and Gray 1980) 67

Figure 2.5 Representative graph showing particle size distribution of HPC powder by laser diffractometry using a Sympatec HELOS/BR particle size analyzer (n=3)..... 76

Figure 2.6 SEM of HPC powder at 50 µm magnification showing somewhat spherical particles with irregular surface 77

Figure 2.7 SEM of LHPC powder at 50 µm magnification showing somewhat elongated particles with irregular surface 77

Figure 2.8 FTIR spectra for HPC and LHPC powders showing higher molecular hydrogen bonding in LHPC 80

Figure 2.9 X-ray diffraction patterns for HPC and LHPC powders showing amorphous humps. The larger size of the amorphous humps in HPC than LHPC correlates with the lower degree of substitution and therefore higher crystallinity of LHPC. 81

Figure 2.10 Out-of-die Heckel's plots for HPC and LHPC pure compacts (n=3). Higher volume reduction and thus lower porosity was observed for HPC, although both powders exhibited similar mean yield pressure values..... 83

Figure 2.11 (A) Photograph of HPC tablet compacted at 5, 10 and 30 kN (left to right); highlighting the appearance of distinct layers (B)..... 85

Figure 2.12 X-ray diffraction patterns highlighting the appearance of small crystalline peaks (highlighted in circles) in LHPC compacted at 10 and 30 kN, and the absence of such peaks in the patterns at 5 kN pressures and the polymer powder..... 86

Figure 2.13 Xray diffraction patterns showing the absence of crystalline peaks in HPC powder and pure tablet compacted at 5, 10 and 30 kN respectively. No difference in diffraction patterns was observed with increasing compaction pressures. 87

Figure 2.14 Comparing FTIR spectra of HPC powder with HPC tablets at different compression forces revealed no difference in -OH stretching bands or other peaks. 88

Figure 2.15 Comparing FTIR spectra of LHPC powder with LHPC tablets at different compression forces revealed no difference in –OH stretching bands or other peaks..... 88

Figure 2.16 SEM of HPC (A,C,E) and LHPC (B,D,F) tablets compacted at 5, 10 and 30 kN respectively, showing consolidation of HPC particles with increasing compaction pressures; particles of LHPC remained fairly constant as compaction pressure increase..... 90

Figure 2.17 Compressibility profiles showing the variation in tablet porosity with increasing compaction pressures. The lower porosity values displayed by HPC depict higher compressibility than LHPC (n=3)..... 91

Figure 2.18 Hardness of tablets containing HPC or LHPC as binder (n=3). Dotted line depicts minimum desirable hardness..... 92

Figure 2.19 Disintegration time of tablets containing HPC or LHPC as binder (n=3). Dotted line depicts maximum acceptable disintegration time acceptable according to BP standards..... 93

Figure 2.20 Friability of tablets containing HPC or LHPC as binder. Dotted line depicts maximum acceptable friability. Missing points show tablets that failed the friability test (broken tablets).. 95

Figure 2.21 Plot showing the effect of increasing compaction pressure on hardness and disintegration time of formulation containing 7% LHPC (n=3). Despite the higher hardness observed with increasing compaction pressures, tablet disintegration time remained significantly constant. 96

Figure 2.22 Plot showing the effect of increasing compaction pressure on friability and porosity of formulation containing 7% LHPC 96

Figure 3.1 Distance to model plot showing the closeness of the various experimental runs to the model. Identified outliers (highlighted with the blue shapes), that did not affect the model detrimentally, were excluded. 112

Figure 3.2 Partial least squares (PLS) fit summary plot for all responses. R^2 represents the extent to which observed data fits the model, Q^2 depicts the per cent of actual data that can be predicted by the model, model validity of >0.25 shows the model has no lack of fit..... 113

Figure 3.3 The lack of fit plots for all responses. As long as the 1st bar is smaller than or equal to the 3rd bar, the model shows no lack of fit. 114

Figure 3.4 ANOVA plots comparing the standard deviations of the model (1st bar) to that of the noise (2nd bar), for all responses. When the first bar is larger than the third bar, the model is good 115

Figure 3.5 The observed vs predicted plots for all responses showing the closeness of the data predicted by the model to the actual data observed. The closer the R^2 value is to 1, the better the model..... 116

Figure 3.6 Main effects plot highlighting the effect on tablet disintegration time when polymer viscosity is increased from its low to high value and other factors maintained at their middle values. The three centre points (black dots) within the white area indicate validity of the effect, as they fall within the confidence limits of ± 95%. 119

Figure 3.7 Main effect plot highlighting the effect on tablet disintegration time when polymer concentration was increased from its low to high value and other factors maintained at their middle values. The three centre points (black dots) within the white area indicate validity of the effect, as they fall within the confidence limits of ± 95%. 120

Figure 3.8 Main effects plot highlighting the change in disintegration time as a function of compaction pressure variations while other factors remained constant at their middle values. The three centre points (black dots) within the white area indicate validity of the effect, as they fall within the confidence limits of ± 95%. 121

Figure 3.9 Interaction plot highlighting strong interaction effect of polymer concentration and compaction pressure on tablet friability. Two lines that cross each other depict a strong interactive effect. 122

Figure 3.10 Main effect plot highlighting the effect on tablet hardness and porosity when compaction pressure is increased from its low to high value and other factors maintained at their middle values. The three centre points (black dots) within/ close to the white area indicate validity of the effect as they fall within the confidence limits of ± 95%. 123

Figure 3.11 Main effect plot highlighting the effect on tablet hardness when polymer concentration is increased from its low to high value and other factors maintained at their middle values. The

three centre points (black dots) within the white area indicate validity of the effect, as they fall within the confidence limits of ± 95%. 124

Figure 3.12 Response surface plot showing the effect on tablet porosity, of varying polymer concentration and compaction pressure, with polymer viscosity held at its mid position. An increase in tablet porosity at high compaction pressures and high polymer concentrations reveal the elastic recovery at high pressures, of polyox polymers..... 125

Figure 3.13 Sweet plot depicting polymer viscosity and compaction pressure ranges for obtaining optimal ODT characteristics when polymer concentration is set at its mid value (1.5%). 126

Figure 3.14 Results showing mucoadhesive efficiencies of ODTs containing various viscosity grades of polyox using CPPs designed by the MODDE software optimiser (n=2). Tablets containing only LHPC without polyox used as control. Only polyox coagulant tablets showed a significant increase above the control. 128

Figure 3.15 Typical plot of compressive load against compressive extension highlighting the energy input into the system and the resulting work of adhesion 128

Figure 4.1 Light microscopy (10x magnification) showing proliferation pattern of TR146 cells grown in normal media on 75cm^3 T-flasks from receipt, sub-culture, until confluence and onward stratification. 142

Figure 4.2 Representative light microscopic images (10x magnification) of TR146 cells cultured on 48-well plates for two days in media fortified with increasing calcium chloride concentrations, with normal (uncalcified) media used as control (n=3). Cell lysis was observed to occur at concentrations >8.4mM. 143

Figure 4.3 Representative light microscopic images (10x magnification) of TR146 cells cultured on collagen-coated microscope coverslips for two days in media fortified with increasing calcium chloride concentrations, with normal (uncalcified) media used as control (n=2). Maximal cell growth was observed at 1.5mM concentrations. 144

Figure 4.4 Representative light microscopic images (40x magnification) of TR146 cells cultured on 25cm^2 T-flasks in media fortified with increasing calcium chloride concentrations, with normal (uncalcified) media as control (n=3). Cell proliferation increased at concentrations between 1.5-1.8 mM, with stratification observed by day 4..... 145

Figure 4.5 Representative confocal microscopic images of TR146 cells grown on collagen coated microscope coverslips in increasing Ca^{2+} fortified media, stained with DAPI (horizontal plane). Arrows indicate areas of stratification; depicted by grouping of nuclei together. 146

Figure 4.6 Representative confocal microscopic images of TR146 cells grown for 8 days on polycarbonate transwell inserts in increasing Ca^{2+} media, stained with DAPI (horizontal plane) 1.5-1.8 Mm Ca^{2+} enhanced cell proliferation. 147

Figure 4.7 Representative confocal microscopic images of TR146 cells grown on collagen coated microscope coverslips in increasing Ca^{2+} fortified media, stained with DAPI (transverse plane). Distinct DAPI-stained nuclei could be seen by day 5, but unclear boundaries were observed as cells begin to flatten out by day 8..... 148

Figure 4.8 Representative confocal microscopic images of TR146 cells grown for 8 days on polycarbonate transwell inserts in increasing Ca^{2+} concentration, stained with DAPI (transverse plane). Indistinct cell boundaries at higher Caa^{2+} may account for higher stratification. 148

Figure 4.9 Results of MTT proliferation assay of TR146 cells grown in media continuously fortified with increasing calcium chloride concentrations, with respect to cells grown in normal (uncalcified) media used as control (n=24). Cells in 2.8 mM Ca^{2+} concentration showed significantly lower proliferation/ viability than the control. 149

Figure 4.10 Results of MTT proliferation assay of TR146 cells grown in media intermittently fortified (every 24 hours) with increasing calcium chloride concentrations, with normal (uncalcified) media used as control (n=24). Cells in 2.8 mM Ca^{2+} concentration showed significantly lower proliferation/ viability than the control. 150

Figure 4.11 Cell count by haemocytometry results for proliferation of cells grown on 25cm2 T-flasks in media fortified with increasing calcium ion concentrations, with normal (uncalcified) media as control (n=12) 151

Figure 4.12 TEER measurements for TR146 cells grown on 24 mm transwell inserts in normal media. Results are the mean of single measurements of 6 different transwell inserts (n=6). Proliferation pattern of cells in lower Ca^{2+} concentrations differed from that at higher concentrations of 1.5-1.8 mM, giving indications of the point when a complete monolayer was formed and stratification commenced. 152

Figure 4.13 Representative confocal microscopic images of FITC-dextran 4kDa localisation (A) in the intercellular spaces of TR146 cells, showing paracellular transport (white arrows). DAPI stained nuclei (blue stain) (B) confirm the absence of the paracellular marker in the cell nucleus. 153

Figure 4.14 Representative confocal microscopic images of FITC-insulin (A) localisation and DAPI nuclear stain (B) on control TR146 cells. DAPI staining confirms localisation of FITC insulin in the nucleus (white arrows) 157

Figure 5.1 Primary structure of insulin showing A and B polypeptide chains, with inter- and intra-molecular di-sulphide bridges (Snyder *et al* 2012) 160

Figure 5.2 The circular dichroism effect. I: Equal absorption of left and right circularly polarised components of plane polarised light resulting in plane polarised radiation. II: Absorption of components to different magnitude resulting in skewed/ elliptical polarisation (Kelly *et al* 2005) 161

Figure 5.3 Circular dichroism spectra showing representative secondary structures of some proteins and peptides (Greenfield (2007), data supplied by W. C. Johnson)..... 162

Figure 5.4 Representative chromatogram of 0.5mg/mL insulin in 0.01N HCl at 214nm. Insulin peak was poorly resolved and eluted off the column in about 1 min..... 169

Figure 5.5 Chromatogram showing elution of the solvent front (blue line) at about the same time as insulin (black line), resulting in poor resolution of the insulin peak. 170

Figure 5.6 HPLC chromatogram showing insulin elution at 6 minute upon gradient elution from solution A:B 80:20 to 20:80. An upward shift in the baseline may be due to the changing gradient. 172

Figure 5.7 Chromatograms showing insulin elution at various wavelengths: 214 nm (black), 230 nm (blue), and 275 nm (pink). 173

Figure 5.8 Chromatogram showing gradient elution of insulin from mobile phase composition A:B of 80:20 to 20:80 at 230 nm UV detection wavelength 174

Figure 5.9 Representative chromatogram showing the developed method for insulin elution employing a gentle gradient at 230 nm detection wavelength and 1.5 mL/min flow rate 175

Figure 5.10 Representative chromatograms showing selectivity and instrument precision of HPLC method. Triplicate measurements of 500 µg/ mL insulin solution produced identical peaks that were well resolved from that of the blank..... 176

Figure 5.11 Beer-Lamberts calibration curve for insulin. 177

Figure 5.12 Representative chromatogram of insulin elution during inter-laboratory validation of HPLC method at Liverpool John Moores University, UK. A well separated insulin peak with no interference from the mobile phase was seen. 179

Figure 5.13 Plot of calculated and experimental CD spectra for neat insulin. The difference between the calculated/ reconstructed data and actual experimental data appears as a straight line, depicting the validity of the results generated..... 183

Figure 5.14 Circular dichroism spectrum of insulin powder (neat insulin) and pure insulin tableted at 10 and 30 kN compaction pressures. Each sample was dissolved in sufficient quantities of PBS to prepare a 1 mg/mL solution 183

Figure 5.15 FTIR spectra of insulin before and after compaction at 10 and 30 kN, showing the amide I and amide II absorption bands. Identical spectral patterns were obtained pre- and post-compaction, highlighting that compaction did not affect the secondary structure of insulin..... 185

Figure 6.1 Primary structure (amino acid sequence) of insulin monomer highlighting basic (black arrows) and acidic (blue arrows) groups which provide ionisable sites to the molecule (adapted from http://www.interactive-biology.com/wp-content/uploads/2012/05/Human-Insulin-Protein-Structure-917x1024.pg..... 190

Figure 6.2 Structures of basic and acidic amino acids that provide ionisable sites on the insulin monomer; adapted from Hames and Hooper (2005)..... 191

Figure 6.3 Schematic representation of active transport of insulin-amino acid ion pair complex. Where (A) represents amino acids transport via their nutrient carriers, (B) represents amino-acid facilitated insulin transport through amino acid carriers. Adapted from https://www.premedhq.com/passive-active-transport..... 191

Figure 6.4 Solubility in water at 25 °C and resulting pH of solutions of insulin in the presence/ absence of basic and acidic amino acids (n=3). Horizontal line depicts the isoelectric point of insulin (1 mg insulin = 27 IU)..... 199

Figure 6.5 Comparing the effect of basic amino acids and the bile salt, Na deoxycholate, on the solubility of insulin in HBSS at 25 °C (n=3). Only lysine was able to alter solution pH and insulin solubility significantly (1 mg insulin = 27 IU)..... 202

Figure 6.6 Comparing the effect of acidic amino acids and Na deoxycholate on the solubility of insulin in HBSS at 25 °C, (n=3) (1 mg insulin = 27 IU). 205

Figure 6.7 Effect of basic and acidic amino acids on octanol/ water distribution of insulin (n=3), as a means of predicting in vivo characteristics (1 mg insulin = 27 IU). 206

Figure 6.8 Transepithelial electrical resistance results for TR146 cells grown on transwell inserts for 30 days (n=9). Cell layer integrity was found to be maintained over the time period used for the permeability studies. 208

Figure 6.9 Percentage of insulin permeated in the presence of various concentrations of arginine (Arg) (n=3). No significant enhancement in insulin permeability ($p>0.05$) was observed in the presence of arginine. 209

Figure 6.10 Comparing the percent enhancement of insulin permeability through TR146 cell layers in the presence of various concentrations of arginine and solution pH (n=3). 211

Figure 6.11 Comparing the solubility in HBSS at 25°C and permeability of insulin through TR146 cells layers, in the presence of various concentrations of arginine (n=3) (1 mg insulin = 27 IU). 212

Figure 6.12 Effect of penetration enhancers on the viability of TR146 cells in the presence of increasing concentrations of amino acids and Na deoxycholate, utilising the MTT assay (n=12).

Na deoxycholate and lysine exhibited the highest toxicity to cells, while histidine, glutamic acid and aspartic acid exhibited the highest safety potential. 215

Figure 6.13 Percentage of insulin permeated in the presence of various concentrations of lysine (n=3). 10, 100 and 200 µg/mL significantly enhanced insulin permeation above the control.... 216

Figure 6.14 Comparing the %enhancement of insulin permeability through TR146 cell layers in the presence of various concentrations of lysine and solution pH (n=3). At higher pH permeation was hindered due to partial dissociation of lysine, and therefore reduced potential for counter-ion formation with insulin. 216

Figure 6.15 Comparing the solubility at 25 °C and permeability of insulin through TR146 cells layers, of insulin in the presence of various concentrations of lysine (n=3). Maximum amount of insulin permeated correlated with the lower ionisation of insulin molecules, enabling the permeability of non-ionised moieties (1 mg insulin = 27 IU). 217

Figure 6.16 Cumulative percentage of insulin permeated in the presence of various concentrations of histidine (n=3). 10 µg/ mL histidine significantly enhanced insulin permeation above the control. 219

Figure 6.17 Comparing the percent enhancement of insulin permeability through TR146 cell layers in the presence of various concentrations of histidine and solution pH (n=3). Enhanced insulin transport in the presence of histidine occurred with no change in solution pH. 219

Figure 6.18 Comparing the solubility at 25 °C and permeability of insulin through TR146 cells layers, of insulin in the presence of various concentrations of histidine (n=3). Significant enhancement observed at 10 µg/ mL due to a balance between ionised and non-ionised states of insulin, and the possible triggering of amino acid transporters (1 mg insulin = 27 IU)..... 220

Figure 6.19 Graph highlighting concentrations of basic amino acids that significantly enhanced insulin permeability with no toxicity to TR146 cells (n=3). 10µg/ mL of both lysine and histidine were effective and safe permeation enhancers. 220

Figure 6.20 Cumulative percentage of insulin permeated in the presence of various concentrations of glutamic acid (n=3). 10, 100 and 200 µg/mL glutamic acid showed significantly higher insulin permeation than the control. Glu 200 and Control were discontinued after 3 hours following a mishap. 221

Figure 6.21 Comparing the percent enhancement of insulin permeability through TR146 cell layers in the presence of various concentrations of glutamic acid and solution pH (n=3). No permeation of insulin was observed at 600 µg/ mL glutamic acid due to the low solubility of insulin at this pH. 222

Figure 6.22 Comparing the solubility at 25 °C and permeability of insulin through TR146 cells layers, in the presence of various concentrations of glutamic acid (n=3) (1 mg insulin = 27 IU). 222

Figure 6.23 Cumulative percentage of insulin permeated in the presence of various concentrations of aspartic acid (n=3). 10 and 200 µg/ mL significantly enhanced insulin permeation above the control. 224

Figure 6.24 Comparing the percent enhancement of insulin permeability through TR146 cell layers in the presence of various concentrations of aspartic acid and solution pH (n=3). 224

Figure 6.25 Comparing the solubility at 25 °C and permeability of insulin through TR146 cells layers, in the presence of various concentrations of aspartic acid (n=3). Low insulin concentration permeated at 400 µg/ mL due to low insulin solubility at pH of this solution (1 mg insulin = 27 IU). 225

Figure 6.26 Highlighting concentrations of acidic amino acids that significantly enhanced insulin permeability with no toxicity to TR146 cells (n=3). 10, 100 & 200 µg/ mL glutamic acid and 10 & 200 µg/ mL aspartic acid significantly enhanced insulin permeation without causing toxicity to cells. 226

Figure 6.27 Cumulative percentage of insulin permeated in the presence of various concentrations of sodium deoxycholate (SDC) (n=3). All concentrations ≥ 200 µg/ mL significantly enhanced insulin permeation above the control. SDC showed higher permeation enhancement than all the amino acids tested. 227

Figure 6.28 Comparing the percent enhancement of insulin permeability through TR146 cell layers in the presence of various concentrations of sodium deoxycholate and solution pH (n=3) 227

Figure 6.29 Comparing the solubility at 25 °C and permeability of insulin through TR146 cells layers, in the presence of various concentrations of sodium deoxycholate (n=3). Insulin enhancement observed for SDC found to be via disruption of cellular membranes lowering cell integrity (1 mg insulin = 27 IU). 228

Figure 6.30 Graph highlighting concentrations of tested penetration enhancers that significantly enhanced insulin permeability with no toxicity to TR146 cells (n=3). Black rectangles signify concentrations that were both effective and safe. 229

Figure 6.31 Confocal microscopic images x40, showing transport pathway of FITC-labelled insulin through TR146 buccal cell layers in the presence of amino acid concentrations that effectively enhanced insulin permeability Insulin observed to traverse transcellularly with localisation in the nucleus. Control (A), Arg 50µg/mL (B), Asp10µg/mL (C), Asp 200 µg/mL (D), Glu 10 µg/mL (E), Glu 100 µg/mL (F), Glu 200 µg/mL (G), Hist 10 µg/mL (H), Lys 10 µg/mL (I), Lys 100 µg/mL (J), Lys 200 µg/mL (K), SDC 200 µg/mL (L). 231

Figure 6.32 Representative confocal microscopic images of FITC-insulin, x40 (A) localisation and DAPI nuclear stain (B) on TR146 cells for control (1) and in the presence of Glu 10µg/mL (2). DAPI staining confirms localisation of FITC insulin in the nucleus (white arrows), with no paracellular transport..... 232

Figure 6.33 Representative confocal microscopic images of FITC-dextran 4kDa localisation, x40 (A) in the intercellular spaces of TR146 cells, showing paracellular transport (white arrows). DAPI stained nuclei (blue stain) (B) confirm the absence of the paracellular marker in the nucleus... 232

Figure 6.34 To investigate active insulin transport in the presence of amino acids. Insulin concentration was fixed at 1mg/mL while amino acid concentration was varied, and permeation experiments carried out at 9 °C for 4 hours (n=3). Note: Results for 200µg/mL at 36 °C, permeated for only 3 hours. Temperature and concentration dependent fall in insulin permeation at suboptimal temperatures confirm the presence of active transport of insulin due to enzyme inactivation that occurs at low temperatures, and early saturation of transporters (1 mg insulin = 27 IU). 233

Figure 6.35 Investigating active and passive transport of insulin-amino acid ion pairs across TR146 buccal cell layers (n=3). Glutamic acid concentration was fixed at 200 µg/mL, and insulin concentration varied. Vectoral transport was investigated by reversing the transport direction from basolateral-to-apical. Results highlight a dependence on initial concentration and direction of transport, pointing to active transport mechanisms (1 mg insulin = 27 IU)..... 235

Figure 7.1 Results highlighting insulin release from buccal tablets formulated from compositions generated by the MODDE software optimiser from chapters 3 and 6 (n=3). High viscosity polyox (coagulant) formulation exhibited some modified release of insulin from tablets..... 246

Abbreviations list

%	Percent
°C	Degrees Celsius
µg	Microgram
µL	Microlitre
µm	Micrometer
ANOVA	Analysis of variance
AOR	Angle of repose
API	Active pharmaceutical ingredient
Arg	Arginine
Asp	Aspartic acid
AUC	Area under the curve
BP	British Pharmacopoeia
C NMR	Carbon nuclear magnetic resonance
Ca^{2+}	Calcium ion
CCF	Central composite face
CD	Circular Dichroism
cm	Centimetre
CO_2	Carbon (IV) oxide
Copt	Optical concentration
CPP	Critical process parameters
CQA	Critical quality attributes
Da	Dalton
DAPI	4′,6′-diamidino-2-phenylinodole
DHA	Docosahexaenoic acid
DMSO	Dimethyl sulphoxide
DoE	Design of experiments
DS	Degree of substitution
ECF	Extracellular fluid
EDTA	Ethylenediamine tetraacetic acid
FBS	Fetal bovine serum
FD4	FITC-labelled dextran
FITC	Fluorescein isothiocyanate
FTIR	Fourier transform infra-red
g	Gram
GIT	Gastrointestinal tract
Glu	Glutamic acid
GRAS	Generally regarded as safe
GSH	Glutathione
HBSS	Hank's balanced salt solution
HCl	Hydrochloric acid
His	Histidine
HPC	Hydroxypropyl cellulose
HPLC	High performance liquid chromatography
HPMC	Hydroxypropyl methyl cellulose
hr	Hour
i.m.	Intramuscular
IU	International units
IBS	Insulin Buccal Spray
ICH	International Conference on Harmonisation
kN	Kilonewton
Leu	Leucine
LHPC	Low-substituted hydroxypropyl cellulose
LOD	Limit of detection

Log D	Distribution coefficient
LOQ	Limit of quantification
Lys	Lysine
m	Metre
M	Molar
MCC	Microcyrstalline cellulose
MCG	Membrane coating granule
mg	Milligram
min	Minute
mL	Millilitres
MLR	Multi-linear regression
mM	Millimolar
MPa	Megapascal
MS	Moles of substitution
MTT	Methylthiazolydiphenyl-tetrazolium bromide
Myr	Myristic acid
N	Normal
N	Newton
NRMSD	Normalised root mean square deviation
ODT	Orally disintegrating tablet
PBS	Phosphate buffered saline
PFA	Paraformaldehyde
pI	Isoelectric point
PLS	Partial least squares
Polyox	Polyethylene oxide
Q^2	Predictability
QbD	Quality by design
QTPP	Quality targeted product profile
R^2	Correlation coefficient
RES	Reticulo-endothelial system
RP-HPLC	Reverse phase high performance liquid chromatography
Rpm	Rounds per minute
RSD	Relative standard deviation
sec	Second
SEM	Scanning electron microscopy
TEA	Triethylamine
TEM	Transmission emission microscopy
TFA	Trifluoroacetic acid
Try	Tryptophan
USP	United States Pharmacopoeia
UV	Ultraviolet
v/v	Volume per volume
VMD	Volume mean diameter
w/v	Weight per volume
w/w	Weight per weight
XRD	X-ray diffraction
2θ	Angular range

Publications List

Peer-reviewed articles

1. **Iyire, A.**; Alayedi, M; Mohammed A.R. (2016) Pre-formulation and systematic evaluation of amino acid assisted permeation of insulin via buccal cell layers. *Scientific Reports* **6**:32498 http://doi.org/10.1038/srep32498

2. ElShaer, A.; Kaialy, W.; Akhtar, N.; **Iyire, A.**; Hussain, T.; Alany, R. *et al* (2015) A methodological evaluation and predictive *in silico* investigation into the multi-functionality of arginine in directly compressed tablets. *European Journal of Pharmaceutics and Biopharmaceutics* **96**:272-281

3. Al-Khattawi, A.; **Iyire, A**.; Dennison, T.; Dahmash, E.; Bailey, C.; Smith, J.; *et al* (2014) Systematic screening of compressed ODT excipients: Cellulosic versus non-cellulosic. *Current Drug Delivery* **11**(4):486-500

4. **Iyire, A**.; Russel, C.; Bailey, C.; Mohammed, A. (2014) Investigating buccal cell cultures to enhance *in vitro* assessment of transmucosal drug delivery. *UKICRS Newsletter* pp 38-40. http://www.ukicrs.org/uploads/1/2/1/5/12158556/ukicrs_2014.pdf

Book chapters

1. **Iyire, A. R.**; Mohammed, A. U. R. (2015) Multiparticulates for paediatrics. In: Rajabi-Siahboomi, A. R. ed. *Multiparticulate drug delivery systems: formulation, processing and manufacture*. London. (accepted).

Oral Presentations

1. **Iyire, A.R.;** Alayedi, M.; Bailey, C.; Mohammed, A.U.R. (2016) Pre-formulation and systematic evaluation of amino acid assisted permeability of insulin across *in vitro* buccal cell layers. *UKICRS, Cardiff, April 2016*

2. **Iyire, A. R.**; Bailey, C.; Mohammed, A.U.R. (2014) A fractional experimental design highlighting the effect of polymer viscosity, polymer concentration and compaction pressure on orally disintegrating tablet (ODT) characteristics. *UKPharmsci, Hertfordshire, 2014*

Conference Proceedings

1. **Iyire, A.**; Bailey, C.; Mohammed, A. A systematic investigation of the role of extracellular calcium in promoting stratification of buccal cell cultures. *CRS, Edinburgh, 2015*

2. **Iyire, A.**; Bailey, C.; Mohammed, A. Effect of viscosity, concentration & pressure on orally disintegrating tablet (ODT) characteristics – a factorial experimental design. *UKICRS, Cork, 2014*

3. **Iyire, A. R**; Bailey, C.; Mohammed, A.U.R. Investigation of the role of substitution in polymers used as direct compression excipients in ODT formulations. *UKPharmsci, Edinburgh, 2013*

Chapter 1

Introduction and literature review

1.1 Introduction

Over the last few decades, tremendous progress has been made in the field of biotechnology, with the consequence of increased availability of large scale production volumes of therapeutic proteins and peptides. However, these macromolecules are still predominantly delivered via the parenteral route due to low bioavailability after oral administration. Limitations of parenteral drug delivery, including, requirement of daily injections, pain at injection site, complications such as injection accesses, psychological trauma, cost, inconvenience and the risk of infection; compromise patient compliance and therefore therapeutic outcomes (Khafagy *et al* 2007). Despite the various advances and developments in drug delivery via new and novel routes of administration, the oral route of drug delivery still holds the highest levels of patient acceptance because of its lower cost, ease of administration and, therefore, patient compliance. However, setbacks of the oral route, including drug degradation in the gastro-intestinal tract (GIT) and first-pass metabolism in the liver leading to low bioavailability, has pushed research in the direction of delivery via other transmucosal routes such as rectal, vaginal, ocular, nasal, pulmonary and the buccal/ oral cavity (Patel *et al* 2011). Amongst the many advantages of these transmucosal routes of drug administration is the possibility for the drug to enter the systemic circulation by escaping first-pass metabolism and/ or pre-systemic degradation along the GIT. However, these transmucosal routes are not without their limitations. In addition to a small absorptive surface area, long term nasal drug delivery could trigger allergies (rhinorrhea, rhinitis), compromise nasal integrity and alter mucociliary activity (Ugwoke *et al* 2005). The vaginal route exhibits poor and highly variable absorption, due to differences in age, and menstrual cycle changes, and poor patient compliance due to low dosage form retention and local irritation (Caon *et al* 2014). Although the transdermal route has advantages of a large surface area and ease of application, limitations such as local irritation and the visible nature of dosage forms (such as patches) may impede patient compliance. The pulmonary route is quite promising, with a very large absorptive surface comprising a monolayer of epithelial cells with high vascularisation, but high alveolar macrophages and metabolising enzymes reduce peptide absorption, in addition to pharmacokinetic differences existing between smokers and non-smokers, while long term use can cause irreversible damage to the lungs (Caon *et al* 2014). The ocular and

rectal routes are reserved for local delivery due to low patient acceptance and low treatment outcomes (Shojaei 1998). However, the robust mucosa and lymphatic system of the oral cavity, along with its high patient compliance, has driven drug delivery in the direction of the oral/ buccal cavity to deliver these highly GIT unstable drugs. Since this route retains the advantages of oral drug delivery while by-passing its shortcomings, this work will centre on peptide delivery via the mucosal membranes of the buccal region of the oral cavity.

1.2 Overview of the oral cavity

The lips, cheek, tongue, gingiva, hard palate, soft palate and floor of the mouth make up the oral cavity; most of which aid mastication and speaking, but the inner lining of the cheek (buccal) and sublingual (under tongue) mucosae are most absorptive (Patel *et al* 2011, Caon *et al* 2014). The oral cavity is covered by the oral mucosa, which is further divided into three types depending on their function (Figure 1.1).

Figure 1.1 Schematic diagram highlighting the anatomical locations of the lining, masticatory and specialised mucosa that cover the oral cavity (Squier and Kremer 2000, Patel *et al* 2011)

The lining mucosa is 100 – 200 µm thick and comprises 60% of total oral surface area in adult humans and covers the buccal (cheek), sublingual (under the tongue/ floor of the mouth) and ventral portion of the tongue (Collins and Dawes 1987, Rossi *et al* 2005). This mucosa is not subject to high masticatory demands, but is flexible to allow for chewing, speaking and swallowing, and therefore has a non-keratinised epithelium and is more absorptive in nature (Squier and Kremer 2000, Veuillez *et al* 2001). The masticatory mucosa (25%) covering the hard palate (roof of the mouth) and the gingiva (gums) are built to withstand stress and strain during eating, and thus, contain a superficial layer of thick keratinised cells similar to that found on the skin (without a stratum corneum). The specialised gustatory mucosa (15%) on the dorsal portion (surface) of the tongue contains both keratinised and non-keratinised cells and papillae (Patel *et al* 2011). The buccal mucosa in its complete definition refers to the lining of the cheeks, upper and lower lips (Rossi *et al* 2005). Unlike the intestinal and nasal epithelia, buccal epithelia lack tight junctions; cells are loosely linked together with the aid of gap junctions, desmosomes and hemidesmosomes (Rossi *et al* 2005).

As a covering tissue, the buccal epithelium (Figure 1.2) is lined with 40-50 layers of stratified squamous epithelia, 500-600µm in thickness, that make up the top 1/4 to 1/3 of the mucosa, covered by a mucus layer (Shojaei 1998, Caon *et al* 2014).

Figure 1.2 A schematic diagram of the human buccal epithelium highlighting possible barriers to drug delivery (Hao and Heng, 2003)

This epithelium protects the underlying tissues and organs from mechanical or chemical stress and prevents moisture loss due to a lipid barrier to permeability (Squier and Kremer 2000). A proteinaceous fibrous matrix called the basement membrane (1-2µm in thickness), from which cells migrate to the upper apical layers during differentiation/ maturation, separates the epithelium from the supporting connective tissue called the lamina propria, which is rich in blood vessels that drain into the jugular vein (Veuillez *et al* 2001, Hao and Heng 2003, Caon *et al* 2014).

1.2.1 Physiological opportunities for drug delivery via the oral cavity

The oral cavity provides various advantages that make it attractive for transmucosal delivery of drugs that cannot withstand the harsh environment of the GIT. This cavity is easily accessed, with a large surface area for absorption (100-200cm^2), large expanse of smooth muscle and a relatively immobile mucosa when compared with that of the GIT (Khafagy *et al* 2007, Heinemann and Jacques 2009). There is direct access to the systemic circulation (leading to high bioavailability) due to its high vascularisation into the internal jugular vein, and by-pass of first-pass metabolism in the liver. There is also a substantial rate of blood flow through the oral cavity vasculature, which yields a somewhat constant and predictable drug concentration to the blood stream. Additionally, compared to the GIT, the oral cavity is free from transit time variability and has lower enzymatic activity (Khafagy *et al.*, 2007). According to Patel *et al* (2011) enzymes found in the oral cavity include: aminopeptidases, esterases, dehydopeptidases and carboxypeptidases. Caon *et al* (2014) reported the absence of digestive enzymes such as pepsin, trypsin and chymotrypsin in the oral mucosa, thus the likelihood for peptide degradation as seen in the GI mucosa will be lower. Walker et al (2002) examined peptidase activity from buccal homogenates of the surface of the porcine oral mucosa, and reported only aminopeptidase N proteolytic activity. However, other groups have argued that this was only observed on the surface of porcine mucosa and more research should be structured and tailored towards various layers, as well as the human oral mucosa (Patel et al, 2011). Compared to the GIT (gastric pH 1-2 and intestinal pH 7-7.4), the oral cavity has a narrow pH range (6.6 – 7.4 depending on rested or stimulated states) maintained by saliva; saliva is also more mobile with less mucin/ enzymatic activity and practically no proteases (Patel *et al* 2011, Caon *et*

al 2014). Also, the robust nature of the mucosa allows it to undergo mechanical, chemical and physical stresses, which allows room for incorporation of formulation additives.

1.2.2 Physiological barriers to oral transmucosal drug delivery and possible solutions

However, despite the various advantages the oral cavity possesses for transmucosal delivery of drugs, there are some physiological barriers to drug delivery that must be considered when administering drugs through this route. Table 1.1 highlights some advantages and disadvantages of buccal drug delivery, with possible strategies to overcome them, and considerations for these strategies. Insufficient membrane permeability poses the largest challenge to buccal drug delivery. The composition and thickness of the mucosal cells vary depending on the site in the oral cavity. For example, the gingival and palatal mucosae (which undergo mechanical stress during mastication) are keratinised, while the soft palate, buccal and sublingual mucosa are non-keratinised. Thus, oral transmucosal drug delivery has been focused on these non-keratinised sites with more emphasis on the sublingual mucosa, which is even thinner than the buccal mucosa (Smart 1993, Patel *et al* 2011). Keratinised cells have been shown to be impermeable to water since they contain neutral lipids like ceramides and acyl ceramides, as opposed to non-keratinised epithelia which contain small amounts of ceramides along with neutral but polar lipids, such as cholesterol sulphate and glucosyl ceramides (Behra *et al* 2012). These differences in lipophilicity may play a role in the delivery of highly polar or highly lipophilic drugs. It has been found that within the oral mucosa, the presence of organelles called membrane coating granules Q (MCGs) serve as a higher permeability barrier than keratinisation (see Figure 1.2). These organelles exist in the first 1/4 - 1/3 of the oral epithelium and occur in both keratinised and non-keratinised cells (Harris and Robinson 1992, Patel *et al* 2011). During cell differentiation, the MCGs fuse with superficial cells and extrude their lipid contents into the intercellular spaces, imparting a higher permeability barrier (Rossi *et al* 2005). It has been reported that cultured epithelium from which MCGs had been removed showed higher permeability for compounds that usually do not penetrate the oral epithelium; and this trend was observed for both keratinised and non- keratinised cells

(Hayward 1979, Salamat-Miller *et al* 2005, Patel *et al* 2011). Thus, it is possible that MCGs may play a higher role in permeability of the oral mucosa than keratinisation of cells.

Table 1.1 Table highlighting pros and cons of buccal drug delivery and possible strategies to overcome these disadvantages, including considerations for each strategy (Salamat-Miller *et al* 2005, Khafagy *et al* 2007, Park *et al* 2011, Patel *et al* 2011, Caon *et al* 2014)

Advantages	Disadvantages	Formulation strategy to overcome disadvantages	Considerations
Excellent accessibility with relatively immobile mucosa suitable for retentive DFs	Insufficient membrane permeation facilitated by MCGs	Absorption enhancers	Increased transport of undesirable molecules present in the oral cavity. Irritant or bitter nature of enhancers may impede patient compliance.
Substantial blood flow with direct access to the systemic circulation, by-pass of hepatic first-pass metabolism and low enzymatic activity.	Enzymatic degradation within the buccal mucosa	Enzyme inhibitors	High toxicity during chronic administration; Non-specific and inhibits degradation of other proteins/peptides; changes metabolic pattern of GIT resulting in reduced digestion of food proteins.
Presence of saliva, with a friendlier pH range, as a solubilising agent for drugs prior to permeation.	Insufficient contact/ residence time at absorption site due to salivary scavenging, dose dilution and accidental swallowing.	Mucoadhesive polymeric systems	Natural mucus turnover in the buccal cavity may pose a drawback.
Painless drug administration, easy dosage form withdrawal and control of direction of drug release.	Direct contact of DFs with taste buds may reduce compliance with bitter or bad tasting formulations.	Taste masking techniques.	Availability of taste masking options.
Short turn-over time of cells enabling the use of excipients that may mildly and reversibly damage the mucosa.	Short turn-over time resulting in changes in permeability characteristics.		

DFs – Dosage forms, MCGs – Membrane coating granules

The presence of mucus in the oral cavity can serve as a further barrier to drug penetration. Mucus is made up primarily of water, but contains large molecules called mucins, which are made up of carbohydrates. At normal body pH, mucin molecules form a three-dimensional network which carries a negative charge (from residues of sulphate and sialic acid) and forms a strongly cohesive gelatinous layer that can bind to the epithelial surface and form a further barrier to drug penetration (Jiménez-Castellanos *et al* 1993, Rathbone *et al* 1994, Patel *et al* 2011). However, this property may be exploited to enhance buccal delivery using mucoadhesive polymers to prolong retention time of the drug/ dosage form in the buccal cavity (Khafagy *et al* 2007, Patel *et al* 2011). The physiological environment of the oral cavity is dictated by the pH, volume and composition of the saliva. Saliva has a resting pH of 6.6, and 7.4 upon stimulation; and 0.5 to 2 litres are produced daily (Salamat-Miller *et al* 2005). The saliva also acts as a dissolution medium for solid dosage forms to be disintegrated/ dissolved in the mouth. However, production of copious volumes of saliva due to the presence of dosage forms in the mouth may lead to accidental swallowing, resulting in dose dilution and diminished contact/ residence time of the dosage form with the buccal mucosa. Thus, transmucosal delivery of the drug cannot be ensured. The use of mucoadhesive retentive systems has been seen to overcome these setbacks (Khafagy *et al* 2007, Patel *et al* 2011, Behra *et al* 2012).

The short turn-over time (estimated time required to replace all cells in the epithelium) of the oral cavity mucosa (3-8 days) as compared with the skin (about 30 days), may serve as a disadvantage, since the continuous changes in mucosal integrity may also lead to changes in permeability characteristics (Squier and Kremer 2000, Patel *et al* 2011). However, this short turn-over time enables the oral mucosa to tolerate drug excipients that cause mild/ reversible damage or irritation to the mucosa, and can therefore be exploited when modifying delivery systems (Khafagy *et al* 2007, Caon *et al* 2014). The lower permeability of the buccal mucosa than the sublingual mucosa makes the former a preferred site for systemic delivery of drugs requiring prolonged/ controlled release, since there is no rapid onset of action; and its relatively immobile mucosa promotes the use of retentive systems (Dixit and Puthli 2009).

1.2.3 Routes of drug transport via the buccal mucosa

Studies using small proteins and dextrans linked to tracers have revealed buccal drug absorption to occur mainly by passive diffusion (along a concentration gradient) via two main pathways (Figure 1.3): the paracellular (intercellular spaces between cells) and the transcellular (intracellular across the cell membrane from one cell to another) routes (Rossi *et al* 2005, Sudhakar *et al* 2006). The paracellular route is more favoured for hydrophilic and small molecules ≤ 300 Da, but the increased lipophilicity of the buccal intercellular spaces following the extrusion of lipid components of the MCGs into the intercellular spaces of superficial cells further compromises paracellular permeation. However, drug transport can occur simultaneously via these two routes, with one route exhibiting predominant permeation (Rossi *et al* 2005, Patel *et al* 2011). The route and rate of drug permeation is dependent on the physicochemical properties such as lipophilicity and molecular weight of the permeant (Sudhakar *et al* 2006). The flux of permeant by passive diffusion through the epithelium traversing the paracellular route (Jp) under sink conditions may be represented as:

$$J_p = \frac{D_p \varepsilon}{h_p} C_d \quad . \quad . \quad . \quad . \quad . \quad . \quad . \quad \text{(Equation 1.1)}$$

where D_p is the diffusion coefficient of the permeant in the intercellular spaces, h_p is the length of the paracellular path the permeant travels, ε is the area fraction of the paracellular route and C_d is the concentration in the donor compartment (Mashru *et al* 2005, Sudhakar *et al* 2006). Correspondingly, the flux of permeant by passive diffusion via the epithelium traversing the transcellular route (J_c) under sink conditions may be represented as:

$$J_c = \frac{(1-\varepsilon) D_c K_c}{h_c} C_d \quad . \quad . \quad . \quad . \quad . \quad . \quad . \quad \text{(Equation 1.2)}$$

where D_c is the diffusion coefficient of the permeant in the transcellular spaces, K_c is the partition coefficient between the aqueous phase and the lipophilic cell membrane and h_c is the length of the transcellular path the permeant travels (Mashru *et al* 2005, Sudhakar *et al* 2006). In addition to passive diffusion, studies have revealed the presence of carrier-mediated transport across the buccal mucosa for nutrients and drugs. This transport may be active (requiring an energy input and can occur against a concentration gradient) or facilitated (not requiring a direct energy input, and cannot

occur against a concentration gradient). Evidence of active carrier mediated transport of monosachharides, amino acids and di-/ tri- peptides across the buccal mucosa have been presented by various studies, using nutrient transporters (Ho *et al* 1990, Rathbone *et al* 1994, Veuillez *et al* 2001). Utoguchi et al (1997) detected the presence of carrier-mediated transport for monocarboxylic acids across buccal epithelial cell layers in primary cell cultures of rabbit epithelium (Rossi *et al* 2005, Sudhakar *et al* 2006). Kurosaki *et al* (1998) suggested the presence of carrier mediated transport for D-glucose from perfusion cells attached to the dorsal side of the tongue of healthy volunteers. Permeation showed saturable kinetics that was absent from the buccal region of the oral cavity (Patel *et al* 2011). According to Sudhakar et al (2006) active carrier mediated transport is not likely to exist in the buccal mucosa. Figure 1.3 shows a schematic representation of the various routes of buccal drug transport.

Figure 1.3 A schematic representation of the possible routes of drug transport across the buccal mucosa (Patel *et al* 2011).

1.3 Considerations for therapeutic peptides and proteins

Many protein and peptide drugs have found application in the management of chronic diseases, such as insulin for diabetes mellitus. However, these therapeutic peptides have been administered mainly via the parenteral route, due to instability and low bioavailability when administered orally for various reasons, including (Veuillez *et al* 2001, Torchilin and Lukyanov 2003, Wilcox 2005, Khafagy *et al* 2007, Caon *et al* 2014):

- Fragility of structure: The ternary and quaternary structures of proteins can aggregate or degrade quite readily.

- Hydrophilic nature which decreases permeation through lipid bilayer of cells. For easy cell permeation, molecules should have a lipophilic nature, which allows for penetration of the cell lipid bilayer via the transcellular pathway. The normally hydrophilic nature of these large molecules results in reduced permeation into the blood stream.
- High molecular weight. Small molecules that are hydrophilic in nature can be transported across cells by squeezing through the intercellular spaces between adjacent cells (the paracellular route). This is a limitation for proteins, which are large molecules.
- Rapid elimination from the blood stream. This is usually due to renal filtration, uptake by the reticulo-endothelial system (RES) and enzymatic degradation.
- Chemical and enzymatic degradation in the GIT: highly acidic conditions accelerate breakage of disulphide bonds; while the presence of enzymes causes total inactivation.

1.3.1 Protein structure

Protein structure is controlled by molecular weight, size, conformation, stereospecificity, immunogenicity and the availability of electrostatic charges (Veuillez *et al* 2001). Small molecules (< 75-100 Da) that are hydrophilic in nature can be transported across cells by squeezing through the intercellular spaces between adjacent cells (the paracellular route) (Siegel 1984). This is a limitation for proteins which are large molecules with sizes ranging from 600 to 100,000 Da. The ability of a permeant to diffuse across the buccal membrane is directly related to its molecular weight and size; with exponential decline in buccal absorption observed as molecular weight increased above 300 Da (Siegel *et al* 1981). Jacques and Buri (1998) reported that *in vivo* permeation studies in humans showed small peptides protirelin (MW: 365) and oxytocin (MW: 1007) crossing the buccal mucosa while larger peptides buserelin (MW:1239) and calcitonin (MW: 3500) did not cross the mucosa (Veuillez *et al* 2001). Thus for proteins larger than 500-1000 Da, addition of permeation enhancers would be necessary.

Peptide drugs in solution may exist in different conformations exhibiting primary, secondary, tertiary or even quaternary structures depending on their size. Since drug permeation is stereospecific, it becomes a challenge to maintain favourable conformations for absorption and

pharmacodynamics during formulation, and in some cases, during sterilisation of proteins. Changes in the microenvironment of the protein due to temperature, pH, solvent, other solutes and protein crystallinity states can alter protein structure and conformation (Carino and Mathiowitz 1999). Ternary and quaternary structures of proteins are fragile and tend to aggregate, denature and degrade quite quickly. Use of inert polymers such as polyethylene glycols (PEGs) in formulations of peptide drugs have also been seen to reduce immunogenicity and enhance peptide resistance to proteolysis (Veuillez *et al* 2001).

It has been found that the distribution of electrostatic charges along the amino acid chain of peptides and proteins may have a higher impact on buccal permeability than the partition coefficient of the molecule (Veuillez *et al* 2001). Ho *et al* (1990) investigated the effect of terminal protein charge on buccal permeation and reported that the presence of terminal charges on small peptide chains impeded buccal permeation, even though the overall partition coefficient on the molecule (calculated using octanol/ water) was high. Interestingly, Gandhi and Robinson (1991) reported that physiological membranes have isoelectric points (pH values where the mucosa has no net charge) ranging from 2.7 – 5.3, with that of the buccal mucosa found to be 2.7. Thus, at pH values below the isoelectric point (pI), buccal membranes possess a negative charge, while at physiologic pH (above the isoelectric point), the membrane has a positive charge. Membrane charges have been found to be due to dissociation of acidic and basic groups on membrane proteins, and the negative charge on the buccal mucosa at physiologic pH has been assigned to the presence of higher numbers of –COOH groups than $–NH_2$ groups in the proteins along the transport pathway. Furthermore, this charge is suspected to accrue from the –COOH groups that make up the proteoglycans of glucoproteins, which are components of the MCGs that get extruded into the intercellular spaces of the buccal epithelium during differentiation (Gandhi and Robinson 1991). This charged effect of the buccal mucosa has been found to have a selective effect on the permeation of charged drugs such as peptides. Accordingly, Veuillez *et al* (2001) reported that the absorption of negatively charged insulin was found to be excluded from the paracellular pathway, while thyrotropin-releasing hormone, a positively charged protein was transported via the paracellular pathway.

1.3.2 Physicochemical properties of proteins

Physicochemical properties affecting protein transport include solubility, hydrophilicity, partition coefficient, aggregation, self-association and hydrogen bonding. The amphoteric nature of peptides makes their solubility profile complex, and highly dependent on solution pH and pKa of their ionisable side chains and end terminals. Thus, at the isoelectric point, most peptide drugs are poorly water soluble, with lipophilicity that gives high partition coefficient and subsequently higher mucosal permeability. As the pH moves away from the pI, aqueous solubility increases, with a decrease in permeation, since the degree of peptide ionisation is dependent on the drug's pKa and the pH at the site of permeation. However, these solubility-partition relationships are not linear for peptide drugs, possibly due to the presence of multiple ionisable sites on the protein chains. Dowty *et al* (1992) showed that the permeability of thyrotropin-releasing hormone was independent on solution pH (Veuillez *et al* 2001). Since a drug must first go into solution before it can be available to permeate the mucosa, solubility/ partition parameters for proteins are not very predictable, and a balance needs to be struck to obtain optimal results (Elshaer *et al* 2014).

The propensity of peptides to self-aggregate interferes with their intrinsic characteristics, with the presence of ionic and phenolic additives increasing this ability (Bondos 2006). For example, the insulin monomer is the therapeutically relevant structure of the molecule, but the hexamer formed in the presence of ions like zinc, is the more stable form. Human insulin has been reported to self-aggregate faster than bovine and porcine insulins (Banga and Chien 1988). Non-ionic surfactants such as PluronicF68 have shown potential as protein stabilisers (Veuillez *et al* 2001). Self-association of peptides is linked to the formation of intermolecular hydrogen bonds and hydrophobic attractions, and this hydrogen bonding reduces the lipophilicity of peptides, and therefore, their ability to permeate the mucosa (Davis 1986). Although the addition of hydroxyl groups triggers hydrogen bonding in peptides, hydroxyl groups have also been shown to enhance protein lipophilicity, due to intramolecular hydrogen bonding leading, to cyclization (Veuillez *et al* 2001).

1.3.3 Enzymatic degradation and intracellular metabolism

The efficacy of a buccally administered peptidic drug would depend on its ability to cross the membrane and enter the systemic circulation intact, without enzymatic degradation during transport. Although the buccal route has been found to have lower enzymatic activity than the GIT and other transmucosal routes (rectal, vaginal and nasal), proteolytic enzymes identified in the buccal mucosa using tissue homogenates or intact mucosal studies are highlighted in Table 1.2. The buccal mucosa is devoid of surface-bound peptidases, unlike that of the small intestines.

Table 1.2 Table highlighting some enzymes identified in the buccal mucosa of various species and their peptide substrates (Veuillez *et al* 2001, Walker *et al* 2002)

Enzyme	Substrate	Species	Test system	Reference
Aminopeptidase	Glutathione	Human	Buccal mucosa (in vivo)	(Hunjan and Evered 1985)
	Leu-enkephalin	Rabbit	Tissue homogenate	(Kashi and Lee 1986)
Carboxypeptidase(s)	Thyrotropin releasing hormone	Rabbit	Excised intact mucosa	(Dowty *et al* 1992)
Dipeptidyl carboxypeptidase Dipeptidyl peptidase	Enkephalin analogues	Rabbit	Tissue homogenate	(Kashi and Lee 1986)
Leucine aminopeptidase	L-Leucine-*b*-naphthylamide	Rabbit, guinea pig	Tissue homogenate	(Zhou and Po 1990)
Serine protease (serine endopeptidase)	Insulin	Rabbit	Tissue homogenate	(Yamamoto *et al* 1990)
	Proinsulin	Rabbit	Tissue homogenate	(Yamamoto *et al* 1990)
	Substance P	Rabbit	Tissue homogenates	(Lee and Yamamoto 1989)

However, most of these studies were carried out using tissue homogenates and, thus, could not differentiate the location of enzymatic activity - whether cytosolic or within the membrane (Walker et al 2002). Insulin and proinsulin have been reported to be degraded by serine proteases but not affected by aminopeptidases (Yamamoto et al 1990, Veuillez et al 2002). Given that peptides are

believed to be transported across the buccal epithelium mainly via the paracellular route, the effect of cytosolic enzymes during drug transport would be expected to be negligible; peptide degradation would provide further insight to the actual route of drug transport present (Veuillez *et al* 2001).

1.4 Formulation strategies for buccal delivery of GIT-sensitive agents

Considering the vast advantages of drug delivery via the oral mucosa, coupled with an understanding of the characteristics of the mucosa, strategies are being investigated to overcome the short-comings of this route. Chemical modification of peptides by prodrug formation has been investigated to enhance lipophilicity and overcome enzymatic degradation during buccal transport; for example, the N-terminal of a dipeptide (Try-Leu) was acylated with myristic acid (Try-Leu-Myr) and permeation through excised porcine buccal epithelium assessed. The acylated peptide was found to accumulate in the epithelium (80%), compared to its unmodified counterpart, which was found in the receiver chamber (53%), depicting high interaction of the prodrug with buccal mucosal proteins and/ or increased peptide stability within the mucosa (Veuillez *et al* 1999, Caon *et al* 2014).

Bundgaard and Moss (1990) achieved improved results with acylation of the imidazoyl group of the histidine moiety of thyrotropin releasing hormone with chloroformates, leading to enhanced lipophilicity as well as enhanced permeation of buccal epithelia compared to the unmodified peptide (Caon *et al* 2014). pH variation and iontophoresis have also been employed as strategies. However, formulation strategies to enhance peptide drug permeation are discussed below and include the use of (Smart 1993, Khafagy *et al* 2007, Behra *et al* 2012, Caon *et al* 2014):

- Absorption/ penetration enhancers to improve drug permeability across the mucosal cells.
- Enzyme inhibitors to reduce the degradation of active ingredients due to enzymatic action.
- Mucoadhesive polymeric systems to increase the contact time of active ingredient with the mucosal surface and prevent drug loss down the GIT.
- Mucolytic agents to break-down mucin
- Anti-aggregating agents to enhance peptide stability
- Targeted (particulate carrier) delivery systems

1.4.1 Permeation enhancers

Penetration enhancers increase the permeability of normally impermeable drug molecules like proteins and peptides through epithelia by increasing their paracellular (between cells) and/ or transcellular (through cells) transport (Mahato *et al* 2003). Mechanisms proposed for this increase in the small intestines include tight junction opening, protein leakage through membranes, decrease in mucus viscosity and changes to membrane fluidity (Mahato *et al* 2003, Khafagy *et al* 2007, Rajeswari 2011); while mechanisms in the buccal mucosa include extraction of intercellular lipids of the buccal epithelium, enhancing drug partitioning into the epithelial cells, interaction with buccal epithelial protein domains, enhancing muco-retention at buccal mucosal surface and possible reduction in mucus viscosity leading to enhanced peptide solubility (Veuillez *et al* 2001, Nicolazzo *et al* 2005, Hassan *et al* 2010, Caon *et al* 2014). Examples of non-specific permeation enhancers include: bile salts, surfactants, fatty acids, salicylates, chelators, zonula occludens toxins and, more recently, polymers such as chitosan (Khafagy et al, 2007) (Table 1.3). Use of absorption enhancers has been extensively studied in the GIT, with increasing data available for their use in the oral cavity (Hoogstraate *et al* 1996a, Hoogstraate *et al* 1996b, Johnston *et al* 1998, Bird *et al* 2001, Sohi *et al* 2010, Oh *et al* 2011). Lane et al (2005) reported improved paracellular absorption of insulin from rat intestines when mixed micellar systems containing bile salts and fatty acids as penetration enhancers were applied. Morishita et al (2000) also reported insulin pharmacological availability of 43.2% when emulsions containing eicosapentanoic acid (EPA) and docosahexaenoic acid (DHA) as permeation enhancers were administered to rat intestines *in situ*.

Since absorption enhancers are site specific due to differences in enzymatic activity, lipid composition, cell morphology, and epithelial thickness at different mucosal sites, it becomes necessary that studies on these enhancers be carried out on the oral mucosa to determine their role in oral transmucosal absorption (Behra *et al* 2012). Hoogstraate *et al* (1996a) investigated the effect of concentration of bile salts (sodium glychodeoxycholate (SDGC), sodium taurodeoxycholate, sodium glycocholate and sodium taurocholate) on extent and route of permeation of fluorescein isothiocyanate labelled dextrans (FITC-dextran) (4, 10 and 20kDa) through excised porcine buccal mucosa.

Table 1.3 Classes and examples of absorption enhancers in common use and their proposed mechanisms of action (Bernkop-Schnürch and Kast 2001, Aungst 2012, Behra *et al* 2012, Caon *et al* 2014)

Absorption enhancer	Proposed mechanism of action	Examples
Bile salts	Extraction of intercellular lipids, and in some cases intracellular lipids. Inhibition of buccal membrane peptidases.	Sodium glycocholate, sodium deoxycholate, sodium taurocholate, sodium glycodeoxycholate, sodium taurodeoxycholate
Chelators	Binding to intercellular Ca^{2+} to alter tight junction integrity. Inhibition of membrane-bound aminopeptidases.	Disodium EDTA, citric acid, sodium salicylate, methosy salicylates
Surfactants	Removal of superficial cell layers. Lipid extraction. Increased intercellular Ca^{2+}leading to apoptosis	Sodium lauryl sulphate, polyoxyethylene, polyoxyethylene-9-laurylether, polyoxyethylene-20-cetyl ether, benzalkonium chloride, 23-lauryl ether, cetylpyridinium chloride, cetyltrimethyl ammonium bromide, lysalbinic acid (natural non-ionic surfactant), sodium cholate (steroidal surfactant)
Non-surfactants		Unsaturated cyclic urea
Fatty acids	Reduction in lipid packing in buccal epithelial cells. Possible increase in partitioning into buccal cells.	Oleic acid, ecosapentaenoic acid, docosahexaenoic acid, capric acid, lauric acid, propylene glycol, cod liver oil methyl oleate, lysophosphatidylcholine, phosphatidylcholine
Thiolated polymers	Enhance residence time of permeant due to mucoretentive properties. Enzyme inhibition by modified chitosans.	Chitosan-4-thiobutylamide, chitosan-4-thiobutylamide/ GSH, chitosan-cysteine, poly(acrylic acid)-homocysteine, polycarbophil-cysteine, polycarbophil-cysteine/ GSH, chitosan-4-thioethylamide/ GSH, chitosan-4-thioglycholic acid
Amino acids	Ion pairing and active transport through amino acid nutrient transporters.	L-arginine, L-lysine
Others		Aprotinin, azone, cyclodextrin (inclusion complexes), dextran sulphate, menthol, polysorbate 80, sulphoxides, various alkyl glycosides

They reported that 10mM SDGC enhanced FITC-dextran 4kDa permeation only paracellularly, but at 100mM concentrations, transcellular permeation was simultaneously enhanced, up to 2000-fold

(Caon *et al* 2014). However, once cell membranes are rendered permeable and intercellular junctions opened, absorption is then enhanced not just for the drug molecule of interest, but also for other undesirable molecules which may be present in the oral cavity (Khafagy et al, 2007). Furthermore, the loss of barrier function of the mucosa may imply mucosal damage. Although the fast recovery of the buccal mucosa compared to that of the skin may reduce this challenge, factors such as effect of concentration and type of enhancer on mucosal irritation, long term toxicity and enhanced permeability to oral pathogens must be investigated before progression to clinical studies (Caon *et al* 2014).

1.4.1.1 Use of amino acids as permeation enhancers

Modified amino acids have been studied as permeation enhancers for peptide drugs. Vávrová et al (2003) reported a 12.5% enhancement in theophylline permeation across skin segments of human cadaver *in vitro* in the presence of undecyl ($C_{11}H_{23}$) – substituted glycine based ceramide analogues. The mechanism of this transport was not elucidated. Sarpotdar *et al* (1988) invented and patented formulations containing L-amino acids in a non-polymeric matrix forming carrier produced from a metal salt (Na or K) of a fatty acid that enhanced transdermal permeation of levonorgestrel across hairless mouse skin; with valine, cysteine, leucine, isoleucine, α-aminobutyric acid, norvaline and norleucine being preferred candidates. The effect of pH on transport rate was investigated and found to be unpredictable. However, the presence of fatty acids which are known permeation enhancers in the formulation could obscure interpretation of the enhancement results observed. Leone-Bay et al (1995) investigated the benefit of N-acylated amino acids as permeation enhancers for the peptides, salmon calcitonin (MW: 3.5kDa) and α-interferon (MW: 20kDa) across the intestinal mucosa of rats and primates *in vivo*. They reported a significant enhancement in permeation of the small peptide, which correlated with partition coefficient (log P) values, but this was not seen for the larger more complex peptide. Acyclic amide amino acid derivatives (N-cyclohexanoylleucine) showed the highest activity, marked by decrease in serum calcium, in both rodents and primates (Aungst 2000). The mechanism of permeation enhancement was not clarified, but was reported not to occur by intestinal enzyme inhibition or solubilisation of the lipid membranes, as revealed by the absence of histological damage to rat's intestines *post*

mortem. Similar results were reported for low molecular weight unfractured heparin and human growth hormone (Leone-Bay *et al* 1998, Aungst 2000, Thanou *et al* 2001). Janůšová *et al* (2013) reported enhanced permeability in the presence of amino acid derivatives (proline attached to a hydrophobic chain via a biodegradable ester linkage). The proline derivative exhibited 40 times enhancement in theophylline permeation across porcine skin *in vitro*, with enhanced permeation and absence of toxicity also observed *in vivo* in rats. More recently, Elshaer *et al* (2014) investigated the ability of cationic amino acids (lysine and arginine) to enhance the permeability of anionic indomethacine across the Caco-2 intestinal cell monolayer *in vitro*. Significant permeation enhancement was observed in the presence of higher molar ratios of drug:amino acid (1:2 and 1:4 for arginine, and 1:2 for lysine). Proposed mechanisms of enhancement included formation of ion pairs between oppositely charges molecules via the counter ion mechanism, and the possible triggering of active transport via peptidyl and anionic transporters for amino acids as described by Bröer (2008). Evidence for this active transport was demonstrated by a decline in indomethacin transport at higher molar ratios (1:8 for arginine and 1:4 and 1:8 for lysine), probably due to transporter saturation. Interestingly, Okuda *et al* (2006) reported the cytoprotective abilities of taurine and L-glutamine by reversing the increase in intracellular Ca^{2+} leading to cytotoxicity caused by the permeation enhancer sodium laurate (Aungst 2012).

1.4.2 Enzyme inhibitors

Formulations for oral drug delivery, containing agents that inhibit the degrading enzymes present in the GIT have shown higher bioavailability. Enzyme inhibitors are usually employed in combination with penetration enhancers and/ or mucoadhesive agents. Their use becomes more important when drugs have to be delivered via the small intestines, where the concentrations of metabolising enzymes are high. Examples of inhibitors used for oral delivery of drugs include sodium glycocholate, camostat mesilate, bacitracin, soybean trypsin inhibitor and aprotinin. Yamamoto *et al* (1994) reported the ability for sodium glycocholate, camostat mesilate and bacitracin to improve the physiological availability of insulin from the large intestines; but they were ineffective as inhibitors in the small intestines. This could have been due to the high concentration of these enzymes in the small intestines (Khafagy et al, 2007). Although enzymatic

activity in the buccal cavity is relatively low as compared with the GIT, Table 1.2 highlights some enzymes found in the buccal mucosa. Chitosan and its derivatives have been recently investigated as multifunctional polymers delivering permeation enhancement, enzyme inhibition and mucoadhesive properties (Bernkop-Schnürch and Kast 2001, Şenel and Hıncal 2001, Rossi *et al* 2005).

1.4.3 Mucoadhesive polymeric systems

Incorporation of polymers into dosage forms enables the adhesion of the dosage form/ drug to the mucin layer of epithelial or mucosal surfaces upon hydration (Behra et al, 2012). This phenomenon is known as mucoadhesion. Mucoadhesion prolongs the contact time of the drug at its administration site, to increase drug concentration gradient, reduce or prevent dilution/ degradation in the saliva and localise drug delivery (Khafagy et al, 2007). The mechanisms of mucoadhesion have been shown to be via hydrogen bond formation and other ionic interactions; according to Roy et al (2009b), these can either be chemical (by adsorption and electronic phenomena) and/ or physical (by wetting, diffusion and cohesion phenomena). Factors that affect mucoadhesion in the oral cavity can either be polymer-related (charge, flexibility, hydrogen bonding capacity, molecular weight, cross linking density, active polymer concentration and degree of hydration); or could be related to the internal environment (initial contact time, application strength, pH, mucin turnover and disease states) (Behra et al, 2012). Examples of mucoadhesive polymers for development of oral mucosal delivery systems are highlighted in Table 1.4 and include: cyanoacrylates, polyacrylates/ ployacrylic acid, sodium carboxy methyl cellulose, hyaluronic acid, hydroxypropyl cellulose, polycarbophil, polyethylene oxide, chitosan derivatives, gellan and cellulose derivatives (Khafagy et al, 2007; Roy et al, 2009; Behra et al, 2012). Morishita et al (2006) noted an insulin pharmacological activity of 9.5% from rat intestinal mucosa using hydrogel polymer-based microparticles, while a pharmacological activity of 14.9% was observed by Pan et al (2002) on administration of bioadhesive chitosan nanoparticles containing insulin, *in vivo* to rats. Hosny et al (2002) also formulated buccal adhesive tablets of insulin using Carbopol 934, hydroxyl propyl cellulose and various absorption enhancers; they reported a significant hypoglycaemic response without detectable fluctuations in blood glucose profile.

Table 1.4 Classes of polymers used to develop buccal mucoadhesive systems with examples (Khafagy *et al* 2007, Roy *et al* 2009b, Behra *et al* 2012)

S/N	Class of mucoadhesive polymer	Examples
1	Hydrophilic polymers	Anionic polyelectrolytes e.g. polyacrylic acid, carboxymethyl cellulose Cationic polyelectrolytes e.g. chitosan and its derivatives Non-ionic polymers e.g poloxamer, hydroxypropyl methyl cellulose, methyl cellulose, poly vinyl alcohol, poly vinyl pyrrolidone Cellulose and its derivatives e.g. carboxymethyl cellulose
2	Hydrogels	Acrylates, polyacrylic acid and methyl cellulose
3	Thiolated polymers	Chitosan-immunothiolane, polyacrylic acid-cycteine, polyacylic acid-homocysteine, chitosanothioglycolic acid, chitosan-thioethylamide, alginate-cysteine,polymethacrylic acid-cysteine, sodium carboxymethylcellulose-cycteine
4	Lectin-based polymers	Lectins extracted from legumes such as soyabeans, peanut, *Lens culinarius*

1.5 Methods for assessing buccal drug transport

During development of dosage forms for buccal drug delivery, drug transport across the mucosa and into the systemic circulation must be modelled both for new chemical entities and for existing drugs requiring a new route of delivery, in order to meet registration requirements by regulatory bodies. Approaches used to model drug transport across the buccal mucosa include *in vivo* methods in animals or healthy human volunteers, as well as *in vitro* methods using excised animal tissues and more recently cultured buccal cells.

1.5.1 *In vivo* methods for assessing buccal drug permeation

In vivo methods are modifications of the buccal absorption tests originally developed by Beckett and Triggs (1967). Here 25 mL of the test solution was swirled in the mouth of healthy human volunteers for 15 minutes, after which the solution was recovered, mouth rinsed, and the concentration of the analyte in both solutions quantified. The test assumed that the difference between initial and final analyte amount depicted the amount absorbed via the buccal cavity. However, accidental swallowing and saliva dilution was not taken into account; and there was no

method of confining the test solution to one particular area of the mouth (Shojaei 1998). Modifications of this test that accounted for possible saliva dilution and accidental swallowing by incorporating markers such as phenol red (Tucker 1988) and polyethylene glycol (Arbab and Turner 1971) in the test solution have since been developed, but the common setback of lack of test solution confinement had still not been overcome (Shojaei 1998, Şenel and Hıncal 2001, Patel *et al* 2012).

Perfusion methods have been developed to localise drug absorption to specific areas of the buccal mucosa and prevent uncontrolled absorption from other regions of the oral cavity (Patel *et al* 2012); this involves the attachment of a perfusion system to the buccal cavity of dogs and pigs (Junginger et al 1999) and humans (Rathbone and Hadgraft 1991, Kurosaki *et al* 1997, Kurosaki *et al* 1998), circulating a test solution through this cavity, and withdrawing samples from both the perfusion chamber and the blood, to correlate the amount of drug lost from the sample to the amount absorbed *in vivo*. In a similar development, Adrian *et al* (2006) correlated the drug lost from the perfusion chamber to its appearance in saliva from the parotid gland, in place of plasma (Patel *et al* 2012). However, the cumbersome nature of this setup and the possibility of drug leakage from the perfusion system are amongst its many limitations (Gandhi and Robinson 1994, Li and Robinson 2005, Patel *et al* 2012).

1.5.2 *In vitro* methods for assessing buccal drug permeation

1.5.2.1 Excised animal tissue

Investigated *in vitro* methods involve the use of either excised animal buccal tissue or buccal cell cultures (Shojaei 1998, Şenel and Hıncal 2001), as it is almost impossible to obtain viable human buccal epithelium on a continual basis (Balimane et al 2000). The general protocol for the use of animal tissues involves the sacrifice of the animal just before experimentation and removal of the buccal mucosa with accompanying connective tissues, after which the buccal epithelium is excised using surgical scissors/ scalpel / dermatome and stored in appropriate buffers (Krebs buffer). Excised epithelium can then be mounted on perfusion/ diffusion chambers such as vertical Franz cells or horizontal Ussing chambers, and permeation experiments commenced (Shojaei 1998, Patel

et al 2012). Issues surrounding *in vitro* methods border around the viability and integrity of the excised tissue, and standardised methods to assess these are unavailable. Furthermore, difficulties in handling/ manipulation, intra- and inter-species variability, and the differences in buccal characteristics of the animal used, to that of humans, pose further challenges. Table 1.5 compares the dimensions and characteristics of available animal buccal tissues to that of humans, and their suitability for modelling buccal drug transport. Porcine buccal epithelium has been identified as being closest to that of man's in terms of morphology, lipid composition and biochemistry (Lesch et al 1989, Davoudi et al 2012).

1.5.2.2 Theory of cell culture (Mather and Roberts 1998, Butler 2003)

Cell culture is a process where cells isolated from animal (or plant) sources are maintained in artificial environments enriched with nutrients and growth factors in an incubator maintained at 37°C and 5% CO_2 for 98% relative humidity. This enables individual cells to function as a whole unit, which can undergo replication by mitosis. Cells cultured in this way will continue to grow until limited by space or depletion of nutrients. Generally, cells are grown in culture to facilitate the study of metabolic/ biochemical processes, to investigate the effect of substances such as drugs, metabolites and hormones on cells, or to produce tissues with modified characteristics, such as producing skin grafts. The cells may be removed from the tissue directly and disaggregated by enzymatic or mechanical means to yield a primary culture; or the cells may be derived from a cell line or cell strain that has already been established (continuous cell line). Cells may then be cultured on solid/ semisolid supports (adherent cultures) or float in culture media (suspension cultures). Examples of solid supports used include cell culture flasks or microscope coverslips, while the membranes of transwell inserts are examples of semisolid supports. Culturing of blood cells is an example of suspension cultures. Primary cell cultures have been found to undergo a maximum of 54 population doublings (passages) before they stop replicating and enter into a phase of senescence (cell ageing with deterioration of functions). This occurs due to the telomere shortening that occurs with each growth generation of somatic cells.

Table 1.5 Comparing the characteristics of available animal tissues used to model buccal drug delivery. Porcine buccal mucosa most closely resembles that of humans in thickness, morphology and biochemical composition. (Lesch *et al* 1989, Shojaei 1998, Patel *et al* 2012)

Animal model	Thickness (μm)	Advantages	Disadvantages
Human	580 ± 90	Ideal	Limited availability
Rat, Hamster	NA 115.3 ± 11.5	Small, size, easy handling, cheap	Thick fully keratinised epithelium
Rabbit	600	Non-keratinised epithelium similar to man	Keratinised margin difficult to isolate from smaller non-keratinised portions.
Monkey	271 ± 50	Non-keratinised	Difficult maintenance. Thin epithelium thus more permeable than humans.
Dog	126 ± 20	Easy maintenance, less expensive than monkeys. Non-keratinised epithelium similar to human; easier to handle than pigs for in vivo studies.	Epithelium thinner than humans, thus more permeable.
Pig	772 ± 150	Non-keratinised epithelium. Closest animal to human in structure, composition, membrane morphology and permeability.	Rapid growth makes it less suitable for in vivo studies. Small size.
Cow	>1000	Non-keratinised epithelium. Readily available and affordable.	Very thick with large protrusions (striations), sectioning is difficult. Smooth areas limited.

Thus when a threshold length is achieved, cells can no longer divide and, thus, undergo senescence. Originally, cells were maintained in media consisting of animal blood until culture media containing specific nutrients in known proportions were developed by Earle and Eagle - Eagle's Minimum Essential Media (EMEM) being the first. EMEM had the advantage over animal products because it enabled the culture of reproducible batches, easy sterility and less chances of contamination. Viral vaccines, monoclonal antibodies and recombinant glycoproteins are examples of valuable products developed from cell culture.

Cells derived from tissues require a surface to adhere to before growth can occur. Figure 1.4 shows the process of cell attachment to a surface (substratum). The process of cell attachment is mediated

by divalent cations (usually Ca^{2+}) and proteins (cell surface glycoproteins, serum derived glycoproteins and conditioning factors secreted by cells) forming an adherent layer between the cells and the substratum.

Figure 1.4 Mechanism of cell adhesion to a solid support. Proteins necessary for cell attachment and spreading: cell surface glycoproteins (v), (o) conditioning factors secreted by cells, (•) serum-derived glycoproteins (Butler 2003).

Transformation of cells *in vitro* by inoculating with a virus leads to the formation of a continuous cell line which can replicate/ divide continuously; also known as immortalised cell lines. Differentiation, which is a process where cells develop different phenotypic characteristics slowly, can be stimulated in cell culture by changing the conditions and composition of the culture media.

1.5.2.3 Buccal cell cultures

Buccal epithelial cell culture models have been introduced to overcome the difficulties encountered with the use of excised animal tissues, and involve the harvesting and growth of cells of buccal origin under standard conditions of humidity, temperature, CO_2 levels and high sterility (Hoogstraate and Boddé 1993). Tavakoli-Saberi and Audus (1989) successfully cultured buccal cells from the hamster's cheek pouch, which formed non-keratinised epithelial cells with higher permeability (different from their original keratinised cells). Thus, this was thought to be a suitable model for predicting buccal drug transport (Patel *et al* 2012). The TR146 buccal cell line is a widely studied and well characterised cell culture model derived from a neck node metastasis of a buccal carcinoma removed from a 65 year old woman who had undergone radiotherapy (Rupniak *et al* 1985, Jacobsen *et al* 1995, Jacobsen *et al* 1996, Nielsen *et al* 1999, Nielsen and Rassing 2000b, Nielsen and Rassing 2000a). When grown in culture for 30 days, TR146 cells produce a buccal epithelium similar to human buccal epithelium in morphology (stratified squamous epithelia),

biochemistry, enzymatic activity and differentiation patterns; and may serve as a model for buccal drug transport (Jacobsen *et al* 1995, Nielsen and Rassing 2000b, Patel *et al* 2012, Xue *et al* 2012). However, these cells have been reported to show higher permeability than human and porcine buccal mucosa to mannitol, nicotine, testosterone, dextrans and tritiated water, which may be due to their cancerous origins (Nielsen and Rassing 1999, Nielsen *et al* 1999, Nielsen and Rassing 2000a, Nielsen and Rassing 2002). To improve on TR146 cell cultures, Selvaratnam *et al* (2001) developed a buccal cell culture derived from biopsies of healthy humans, which showed similar barrier properties to intact human buccal mucosa as well as similar morphology, lipid composition and the presence of membrane coating granules (Patel *et al* 2012). SkinEthic Laboratories (Nice, France) also developed a reconstituted human oral epithelium (RHOE), which is a commercially available tissue engineered oral mucosal model derived from TR146 cells cultured at the air-liquid interface on polycarbonate transwell inserts (http://www.episkin.com/HOE.asp). These have similar properties to that of TR146 cells in that they form a three dimensional, not fully differentiated, multi-layered buccal epithelium that is non-keratinised; similar in histology to that in humans (Moharamzadeh *et al* 2007). This tissue has been reported to express keratin 6 and 16, and involucrin differentiation markers, and has been employed to investigate candidal invasion in the oral cavity (Jayatilake *et al* 2005, Lu *et al* 2006). EpiOral™ is also commercially available from MatTek Corporation (Ashland, MA, USA) and is a three-dimensional reconstruct derived from normal human buccal epithelial cells; they form a multilayer stratified squamous epithelium, which is non-keratinised with similar growth and morphological characteristics as seen *in* vivo in humans (Moharamzadeh *et al* 2007). These cells have been reported to produce naturally occurring antimicrobial peptides, human beta defensins as well as cytokeratin K13 and K14. EpiOral™ has also been reported to show good in vitro - in vivo correlations for fentanyl transport and its bioavailability in humans (Agarwal *et al* 2005). Among the attractions to buccal cell cultures is the relative ease of handling, availability and the potential for mass testing.

Table 1.6 compares the characteristics of excised animal tissues to that of cell cultures to model buccal drug transport.

Table 1.6 Comparing the use of excised animal tissues against buccal cell culture for modelling buccal drug delivery (Balimane et al 2000, Reichl et al 2004)

Animal Tissues	Cell Culture
Low reproducibility due to inter - animal differences (e.g. damaged buccal mucosa in pigs due to chewing).	High consistency and reproducibility when cells of a homogeneous population are used
Isolation of buccal epithelium not straight forward.	Initially time consuming requiring high sterility, but immortalised cell lines grow rapidly yielding high throughput.
Difficulty in ensuring and maintaining viability and integrity of dissected tissue.	Characterisation and control of number of cell layers and lipid composition required.
High number of animals that need to be sacrificed to obtain sufficient tissues.	Hard to obtain the same level of differentiation/ stratification observed in animal species.
	As number of passage increases, cells may show different phenotypic characteristics than initial donor organism.

1.6 Model Protein – Insulin

The biologically active and circulating form of human insulin (Figure 1.5) is a 51 amino acid polypeptide comprising 2 amino acid chains joined by two di-sulfide linkages afforded by the amino acid, cysteine. 21 amino acids make up the A chain and 30 make up the B chain, with total molecular weight of 5800 Da. A di-sulphide linkage also exists within the A chain (Sarmento et al 2006). Insulin is produced by the beta cells of the Islets of Langerhans in the pancreas and is the most important hormone in the regulation of glucose homeostasis in the body (Xu *et al* 2006). Insulin was isolated in 1922 from the bovine pancreas by Frederick Banting and Charles Best in John Macleod's laboratory in Canada; Banting and Macleod later won a Nobel prize for this work (Khafagy et al 2007). The protein has since been administered subcutaneously, due to stability and bioavailability challenges associated with oral administration, for the management of insulin-dependent diabetes in patients whose pancreas does not produce insulin (Type I), or those whose cells have developed low insulin sensitivity (Type II).

Figure 1.5 Primary structure of insulin showing A and B polypeptide chains, with inter- and intra-molecular di-sulphide bridges (Snyder et al 2012)

Diabetes is currently one of the most common metabolic disorders in the world, with global burden on a steady rise over that last three decades (Guariguata *et al* 2014). Insulin was the first therapeutic protein to be fully syntheisised, first to get its three-dimensional nomenclature elucidated, and the first protein to be produced by recombinant DNA technology and marketed in large quantities; it is, therefore, one of the most studied therapeutic peptides in history (Heinemann 2008, Muheem *et al* 2014). Complications associated with insulin parenteral therapy have driven the on-going search for non-invasive methods for insulin delivery.

1.6.1 Previous work done on oral transmucosal delivery of insulin

Numerous data have been published on the oral delivery of insulin (along the entire GIT); however, although various reviews on insulin buccal delivery abound, actual research articles are few. Morishita et al (2001) reported the reduction in blood sugar in normal rats, after buccal administration of pluronic gels containing insulin with unsaturated fatty acids. Formulations containing oleic acid were found to exhibit the highest bioavailability of 15.9 ± 7.9 %. Yang et al (2002) also reported a 15.59% relative pharmacological bioavailability (relative to subcutaneously administered insulin solution), of insulin from phospholipid deformable vesicles delivered via the rabbit buccal mucosa. Aungst and Rogers (1988) had earlier compared the hypoglycaemic effects of insulin preparations containing absorption enhancers/ adjuvants administered transmucosally via the rectal, buccal and nasal routes in rabbits, to that of intramuscular (i.m.) insulin. The three routes investigated showed 30% of the hypoglycaemic effect from i.m. insulin, with sodium

salicylate and disodium ethylene diaminetetraacetic acid enhancing rectal insulin effect up to 40% of its i.m. counterpart. Aungst and Rogers (1989) reported similar findings when sodium lauryl sulphate was used as an absorption enhancer for buccal insulin delivery. Xu et al (2002) reported an Insulin Buccal Spray (IBS) comprising a combination of soybean lecithin and propandiol as absorption enhancers, to have improved significantly, the hypoglycaemic side effect of insulin in diabetic rats and rabbits. Modi (2002) patented mixed micellar formulations containing an alkyl sulphate for buccal insulin delivery while Modi et al (2010) patented a technology for administering insulin to the buccal mucosa via an atomiser, while restricting inhalation. A summary of the outcomes of studies employing bile salts and surfactants to enhance buccal insulin absorption is presented in Table 1.7 below.

1.6.2 Non-invasive buccal insulin formulations on the market or under development

A number of companies have oral (GIT) insulin preparations that are currently on the market or undergoing clinical development (Table 1.8). However, till date, only one marketed buccal formulation for insulin (Oralyn™ by Generex Biotechnology, Canada) has been approved and is in use in countries like Ecuador and India, while awaiting approval in others (Heinemann and Jacques 2009). Oralyn™ is a liquid preparation of regular recombinant human insulin administered just before meals, formulated with a propellant for aerosol administration via Rapidmist™ patented technology which sprays the solution into the mouth towards the throat as micelles in a fine mist; and particle size of droplets (85% >10μm) are too large to enter deeply into the lungs (Heinemann and Jacques 2009, Bansal *et al* 2014, Verma *et al* 2014).

Table 1.7 Summary of insulin buccal transport studies employing bile salts and surfactants as permeation enhancers (Caon *et al* 2014); adapted

Surfactant/ Bile salt	Test model	Outcome	Reference
Laureth-9	Insulin solution administered to rats in vivo.	Increase in hypoglycaemic response from 3.6% to 27.2%	(Aungst and Rogers 1988)
Laureth-9 (L9) polysorbate 20, PEG laurate, propylene glycolaurate, sorbitan laurate, glyceryl monolaurate, octoxynol-9, sodium dodecyl sulphate (SDS), sodium glycocholate (SGC), sodium deoxycholate (SDC), sodium, laurate (SL), sodium lauryl sulphate (SLS)	Insulin solutions administered in vivo in rats.	Presence of bile salts (SGC, SDC) and surfactants (SL, SLS and L9) showed maximum efficacy with >20% efficacy over i.m. insulin	(Aungst and Rogers 1989)
Sodium cholate (SC), sodium taurochlorate (STC) , lysophosphatidyl choline (LPC)	Buccal insulin administered in anaesthetised dogs in vivo.	Enhanced hypoglycaemic effect with glucose back permeation lowered by 80% 5-8 hours after exposure to STC, but remained unchanged for SC.	(Zhang *et al* 1994)
Brij-35, STC.SLS, SDC	Formulation solutions administered to rabbits in vivo	Hypoglycaemic effect increased in the order SDC<SLC<STC<Brij-35	(Oh and Ritschel 1990)
Octylglucoside and dodecylmaltoside	Buccal administration of formulation solutions to rats in vivo	Hypoglycaemic effect increased from 1% in the control to 20% and 30% respectively for octylglucoside and dodecylmaltoside	(Aungst 1994)
Soybean lecithin	Application in rats and rabbits in vivo	Significant blood glucose decrease by 60% and 54% in rats and rabbits respectively.	(Xu *et al* 2002)
Lysalbinic acid	In vitro permeation using excised hamster cheek pouch	5-fold increase in buccal FITC-insulin permeation	(Starokadomskyy and Dubey 2006)

Table 1.8 Oral insulin formulations in development; adapted from (Heinemann and Jacques 2009)

Company	Product	Stage	Dose (IU)	Daily dose (IU)	Functional bioavailability	Mechanism
Biocon, India	IN-105, tablet, (NCE)	Phase I	300-500	1200-2000	Low	Active transport
Diabetology, UK	Capsulin™ Enteric-coated capsule	Phase I Phase IIa	150 or 300	600-1200	Low	Active transport
Diasome, US	HDV-1, Oral gel capsule	Phase II	5	20	High	Tight junction with hepatic targeting
Emisphere, US	Oral capsule	Phase I, Phase IIa	300	1200	Low	Active transport
Oramed, US	Oral capsule	Phase I	236	944	Low	Active transport with possible hepatic targeting

NCE- new chemical entity

This insulin formulation is stable at room temperature for over 6 months, contains "a surfactant, a solubiliser, a micelle-creating agent, and emulsifying agents—all generally regarded as safe (GRAS)" and is presented in an asthma-type inhaler that releases 10 IU of insulin per puff; reported to rapidly penetrate the buccal mucosa and achieve fast absorption within 5-10 minutes *in vivo* (Heinemann and Jacques 2009, Bansal *et al* 2014). Advantages of Oralyn™ include patient acceptance of the inhaler-type device which is somewhat familiar and non-invasive. However several limitations exist including the training required to correctly operate the device to deliver insulin accurately; drug loss could occur due to non-compartmentalised delivery to the buccal region of the mouth, with some aerosol droplets travelling down the GIT with onward insulin inactivation. Furthermore, the specific formulation additives have not been disclosed, specific descriptions of mechanism and route of insulin transport have not been described for this system, and relative biopotency studies are still outstanding since 95% of the formulation is ingested by patients (Heinemann and Jacques 2009, Bansal *et al* 2014).

1.7 Orally Disintegrating Tablets (ODTs)

Orally disintegrating tablets (ODTs) have been described as solid dosage forms that disintegrate and dissolve in the mouth (either on or beneath the tongue or in the buccal cavity) without water within 30 seconds (USP specification) or 3 minutes (BP specification) (Pfister and Ghosh 2005). ODTs are particularly useful to patients who have difficulty in swallowing (dysphagia) such as children and the elderly. Wagh et al (2011) reported that 30-40% of the elderly and 18-22% of persons in long-term care homes, as well as 35% of the general populace suffer from dysphagia. ODTs have advantages over chewable tablets in patients who have difficulty chewing or in children who have lost their milk teeth but are yet to grow their permanent teeth (Hirani *et al* 2009); also there would be no leaching out of unpleasant tasting drugs which occurs during chewing of taste-masked chewable tablets (Alhusban *et al* 2010). ODTs are preferred to oral liquid dosage forms like suspensions and granules because they do not need a preparatory step before administration (AlHusban et al 2010). In disease conditions such as nausea and motion sickness, for psychiatric patients, patients on reduced fluid intake/ diet and even when there is no access to water such as when travelling, ODTs have proven to be a useful alternative to conventional solid dosage forms such as tablets/ capsules (Hirani et al 2009). Some market surveys revealed that over 50% of the population would choose ODTs over other dosage forms; about 70% would request ODTs from their physicians, 70% would buy ODTs and over 80% would choose ODTs over conventional tablets/ capsules (Hirani et al 2009). Since ODTs disintegrate and dissolve rapidly in the mouth, which has a very high number of blood vessels (highly vascularised), the drug molecules can be rapidly absorbed from the pre-gastric area (the mouth, pharynx and oesophagus); though some absorption can still take place in the stomach and intestines. Pre-gastric absorption has the benefit of rapid onset of drug action because the drug reaches the blood stream faster and does not depend on gastric emptying (Wagh *et al* 2011). This may result in higher bioavailability than conventional tablets, as ODTs evade hepatic first pass metabolism which is a major problem of the oral route of drug administration (Pfister & Ghosh 2005).

1.7.1 Characteristic Limitations/ Possible Solutions of ODTs

Despite the numerous advantages of ODTs, a major limitation is the amount of drug the dosage form can contain. For ODTs produced by freeze-drying, drug content must be less than 60mg for soluble drugs and less than 100 mg for an insoluble drug (Pfister and Ghosh 2005). Directly compressed ODT have overcome this set-back (Al-Khattawi and Mohammed 2013). To ensure rapid disintegration, dissolution and drug release in the mouth, ODTs have to be porous enough to enhance wettability by saliva. However, the more porous a tablet, the less its mechanical strength and ability to withstand stress during manufacture, transportation and handling. Also, many ODTs are hygroscopic and can therefore not withstand humidity or elevated temperatures (Hirani et al, 2009). Thus, some ODTs such as freeze- dried wafers have to be packed in specialised unit-dose blisters, which are only opened prior to administration. These, however, have higher cost implications (Pfister and Ghosh, 2005). Since ODTs disintegrate and dissolve in the mouth, the drug is released very near the taste buds. Thus, the taste of the drug is of paramount importance if compliance is expected. This is not a problem for drugs which are generally tasteless, but becomes a concern for drugs with bitter/unpleasant tastes. Taste masking is therefore an integral component of ODT manufacture and novel taste-masking methods are being investigated; however, whichever technique is employed for taste masking, it should not alter the characteristics of the ODT (Giri *et al* 2010). Shukla et al (2009) reported the development of pleasant tasting risperidone ODT fabricated using an ion-exchange resin that completely masked the bitter taste of risperidone. Saccharides and polyols are used extensively in lyophilised ODTs and this is a limitation for their long-term use in paediatric, diabetic or obese patients or those on multiple-dose regimens because of the narrow daily limit for these substances (Al-Khattawi and Mohammed 2014). In an attempt to overcome this drawback, AlHusban et al (2010) formulated freeze-dried ODTs with a novel amino acid (proline/serine) combination in place of saccharides and reported improved formulation characteristics. However, polyols such as mannitol with zero calorie content and good mouth-feel have been utilised (Al-Khattawi and Mohammed 2013). Rapid disintegration limits the use of ODTs for controlled-release of drugs except when formulated with "slow-dissolving, microparticulate-coated drugs" that disperse on disintegration and are swallowed (Pfister & Ghosh

2005). Fini et al (2008) however reported the successful production of fast-dispersible, slow-release ibuprofen ODTs prepared by wet granulation method using lecithin and coating agents. Cilurzo (2005) investigated the feasibility of preparing fast dissolving tablets containing microparticles with mucoadhesive properties to enhance residence time of the dosage form on the sublingual mucosa. A formulation containing 70% piroxicam and 30% Eudragit®L100 sodium salt was found to impart mucoadhesive properties and enhanced apparent drug solubility while incorporating the lowest concentration of polymer.

1.7.2 ODT formulation

Properties of ODTs depend on the technology used in their manufacture. Techniques/ technologies employed in production of ODTs can be grouped as: heat-based technologies (such as mass extrusion, melt granulation, flash heating, phase transition, tablet moulding, sintering, sublimation, and wet granulation processes); and non-heat-based technologies such as freeze-drying, direct compression/ spray drying processes and effervescent disintegration systems (Goel *et al* 2008, Hirani *et al* 2009, Giri *et al* 2010, Wagh *et al* 2011). Of the various technologies for producing ODTs, studies have shown that lyophilisation seems to be the most successful because it provides highly porous tablets, resulting in rapid disintegration and ease of swallowing; however high friability is a concern with lyophilised tablets (AlHusban et al, 2010). Direct compression is gaining grounds as a simple, cost effective method not requiring the use of moisture or heat that produces ODTs with good mechanical properties (Al-Khattawi *et al* 2014). Gosai et al (2008) formulated ondansetron ODTs by direct compression using super disintegrants. The ODTs were found to disintegrate in the mouth within 3-5 seconds, and showed higher dissolution/ release rates than both the pure drug and the conventional tablets available in the market.

1.8 Research aims and objectives

Unfortunately, the use of peptides for chronic illnesses requires one or more injections per day on patients and this comes with inherent setbacks such as pain, psychological and physiological stress, risk of infection, and depositions at the site of administration; which all lead to poor patient compliance and probably therapeutic failure. Also, although parenteral routes result in delivery of

adequate doses to the bloodstream, some common problems with the administration of a protein like insulin include hyperinsulinaemia in the peripheral systems, entrance of insulin into arterial wall lipids, increase in smooth muscle cell growth; all leading to angiopathy at micro and macro levels (Khafagy *et al* 2007). Thus, with advancements in mass protein and peptide production via recombinant technologies, research has been directed towards novel, non-invasive methods to deliver these agents. Although these alternative routes have so far not recorded overwhelming successes in terms of improved or comparable bioavailability and efficacy, scientists are still working towards non-invasive delivery, because of the promise of an improved quality of life for the patients (Caon *et al* 2014).

The advantages of buccal drug delivery, as discussed above, and the high acceptability of ODTs necessitate further studies into the applicability of this dosage form to deliver large molecule therapeutics such as peptides and proteins like insulin, which cannot withstand the harsh environment of the GIT. However, there are various gaps in currently available knowledge. No literature exists that explores the buccal delivery of proteins formulated as an ODT. The unavailability of standardised, cost effective methods for *in vitro* modelling of buccal transport is still a concern. Most of the published literatures report the use of amino acid derivatives as permeation enhancers with little or no elucidation of mechanisms of such enhancement; few studies employed unmodified amino acids. However till date, no evidence exists on the use of amino acids as permeation enhancers across the buccal cavity, or for the peptide insulin. Thus, it becomes pertinent that a multivariate study employing strategies that overcome the physiological barriers of peptide drug delivery via the buccal cavity be carried out, to investigate increases in bioavailability, if any, of peptide drugs administered via this route. The objectives of this work therefore include:

- To systematically investigate the tabletting properties of novel multifunctional excipients and their applicability in ODT manufacture by direct compression method.
- To employ quality by design (QbD) principles in the fabrication of ODTs exhibiting mucoadhesive properties which still meet ODT criteria of good mechanical strength and fast disintegration.

- To investigate the development of a robust and cost effective cell culture based method for *in vitro* assessment of buccal drug transport exhibiting characteristics similar to that expected *in vivo*.
- To characterise and quantify the model protein, insulin and determine the effect of ODT manufacturing process parameters on protein stability and secondary structure.
- To model insulin transport across the buccal mucosa *in vitro* in order to identify preferred candidates, as well as elucidate exact routes and mechanisms of insulin transport in the presence of amino acids as permeation enhancers.
- To formulate and characterise insulin ODTs containing amino acids and mucoadhesive agents.

Research Hypothesis

The overall hypothesis of this work was built on the premise that the absorption of large molecules like proteins and peptides which are degraded in the harsh environment of the GIT can be significantly increased via buccal transmucosal delivery, when formulated as ODTs including penetration enhancers and mucoadhesive agents.

Chapter 2

Investigation of the role of low substituted hydroxypropyl cellulose (LHPC) and HPC in the formulation of orally disintegrating tablets by direct compression

Publications relating to chapter 2

Al-Khattawi, A.; **Iyire, A**.; Dennison, T.; Dahmash, E.; Bailey, C.; Smith, J. et al (2014) Systematic screening of compressed ODT excipients: Cellulosic versus non-cellulosic. *Current Drug Delivery* **11**(4):486-500

ElShaer, A.; Kaialy, W.; Akhtar, N.; **Iyire, A.**; Hussain, T.; Alany, R.; Mohammed, A. (2015) A methodological evaluation and predictive *in silico* investigation into the multi-functionality of arginine in directly compressed tablets. *European Journal of Pharmaceutics and Biopharmaceutics* **96**:272-281

2.1 Introduction

Cellulose is the most abundant and renewable naturally occurring polymer or raw material presently available (Roy *et al* 2009a). It is a component of the cell wall of green plants, some algae and bacteria amongst others. Cellulose consists of repeating linear chains of anhydrous D-glucose molecules linked by β(1→4)-glycosidic linkages (Figure 2.1). The abundance and easy accessibility of cellulose has driven its application in various industries such as food, pharmaceutical and textile (Roy *et al* 2009a). However, comparing the current applications of cellulose to its high abundance, it is an under-utilised natural resource.

The multiple hydroxyl groups in the cellulose polymer backbone enable hydrogen bond formation (Figure 2.2 and Figure 2.3) between hydroxyl hydrogen and the oxygen atom in the glucose ring. This inter- and/ or intra-molecular hydrogen bonding imparts high crystallinity and a very rigid structure on cellulose (Sharma *et al.*, 2009). Therefore, pure cellulose is insoluble in water and most organic solvents and has limited applications, especially in the pharmaceutical industry. Structural modifications of the cellulose backbone have provided polymers with better characteristics for diverse applications. Cellulosic polymers such as microcrystalline cellulose (MCC) and low substituted hydroxypropyl cellulose (LHPC) have been employed in the development of compressed ODTs, with tablets exhibiting high hardness and fast disintegration (Al-Khattawi and Mohammed 2013). Cellulosic polymers offer the advantage of their natural origin, biodegradability and accessibility. A major setback to the use of cellulosics in compressed ODT formulation is the poor mouth-feel or grittiness due to large particle size (Al-Khattawi and Mohammed 2013). Thus research has been geared into improving the physical characteristics of these excipients.

Figure 2.1 Molecular structure of cellulose showing repeating anhydrous glucose molecules linked by β(1,4)-glycosidic linkages (Roy *et al* 2009a)

Figure 2.2 Intra-molecular hydrogen bonding in cellulose (Roy *et al* 2009a)

Figure 2.3 Inter-molecular hydrogen bonding in cellulose (Roy *et al* 2009a)

One of such efforts was reported by Ishikawa et al (2001) where new grades of MCC (PH-M series) were reported, which were spherical with smaller particle size, to reduce the gritty mouth-feel of the original excipient.

To continue the investigation of cellulosics, a new grade of hydroxypropyl cellulose with small particle size was investigated. This grade of HPC had been reported by the manufacturers to impart desirable tablet characteristics to ODT formulations. HPC is a non-ionic ether of cellulose which is obtained when some or all the hydroxyl groups of the glucose units on the cellulose backbone have been hydroxypropylated to $-CH_2CH(OH)CH_3$ groups using propylene oxide (Sharma *et al* 2009). HPC possesses advantageous features such as biocompatibility, biodegradation, hydrophilicity/ water solubility and phase transition behaviors that change depending on polymer concentration (Gong *et al* 2011). According to the number of substituted hydroxyl groups on the cellulose backbone, various HPCs can be obtained differing in their degree of substitution (DS). The maximum DS obtainable is 3, since only 3 hydroxyl groups exist per anhydrous glucose unit of cellulose. A second important parameter for HPC is the moles of substitution (MS), which represents the total number of moles of propylene oxide molecules that have reacted per glucose moiety (Samuels 1969). MS may be greater than 3 because the –OH groups of the hydroxypropoxy

substituents are available for further etherification to incorporate more propylene oxide groups during the preparation of HPC (Sharma *et al* 2009). For HPC to be soluble in water, it must have an MS of at least 4, because of the high crystallinity of cellulose (Gong *et al* 2011). An idealised structure of HPC is shown in Figure 2.4 indicating that the propylene oxide moieties can either react with the hydroxyl group of the anhydrous glucose moiety, or the hydroxyl group on the previously attached hydroxypropyl substituent (Werbowyj and Gray 1980).

Figure 2.4 Idealised structure of hydroxypropyl cellulose portraying hydroxypropylation occurring either on the hydroxyl group of glucose, or on previously hydroxypropylated side chains (Werbowyj and Gray 1980)

The specific application of HPC in pharmaceutical dosage formulation depends on different variables, especially its structural features, which can be defined by its DS. DS of HPC determines its behavior in the presence of water; thus, HPCs with medium or high DS which are characteristically soluble in water, are applied as thickeners and in the formulation of matrix tablets; while those with low DS reported not to dissolve, but swell in the presence of water, are applied as disintegrants during formulation of conventional tablets (Alvarez-Lorenzo *et al* 2000). HPC has been reported to exhibit properties as a binder, disintegrant, and/or mucoadhesive agent for drug delivery systems (Machida 1974, Sakagami *et al* 2001, Francis *et al* 2003). Studies employing low-substituted hydroxypropyl cellulose (LHPC) have used it as a co-excipient in conventional or orodispersible tablet formulations. Little or no data exists for the use of HPC or LHPC as the main excipient for ODT studies. Alvarez-Lorenzo et al (2001) studied the

characteristic effect of 5 varieties of LHPC on the behaviors of conventional tablets prepared by direct compression. Thus it is important to investigate and highlight the roles these polymers play in ODT formulation development.

Orally disintegrating tablets (ODTs) have gained popularity and are useful for drug delivery to paediatric and geriatric populations (Wagh *et al* 2011). These tablets are required to disintegrate in the mouth in less than 30 seconds (USP requirement), without the need to drink water (Pfister and Ghosh 2005). One of the constraints of ODT usage is the small quantity of drug it can accommodate (Aurora and Pathak 2005). Thus, to maximise drug loading without producing very large tablets, it is necessary to employ excipients with multi-functionalities. Scant data is available on the use of HPCs on their own as binders and/or disintegrants for formulation of ODTs. The availability and incorporation of multi-functional excipients into oral tablets is becoming more popular due to the potential for reduced excipient load, increased dose capacity, smaller tablet size enhancing patient compliance and suitability for ODT manufacture by direct compression, without the need for granulation (Al-Khattawi *et al* 2014).

The objective of this study was to investigate the tableting properties of a novel grade of HPC, which was claimed by the manufacturers to be applicable as a binder/ disintegrant in ODT formulation (to substantiate or refute their claims) and compare with a low substitution HPC (LHPC), with the overall aim of obtaining an optimised ODT formulation by direct compression.

2.2 Materials and methods

2.2.1 Materials

Hydroxypropyl cellulose (HPC-SSL-SFP) was a gift from Nisso Soda Co. Ltd (Japan). Low-substituted hydroxypropyl cellulose (L-HPC, NBD-022) was a gift from Shin-Etsu Chemical Co (Tokyo, Japan), while magnesium stearate and D-mannitol were purchased from Sigma-Aldrich (Pool, UK).

2.2.2 Methods

2.2.2.1 Bulk/ pre-formulation characteristics of powders

Pre-formulation characterisation was carried out on HPC and low substituted HPC (LHPC) to serve as a basis for comparing behaviours when tablets were formulated.

2.2.2.1.1 Particle size analysis (Diffractometry)

Approximately 2 g of the dry powders was spread on a VIBRI/L feeder tray, and dispersed through a RODOS disperser attached to a Sympatec HELOS/BR particle size analyser (Clausthat-Zellerfeld, Germany) at trigger condition of 2% Copt for 10 sec using compressed air at 3 bar pressure. As a beam of monochromatic light passed through the chamber, the powder particles diffracted the light at certain angles depending on their particle size through lens range of 0-175µm and results were produced as a volume distribution. Triplicate measurements were made and the accompanying software calculated the 10% (D10), median (D50%), 90% (D90) particle sizes, as well as the volume mean diameter (VMD) of particles (n=3).

2.2.2.1.2 Angle of repose (ɵ)

The angle of repose has been described as 'an engineering property of granular materials' and is 'the maximum angle of a stable slope with the horizontal determined by friction, cohesion and the shape of the particle' (Deshpande and Yadav 2009). The fixed height cone method (Fahmy and Kassem 2008) was adapted for this test. A funnel was attached to a retort stand at a specific height and the powders were poured freely through the funnel until a conical heap was achieved. The height (h) and diameter (d) of the heap were measured. The angle of repose ɵ, which is the internal angle between the horizontal surface and the powder surface, was then calculated from the equation:

$$\text{Tan } \theta = \frac{2h}{d} \quad . \quad . \quad . \quad . \quad . \quad . \quad . \qquad \text{(Equation 2.1)}$$

The test was performed in triplicate (n=3) for each sample and the mean angle recorded in degrees.

2.2.2.1.3 Bulk and tapped density

A specific weight (20 g) of the sample was poured into a 100 mL measuring cylinder attached to a Sortax tap density tester USP I apparatus (Allschwil, Switzerland). The initial volume (volume at zero tap or bulk volume) was recorded. The machine was set to vibrate and the volumes at 50, 100,150, 200 and 250 taps were obtained and recorded. This was repeated for all the samples. The tapped and bulk densities, Hausners ratio and Carrs' index were calculated for the samples using the equations below:

$$Tapped\ density = \frac{Mass\ of\ powder}{Final\ powder\ volume} \quad . \quad . \quad . \quad . \quad . \quad \text{(Equation 2.2)}$$

$$Bulk\ density = \frac{Mass\ of\ powder}{Initial\ powder\ volume\ (at\ zero\ tap)} \quad . \quad . \quad . \quad \text{(Equation 2.3)}$$

$$Hausner's\ ratio = \frac{Tap\ density}{Bulk\ density} \quad . \quad . \quad . \quad . \quad . \quad \text{(Equation 2.4)}$$

$$Carr'sindex = \frac{Tap\ density - Bulk\ density}{Tap\ density}\ x\frac{100}{1} \quad . \quad . \quad . \quad . \quad \text{(Equation 2.5)}$$

2.2.2.1.4 True density and porosity of powders

A multipycnometer from Quantachrome Instruments (Syosset, USA) utilising helium gas was used to measure the true density of the powders at ambient temperature. Tablet true volume measurement was based on Archimedes principle of fluid displacement since helium gas can penetrate tiny pores of up to 1 angstrom (10^{-10} m) in diameter. Weighed samples (0.9-1.1 g) were employed. The true density of the sample was automatically calculated by the accompanying software using equation 2.6 below. The bulk volume of the powder was further measured by pouring the weighed sample into a 1mL volumetric cylinder. The tests were performed in triplicates for each of the samples. The porosity of the powders was calculated from equation 2.7:

$$V_t = V_c - V_r\left(\frac{P_1}{P_2} - 1\right) \quad . \quad . \quad . \quad . \quad . \quad . \quad . \quad \text{(Equation 2.6)}$$

$$Porosity\ (\varepsilon) = 1 - \frac{bulk\ density}{true\ density} \quad .. \quad . \quad . \quad . \quad \text{(Equation 2.7)}$$

Where V_t, V_c and V_r are the sample true volume, sample cell volume and known reference volume respectively. P_1 and P_2 represent the atmospheric pressure and air pressure change during determination. The true and bulk densities of the tablet can then be calculated from V_t and bulk volume.

$$True\ density = \frac{Powder\ weight}{Powder\ volume\ (Vt)} \quad . \quad . \quad . \quad . \quad . \quad \text{(Equation 2.8)}$$

$$Bulk\ density = \frac{Weight\ of\ powder}{bulk\ volume\ of\ powder} \quad . \quad . \quad . \quad . \quad . \quad \text{(Equation 2.9)}$$

2.2.2.1.5 Powder moisture content

The moisture content of the powders was determined by the 'loss on drying method' using a thermobalance (Sartorius, Surrey, UK). Samples of <200 mg were loaded unto the balance and the initial weight recorded. After heating at a constant rate, the final weight was recorded. Moisture content was then calculated as the percentage weight loss from the sample using equation 2.10.

$$Moisture\ content = \frac{initial\ weight - final\ weight}{initial\ weight}\ x\frac{100}{1} \quad . \quad . \quad . \quad \text{(Equation 2.10)}$$

The samples were tested in triplicates and reported as mean ± standard deviation.

2.2.2.1.6 Scanning electron microscopy (SEM)

For powders, approximately 1mg samples were lightly sprinkled on the carbon surfaces of universal specimen stubs taped with double-sided adhesive strip, while tablets were dissected with a blade and a thin section was added to the specimen stub. Samples were then double coated with a thin layer of gold under low vacuum for about 3 minutes in the presence of Argon gas using a sputter coater, Polaron SC500 (Polaron Equipment Ltd, Watford, UK) at 20 mA. The particle surface morphology was captured using a Cambridge Stereo Scan (S90) Electron Microscope to produce micrographs including acceleration voltage and magnification.

2.2.2.1.7 Fourier transform infrared (FTIR) spectroscopy

FTIR spectroscopy was carried out on the powders using a Nicolet IS5 FTIR spectrometer equipped with an iD5 attenuated total reflectance (ATR) diamond from Thermo Fisher

(Massachusetts, USA). A small mass of dry powder was lightly spread on the lens and after measurements the accompanying software identified the available peaks.

2.2.2.1.8 X-ray diffractometry (XRD)

To investigate the absence or presence of crystallinity in the polymers, x-ray diffraction using a D2 Phaser from Bruker (Massachussetts, USA) was carried out on the polymer powders. The angular range (2ɵ) varied from 4 – 50° with increment steps of 0.02° and measured at 0.25 seconds/ step. Diffractive patterns were generated as counts per step and thereafter analysed using Eva 18.0.0.0 software (Bruker, AXS). Runs were carried out in triplicate and representative results reported.

2.2.2.2 Tablet preparation and characterisation

500 mg tablets consisting of 100% polymer were compacted using a manual bench-top hydraulic tablet press from Specac Ltd (Slough, UK) equipped with 13mm flat-faced dies. The punches were externally lubricated with a suspension of magnesium stearate in acetone (5% w/v) and powders were manually filled into dies. Tablets were punched at a pressure range of 5-30 kN and 5sec dwell time. Six batches of 500 mg placebo tablets were prepared. The tablets were individually weighed from mixes that contained 0.5% magnesium stearate as lubricant, D-mannitol as filler and 0-10% polymer (HPC or LHPC) as binder/ disintegrant. The composition of the batches is shown in Table 2.1.

Table 2.1 Composition of placebo tablets

Formulation	D-Mannitol (%)	Polymer (%)	Magnesium stearate (%)
F0 (control)	99.5	0.0	0.5
F1	98.5	1.0	0.5
F2	96.5	3.0	0.5
F3	94.5	5.0	0.5
F4	92.5	7.0	0.5
F5	89.5	10.0	0.5

2.2.2.2.1 Tabletting behaviour of pure polymer tablets

In order to examine powder densification mechanisms and obtain mean yield pressure (P_y) values, out-of-die Heckel's profiles were generated for the pure polymer tablets. This analysis involves compaction of the tablets at different pressures and measuring the porosity after tablet ejection. P_y can be obtained from the reciprocal of the slope (K) of the linear portion of the Heckel plot (–Ln porosity vs compaction pressure), which is represented by equation 2.11 (Paronen 1986):

$$Ln\left(\frac{1}{1-D}\right) = KP + A \quad . \quad . \quad . \quad . \quad . \quad . \quad . \quad \text{(Equation 2.11)}$$

where D = relative density (apparent tablet density/ effective particle density) of powder bed during compression, P = applied pressure, K = constant which reciprocal gives the material's mean yield pressure that shows the ability of a material to undergo deformation under pressure; and the intercept, A, sheds light on the movement of particles at the initial compaction stage.

FTIR spectroscopy, SEM and XRD (described above) were also carried out on the pure polymers compacted at pressures of 5, 10 and 30 kN, to attempt an elucidation of the bonding processes that occur during their compaction.

2.2.2.2.1 Tablet hardness

The hardness (crushing strength) of the tablets was measured using a 4M hardness tester from Schleuniger (Thun, Switzerland). Tensile strength, σ was calculated from equation 2.12:

$$Tensile\ strength\ (\sigma) = \frac{2\ x\ Hardness}{\pi d\mathrm{h}} \quad . \quad . \quad . \quad . \quad . \quad \text{(Equation 2.12)}$$

Where d and h represent the diameter and thickness of the tablet, measured using a digital Vernier calliper.

2.2.2.2.2 Tablet porosity

The apparent density of the tablets was measured using the helium pycnometry method described above (section 2.2.2.1.4). Bulk volume, calculated from tablet diameter (d) and thickness (h) using

equation 2.13, was used to compute bulk density (equation 2.14) while porosity was calculated using equation 2.7 above.

$$Bulk\ volume = \pi\left(\frac{d}{2}\right)^2 h \quad . \quad . \quad . \quad . \quad . \quad \text{(Equation 2.13)}$$

$$Tablet\ bulk\ density = \frac{mass\ of\ tablet}{bulk\ volume} \quad . \quad . \quad . \quad . \quad \text{(Equation 2.14)}$$

2.2.2.2.3 Tablet friability

The ability of the tablets to withstand mechanical stress, known as friability was measured using a rotating drum friabilator from J. Engelsmann AG (Ludwigshafen, Germany). 6 tablets were utilised at 25 rpm for 100 revolutions or 4 minutes. Tablets were carefully de-dusted before and after the test, and friability expressed as the percentage loss in weight.

$$Friability = \frac{initial\ weight - final\ weight}{initial\ weight}\ x\frac{100}{1} \quad . \quad . \quad . \quad . \quad \text{(Equation 2.15)}$$

2.2.2.2.4 Tablet disintegration time

The time taken for the tablet to disintegrate and completely pass through the mesh of a disintegration basket was determined according to the official USP monograph 701, on a ZT3 USP II disintegration test apparatus (Erweka, Heusenstamm-Germany). A tablet was placed in the disintegration basket and covered with a disk. The basket was then raised and lowered at a constant frequency of 30 cycles/ min in the disintegration medium (800 mL distilled water) maintained at 37°C. Measurements were carried out on tablets individually to improve operator accuracy and precision.

2.2.2.2.5 Formulation optimisation

The formulation which showed the best overall tablet characteristics, of low friability and disintegration time, but high hardness and porosity, was optimised by compacting at various pressures and tablet characterisation repeated as above.

2.2.2.6 Statistical analysis

All data generated in triplicates were presented as mean ± standard deviation (SD), where n=3. The data was then analysed for statistical significance using one-way analysis of variance (ANOVA) and Tukey-Kramar multiple comparison post-test from Graphpad Prism® version 5.04 (Graphpad Software, San Diego, CA, USA). The level of significance was quoted as $p<0.05$ (probability values of 95%).

2.3 Results and discussion

2.3.1 Pre-formulation characterisation

2.3.1.1 Effect of morphology on power characteristics

Table 2.2 and Figure 2.5 present the particle sizes of the polymers using laser diffractometry. The results showed HPC as a much finer powder than LHPC. These results were consistent with that from SEM studies displaying HPC particles (Figure 2.6) as smaller than that of LHPC (Figure 2.7). The morphology of HPC particles was somewhat spherical, non- elongated, with an irregular surface; while that of LHPC particles was fibrous, needle-shaped/ elongated with an irregular surface. Picker-Freyer and Durig (2007) reported that for fine particle grades of HPC, the morphology of the smaller particle size grades was spherical, while those with larger particle size showed more elongated structures. The irregular surface of the particles would be expected to lend to higher interactions and hardness on compaction (Korhonen *et al* 2002). Particle size becomes important because it may control many properties such as flowability, agglomeration and dissolution of powders (Sinko 2011). Small particle size is advantageous because it increases the particle surface area and thus decreases dissolution time, but particles smaller than a critical dimension (approximately 20 µm) tend to agglomerate and thus impede tablet dissolution (Sinko 2011).

Table 2.2 Particle size analysis of powders using difractometry (n=3). HPC exhibited significantly smaller particle size than LHPC

Property	HPC	L-HPC
D_{10} (µm)	2.57 ± 0.05	16.15 ± 0.13
D_{50} (µm)	15.08 ± 0.21	42.30 ± 0.22
D_{90} (µm)	39.21 ± 1.52	85.51 ± 2.09
VMD (µm)	19.12 ±0.44	47.02 ± 0.82

On the other hand, particles with large sizes tend to exhibit good flow characteristics (Sinko 2011). Flowability of powders is important because small particle sizes can result in poor die fill and inconsistent content uniformity, which in turn can cause entrapment of air within the tablet upon compaction, resulting in lamination and capping (Al-Khattawi *et al* 2014).

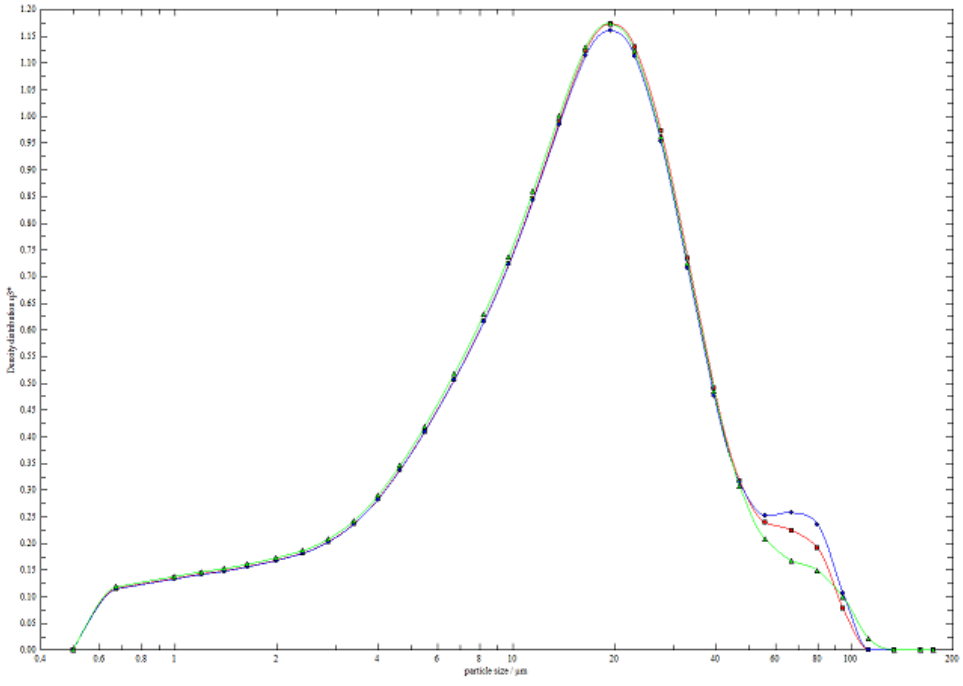

Figure 2.5 Representative graph showing particle size distribution of HPC powder by laser diffractometry using a Sympatec HELOS/BR particle size analyzer (n=3)

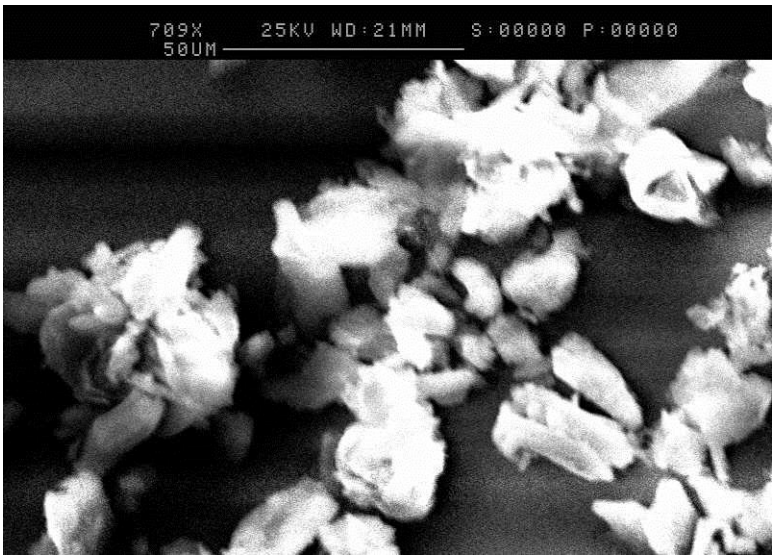

Figure 2.6 SEM of HPC powder at 50 µm magnification showing somewhat spherical particles with irregular surface

Table 2.3 is a summary of the pre-formulation characteristics of the powders. According to the USP 29, the angle of repose (AOR) is a characteristic related to the inter-particulate friction or resistance to movement between particles. The lower the AOR, the better would be the flowability of the powder. HPC showed a high angle of repose indicative of very poor flow (Table 2.4). This was expected considering its small powder particle size. According to Elshaer et al (2013) AOR values above 40° describe powders that possess very poor flowability. Based on this classification, HPC can be said to have poor flowablity and L-HPC passable flowability. This can be explained based on the smaller mean particle diameter of HPC (<20µm).

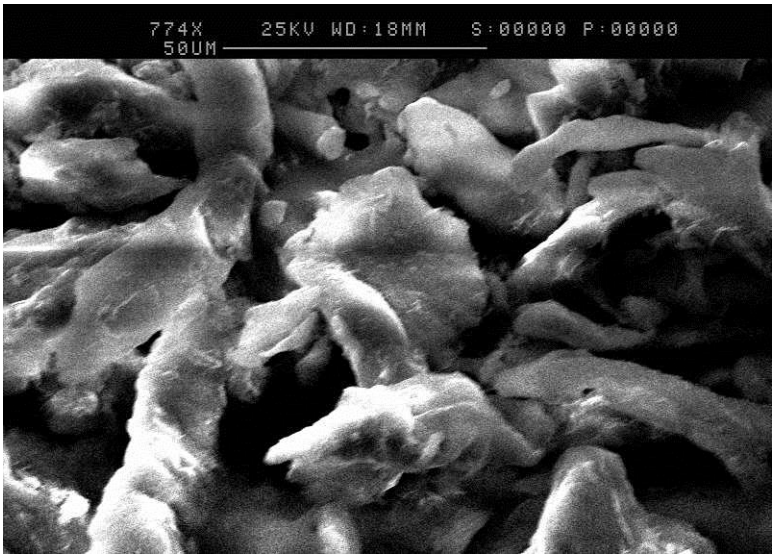

Figure 2.7 SEM of LHPC powder at 50 µm magnification showing somewhat elongated particles with irregular surface

Table 2.3 Summary of pre-formulation characteristics of HPC and LHPC powders (n=3)

Parameters	HPC	LHPC
Angle of repose (°)	40.68 ± 0.57	34.42 ± 1.13
Bulk Density (g/cm^3)	0.341 ± 0.01	0.330 ± 0.01
Tap Density (g/cm^3)	0.408 ± 0.01	0.445 ± 0.02
Hausner's ratio	1.197 ± 0.01	1.349 ± 0.05
Carr's Index (%)	16.48 ± 0.88	25.82 ± 2.50
True Density (g/cm^3)	1.46 ± 0.02	1.90 ± 0.03
Porosity	0.84 ± 0.01	0.86 ± 0.01
Moisture content (%)	9.91 ± 0.94	12.08 ± 1.92

Hancock et al (2001) reported low particle size grades of HPC to exhibit very poor flow properties. The Carr's index gives a representation of changes that occur in the packing arrangement of a powder when it is tapped and this can then be extrapolated to the effect expected during movement, shipping and handling (Nerurkar *et al* 2005). However, using the Carr's indices, LHPC would be classified as having poor flow and HPC as having fair flow. This was an unexpected result and may be explained by the fact that Carr's index is based on bulk density measurements.

Table 2.4 AOR and Carr's index as indicators of powder flowability (Aulton, 2002, adapted)

S/N	Type of Flow	AOR (°)	Carr's index (%)
1	Excellent	<20	5-15
2	Good	20-30	12-16
3	Fair to passable	30-34	18-21
4	Poor	34-40	23-35
5	Very poor	>40	33-38
6	Extremely poor	-	>40

According to Sinko (2011), the bulk density of a powder is not a fixed value, but is dependent on various factors including: particle size and size distribution, particle shape, true density, the ability of the particles to adhere to one another and the method of measurement. Nerurkar *et al* (2005) reported similar results for bulk density and Carr's index measurements for a small particle size grade of HPC.

The true density of a powder usually depicts the powder's basic chemical properties, such as unit cell dimensions, molecular weight and molecular formula (Hancock *et al* 2003). As explained above, the bulk density, unlike the true density, is not constant and changes depending on different factors. Although there is no direct correlation between the bulk density of a powder and its flowability, this density becomes important in determining the fill of tablet powders from hoppers and into dies, as well as the size of tablets to be used for a powder of a certain mass, to ensure a reproducible and constant content (Sinko 2011). The true density of LHPC was significantly higher than that of HPC (Table 2.3), which could be explained based on the lower degree of hydroxypropyl substitution in LHPC. Thus, although the chemical compounds present are similar, their compositions differ. Alvarez-Lorenzo *et al* (2000) reported that LHPC powders with lower degrees of hydroxyl substitution had higher true densities than those with higher degrees of substitution. However, the two powders showed bulk and tapped densities with no significant differences between them.

Tablet porosity is a derived value and gives an indication of the solid fraction available for bonding in the tablet. Porosity has been shown to affect various properties of tablets including hardness/ tensile-strength, friability, disintegration time and dissolution characteristics (Bredenberg *et al* 2003). As with the bulk density measurements, porosities of LHPC and HPC powders (Table 2.3) were in the same range, with no significant difference between them.

2.3.1.2 Effect of degree of substitution on powder properties

FTIR spectra (Figure 2.8) were obtained to identify the peaks corresponding to functional groups present in the polymers. HPC and LHPC spectra exhibited absorption peaks that are characteristic for the cellulose backbone; (-OH 3418 cm^{-1}, -CH- 2873 cm^{-1}, -COC- 1049 cm^{-1}, β-linkage 839 cm^{-}

[1]) for HPC and (-OH 3333 cm^{-1}, -CH- 2879 cm^{-1}, -COC- 1020 cm^{-1}, β-linkage 897 cm^{-1}) for LHPC. The broad -OH absorption peak observed at 3418 cm^{-1} in the HPC spectrum shifted downwards to 3333 cm^{-1} and was larger in the LHPC spectrum. This confirms that the –OH groups in LHPC are not completely substituted and there is higher inter-molecular and intra-molecular hydrogen bonding available in LHPC (Wang *et al* 2003). The replacement of the hydroxyl groups of cellulose with ether linkages that occurs in HPC, reduces the intra-molecular hydrogen bonding. Shifting of IR peaks from lower to higher intensities are associated with destruction of intermolecular hydrogen bonds; as seen in HPC (Yamada *et al* 1999). C-H stretching vibrations from 2969 to 2873 cm^{-1} were observed in HPC and were consistent with results obtained by Kim and Park (2011). This C-H vibration of HPC characteristically shows a shoulder at 2969 cm^{-1} which is assigned to the CH stretching of the methyl group indicative of the hydroxypropyl groups (Sharma *et al* 2009). This shoulder was not noticed in the spectra for LHPC as hydroxypropyl substitution is low in LHPC. Alvarez-Lorenzo et al (2000) reported that lower degrees of substitution in LHPC impart higher crystallinity to the polymer structure.

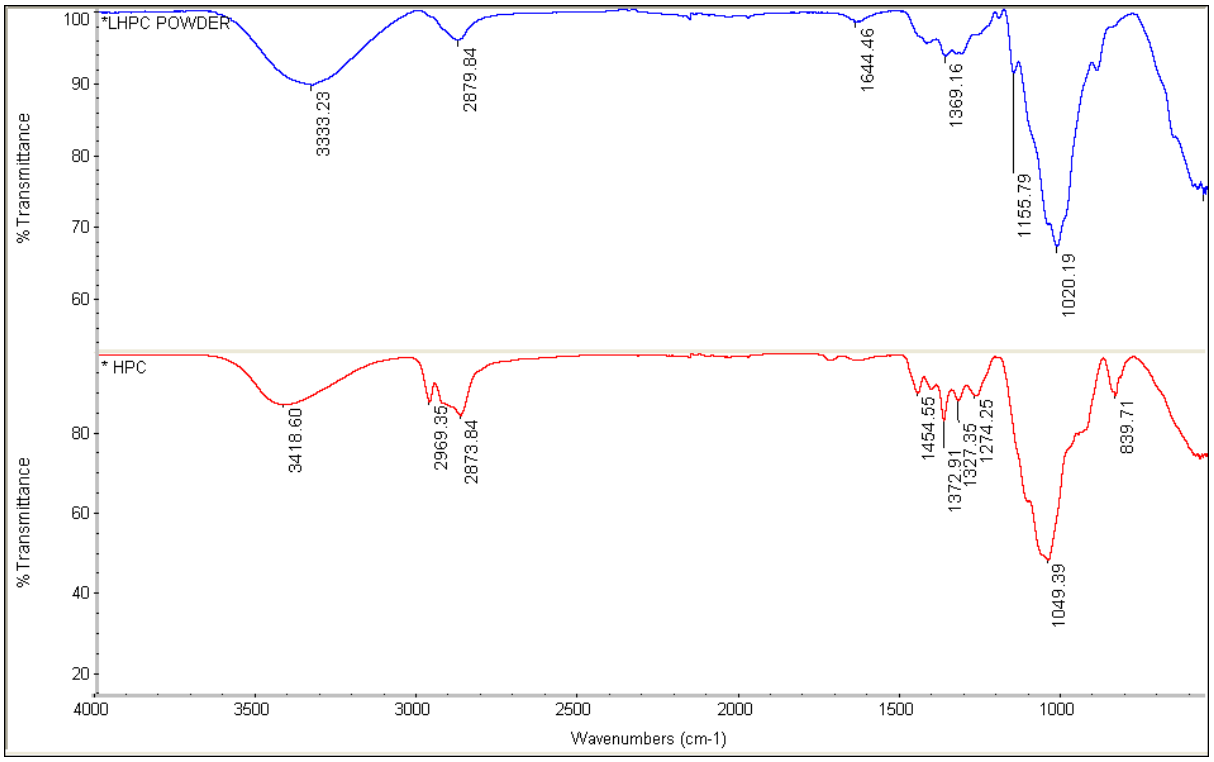

Figure 2.8 FTIR spectra for HPC and LHPC powders showing higher molecular hydrogen bonding in LHPC

The actual degree of substitution of HPC and LHPC can be determined by gas chromatography or NMR (Alvarez-Lorenzo *et al* 2000). Alvarez-Lorenzo et al (2000) also reported that crystallinity indices of different varieties of LHPC decreased with increasing hydroxypropyl content. Therefore, the degree of crystallinity in LHPC would be expected to be higher than that of HPC.

The x-ray diffraction patterns for the powders are depicted in Figure 2.9 . Amorphous humps were obtained for both HPC and LHPC. The absence of crystalline peaks in the diffraction patterns of the polymers showed that they existed in the amorphous state (Yang *et al* 2004, Cilurzo *et al* 2005). Yamada et al (1999) reported similar findings for x-ray diffraction of HPC powders. However, the larger amorphous humps found in the HPC patterns than that in LHPC is consistent with the higher amorphous character of HPC, revealed by FTIR results.

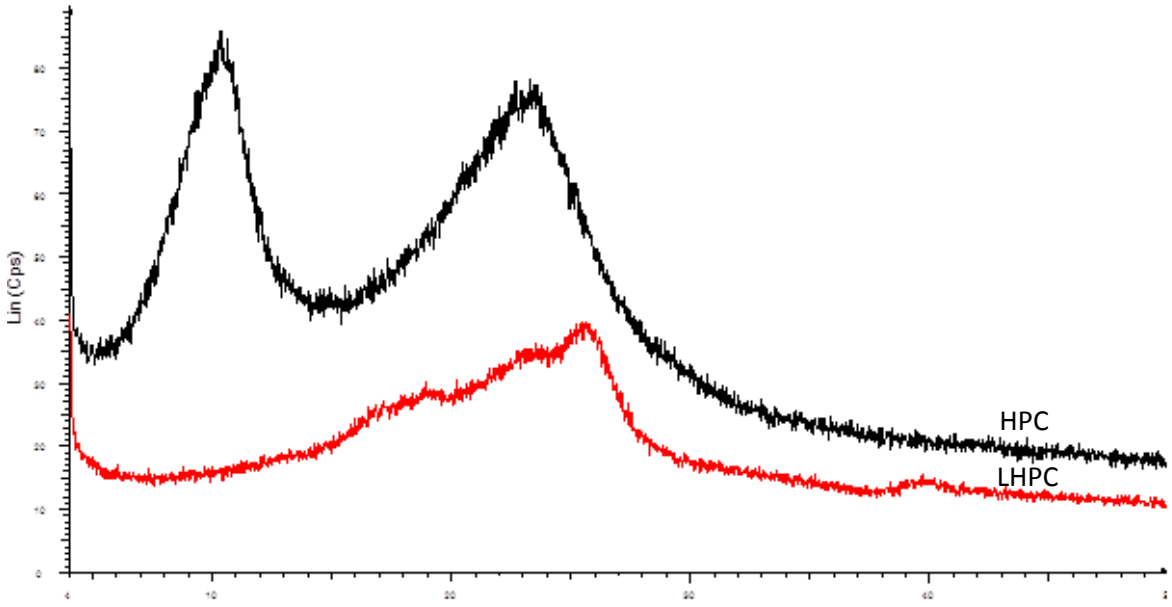

Figure 2.9 X-ray diffraction patterns for HPC and LHPC powders showing amorphous humps. The larger size of the amorphous humps in HPC than LHPC correlates with the lower degree of substitution and therefore higher crystallinity of LHPC.

2.3.2 Compaction characteristics of polymers

2.3.2.1 Compaction mechanisms

When pressure is applied to a powder mass during compaction, different processes come into play (Alderborn and Nystrom 1995): First, the particles of the powder rearrange themselves in the die to produce a closer packing structure until a certain pressure, where friction between particles prevents any further movement of particles. Thus, to continue the compaction process, plastic deformation of the particles may ensue, leading to volume reduction, which is irreversible after the pressure is removed. Some particles undergo elastic recovery, which occurs when the particles initially deform with increased pressure, leading to volume reduction, but upon removal of the pressure, the particles rebound, leading to increase in volume. Elastic recovery is associated with capping at higher pressures, resulting in tablets with low tensile strength or hardness (Alderborn and Nystrom 1995). Some other materials undergo fragmentation, which is the breakdown of particles into smaller fragments under pressure. As the compaction process continues, these smaller fragments may undergo further deformation. Thus, a single particle may undergo one or more of these processes before a compaction cycle is completed. Plastically deforming particles result in higher volume reduction and increased inter-particulate bonding, and thus may produce harder tablets (Alderborn and Nystrom 1995). Since pharmaceutical powders undergo compaction by one or more of these mechanisms, adequate powder characterisation is important.

Figure 2.10 shows the Heckel's plots for HPC and LHPC. The mean yield pressure, P_y gives an indication of the plastic deformation of a substance under pressure (Odeku *et al* 2005). The lower the P_y value, the higher the plastic deformation of the material upon compaction, and vice versa. The yield pressure has been reported to be affected by various factors, including particle fracture, particle and die wall friction, inter-particulate rearrangement, plastic or elastic deformation, and inter-particulate friction (that is the prevention of increased closeness of particle surfaces due to inter-particulate bonding) (Eriksson and Alderborn 1995).

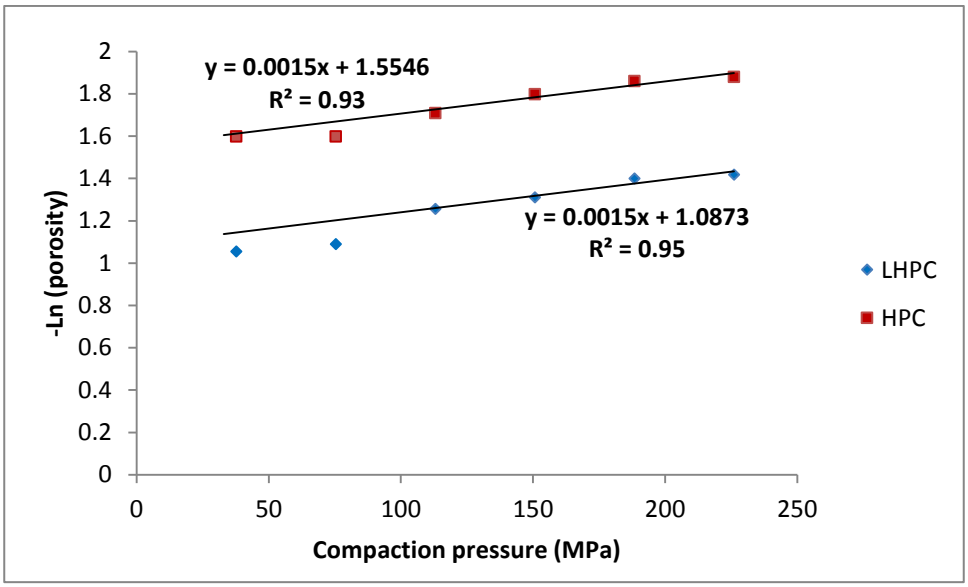

Figure 2.10 Out-of-die Heckel's plots for HPC and LHPC pure compacts (n=3). Higher volume reduction and thus lower porosity was observed for HPC, although both powders exhibited similar mean yield pressure values.

P_y value calculated as the reciprocal of the gradient of the linear portion of the Heckel's plot was found to be 666.67 MPa^{-1} for both HPC and LHPC. This yield pressure value indicates that some plastic deformation occurs during compaction of the two polymers, since the out-of-die method of porosity measurement was employed (Al-Khattawi *et al* 2014). HPC and LHPC have been reported as plastically deforming materials by some authors (Khossravi and Morehead 1997, Picker-Freyer and Dürig 2007); however, Sonnergaard (1999) stated that the Heckel's plot yield pressure value alone cannot totally describe the compaction behaviour of powders. Moreover, Hiestand (1997) argued that materials do not undergo plastic deformation or fracture exclusively, but that the higher the plastic deformation, the less the tendency for fracture/ fragmentation and vice versa. Thus, both events may occur during a single compaction process.

The yield pressure value obtained for HPC was expected to be lower than that obtained for LHPC, because crystalline portions of materials deform by fragmentation while amorphous portions deform plastically (Suzuki and Nakagami 1999). Thus, HPC with a more amorphous nature (as confirmed from FTIR and XRD results) would be expected to yield a lower mean yield pressure. Suzuki and Nakagami (1999) reported an increase in the mean yield pressure and tablet hardness of MCC as degree of crystallinity increased. The opposite trend was seen here, as both polymers

showed equal yield pressures, but HPC tablets showed higher hardness at similar compaction forces than LHPC (Table 2.5).

Table 2.5 Characteristics of pure HPC and LHPC tablets compacted at various pressures (n=3)

Compaction pressure (MPa)	**Hardness (N)**		**Disintegration time (s)**		**Porosity**	
	HPC	LHPC	HPC	LHPC	HPC	LHPC
38.00	340.27 ± 19.04	122.90 ± 41.00	>1800.00	30.00 ± 4.00	0.20 ± 0.02	0.35 ± 0.02
75.00	>520.00	240.57 ± 15.17	>1800.00	130.30 ± 7.51	0.20 ± 0.04	0.34 ± 0.01
113.00	>520.00	374.37 ± 11.77	>1800.00	212.20 ± 2.11	0.18 ± 0.0	0.2846 ± 0.01
151.00	>520.00	484.60 ± 5.46	>1800.00	332.40 ± 2.75	0.17 ± 0.01	0.27 ± 0.01
188.00	>520.00	488.43 ± 6.25	>1800.00	338.20 ± 19.56	0.16 ± 0.02	0.25 ± 0.04
226.00	>520.00	>520.00	>1800.00	366.80 ± 5.70	0.16 ± 0.04	0.24 ± 0.02

An interesting observation was made upon compaction of the pure HPC tablets. First, a change in colour of the tablets from white to cream occurred at compaction pressures from 10-30 kN (75-226 MPa). Also on visual observation of tablets within this pressure range, two distinct layers could be noticed (Figure 2.11) and the tablets appeared to have melted and solidified. Hardness of tablets within this pressure range could not be verified because the hardness recorded was >520N which is the maximum hardness the instrument can record. For LHPC tablets, no colour change was observed and although the tablet hardness was very high (122->520 N), only the tablets compacted at 30 kN recorded hardness values >520N (Table 2.5). HPC compacts did not disintegrate even

after 30 minutes at all compaction pressures tested, and this was expected considering the high hardness recorded. However, despite the high hardness of LHPC compacts, disintegration time at maximum pressure was less than 6 minutes, and disintegration time increased with increasing compaction pressure (Table 2.5). This difference in disintegration characteristics between HPC and LHPC, despite the high hardness, can be attributed to the behaviour of the polymers in the presence of water. HPC is more soluble in water and, therefore, dissolves on contact with water, thus dissolution occurs by tablet erosion and is slower (Alvarez-Lorenzo *et al* 2000); while insoluble LHPC swells on contact with water. This swelling action disrupts the tablet, leading to faster disintegration (Shirai *et al* 1993, Fukami *et al* 2006).

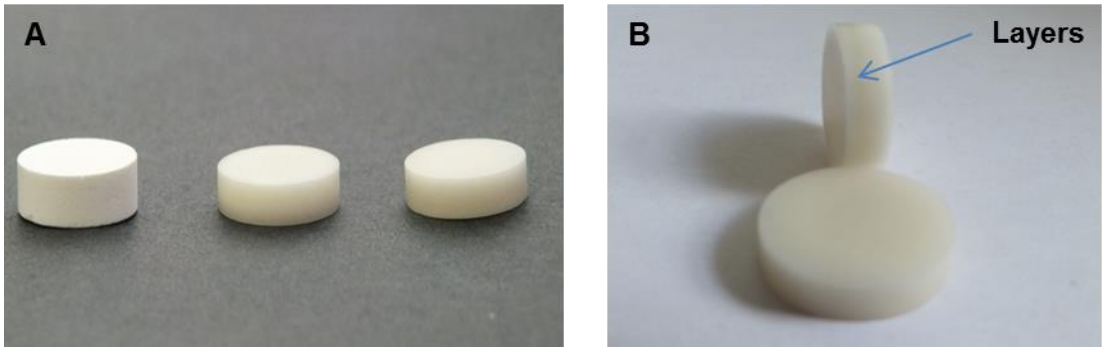

Figure 2.11. (A) Photograph of HPC tablet compacted at 5, 10 and 30 kN (left to right); highlighting the appearance of distinct layers (B)

The extremely high tablet hardness exhibited by LHPC tablets at 30 kN may be substantiated by x-ray diffraction patterns for these tablets. Figure 2.12 shows the XRD patterns for pure LHPC tablets compacted at 5, 10 and 30 kN respectively. The appearance of small crystalline peaks can be seen as compaction pressure increased to 10 and 30 kN, respectively. This introduction of crystallinity to LHPC upon compaction, would lead to more ordered arrangement of the LHPC molecules, and thus impart higher hardness to the compacts. Ek et al (1995) reported an increase in crystallinity of MCC with increasing compaction pressure, up to 125 MN/m^2 after which crystallinity decreased. This increase was said to be due to alteration of stressed structures in the polymer particles, resulting in a more ordered form as compression increased. This is also in line with reports by Suzuki & Nakagami (1999) who investigated the effect of degree of crystallinity on the compaction properties of MCC. They reported a decrease in tablet hardness (and energy

required for crushing tablets) with a decrease in MCC crystallinity. Gracias & Somorjai (1998) also reported an increase in hardness of polymers as crystallinity increased.

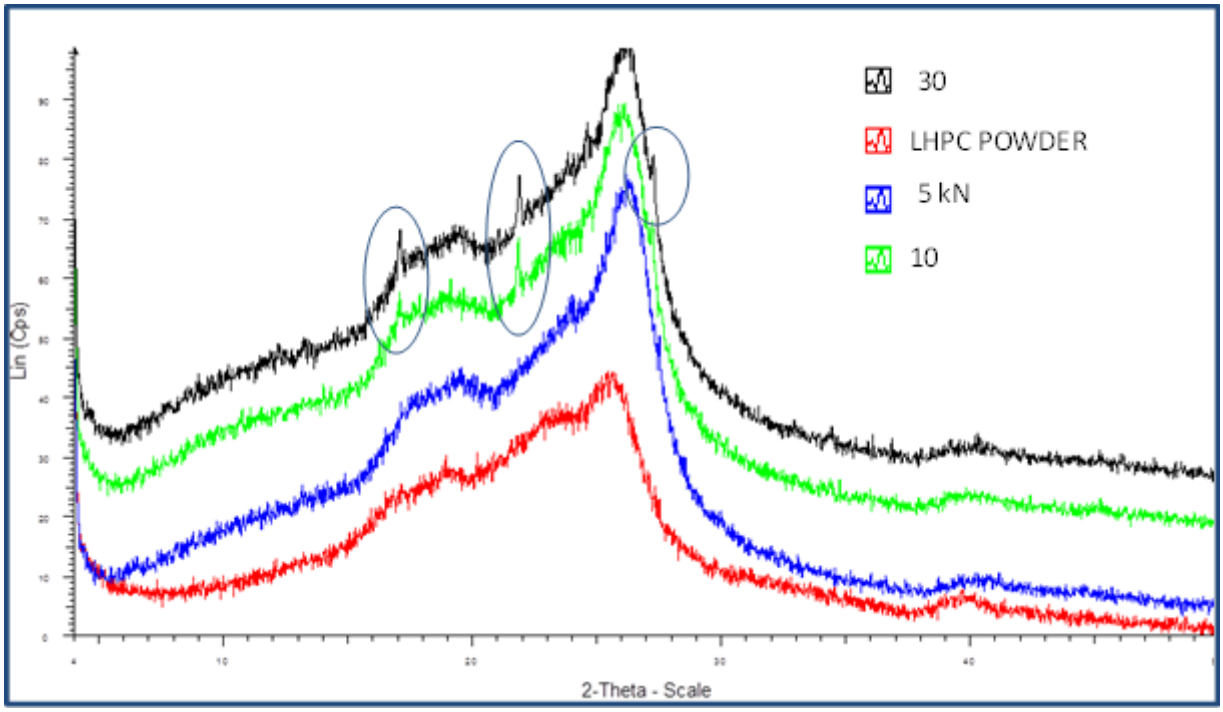

Figure 2.12 X-ray diffraction patterns highlighting the appearance of small crystalline peaks (highlighted in circles) in LHPC compacted at 10 and 30 kN, and the absence of such peaks in the patterns at 5 kN pressures and the polymer powder

The above crystallinity trend was not observed in compacts of pure HPC compacted at equal pressures (Figure 2.13). This could be because HPC was more amorphous than LHPC, and might therefore require much higher pressures to impart any measureable crystallinity to the polymer molecules (Al-Khattawi *et al* 2014). It was, therefore, important to attempt an elucidation of the mechanism of the hard compact formation observed with the HPC compacts. Various hypotheses have been given for high tablet strength upon compaction, and they are discussed as possibilities below: **Hydrogen bonding** has been shown to contribute to tablet hardness due to the presence of OH groups in the HPC structure. But, hydrogen bonding has been reported to provide a lower contribution to tablet hardness than other bonding mechanisms (Alderborn and Nystrom 1995, Hiestand 1997). However, careful observation of the FTIR spectra for HPC and LHPC compacts at different compaction pressures (Figure 2.14) showed identical peaks as those observed in the powders.

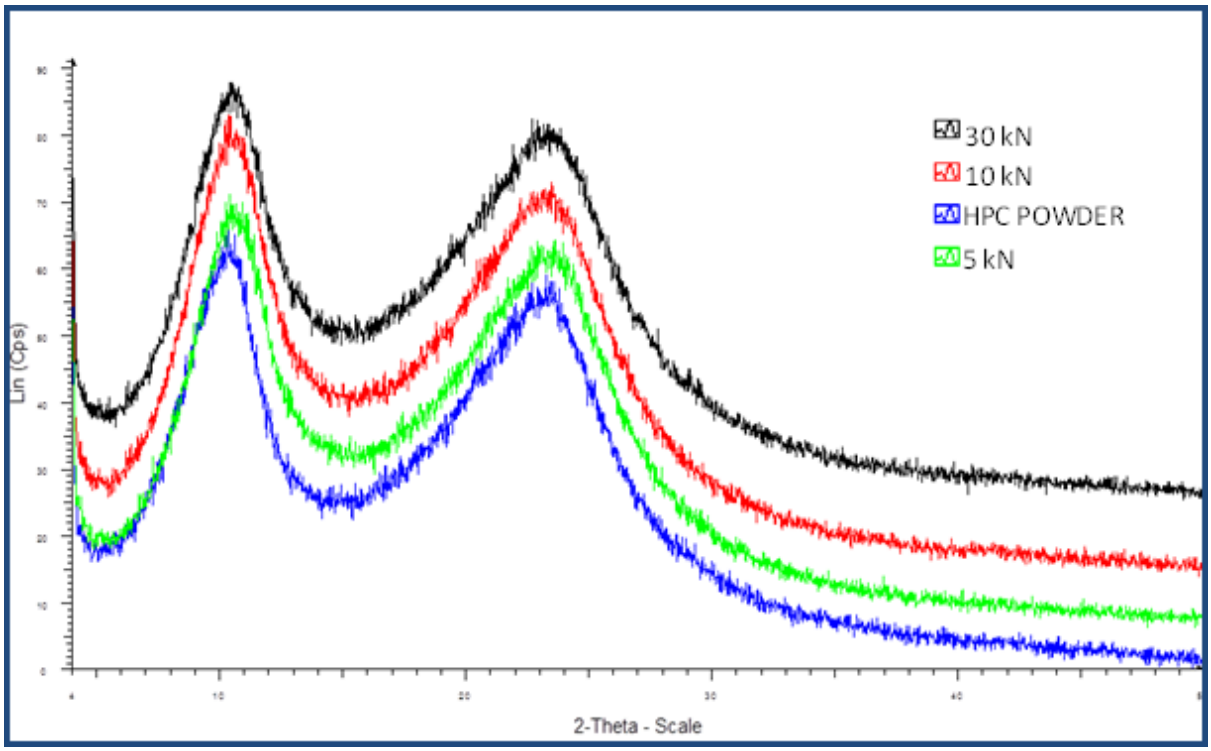

Figure 2.13 Xray diffraction patterns showing the absence of crystalline peaks in HPC powder and pure tablet compacted at 5, 10 and 30 kN respectively. No difference in diffraction patterns was observed with increasing compaction pressures.

Peak location and intensity was not observed to vary with compaction pressure for both polymers. Thus, the increase in compact hardness for two polymers may not be attributable to increased hydrogen bonding. Smaller **particle size** results in higher surface area which lends to higher inter-particle attraction (Adolfsson *et al* 1998). Small particle size of plastically deforming materials also promote volume reduction during compaction, resulting in closer packing of particles in the compact (Korhonen *et al* 2002). Comparing LHPC to HPC, the smaller particle size and lower porosity of HPC particles than LHPC, as seen from laser diffractometry (Table 2.2) and SEM results (Figure 2.6 and Figure 2.7), would produce a higher surface area for interaction and, therefore, higher binding and consequently harder compacts for HPC. Also, the Heckel's plot for the polymers shows a higher volume reduction (lower porosity) of HPC than LHPC, on compaction (Figure 2.10).

Solid bridge formation has been reported for coarse, plastically deforming materials that melt upon compaction (Hiestand 1997). Alderborn & Nystrom (1995) reported that formation of solid

bridges occurs as a result of crystallisation, sintering, binder hardening, melting and chemical reactions.

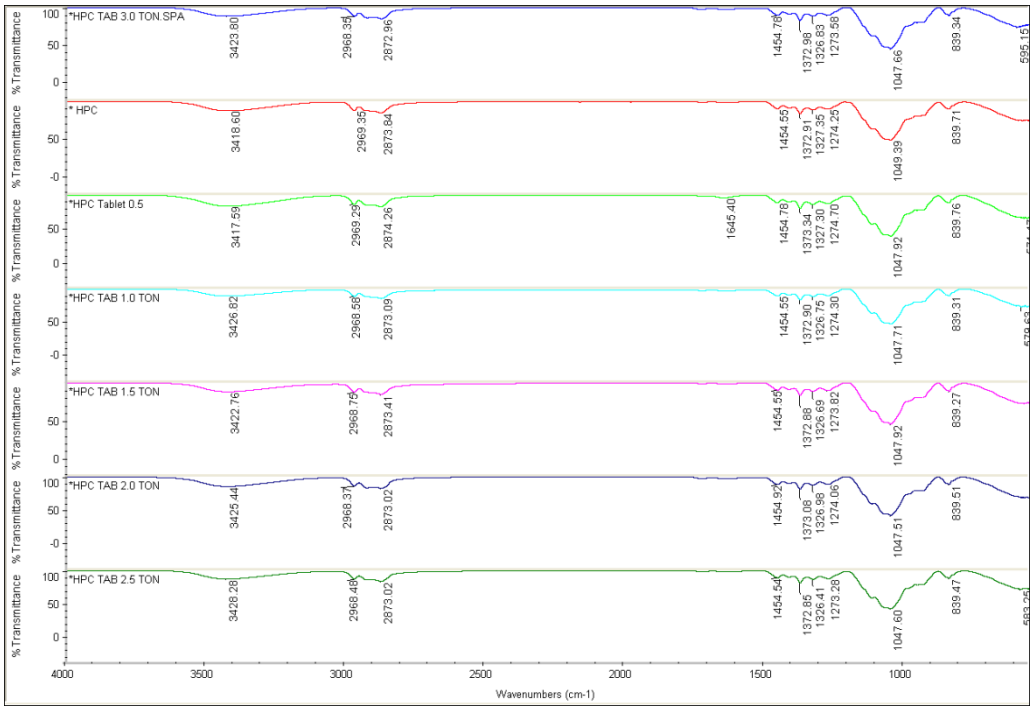

Figure 2.14 Comparing FTIR spectra of HPC powder with HPC tablets at different compression forces revealed no difference in -OH stretching bands or other peaks.

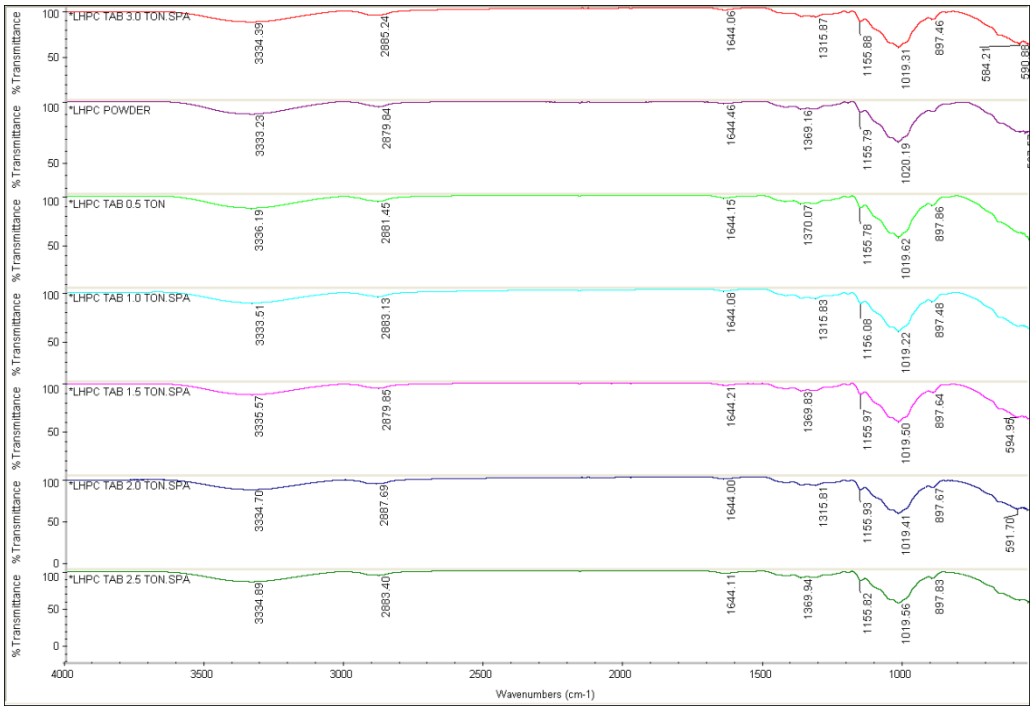

Figure 2.15 Comparing FTIR spectra of LHPC powder with LHPC tablets at different compression forces revealed no difference in –OH stretching bands or other peaks

Nystrom et al (1993) investigated the bonding mechanisms that come into play when powders are compacted into tablets. They reported the formation of solid bridges for highly plastically deforming particles, which could confer high compact strengths on the tablets. However, solid bridges were observed with coarse materials such as sodium chloride. The HPC compacts, when viewed with the naked eyes, appeared to have melted during compaction (Figure 2.11). Figure 2.16 shows SEM micrographs (all at 50 μm magnification) of the pure HPC and LHPC polymers compacted at 5, 10 and 30 kN respectively. At 5 kN pressure, HPC was somewhat compacted into sheets, with a general loss of its individual particle morphology, while the LHPC tablets retained some of the elongated structures, as seen from the SEM of its powder. With increasing compaction pressure, the pores in the tablets were observed to decrease, and this is consistent with the compressibility results for both powders (Figure 2.17) where porosity decreased with increasing compression force. However, there was greater decrease in the observed pores for HPC compacts than LHPC. Interestingly, with increasing compaction force, the HPC particles appeared to have coalesced to form a cohesive layer, which appeared larger than that observed at lower pressure; while the micrograph of LHPC remained fairly constant. This observation might be indicative of some fusion and/or bonding between HPC particles, which might be indicative of solid bridge formation, and give an insight into the high hardness of these HPC compacts.

2.3.2.2 Compressibility, compactability & tabletability

Compressibility shows the ability of a material to undergo volume reduction when pressure is applied to it (He *et al* 2007). This is determined from a plot of porosity against compaction pressure. Compactability reflects the material's ability to form compacts of reasonable strength upon densification, and is determined from a plot of tensile strength against porosity (Tye *et al* 2005). While tabletability demonstrates how effective the applied pressure is at increasing the strength of the compacted tablet (Tye *et al* 2005). Tabletability can be represented by plotting the tensile strength against compaction pressure.

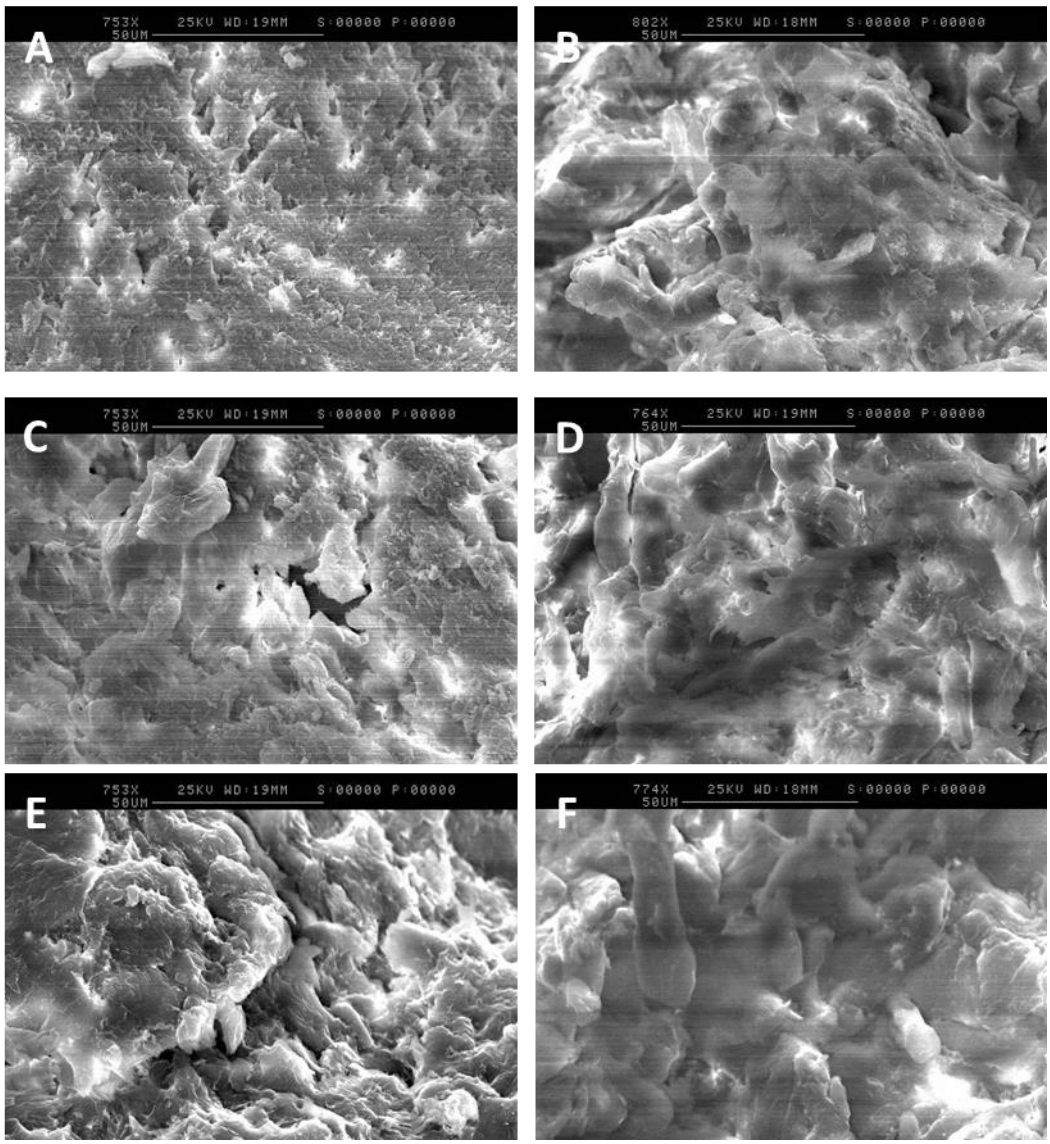

Figure 2.16 SEM of HPC (A,C,E) and LHPC (B,D,F) tablets compacted at 5, 10 and 30 kN respectively, showing consolidation of HPC particles with increasing compaction pressures; particles of LHPC remained fairly constant as compaction pressure increase.

Figure 2.17 shows the compressibility profile for HPC and LHPC at dwell time of 5 secs. There was generally a decrease in porosity with increase in compaction pressure, resulting in higher solid fraction for both powders. However, the compressibility and solid fraction of LHPC was lower than that of HPC, as would have been expected considering the smaller particle size of HPC. LHPC has been reported to impart high porosity to tablets (Watanabe *et al* 1995). Materials with high plastic flow and solid fraction have been reported to exhibit higher surface areas for bonding between particles (Tye *et al* 2005). Since the more porous a tablet, the easier and faster its disintegration, it is important to determine the compressibility of a tablet upon densification.

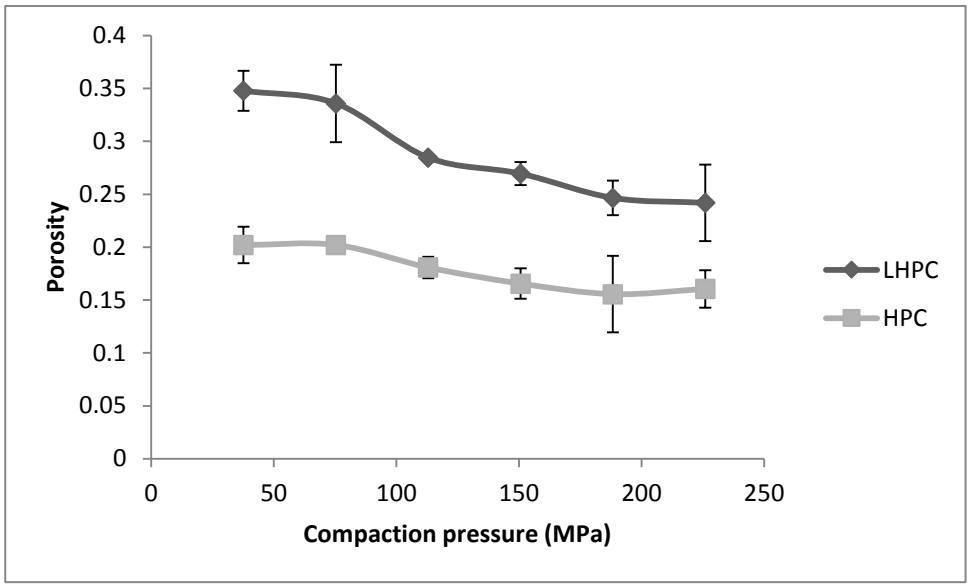

Figure 2.17 Compressibility profiles showing the variation in tablet porosity with increasing compaction pressures. The lower porosity values displayed by HPC depict higher compressibility than LHPC (n=3).

Unfortunately, because tablet hardness could not be estimated, compactability and tabletability profiles were not generated for the polymers. Nevertheless, the high hardness values of 340 and 122 kN recorded at compression force of 5 kN indicates that HPC and LHPC, respectively, showed high tabletability even at low compression pressures. Picker-Freyer and Durig (2007) had earlier reported that low particle sized HPC powders (D_{50} about 66µm) formed very hard tablets (about 200N) at significantly lower compression forces, when compared to other powders and even HPC powders with larger particle size.

2.3.3 Placebo tablet characterisation

To assess the application of the characterised polymers in ODT formulations, placebo tablets containing mannitol as filler, magnesium stearate as lubricant and either HPC or LHPC (concentrations 0 - 10%) were compacted at 10 kN and characterised. For a tablet to be useful as an ODT, it should show considerable hardness, fast disintegration time (<1 minute) and low friability to be able to withstand stress during packing and shipping (Alhusban *et al* 2010).

2.3.3.1 Tablet hardness

Figure 2.18 compares the hardness of mannitol tablets containing either HPC or LHPC (0 -10%) as binder. As was expected, there was a general increase in tablet hardness with increasing HPC

concentration, depicting the binding property of HPC. Contrary to what would have been expected following the high hardness values recorded for the HPC compacts (>520N), the hardness of the mannitol formulations incorporating HPC was not very high (<60N at 10% HPC concentration). Elshaer *et al* (2015) highlighted the unavailability of simple relationships to predict tablet characteristics of binary mixtures from the behaviours of their pure polymer compacts. Maggi (2002) reported higher hardness for compacted pure polymer tablets when compared to formulation tablets compacted at the same compaction pressures due to the influence of other additives/ excipients in the system. This suggests that the incorporation of mannitol (with low tabletability) had a significantly large influence on the cohesiveness of HPC (Al-Khattawi *et al* 2014). But the prepared tablets exhibited sufficient hardness for practical use. HPC has been reported to act as a binder in concentration ranges from 2-8% w/w, in combination with other excipients (Picker-Freyer and Dürig 2007).

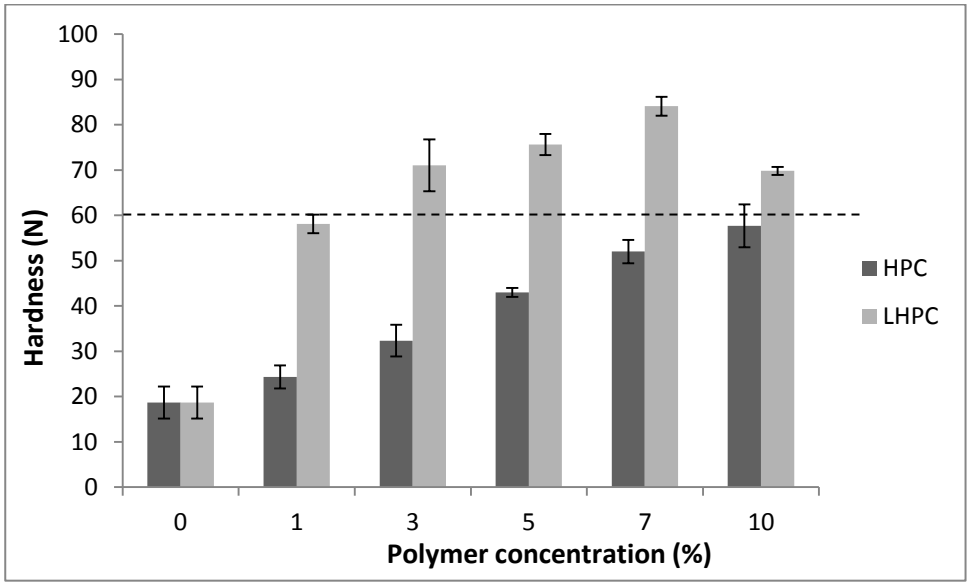

Figure 2.18 Hardness of tablets containing HPC or LHPC as binder (n=3). Dotted line depicts minimum desirable hardness.

There was also generally an increase in hardness of tablets with increasing LHPC concentration. However, a decline in hardness was observed when LHPC concentration increased from 7% to 10%. Watanabe et al (1995) had reported a similar decline in crushing strength of tablets comprising LHPC and other excipients, when LHPC concentration was increased from 10% to 30%; though reasons for this anomaly were not presented. When compared to HPC tablets, LHPC

tablets exhibited significantly higher hardness at the same polymer concentrations. The appearance of crystallinity peaks in LHPC tablets compacted at 10 kN (Figure 2.12), may account for the higher hardness of LHPC placebo tablets compared to that of HPC. Wantanabe et al (1995) also reported lower hardness for tablets comprising crystalline cellulose and LHPC with smaller particle size, than systems containing larger particle sizes.

2.3.3.2 Tablet disintegration time

The higher tablet disintegration times observed with increasing concentrations of HPC (Figure 2.19) infer that HPC may not have disintegrant properties as reported previously (Machida 1974, Francis *et al* 2003). The tablets comprising HPC were visually observed to disintegrate by erosion. Fast disintegration is a requirement, especially for ODTs which must disintegrate in the mouth in <30 seconds (USP standard) or <3 minutes (BP standard). However, tablets containing LHPC maintained a relatively fast disintegration time (all <60s) irrespective of polymer concentration. LHPC tablets were visually observed to disintegrate by flaking off.

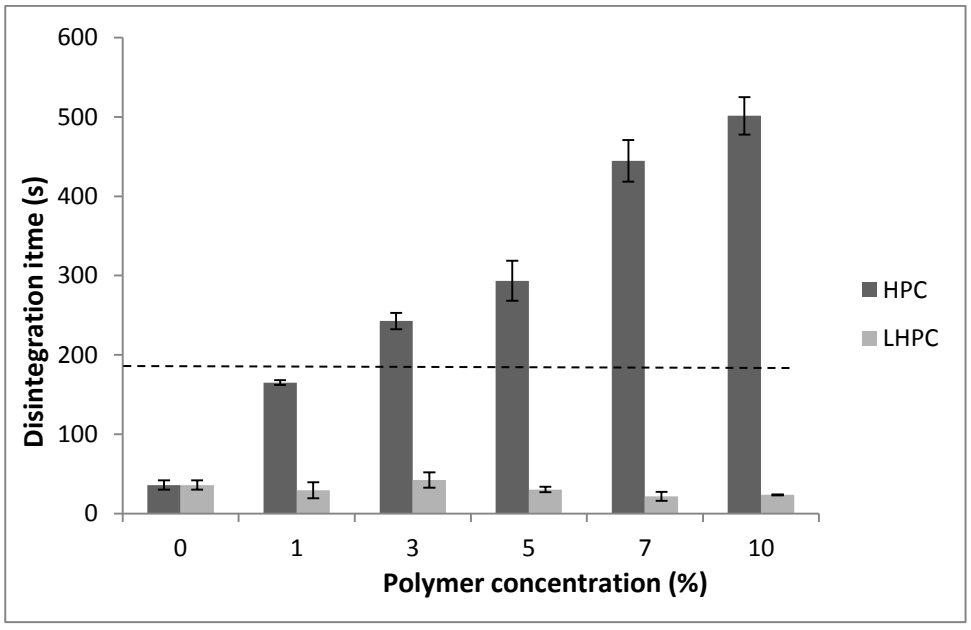

Figure 2.19 Disintegration time of tablets containing HPC or LHPC as binder (n=3). Dotted line depicts maximum acceptable disintegration time acceptable according to BP standards.

The much faster disintegration of LHPC tablets than those of HPC can occur for various reasons. Differences in disintegration behaviours of similar substances has been attributed to factors such as level of cross-linkage, degree of substitution and particle size of disintegrants (Fukami *et al*

2006). Firstly, LHPC tablets showed significantly higher porosities than those from HPC (Table 2.5). Thus, the availability of more pores within the tablet makes water penetration easier, thereby facilitating disintegration. Watanabe et al (1995) ascribed the fast disintegration of tablets containing LHPC to its ability to form relatively porous tablets, and therefore promote capillary action via these hydrophilic pores. Secondly, as confirmed by FTIR results, some of the molecular hydrogen bonding present in cellulose had been destroyed by hydroxypropylation in HPC; thus, HPC is more amorphous and dissolves in the presence of water. This dissolution causes the tablet to disintegrate slowly by erosion (this disintegration mechanism was noticeable upon visual observation), thereby prolonging disintegration time. On the other hand, LHPC with lower degree of substitution, retains some of the crystalline nature of cellulose and is thus insoluble in water (Gómez-Carracedo *et al* 2003). LHPC has been reported to swell in the presence of water and not dissolve (Shirai *et al* 1993, Fukami *et al* 2006) which causes the tablet to disintegrate. Alvarez-Lorenzo et al (2000) characterised different LHPCs with varying degrees of hydroxyl substitution, and reported an increase in disintegration time with increasing degrees of substitution.

2.3.3.3 Tablet friability

The friability of the placebo tablets also decreased with increasing HPC concentration (Figure 2.20), but even at the highest concentration tested (10%), friability did not meet the BP standard of <1%. Increasing the proportion of HPC as binder in the formulations to yield better friability results would be expected to further compromise tablet disintegration time. Furthermore, at about 20% concentration, HPC has been reported to act as a matrix forming polymer (Picker-Freyer and Dürig 2007). LHPC tablets exhibited similar friability to HPC tablets, with friability still significantly above the specification for tablets. Both polymers, however, greatly reduced the friability of mannitol tablets (>12% when compacted without a binder). The high friability recorded even at 10% polymer concentration may be attributed to the fragmenting nature of mannitol tablets, which causes the tablet to lose its cohesion and, thus, exhibit lower hardness and higher friability (Al-Khattawi and Mohammed 2013). However, to utilise LHPC for ODT formulations, methods to decrease tablet friability would be necessary.

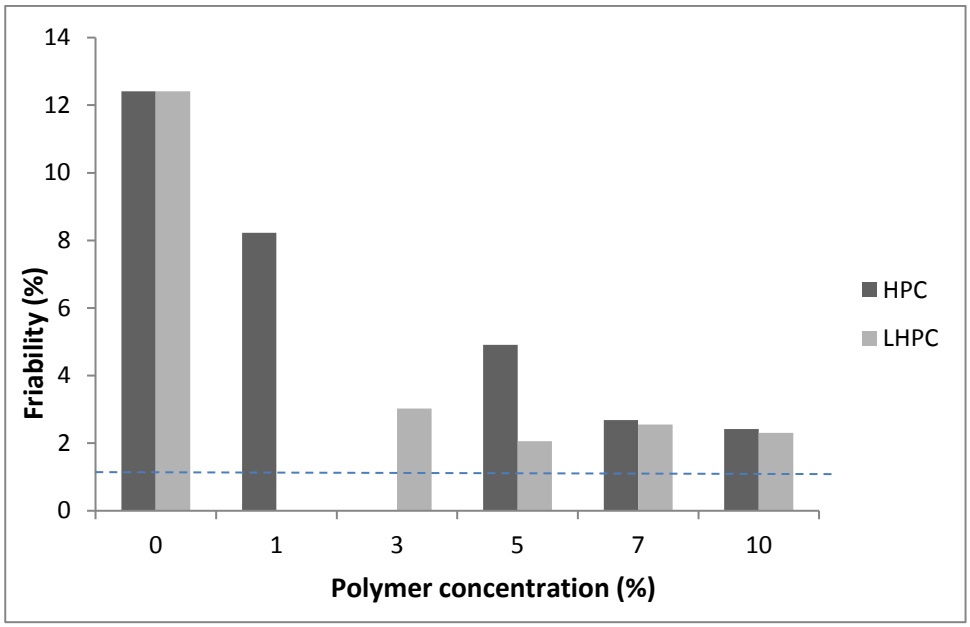

Figure 2.20 Friability of tablets containing HPC or LHPC as binder. Dotted line depicts maximum acceptable friability. Missing points show tablets that failed the friability test (broken tablets)

2.3.4 Formulation optimisation

Considering the tablet characteristics discussed above, the LHPC formulation containing 7% LHPC showed the best overall tablet properties with high hardness and fast disintegration time (Figure 2.18 and Figure 2.19). This formulation was chosen for optimisation to decrease friability which was >2%, and incorporation of other excipients. These tablets were compacted at various pressures (5, 10, 15, 20, 25 and 30 kN) to attempt a reduction in tablet friability upon higher compaction. Results showed a linear increase in hardness as compaction pressure increased, but no significant change in disintegration time was observed, due to the behaviour of LHPC in water (Figure 2.21). Tablet friability was observed to decrease, alongside porosity with increasing compression pressure (Figure 2.22). However, there was an increase in both friability and porosity of the tablets at maximum compaction pressure tested; highlighting the direct relationship between tablet friability and porosity. Although the lowest friability was achieved at 25 kN pressure, this value (1.52%) was still higher than the acceptable limit for tablet friability. Additional steps will be required to further improve the friability of the formulation.

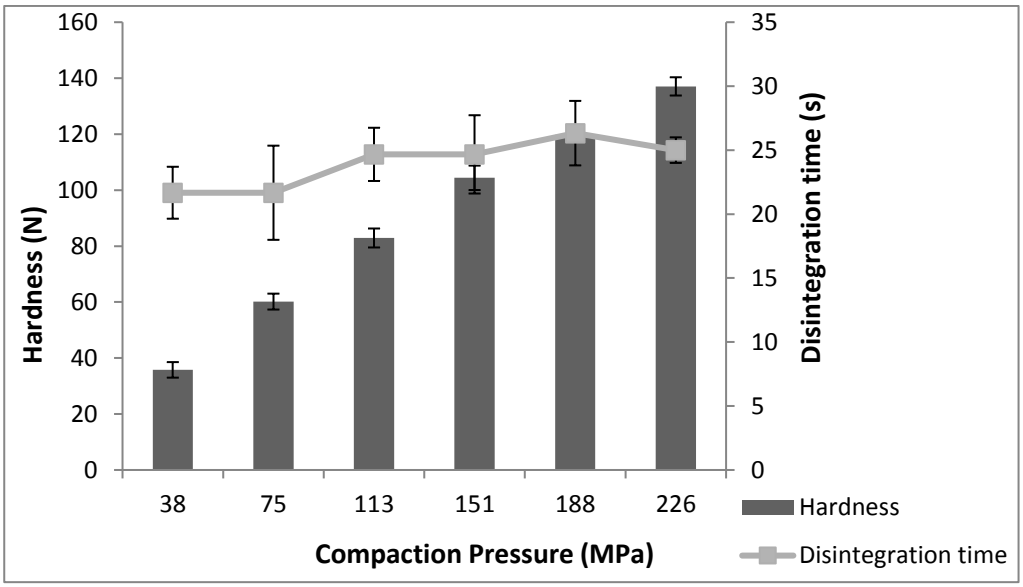

Figure 2.21 Plot showing the effect of increasing compaction pressure on hardness and disintegration time of formulation containing 7% LHPC (n=3). Despite the higher hardness observed with increasing compaction pressures, tablet disintegration time remained significantly constant.

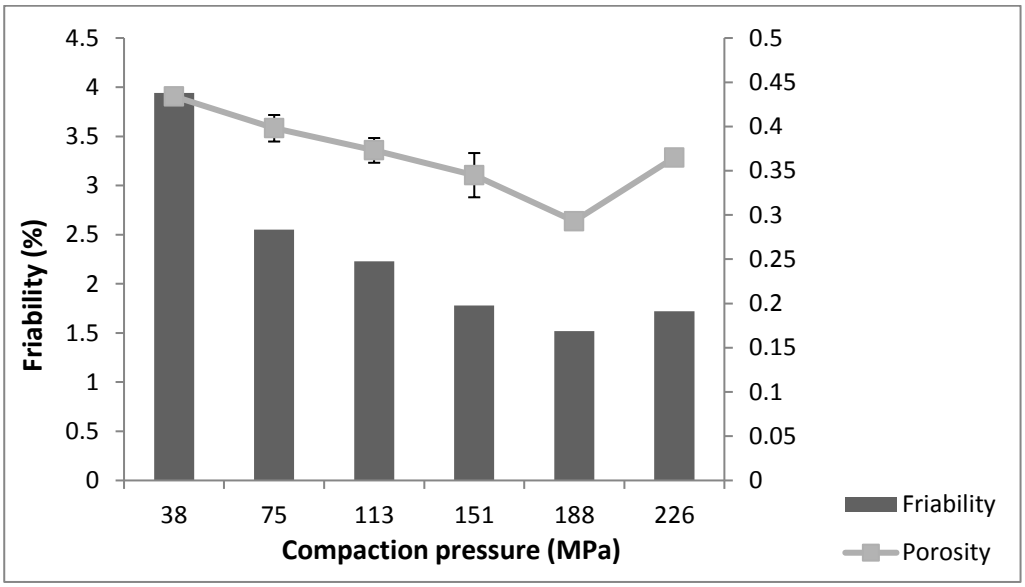

Figure 2.22 Plot showing the effect of increasing compaction pressure on friability and porosity of formulation containing 7% LHPC

2.4 Conclusion

During the development of successful ODT formulations, it becomes important to systematically investigate the role each excipient plays individually in the ODT, to locate multi-functional excipients and use this information to design intelligent dosage forms with favourable attributes built into them. The degree of substitution (DS) in HPC and LHPC polymers played a key role in their behaviour as binders and/ or disintegrants. The lower DS in LHPC made it more crystalline yielding higher hardness, practically insoluble in water, with high disintegrant properties. However, the higher DS of HPC made it more amorphous (as confirmed from XRD and FTIR results) exhibiting lower hardness and high water solubility, which diminished its ability to act as a disintegrant. HPC and LHPC exhibited an interesting characteristic of forming pure compacts with extremely high hardness at elevated compaction pressures (>520N). However, this high hardness of pure polymer compacts could not be translated to ODTs containing polymers and D-mannitol only, with HPC ODTs exhibiting hardness of <60N even at 10% polymer concentration; thus highlighting the detrimental effect of low tabletability grades of mannitol on ODT characteristics. However, the results obtained suggest that this grade of HPC may not be suitable for use by itself in ODT formulations. ODTs require fast disintegration in the mouth, sufficient friability to withstand mechanical stress, and the use of multi-functional excipients to allow for higher drug loading without compromising tablet size. LHPC on the other hand showed good hardness and disintegration time acceptable for ODT formulation. With formulation optimisation to reduce tablet friability, LHPC may be useful as a single multifunctional excipient in the formulation of ODTs.

Chapter 3

Effect of polymer viscosity, concentration and compaction pressure on ODT characteristics – a quality by design (QbD) approach

3.1 Introduction

Critical qualities or attributes of a successful ODT include sufficient hardness to impart low friability and withstand mechanical stress encountered during packaging and transport, and optimal porosity to enable imbibing of water into the ODT, thereby facilitating fast disintegration. However, these attributes have opposing effects. For instance, increased hardness tends to lower porosity and thus elongate disintegration time. The formulation scientist is thus faced with the dilemma of optimising ODT formulations in combinations that provide the best qualities. If all factors affecting the critical ODT qualities are to be investigated one after the other, a huge amount of resources (time, man power and money) would be required. Thus, the Quality by Design (QbD) theme incorporating Design of Experiments (DoE) has become popular in the pharmaceutical terrain. QbD is based on the philosophy that quality should be designed into a product before manufacture, and not just tested after manufacture (ICH 2009). QbD has been defined by the International Conference on Harmonisation (ICH Q8) as "a systematic approach to development that begins with predefined objectives and emphasizes product and process understanding and process control, based on sound science and quality risk management" (ICH 2009). QbD incorporates a step-by-step mechanistic process that identifies product features and pre-empts potential sources of inconsistency in order to apply robust manufacturing procedures to generate a reliable product over time, with quality strategically built into it (Lionberger *et al* 2008). QbD usually begins with setting the quality targeted product profile (QTPP) which outlines prerequisites for product quality, efficacy and safety, while incorporating elements such as dosage form/ strength and administration route (Lawrence 2008, Lionberger *et al* 2008). From here, critical process parameters (CPPs) that are vital to the manufacturing process are identified and ranked in order of importance based on their influence on critical quality attributes (CQAs) of products. Assessment of potential risks is completed by measuring the intended QTPP against the CPP and their effect on CQAs. These can then be included in a design of experiments (DoE) study.

DoE enables one to design a set of experiments that can simultaneously assess the contributions of various factors or variables (CPP) on responses or outcomes (CQA). Because these experiments

are run in combinations, less time and resources are required (Anderson and Whitcomb 1974). Factors may be described as tools used to control or manipulate a system, while responses provide information about the characteristics and state of the system (Eriksson 2008). Factors are variables that, when changed, cause changes in the responses and thus the system. Three major experimental objectives can be achieved using an experimental design and they include: screening – this highlights the effects that many factors have on the system, to identify the important/ dominating factors; optimisation – this provides information on the optimal factor combinations to produce expected responses; and robustness testing – to confirm the vigorousness/ strength of the model/ system (Eriksson 2008).

Polyethylene oxide (PEO), popularly known as Polyox™, is a trademark of the DOW company. Polyox™ are non-ionic, water-soluble resins exhibiting high swelling and thermoplastic capacity with molecular formula $(-OCH_2CH_2)_n$, where n represents the average number of oxyethylene moieties per polymer chain (Tadokoro *et al* 1964). Polyox has been found to exhibit stability, non-toxicity, good flow properties, high compressibility enabling direct compression, good mucoadhesive properties and faster hydration (Dimitrov and Lambov 1999). Thus, polyox has been applied as a mucoadhesive agent, binder, coating and viscosity imparting agent with pharmaceutical applications such as hot-melt extrusion, immediate and delayed/sustained-release formulations (Maximilien 2013).

One of the challenges of conventional ODTs is the short residence time in the mouth due to saliva scavenging and accidental swallowing. To improve this short-coming, the addition of multi-functional excipients with mucoadhesive properties was proposed. Cilurzo et al (2005) had investigated the feasibility of producing fast-dissolving mucoadhesive microparticulate systems to prolong residence time of disintegrated formulations on the sublingual mucosa. Eudragit sodium salts were used as mucoadhesive polymers. They reported an optimal formulation with good drug release and mucoadhesion, which was dependent on drug loading.

The aim of this work was, therefore, to apply QbD principles in a DoE to determine the effects of significant factors (polyox viscosity, polyox concentration and compaction pressure) on ODT

characteristics (responses) in order to produce ODTs with good mechanical properties and fast disintegration that promote mucoadhesion of the dosage form upon disintegration/ disaggregation in the buccal cavity. The objectives of this initial DoE were two-fold. Firstly, to identify the influence of variations and interactions of the chosen factors on the responses highlighted; and secondly, to optimise the system to determine the optimal factor combinations that would yield desired or targeted responses.

3.2 Materials and methods

3.2.1 Materials

Sentry Polyox® (polyethylene oxide) WSR N10 (MW 100,000 Da), 1105 (MW 900kDa), N-60K (MW 2000 kDa) and Coagulant (MW 5000 kDa) were a gift from Colorcon (Kent, UK). L-HPC grade NBD-022 was a gift from Shin-Etsu (Tokyo, Japan). D-Mannitol, magnesium stearate and Krebs buffer were purchased from Sigma Aldrich Chemicals (Poole, UK). All materials were of pharmaceutical grade and used as received.

3.2.2 Methods

3.2.2.1 Pre-formulation characterisation of polymers

The various viscosity grades of polyox were characterised according to flow properties, true, bulk and tapped densities; porosity and moisture content as described below:

3.2.2.1.1 Angle of repose (ɵ)

The angle of repose has been described as ‘an engineering property of granular materials’ and is ‘the maximum angle of a stable slope with the horizontal determined by friction, cohesion and the shape of the particle’ (Deshpande and Yadav 2009). The fixed height cone method (Fahmy and Kassem 2008) was adapted for this test. A funnel was attached to a retort stand at a specific height and the powders were poured freely through the funnel until a conical heap was achieved. The height (h) and diameter (d) of the heap were measured. The angle of repose ɵ, which is the internal

angle between the horizontal surface and the powder surface, was then calculated from the equation:

$$\text{Tan } \theta = \frac{2h}{d} \quad . \quad . \quad . \quad . \quad . \quad . \quad . \quad \text{(Equation 3.1)}$$

The test was performed in triplicate for each sample and the mean angle recorded in degrees.

3.2.2.1.2 Bulk and tapped density

A specific weight (20g) of the sample was poured into a 100mL measuring cylinder attached to a Sortax tap density tester USP I apparatus (Allschwil, Switzerland). The initial volume (volume at zero tap or bulk volume) was recorded. The machine was set to vibrate and the volumes at 50, 100,150, 200 and 250 taps were obtained and recorded. This was repeated for all the samples. The tapped and bulk densities, Hausner ratio and Carr's index were calculated for the samples using the equations below:

$$Tapped\ density = \frac{mass\ of\ powder}{final\ powder\ volume} \quad . \quad . \quad . \quad . \quad . \quad \text{(Equation 3.2)}$$

$$Powder\ bulk\ density = \frac{mass\ of\ powder}{initial\ powder\ volume} \quad . \quad . \quad . \quad . \quad \text{(Equation 3.3)}$$

$$Hausner's\ ratio = \frac{tapped\ density}{bulk\ density} \quad . \quad . \quad . \quad . \quad . \quad \text{(Equation 3.4)}$$

$$Carr'sindex = \frac{tapped\ density - bulk\ density}{tapped\ density}\ x\frac{100}{1} \quad . \quad . \quad . \quad \text{(Equation 3.5)}$$

3.2.2.1.3 True density and porosity

A multipycnometer from Quantachrome Instruments (Syosset, USA) utilising helium gas was used to measure the true density of the powders at ambient temperature. Powder true volume measurement was based on Archimedes principle of fluid displacement. Helium gas can penetrate tiny pores of up to 1 angstrom (10^{-10} m) in diameter. Weighed samples (0.9-1.1g) were employed. The true density of the sample was automatically calculated by the software using equation 3.6 below. The bulk volume of the powder was further measured by pouring the weighed sample into

a 1mL volumetric cylinder. The tests were performed in triplicates for each of the samples. The porosity of the powders was calculated from the equation 3.7:

$$V_t = V_c - V_r \left(\frac{P_1}{P_2} - 1\right) \quad . \quad . \quad . \quad . \quad . \quad . \quad . \quad \text{(Equation 3.6)}$$

$$Porosity\ (\varepsilon) = 1 - \frac{bulk\ density}{true\ density} \quad .. \quad . \quad . \quad . \quad \text{(Equation 3.7)}$$

Where V_t, V_c and V_r are the sample true volume, sample cell volume and known reference volume respectively. P_1 and P_2 represent the atmospheric pressure and air pressure change during determination. The true and bulk densities of the tablet can then be calculated from V_t and bulk volume.

$$True\ density = \frac{Powder\ weight}{Powder\ volume\ (Vt)} \quad . \quad . \quad . \quad . \quad . \quad \text{(Equation 3.8)}$$

$$Bulk\ density = \frac{Weight\ of\ powder}{bulk\ volume\ of\ powder} \quad . \quad . \quad . \quad . \quad . \quad \text{(Equation 3.9)}$$

3.2.2.1.4 Powder moisture content

The moisture content of the powders was determined by the 'loss on drying method' using a thermobalance (Sartorius, Surrey UK). Samples of <200mg were evenly loaded unto the balance and the initial weight recorded. After heating at a constant rate, the final weight was recorded. Moisture content was then calculated as the percentage weight loss from the sample using the equation:

$$Moisture\ content = \frac{initial\ weight - final\ weight}{initial\ weight}\ x\frac{100}{1} \quad . \quad . \quad . \quad \text{(Equation 3.10)}$$

Three samples were tested in triplicates and reported as mean ± standard deviation.

3.2.2.2 Elements of quality by design (QbD)

Information from preliminary studies and literature reviews was used to identify QTPP and CQA, which were then assessed against each other using ICH Q9 risk assessment guidelines, information from previous developmental work and current knowledge to ascertain the level of risk (ICH 2009). Each outcome was assigned a ranking of low, medium or high depicting the magnitude of influence

the QTPP had on the CQA. All QTPP with medium or high ranking were then inserted into the DoE as CPP representing fundamentally independent factors (ICH 2009).

3.2.2.2.1 Design of experiments (DoE)

The experimental design for incorporation of polyox into the selected formulation (F4 containing 7% LHPC from chapter 2) was carried out using the MODDE 8.0.2 software (Umetrics Inc., USA). A central composite face-centred (CCF) design comprising 17 experiments with 3 replicated centre points was selected by the software to investigate the influence of variations in three independent variables (factors) on the dependent variables (responses). The total number of experiments was computed from the equation:

$2^k + 2k + 3$, where k = number of factors (variables) . . (Equation 3.11)

The factors investigated were polyox polymer viscosity (X_1), polymer concentration (X_2) and compaction pressure (X_3); and the critical responses investigated were tablet disintegration time (Y_1), tablet friability (Y_2), tablet hardness (Y_3) and tablet porosity (Y_4). The levels of the investigated factors are summarised in Table 3.1 and these levels were chosen based on literature and preliminary experiments. The design of experiments with run order developed by MODDE software is shown in the appendix. Each experiment was carried out in triplicate according to their run order, and the means of the responses incorporated into the software. The resultant data was fit using partial least squares (PLS) model and the relationship between factors and responses studied and interpreted using response surface and contour plots generated by the software.

3.2.2.2.2 Regression model verification & interpretation

A statistical model comprising both interactive and polynomial terms was used to evaluate the responses and is depicted in the regression model equation below (Montgomery 2004, Eriksson 2008).

Table 3.1 List of independent variables (factors/ CPP) with their feasible investigational ranges that were employed in the optimisation DoE

Process parameter	**Level**		
	High level	**Medium level**	**Low level**
Polymer viscosity (cP)	5,500 -7,500[a] (1)	8,800 – 17,600[b] (0)	12 -50[b] (-1)
Polymer concentration (%)	2.5	1.5	0.5
Compaction pressure (tons)	3.0	2.0	1.0

a = 1% solution, b = 5% solution. The number between brackets was used to represent the viscosity levels in the DoE with 1 as the highest and -1 as the lowest.

$$\boldsymbol{Y_i = \beta_0 + \beta_1 X_1 + \beta_2 X_2 + \beta_3 X_3 + \beta_{12} X_1 X_2 + \beta_{12} X_1 X_2 + \beta_{13} X_1 X_3 + \beta_{23} X_3 + \beta_{11} X_1^2 + \beta_{22} X_2^2 + \beta_{33} X_3^2 + \beta_{123} X_1 X_2 X_3} \quad . \quad . \quad . \quad \text{(Equation 3.12)}$$

where Y_i is the modelled response, β_0 is the arithmetic mean response of the runs; β_1, β_2 and β_3 are the estimated coefficients for the factors X_1, X_2 and X_3 respectively. The main effects (X_1, X_2 and X_3) represent the mean results when one factor at a time is changed from its low to its high value, and other factors are kept at their centre points; the interactive terms (X_1X_2, X_1X_3, X_2X_3 and $X_1X_2X_3$) represent the mean effect when factors are varied simultaneously, while the polynomial terms (X_1^2, X_2^2 and X_3^2) were included to investigate non-linear correlations in the model (Gohel *et al* 2004, Alhusban *et al* 2011). For each of the regression coefficients (e.g., B_1) accompanying X_1, the value was scaled and centred which allows for its interpretation. Therefore, if Y_1 is the disintegration time, the constant β_0 is the estimated disintegration at the design centre point when the other factors have their values as zero. In order to compare responses with different ranges, the values of the coefficients were divided by the standard deviation of the individual responses for normalisation (by the MODDE software).

Results obtained from the DoE were fit using partial least squares (PLS) model and the model verified using PLS parameters including the distance to model, summary fit, lack of fit, analysis of variance (ANOVA), and predicted versus observed plots generated by the MODDE software. During model verification, outliers and insignificant terms that did not affect the model were eliminated, since the presence of insignificant terms in a model may reduce the model's prediction

power (Eriksson 2008). After model verification was complete, evaluation and prediction tools (main effect, interaction, contour and/ or response surface model plots) were employed to identify the effect of individual or interactive CPP on CQA, and the results utilised for further optimisation and prediction of design space.

3.2.2.3 Tablet preparation & characterisation

500 mg tablets consisting of 7% LHPC as binder/ disintegrant, 0.5% magnesium stearate as lubricant, D-mannitol as filler, varying polymer viscosity, concentration and compaction pressure with 30 second dwell time were compacted using a manual bench-top hydraulic tablet press from Specac Ltd (Slough, UK) equipped with 13mm flat-faced dies. Tablets were prepared according to the run order generated by MODDE software; and then characterised for disintegration/ disaggregation time, friability, hardness and porosity.

3.2.2.3.1 Tablet disintegration time

The disintegration/ disaggregation time was determined according to the USP, on a ZT3 USP II disintegration test apparatus (Erweka, Heusenstamm-Germany), and for these experiments was taken as the time for the tablet to disaggregate into a slurry still held together by the mucoadhesive polymer. Measurements were made at 37°C and 30 cycles/ min.

3.2.2.3.2 Tablet friability

The ability of the tablets to withstand mechanical stress, known as friability was measured using a rotating drum friabilator (J. Engelsmann AG, Ludwigshafen, Germany). 6 tablets were utilised at 25 rpm for 100 revolutions or 4minutes. Tablets were carefully dusted before and after the test, and friability expressed as the percentage loss in weight.

$$Friability = \frac{initial\ weight - final\ weight}{initial\ weight}\ x\frac{100}{1} \quad . \quad . \quad . \quad . \quad \text{(Equation 3.13)}$$

3.2.2.3.3 Tablet hardness

The hardness (crushing strength) of the tablets was measured using a 4M hardness tester (Schleuniger, Thun-Switzerland). Tensile strength, σ was calculated from the equation:

$$Tensile\ strength\ (\sigma) = \frac{2\ x\ Hardness}{\pi d \mathrm{h}} \quad . \quad . \quad . \quad . \quad . \quad \text{(Equation 3.14)}$$

Where d=tablet diameter and h=tablet thickness; measured using a digital Vernier calliper.

3.2.2.3.4 Tablet porosity

The apparent/true density of the tablets was measured using the helium pycnometer described above (section 3.2.2.1.3). 500mg tablets were used in place of powder. Tablet bulk volume was calculated from the volume of a cylinder by measuring tablet diameter (d) and thickness (h) using a digital Vernier calliper (equation 3.15) and was used to compute tablet bulk density. Tablet porosity was calculated by substituting with the relevant equations below:

$$Bulk\ volume = \pi \left(\frac{d}{2}\right)^2 h \quad . \quad . \quad . \quad . \quad . \quad . \quad \text{(Equation 3.15)}$$

$$Tablet\ bulk\ density = \frac{mass\ of\ tablet}{bulk\ volume} \quad . \quad . \quad . \quad . \quad . \quad \text{(Equation 3.16)}$$

$$Tablet\ true\ density = \frac{mass\ of\ tablet}{true\ volume} \quad . \quad . \quad . \quad . \quad . \quad \text{(Equation 3.17)}$$

3.2.2.3.5 Mucoadhesive efficiency

Optimal formulations obtained from the results of the DoE were carried forward to test their mucoadhesive efficiency and was adapted from Cappello et al (2006). Porcine buccal mucosa was obtained from freshly killed pigs (abattoir in Wolverhampton, UK).The buccal epithelium was separated from the connective tissues using surgical scissors and a scalpel and immediately stored at -80 °C until required. Porcine buccal mucosa defrosted in Krebs buffer at room temperature and was fixed on a stainless steel surface of a MicroTest 5848 mechanical tester (Instron, Buckinghamshire, UK) and hydrated with deionised water. Test tablets were fixed using double adhesive tape to the probe of the mechanical tester and probe moved at a constant speed until contact was made with the mucosa and a force of 1.6 N exerted for 60 seconds; the probe was thereafter withdrawn at a constant speed. The accompanying software plotted a graph of compressive load against compressive extension. Mucoadhesive efficiency was determined from equation 3.18 below:

$$Mucoadhesive\ efficiency = \frac{AUC_{output\ (extension)}}{AUC_{input\ (compression)}} \quad . \quad . \quad . \quad \text{(Equation 3.18)}$$

where AUC_{input} and AUC_{output} represent the calculated area under the curve during contact (load) and withdrawal (extension) of tablet respectively.

3.2.2.4 Statistical analysis

All data generated in triplicates were presented as mean ± standard deviation (SD), where n=3. The data was then analysed for statistical significance using one-way analysis of variance (ANOVA) and Tukey-Kramar multiple comparison post-test from Graphpad Prism® version 5.04 (Graphpad Software, San Diego, CA, USA). The level of significance was quoted as $p<0.05$ (probability values of 95%).

3.3 Results and discussion

3.3.1 Bulk characteristics of polyox

Preformulation characteristics of the polymers are highlighted in Table 3.2. The three powders showed similar results with no significant difference for all parameters measured except the true density. The powders were characterised by good flow properties based on angle of repose, Hausner's ratios and Carr's index (2.3.1.1, page 75). Shah & Bhandary (2010) reported that various grades of polyox exhibited similar flow properties and are generally free-flowing. There was no significant difference between the true densities of the medium and high viscosity grades of the polymers, but a significant difference was seen between true densities of the low and medium, as well as the low and high polymer grades (Tukey-Kramar post-test). This difference in true density may be related to the molecular weight of the polymers, as polymer viscosity increases with increasing molecular weight (Shah and Bhandary 2010); and the lower the true density of a powder, the higher the possibility of the presence of enclosed voids (Nerurkar *et al* 2005).

Table 3.2 Preformulation characterisation of different viscosity grades of polyox polymers. No significant difference was observed for all characteristics tested, except that of true density.

PARAMETERS	LOW	MEDIUM	HIGH
Angle of repose (°)	23.90 ± 2.87	22.81 ± 2.70	25.48 ± 0.33
Bulk density (g/cm^3)	0.47 ± 0.03	0.45 ± 0.05	0.42 ± 0.01
Tapped density (g/cm^3)	0.59 ± 0.05	0.52 ± 0.01	0.54 ± 0.01
Hausner's ratio	1.26 ± 0.03	1.16 ± 0.11	1.28 ± 0.02
Carr's index (%)	20.37 ± 1.97	12.90 ± 8.98	21.68 ± 1.10
True density (g/cm^3)	1.51 ± 0.02	1.44 ± 0.01	1.42 ± 0.01
Porosity	0.73 ± 0.01	0.74 ± 0.01	0.72 ± 0.01
Moisture Content (%)	8.36 ± 1.16	7.96 ± 1.37	9.45 ± 0.92

3.3.2 Elements of quality by design (QbD)

The aim of this work was to develop a new dosage form with robust mechanical strength and optimal disintegration time, imbibing a mucoadhesive polymer which could retain the formulation in the mouth and enhance epigastric absorption. Using QbD, a study to determine the effects of viscosity grade and concentration of polyethylene oxide (as model excipient) and compaction pressure (factors) on ODT characteristics (responses) was run. QTPP were selected based on the targeted properties from which CQAs were determined, as depicted in Table 3.3, while CQAs were based on compendia regulations and preliminary studies.

Table 3.3 QTPP and CQAs of the final ODTs used for risk assessment

Quality Attribute	Targeted outcome	CQA	Comments
Disintegration time	Conforms with BP specification of < 3 minutes (BP 2012)	Yes	Successful ODTs include sufficient hardness to impart low friability and withstand mechanical stress encountered during packaging and transport. Optimal porosity is targeted to enable imbibing of water into the ODT, thereby facilitating fast disintegration time in seconds (Al-Khattawi *et al* 2014).
Tablet friability	<1%	Yes	
Tablet Hardness	≥60N	Yes	
Tablet porosity	>0.2	Yes	

Results of risk assessment to determine the risk score of each process parameter on each of the assigned CQA are shown in Table 3.4. Those with risk ranking of medium or high were used as factors/ responses in the DoE.

Table 3.4 Risk assessment of the process parameters against the CQAs including justification for assigning these risk values.

Process parameter	**Critical Quality Attributes**				
	Disintegration time	**Friability**	**Tablet porosity**	**Hardness**	**Justification**
Polymer viscosity	High	Low	Low	Medium	High polymer viscosity will increase the viscosity of the disintegration medium thereby adversely affecting disintegration time (Efentakis and Vlachou 2000).
Polymer concentration	High	High	Low	High	At higher polymer concentrations, more molecules interact to form a strong matrix that impedes entrance of water and disintegration time, while enhancing hardness and reducing friability due to its binding capacity (Nerurkar *et al* 2005).
Compaction pressure	High	Medium	High	High	High compaction pressures should increase compactability, increase hardness, decrease porosity and possibly decrease friability, thereby hindering tablet disintegration (Al-Khattawi *et al* 2014).

The present work was aimed at determining the influence of three independent variables (factors): polymer viscosity (X1), polymer concentration (X2) and compaction pressure (X3) on the characteristics (responses) of tablets prepared by direct compression. The investigated responses included tablet disintegration time (Y1), tablet friability (Y2), tablet porosity (Y3) and tablet

hardness (Y4). A CCF design with highest efficiency factor was selected by the software and resulting data was fitted using a partial least squares (PLS) model. PLS was chosen as the fitting method instead of multiple linear regression (MLR) because PLS is utilised when more than 3 responses are investigated. PLS takes into cognisance, the covariance of the various responses, and the influence/ relationship the various responses have on each other. MLR on the other hand, generates separate regression models for each response (Eriksson 2008).

3.3.2.1 Model verification

3.3.2.1.1 PLS model summary fit plot

In order to obtain a good model, the presence of outliers in the data set must first be identified and excluded. Also, the presence of insignificant factor terms in the model can reduce the model's prediction power (Q^2). Therefore, it is important to identify insignificant terms and delete them from the model, thereby improving the model's usability (Eriksson 2008). However, this exclusion should be undertaken carefully, ensuring that only model factor terms that are insignificant to all responses are excluded. Based on the foregoing, three experiments detected as outliers, which did not compromise the model, were excluded. The 'distance to model' plot is shown in Figure 3.1, highlighting the excluded data sets. Also, being a quadratic model, all quadratic terms were initially included in the model. The terms which were found to be insignificant to all the responses, and did not interfere with the model hierarchy, were excluded from the model. The resulting regression equation is shown in equation 3.19:

$$\boldsymbol{y = \beta_0 + \beta_1 X_1 + \beta_2 X_2 + \beta_3 X_3 + \beta_{13} X_1 X_3 + \beta_{23} X_3 + \beta_{22} X_2^2} \quad . \qquad \text{(Equation 3.19)}$$

Data generated from the experimental design is highlighted in the appendix. The PLS summary fit plot of the design is shown in Figure 3.2. Four important parameters can be highlighted from this plot, analyses of which give the goodness or strength of the model. The $\mathbf{R^2}$ is the correlation coefficient and gives an idea of the "goodness of fit" of the model, i.e. the extent to which the model fits the data generated. R^2 gives the per cent of variation in a response that is explained by

the model. An R^2 value of 1 depicts a perfect fit (minimal residuals (noise), observed points/ means equals predicted means).

.

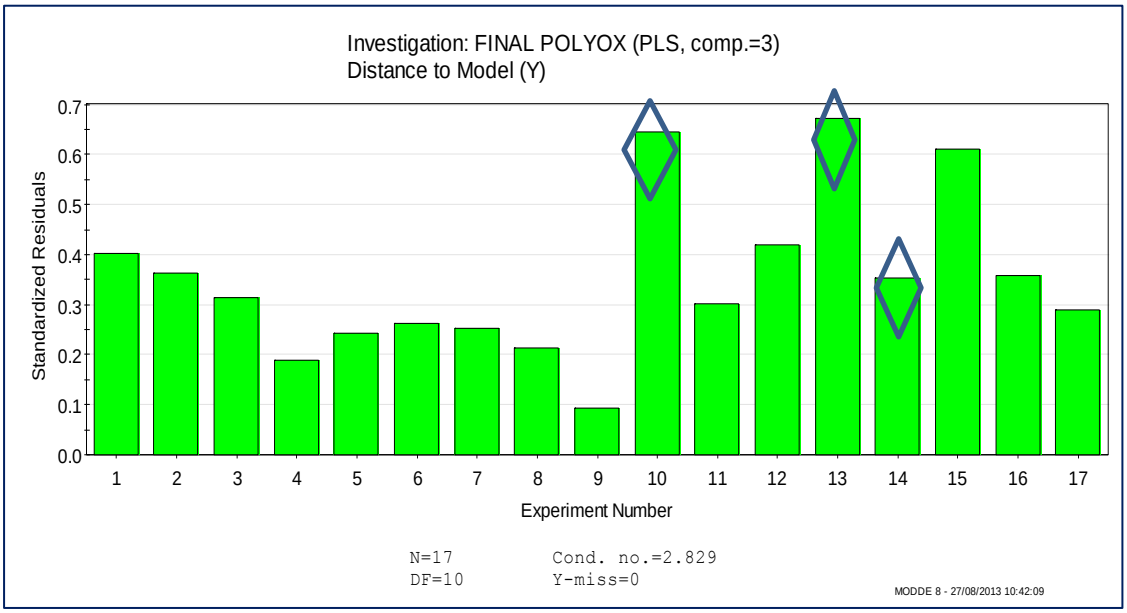

Figure 3.1 Distance to model plot showing the closeness of the various experimental runs to the model. Identified outliers (highlighted with the blue shapes), that did not affect the model detrimentally, were excluded.

An R^2 value of 0.75 gives a rough but stable and useful relationship (Eriksson 2008). However, R^2 is not the only parameter required to confirm the goodness of a model. The $\mathbf{Q^2}$ value gives the percent of variation in the responses that is predicted by the model. A large Q^2 value is useful; however, it is more important that the R^2 and Q^2 values are not far apart from each other. A low Q^2 value may be obtained when there are insignificant terms in the model, removal of which would enhance the model's predictive power.

The model **validity** bar gives an indication of the validity of the model. When this bar is below 0.25, there is a lack of fit, i.e. the model error is significantly larger than the pure error. A model validity of unity implies a perfect model. The fourth important parameter is the model **reproducibility** bar. This bar reveals the variation in the response carried out under identical situations, compared to the total variation of the response; and this is mostly at the centre points. A reproducibility bar of unity depicts a pure error of zero, thus under the same conditions, the results for the responses were always the same.

From Figure 3.2 it can be seen that the model showed good R^2, Q^2, model validity and reproducibility values. Because the Q^2 values for each of the responses is not too far from the corresponding R^2 values for the actual data (less noise), the amount of the data that can be predicted by the model is high.

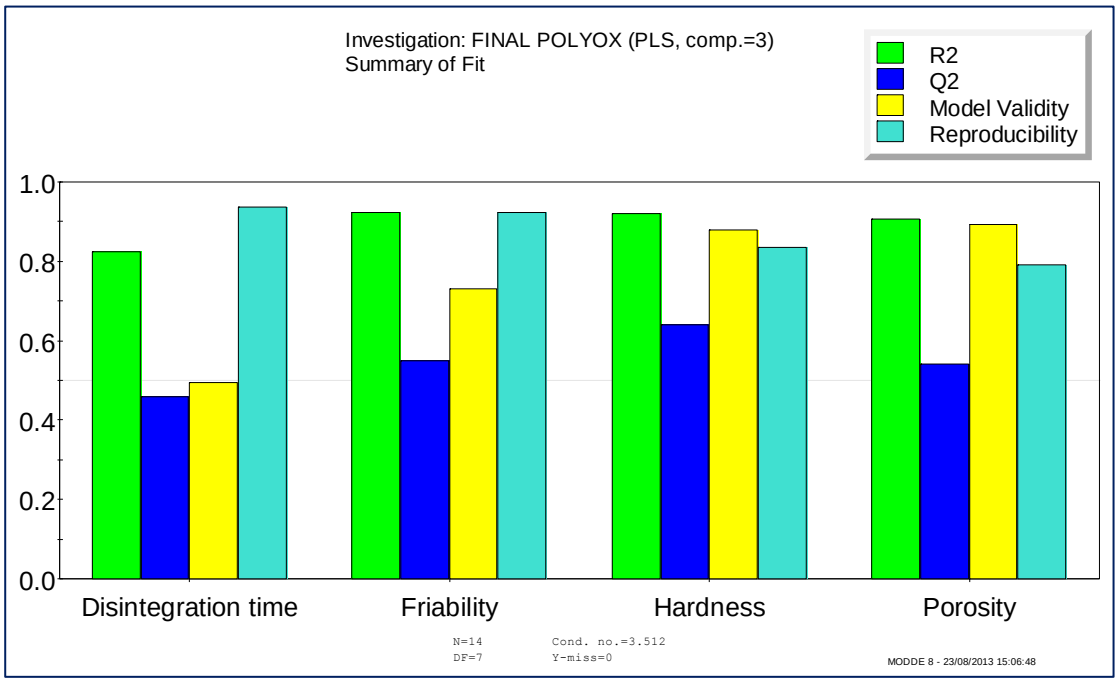

Figure 3.2 Partial least squares (PLS) fit summary plot for all responses. R^2 represents the extent to which observed data fits the model, Q^2 depicts the per cent of actual data that can be predicted by the model, model validity of >0.25 shows the model has no lack of fit.

For example, for the response tablet hardness (Y_3) with R^2 and Q^2 values of 0.92 and 0.64 respectively, 92% was actual data while 8% can be attributed to noise; and from the 92% of actual data, 64% of that data is predicted by the model, and vice versa (Eriksson 2008). Generally, for the actual data obtained for all the responses, over 60% of the data was predictive. The lowest predictive ability was seen with the disintegration time response. This may be due to the fact that the test is subjective and depends on the visual evaluation of the test endpoint by the experimenter; unlike the other tests which are more instrument-dependent. Thus, any inefficiency in evaluating disintegration time to the tune of a few seconds can produce errors in the model (Alhusban *et al* 2011).

Figure 3.3 shows the lack of fit plots for the various responses. For a model to show no lack of fit, the first bar (the model error) must be smaller than or equal to the third bar (the pure error adjusted

for uncertainties). The middle bar is the standard deviation of the pure error (the standard deviation of the responses at the centre points). From this figure, it can be seen that all the responses showed no lack of fit, and, thus, the absence of significant model error. The lack of fit plot is an expatiation of the information obtained from the model validity bar in the summary fit plot (Figure 3.2) (Eriksson 2008).

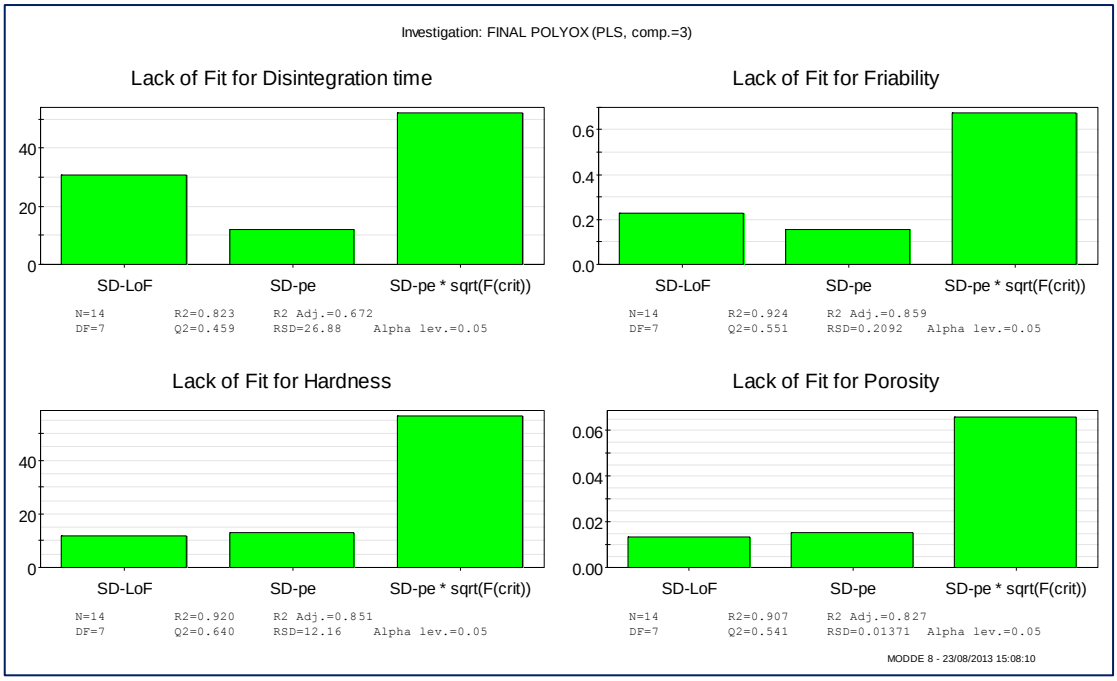

Figure 3.3 The lack of fit plots for all responses. As long as the 1st bar is smaller than or equal to the 3rd bar, the model shows no lack of fit.

3.3.2.1.2 Analysis of variance (ANOVA)

The analysis of variance (ANOVA) plot compares the standard deviations of the regression line (the model) to the standard deviation of the residuals (the noise). These are depicted as the first and third bars, respectively, in Figure 3.4. As long as the first bar is larger than the third bar (the standard deviation of the noise at its upper confidence level), then the model is good. From Figure 3.4, it can be seen that all the models were good. Summary of ANOVA results showing model significance ($p<0.05$) for all assessed factors are shown in Table 3.5, depicting minimal model error.

3.3.2.1.3 Observed vs predicted plot

This important plot displays the relationship between the observed responses of the model and the responses predicted by the model. For good models, the points should fall around a 45 degree regression line and the correlation coefficient should be as close to unity as possible (Eriksson 2008).

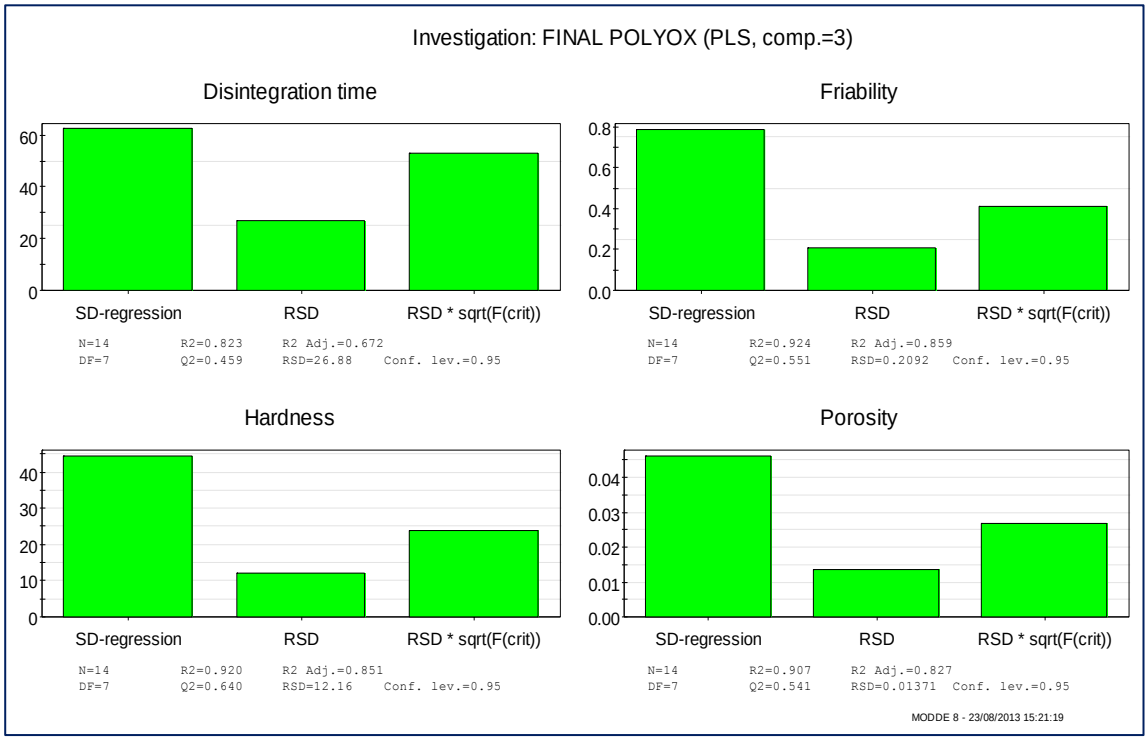

Figure 3.4 ANOVA plots comparing the standard deviations of the model (1st bar) to that of the noise (2nd bar), for all responses. When the first bar is larger than the third bar, the model is good

Generally, regression coefficients above 0.75 are acceptable within the limits of experimental error (Eriksson 2008). From Figure 3.5, which depicts this plot for our model, all the responses had R^2 values greater than 0.9, except for disintegration time with a slightly lower value of 0.82. A possible explanation for this has been given above. However, these values are still representative of a good model.

Table 3.5 Summary of results obtained from ANOVA of four responses to test model validity. P is the probability and R^2 is the regression coefficient.

CQA	P value	R^2
Disintegration time		
Regression	0.02	0.82
Lack of fit	0.13	
Friability		
Regression	0.00	0.92
Lack of fit	0.34	
Hardness		
Regression	0.00	0.92
Lack of fit	0.62	
Porosity		
Regression	0.00	0.91
Lack of fit	0.65	

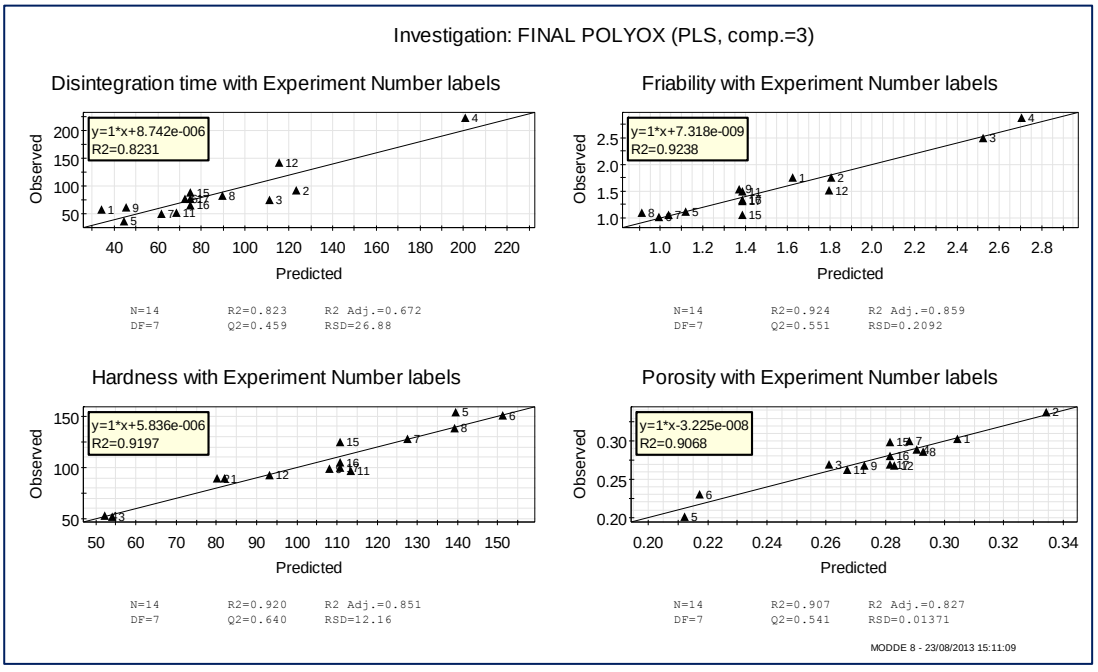

Figure 3.5 The observed vs predicted plots for all responses showing the closeness of the data predicted by the model to the actual data observed. The closer the R^2 value is to 1, the better the model.

3.3.2.2 Effect of factor variation on responses

The disintegration time of the tablets varied from 51.0 to 223.33 secs, friability from 2.02 to 2.92 %, hardness from 48.04 to 154.1 N, and porosity from 0.201 to 0.337 (data in the appendix) indicating that these responses were strongly dependent on the factors varied (Alhusban *et al* 2011). Three parameters will be employed to discuss the effect of changes in the various factors on the responses and they include:

- **The model equation/ ANOVA coefficients list with significance level:** The ANOVA coefficients list gives the magnitude and direction of the effect a factor has on a response. It also highlights the significance of such effects. Generally, at 95% confidence limit, all p values <0.05 are considered significant. Table 3.6 shows the effect of the various factors on the observed responses and their significance at 95% confidence interval (ANOVA $p<0.05$).
- **The main effects plots to explain linear models**: This plot depicts the change in a response, when one factor is increased from its low to high value while keeping other factors at their middle (or centre) values. With response surface modelling (RSM) objective is chosen, the three centre points (the black dots in Figure 3.6) must be within or close to the confidence interval, for the effect to be valid. From our model, because the dots are within, or in a few cases close to, the confidence intervals, these effects are valid. Also because a PLS fitting model was used, the main effect of one factor can be generated without interference from the other factors (Eriksson 2008). The quantitative effects of the various factors on the responses are summarised in Table 3.6. These effects are discussed in detail in later sections of this work.
- **The response surface model (RSM) and interactive plots** to interpret interaction or quadratic models where available. These plots highlight the interactions between two factors and how they affect a particular response, while keeping other factors at their middle levels.

Table 3.6 Quantitative factor effects on the responses and their corresponding p values. A (+) sign indicates a direct proportionality while a (-) sign indicates a reverse proportionality.

Term	Disintegration time		Friability		Hardness		Porosity	
	Effect	**P value**	**Effect**	**P value**	**Effect**	**P value**	**Effect**	**P value**
X_1	58.70	0.02	0.03	0.85	4.99	0.56	0.02	0.10
X_2	47.11	0.028	0.41	0.02	-20.02	0.04	0.02	0.11
X_3	-48.24	0.04	-1.14	0.00	71.79	0.00	-0.04	0.00
X_2^2	34.23	0.32	0.41	0.15	-14.82	0.34	-0.02	0.46
X_1X_3	-30.67	0.15	-0.15	0.34	6.72	0.46	-0.01	0.24
X_2X_3	-29.85	0.16	-0.49	0.01	7.92	0.39	0.06	0.00

3.3.2.2.1 Regression models for all CQA

The data was fitted using quadratic models containing 6 model terms (constant, concentration, viscosity, compaction pressure, concentration*concentration, viscosity*pressure and concentration*pressure) to yield the following model equations:

$$Y_1 = 92.39 + 30.09X_1 + 19.75X_2 - 20.60X_3 \quad . \quad . \quad . \quad . \quad \text{(Equation 3.20)}$$

$$Y_2 = 1.38 + 0.18X_2 - 0.45X_3 - 0.17X_2X_3 \quad . \quad . \quad . \quad . \quad \text{(Equation 3.21)}$$

$$Y_3 = 110.53 - 8.78X_2 + 28.16X_3 \quad . \quad . \quad . \quad . \quad . \quad \text{(Equation 3.22)}$$

$$Y_4 = 0.28 - 0.017X_3 + 0.02X_2X_3 \quad . \quad . \quad . \quad . \quad . \quad \text{(Equation 3.23)}$$

where Y_1 is the disintegration time, Y_2 is tablet friability, Y_3 is tablet hardness and Y_4 is tablet porosity. X_1 is polyox polymer viscosity grade, X_2 is polyox concentration, and X_3 represents compaction pressure.

3.3.2.2.2 Effect on disintegration time (Y_1)

Tablet disintegration time response was significantly affected by the linear models of polymer viscosity, polymer concentration and compaction pressure (Equation 3.20 and Figure 3.6, Figure **3.7** & Figure **3.8**). An increase in polymer viscosity or polymer concentration increased

disintegration time significantly, while an increase in compaction pressure resulted in a decrease in disintegration time; as shown by the positive and/ or negative signs in the model equation (3.20) above. The largest effect coefficient (+30.09) was seen for polymer viscosity and this suggests that polymer viscosity had a larger effect on disintegration time than polymer concentration and compaction pressure. The increase in disintegration time upon increasing viscosity of polymer was expected, since viscosity of polyox is directly proportional to its molecular weight (Royce 1993). The more viscous the polymer in solution, the harder it is for water to diffuse into and wet the tablet, thereby slowing down the disintegration process (Alhusban *et al* 2011). Higher molecular weight matrix forming polymers with longer polymer chains exhibit increased chain entanglement, which is synonymous with extended release formulations, thereby inhibiting matrix erosion and tablet disintegration (Royce 1993, Lee *et al* 1999, Efentakis and Vlachou 2000, Streubel *et al* 2003).

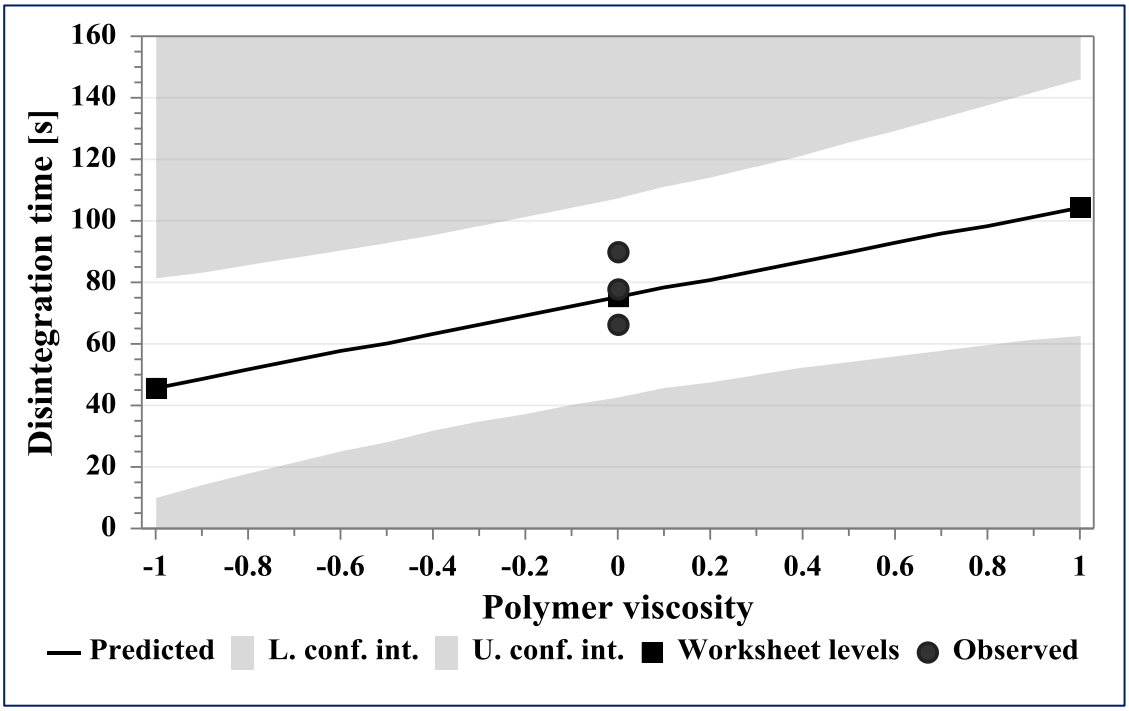

Figure 3.6 Main effects plot highlighting the effect on tablet disintegration time when polymer viscosity is increased from its low to high value and other factors maintained at their middle values. The three centre points (black dots) within the white area indicate validity of the effect, as they fall within the confidence limits of ± 95%.

Physical observation of the disintegration of tablets containing higher viscosity polyox showed the formation of a sticky gel-like mass that did not disintegrate within a couple of minutes. A similar observation was reported by Nerurkar *et al.* (2005) and Khan *et al*. (2007). The main effect of

polymer concentration on disintegration time (Figure 3.7) varied depending on concentration used. Disintegration time was found to incline slightly from 0.5 to 1.5% polymer concentration, after which there was a steeper increase between 1.6-2.5%. This implies that disintegration time is more significantly affected at higher polymer concentrations. This can be explained because at low polymer concentrations, there are less molecules of polyox interacting to form the gelatinous matrix that interacts to impede disintegration time via formation of a discontinuous gel layer; the reverse occurred at higher polymer concentrations (Sung *et al* 1996, Nerurkar *et al* 2005). Similar results have been reported by Al-Khattawi *et al* (2014).

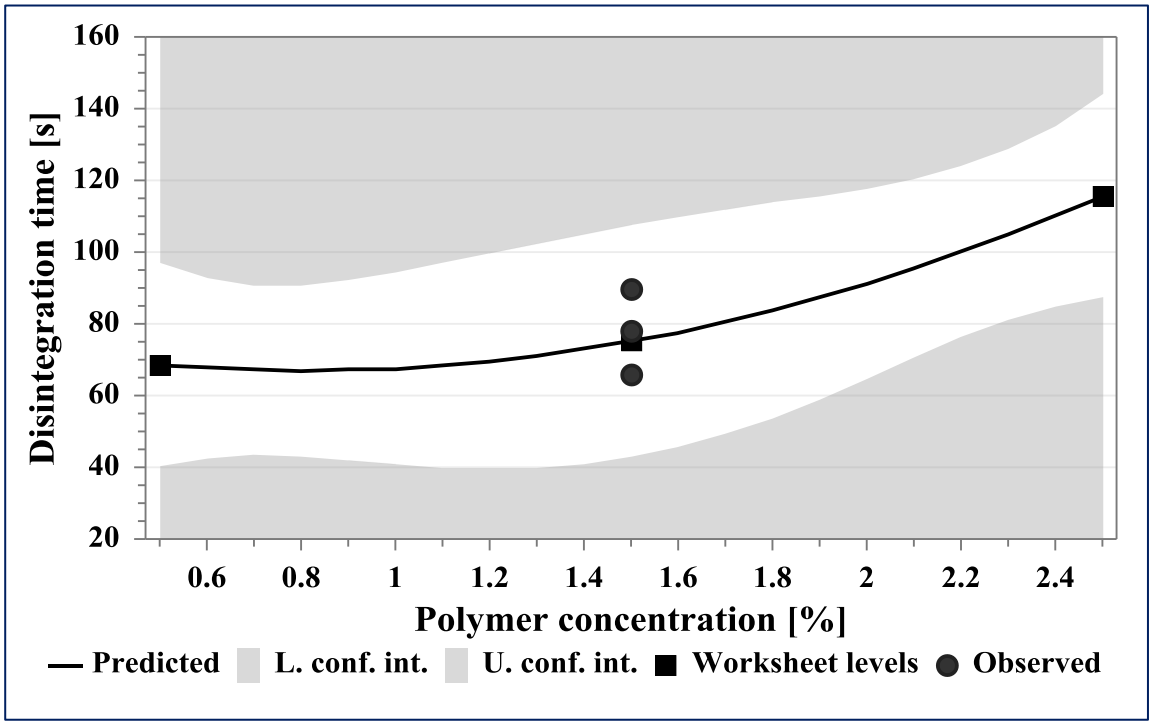

Figure 3.7 Main effect plot highlighting the effect on tablet disintegration time when polymer concentration was increased from its low to high value and other factors maintained at their middle values. The three centre points (black dots) within the white area indicate validity of the effect, as they fall within the confidence limits of ± 95%.

The main effect of compaction pressure on disintegration time (Figure 3.8) showed that this response decreased linearly as compaction pressure increased. This was contradictory to our expectations as increasing compaction pressure would generally increase tablet hardness and thereby extend disintegration time (Al-Khattawi *et al* 2014). This effect has been observed in materials that show elastic recovery upon compression, where increase in compaction pressure increases the elastic energy of the system, leading to recovery of tablet shape, low hardness and

low disintegration time, especially at high compaction pressures (Yoshinari *et al* 2003, Kleinebudde 2004). Accordingly, Picker (2004) and Yang (1996) reported polyox polymers as exhibiting elastic recovery or viscoelastic properties with increasing compaction pressures.

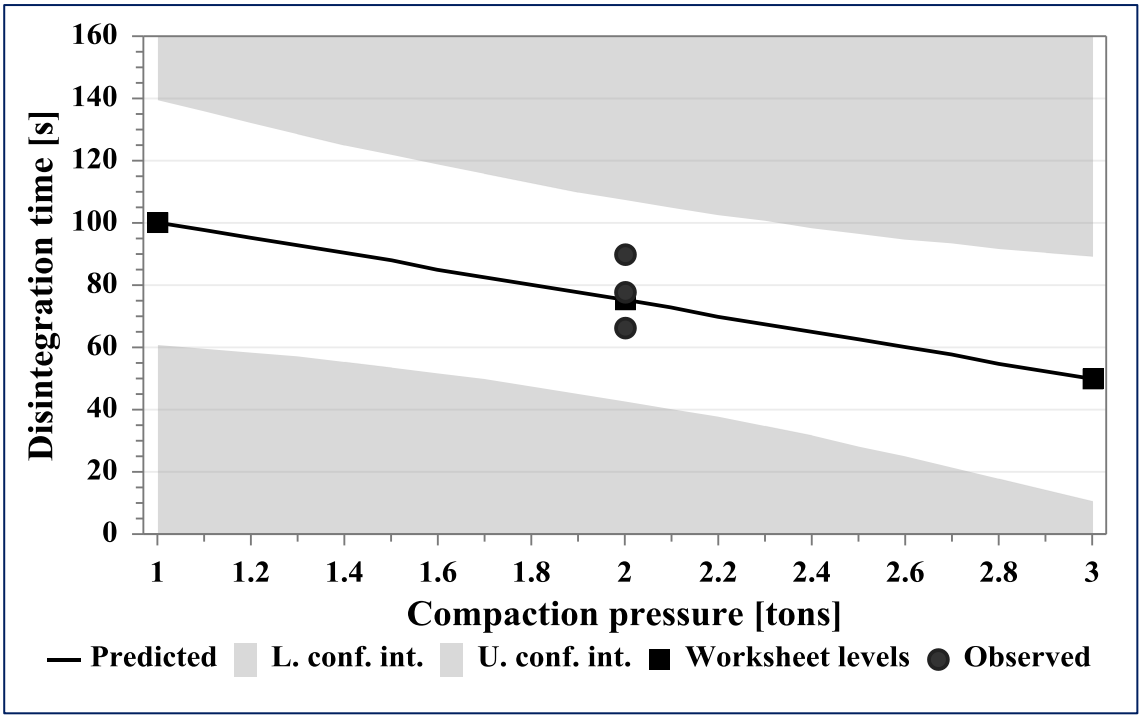

Figure 3.8 Main effects plot highlighting the change in disintegration time as a function of compaction pressure variations while other factors remained constant at their middle values. The three centre points (black dots) within the white area indicate validity of the effect, as they fall within the confidence limits of ± 95%.

3.3.2.2.3 Effect on tablet friability (Y_2)

Tablet friability was only significantly influenced by the linear models of polymer concentration and compaction pressure, as well as the interactive model of both factors (Equation 3.21). The effect coefficient for compaction pressure (-0.45) was much higher than that for polymer concentration (+0.18), implying that compaction pressure plays the highest role in tablet friability. This was further seen in the negative effect coefficient of the interactive term (-0.17), which implies that the detrimental effect of polymer concentration on friability is minimised when combined with increasing compaction pressure. Pinto (2004) reported that tablets containing polyox as a binder/ matrix forming agent showed a decrease in friability on increasing the compaction pressure. This observation can be explained by the fact that higher forces lead to increased binding capacity. Also,

previous work in the literature showed no significant difference in tablet friability (Al-Khattawi *et al* 2014) or a decrease in friability (Shahi *et al* 2013) with increasing polyox concentration. Figure 3.9 is a plot of the interactive effect of polymer concentration and compaction pressure on tablet friability. From this plot, it can be seen that at low pressures and high polymer concentrations there was high friability. However, as we navigate to a higher compaction pressure, an interactive relationship can be seen where low friability values are recorded at high compaction pressures and high polymer concentrations. The elastic recovery property of polyox can account for this interaction effect, as explained above.

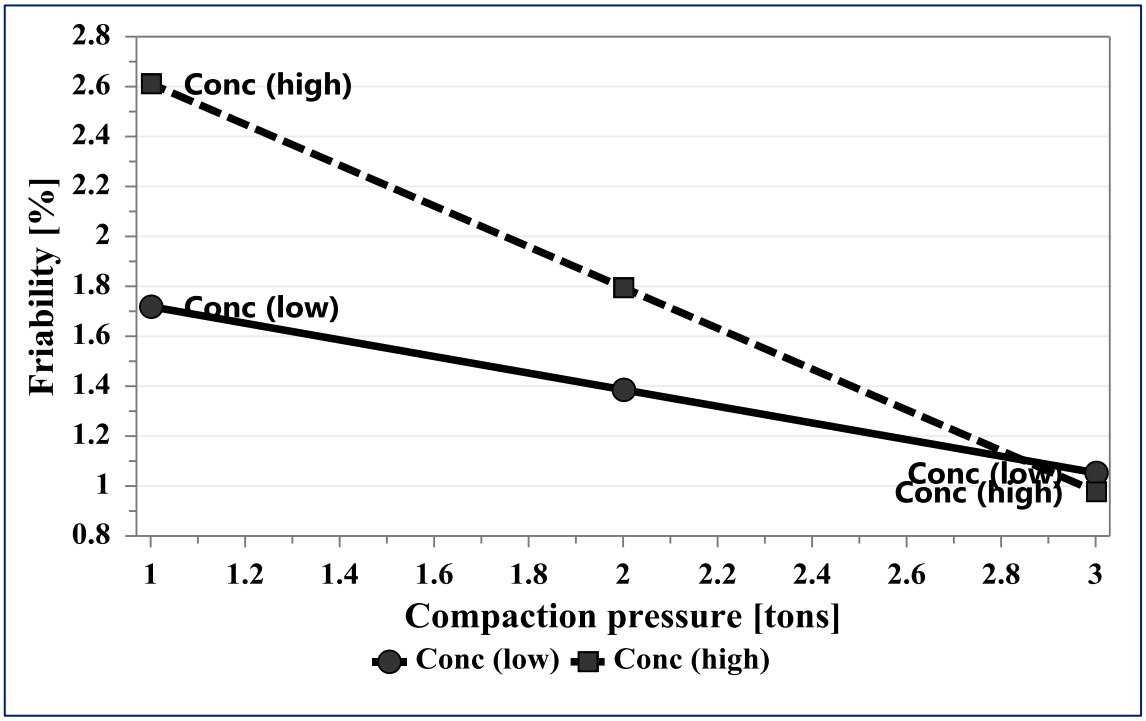

Figure 3.9 Interaction plot highlighting strong interaction effect of polymer concentration and compaction pressure on tablet friability. Two lines that cross each other depict a strong interactive effect.

3.3.2.2.4 Effect on tablet hardness (Y_3) and porosity (Y_4)

The regression model equation for tablet hardness (Equation 3.22) showed that the only factors that significantly affected tablet hardness were the linear model terms of polymer concentration and compaction pressure; with compaction pressure contributing the major impact. Tablet porosity was only influenced by the linear model of compaction pressure and the interaction model of polymer concentration and compaction pressure (Equation 3.23). As expected, compaction

pressure was directly proportional to hardness and inversely proportional to porosity as seen in their main effect plots (Figure 3.10). This was expected since high compaction pressures bring particles into closer proximity which yields lower porosity and, therefore, higher solid fraction. Thus providing more contact points for inter-particle bonding, leading to higher cohesiveness and hardness of the tablet (Bi *et al* 1996, Tye *et al* 2005).

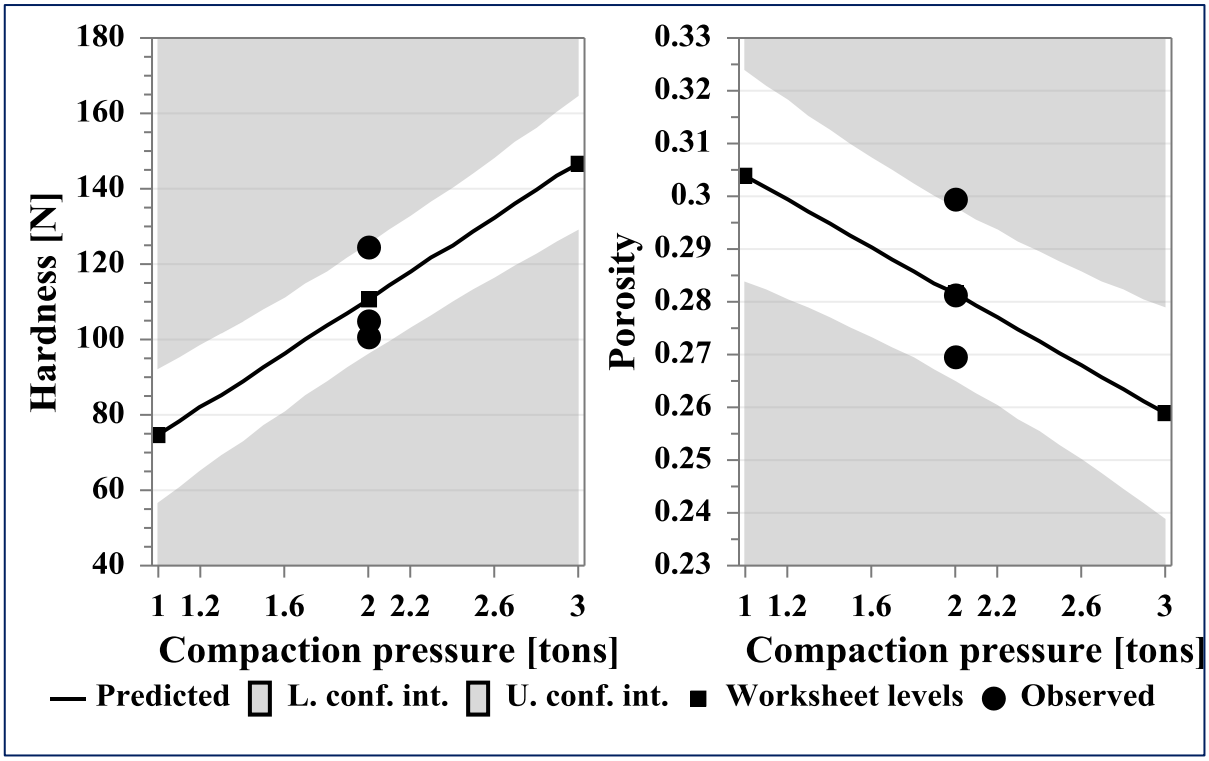

Figure 3.10 Main effect plot highlighting the effect on tablet hardness and porosity when compaction pressure is increased from its low to high value and other factors maintained at their middle values. The three centre points (black dots) within/ close to the white area indicate validity of the effect as they fall within the confidence limits of ± 95%.

Interestingly, there was an insignificant decrease in tablet hardness with increase in polymer concentration from 0.5-1.5% (Figure 3.11). Similar results have been reported (Al-Khattawi *et al* 2014) using low viscosity grades of polyox. However, tablet hardness was observed to decrease markedly above 1.5% polymer concentration. This was a totally unexpected trend because one would expect that increase in binder concentration would increase the cohesiveness of the powder mix, and therefore result in higher hardness. However, an examination of the response surface model (RSM) plot of polymer concentration and compaction pressure on porosity (Figure 3.12) reveals a decrease in tablet porosity with increasing compaction pressures (at low polymer

concentrations); however, at higher concentrations, tablet porosity was seen to increase. Thus, the elastic recovery of polyox increased with increasing polymer concentration and this effect supersedes the effect of increasing compaction pressure, thereby resulting in increased tablet porosity and subsequently decreased hardness. Bi *et al* (1999) reported lower tablet tensile strength and increased porosity with increase in polymer concentration. In our model, polymer viscosity did not significantly affect tablet hardness.

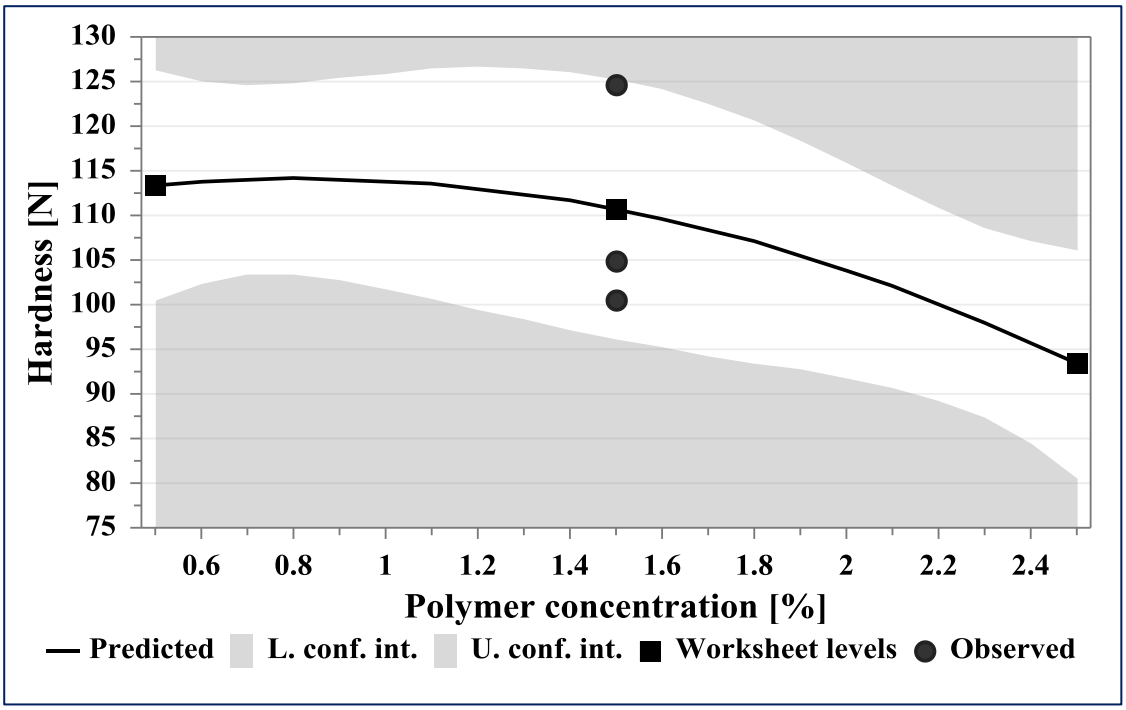

Figure 3.11 Main effect plot highlighting the effect on tablet hardness when polymer concentration is increased from its low to high value and other factors maintained at their middle values. The three centre points (black dots) within the white area indicate validity of the effect, as they fall within the confidence limits of ± 95%.

L'hote-Gaston *et al* (2009) reported a small increase in tablet hardness/ breaking force, with increasing polyox viscosity. On the other hand, Nokhodchi et al (1995) reported a decrease in tensile strength/ hardness of HPMC tablets with increasing polymer viscosity grades. However, a slight increase in porosity was observed on increasing polymer viscosity. This increase in porosity may be explained by the densification behaviour of the polymers upon compression. Polymers with lower viscosities and molecular weights have been reported to deform easily to fill the voids in the dies, during tablet compaction. Nokhodchi et al (1996) reported a linear increase in porosity of HPMC tablets with increasing polymer viscosity grades. However, in our model, the increase in

porosity seen with increasing polymer viscosity was regarded as insignificant by ANOVA (Table 3.5).

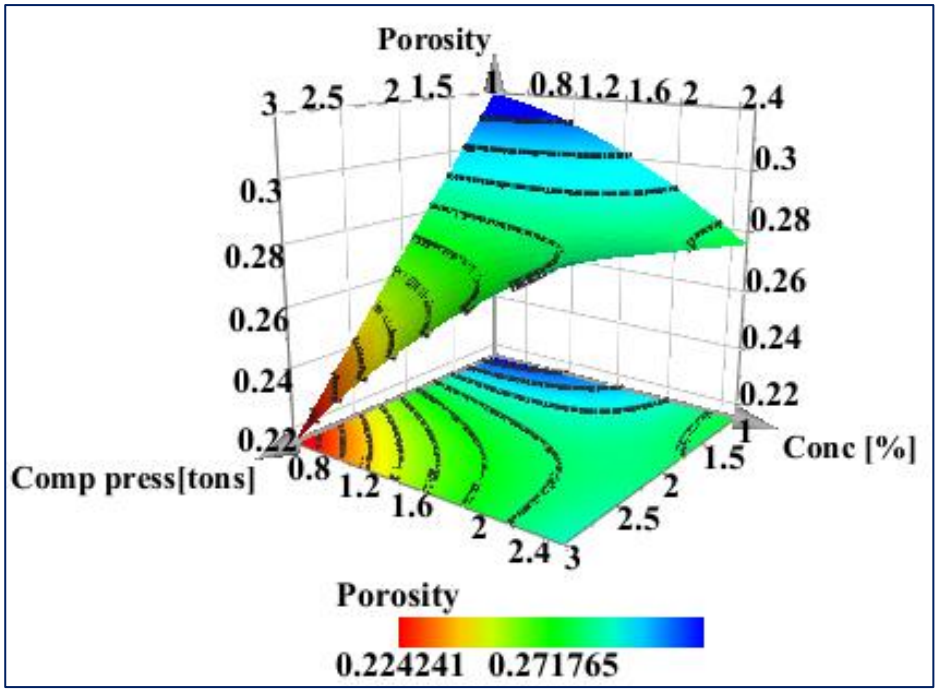

Figure 3.12 Response surface plot showing the effect on tablet porosity, of varying polymer concentration and compaction pressure, with polymer viscosity held at its mid position. An increase in tablet porosity at high compaction pressures and high polymer concentrations reveal the elastic recovery at high pressures, of polyox polymers

3.3.2.3 Prediction of design space/ formulation optimisation

Low polymer viscosity and concentration combined with high compaction pressures were identified as necessary CPPs for formulating desirable ODTs containing polyox. Figure 3.13 represents the sweet spot plot highlighting combinations of factors that would yield ODTs with disintegration times <180 secs, tablet hardness >60 kN and possible friability <1%. From here, it can be seen that low to medium viscosity polyox grades should be used at about 1.5% concentration and compacted at pressures between 2.6 – 3.0 tons to achieve ODTs with desirable characteristics. Based on this information, the MODDE software optimiser was used to set specific parameters (CPP levels) to yield ODT characteristics that would maximise tablet hardness, while minimising tablet disintegration time and friability. Tablet porosity was allowed to run free. ODTs were then formulated using these parameters for the various grades of polyox polymer viscosities tested.

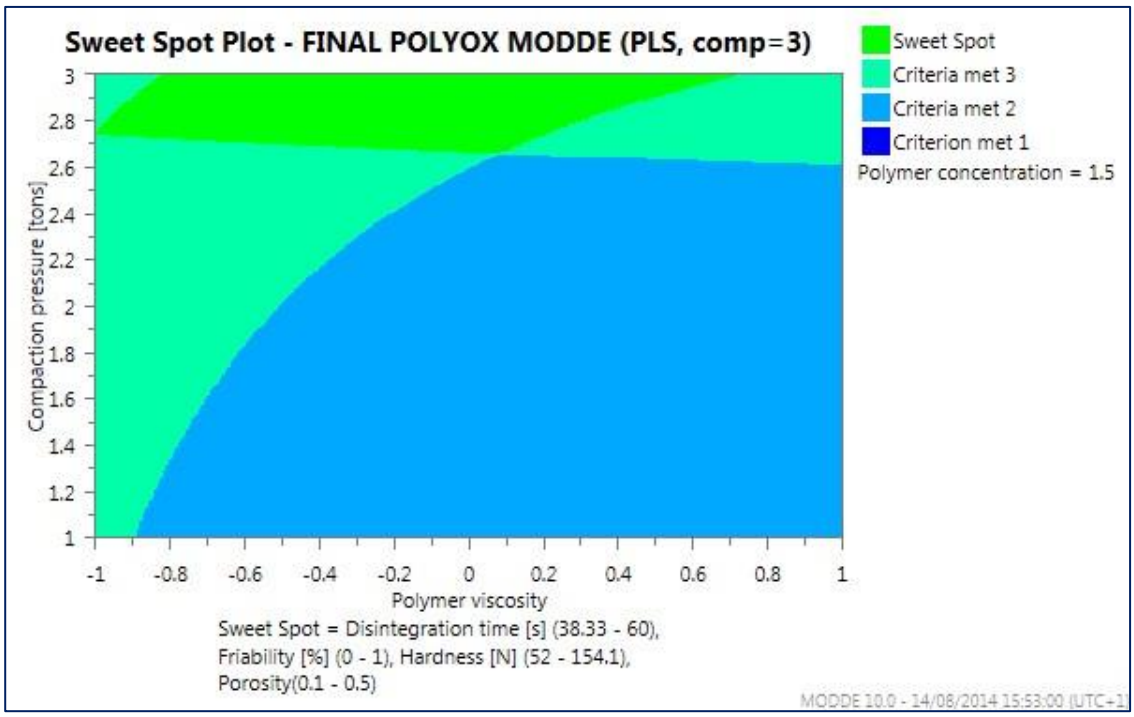

Figure 3.13 Sweet plot depicting polymer viscosity and compaction pressure ranges for obtaining optimal ODT characteristics when polymer concentration is set at its mid value (1.5%).

From experimental results highlighted in Table 3.7, tablets produced with the various viscosity grades of polyox were able to disintegrate/ disaggregate in < 60s, except those containing the highest viscosity grade of polyox. Hardness was > 110N for all tablets including the control, and tablet friability was much lower than for previous formulations (1.08 – 1.14%). Thus, using any combination of chosen factors designed by the MODDE optimiser, ODTs with optimal characteristics could be produced, although strategies to decrease friability would still need to be employed, as suggested by Al-Khattawi *et al* (2014).

3.3.3 Mucoadhesive efficiency

The ability of the ODT formulations to adhere to the surface of excised porcine buccal mucosa was assessed to determine the mucoadhesive efficiencies of the polymers. Results of the mucoadhesive efficiencies obtained for the optimised formulations are shown in Figure 3.14 while a typical compressive load vs compressive extension graph produced by the software is depicted in Figure 3.15. From Figure 3.14, only ODTs containing the polymer with the highest viscosity (Polyox coagulant) showed any significant enhancement in mucoadhesive efficiency, compared to formulations with other polyox polymers and the control which contained only LHPC.

Table 3.7. Table highlighting CPP levels chosen by the MODDE optimiser to yield ODTs with favourable characteristics, and results obtained after testing the ODTs (n=3). ODTs prepared without polyox were used as control.

FACTORS (CPP)			**RESPONSES (CQA)**			
Polymer viscosity grade	**Polymer concentration (%)**	**Compaction Pressure (tons)**	**Disintegration time (s)**	**Hardness (N)**	**Friability (%)**	**Porosity**
Polyox N10	1.39	2.99	37.00 ± 5.57	125.03 ± 5.56	1.12	0.43 ± 0.06
Polyox 1105	1.36	2.99	49.67 ± 2.52	121.87 ± 5.41	1.08	0.43 ± 0.03
Polyox N60K	1.32	2.99	51.00 ± 3.00	129.63 ± 0.60	1.13	0.47 ± 0.04
Polyox Coagulant	1.32	2.99	65.67 ± 1.53	119.93 ± 7.16	1.14	0.42 ± 0.03
Control	-	2.99	27.67 ± 3.05	118.70 ± 5.06	1.12	0.42 ± 0.02

Mucoadhesion has been reported to be directly proportional to polymer viscosity/ molecular chain length from molecular weights above 100,000 Da, for polyox polymers (Boddupalli 2010, Manly 2012). Shah *et al* (2014) reported that polyox polymers with molecular chain lengths 4,000,000 and above, showed the highest mucoadhesive potential. Mucoadhesion is affected by various properties of polymers, including molecular weight/ viscosity, flexibility, cross-linking density, hydrogen bonding capacity, hydration, charge and concentration (Boddupalli 2010). Considering that the concentration of the polymers in the formulations were almost constant, the similarities in mucoadhesive efficiencies of the low to medium viscosity polyox polymers may be related to the lower ability of these polymers to interact with water to form the interlinking chains with mucus (Cilurzo *et al* 2005). Conversely, Di Colo *et al* (2001) reported the mucoadhesive potential of low molecular weight polyox polymers to be higher than that of higher molecular weight polyox.

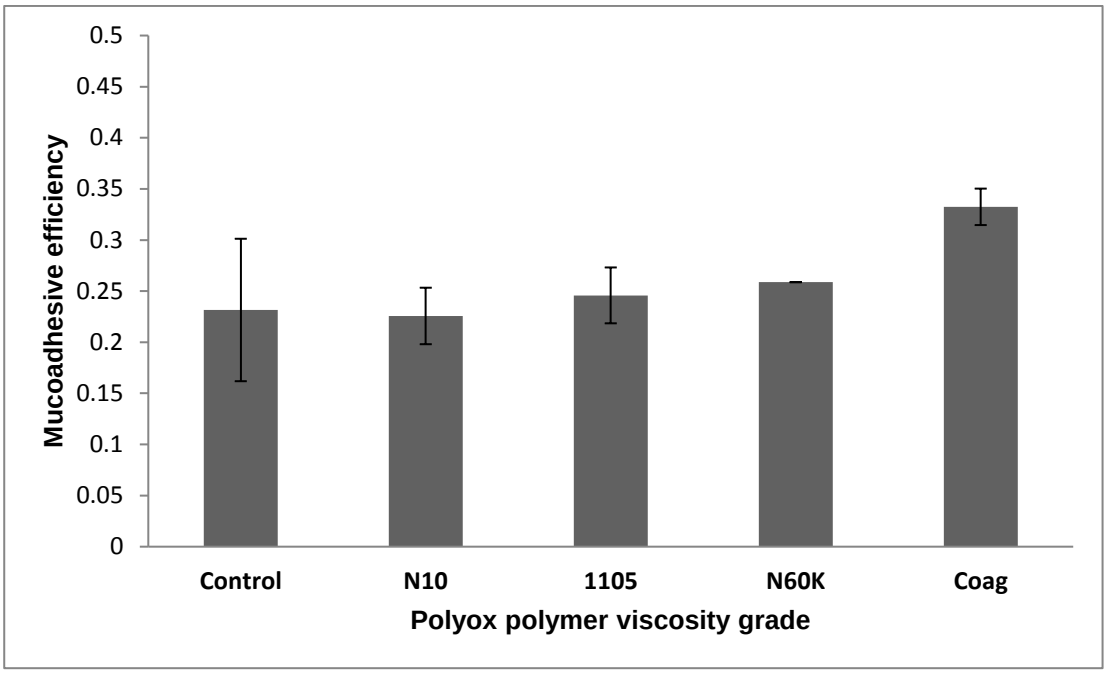

Figure 3.14 Results showing mucoadhesive efficiencies of ODTs containing various viscosity grades of polyox using CPPs designed by the MODDE software optimiser (n=2). Tablets containing only LHPC without polyox used as control. Only polyox coagulant tablets showed a significant increase above the control.

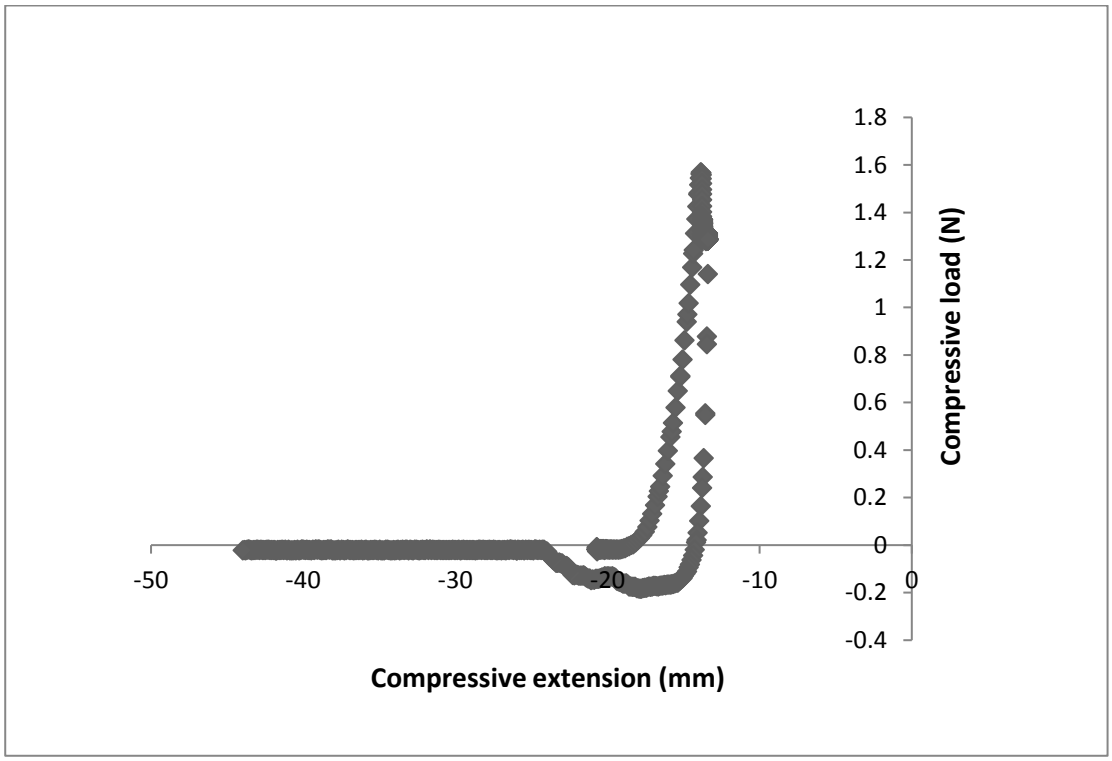

Figure 3.15. Typical plot of compressive load against compressive extension highlighting the energy input into the system and the resulting work of adhesion

3.4 Conclusion

Quality by design (QbD) incorporating design of experiments (DoE) proved an effective tool for designing quality into ODTs to yield optimal tablet characteristics. Furthermore, an understanding of the interactive and polynomial relationships generated by the model, brought to light the effect of the elastic recovery exhibited by polyox on the tablet characteristics of ODTs. From our model, tablet disintegration time was found to be directly proportional to polymer viscosity and concentration, but inversely related to compaction pressure. This effect of compaction pressure on disintegration time was unexpected but was found to be due to the elastic recovery of polyox that occurs at high compaction pressures and polymer concentrations, resulting in increased tablet porosity. Tablet friability decreased with lower polymer concentrations and higher compaction pressures. Tablet hardness was inversely related to polymer concentration and directly related to compaction pressure; while tablet porosity was found to decrease with increasing compaction pressures. These factors were successfully combined to intentionally produce ODTs with optimal characteristics and mucoadhesive properties that would enhance residence time of the ODT in the mouth, prevent saliva scavenging/ unintentional swallowing, and therefore enhance therapeutic outcomes.

Chapter 4

A systematic investigation of the role of extracellular calcium ion in promoting stratification of buccal cell cultures

Publications relating to chapter 4

Iyire, A.; Russel, C.; Bailey, C.; Mohammed, A. (2014) Investigating buccal cell cultures to enhance *in vitro* assessment of transmucosal drug delivery. *UKICRS Newsletter* pp 38-40. http://www.ukicrs.org/uploads/1/2/1/5/12158556/ukicrs_2014.pdf

4.1 Introduction

On delivery of a solid dosage form into the buccal cavity, the drug must diffuse out of the dosage form rapidly, dissolve in the saliva, partition into the lining of the epithelium, then across the whole epithelium, and thereafter diffuse into the systemic circulation via the internal jugular vein (Mathias and Hussain 2010). Because the buccal route is used mainly as an alternative non-invasive route to maximise the advantages of oral delivery while minimising its challenges, the formulation scientist must ensure that pharmacokinetic and pharmacodynamic parameters are similar between the two routes of administration. During formulation of potential buccal dosage forms, drug permeation via the buccal cavity has to be modelled. One area of continuous concern is the availability of effective *in vitro* methods to assess buccal drug delivery which are reproducible and representative of the *in vivo* environment (Shojaei 1998, Şenel and Hıncal 2001).

Ideally *in vivo* methods, if properly developed, would give the best representation of the fate of delivery systems upon buccal administration. *In vivo* methods available are modifications of the buccal absorption tests originally developed by Beckett and Triggs (1967). This test had limitations of accidental swallowing and saliva dilution that were not accounted for; and there was no method of confining the test solution to one particular area of the mouth (Shojaei 1998). Modifications of this method which accounted for possible saliva dilution and accidental swallowing have since been developed, but the common setback of lack of test solution confinement had still not been overcome (Shojaei 1998, Şenel and Hıncal 2001). Other *in vivo* methods include the attachment of a perfusion system to the buccal cavity of dogs and pigs, circulating a test solution through this cavity, and withdrawing samples from both the perfusion chamber and the blood, to correlate the amount of drug lost from the sample to the amount absorbed *in vivo* (Junginger et al 1999). Thus, *in vivo* methods for modelling buccal delivery are cumbersome and non-standardised. However, the use of mucoadhesive polymers to localise test systems to one site in the oral cavity would greatly improve the applicability of these tests (Sudhakar et al 2006).

Available *in vitro* methods involve the use of either excised animal buccal tissue or buccal cell cultures (Shojaei 1998, Şenel and Hıncal 2001); as it is almost impossible to obtain viable human

buccal epithelium on a continual basis (Balimane *et al* 2000). Here, excised animal buccal epithelium is mounted on perfusion/ diffusion chambers such as Franz cells, and permeation experiments carried out (Shojaei 1998). Table 1.5 (section 1.5.2, page 51) compares the dimensions and characteristics of available animal buccal tissues to that of humans. Porcine buccal epithelium has been identified as being closest to man's in terms of morphology, composition and biochemistry (Lesch et al 1989, Davoudi et al 2012). In order to overcome the disadvantages associated with the use of animal tissues, buccal cell cultures have been investigated as a high throughput method of buccal transport assessment.

Table 1.6 (section 1.5.2, page 54) compares the use of animal tissues and buccal cell cultures for modelling buccal delivery.

At present, commercially available buccal cell culture models include the TR146 cell line, reconstituted human oral epithelium (RHOE) and Epioral tissues. TR146 is a continuous cell line derived from a neck node metastasis of a buccal squamous cell carcinoma in a 67 year old woman who had undergone radiotherapy prior to incision (Rupniak et al 1985, Moharamzadeh et al 2007). They are reported to form a non-keratinised epithelium, 7-10 cell layers thick, with organelles identified as membrane coating granules (MCGs) and they cost approximately £800 including freight. RHOE are modified cells derived from the TR146 cell line and grown at the air-liquid interface on polycarbonate membranes in media supplemented with insulin, hydrocortisone and calcium chloride (Moharamzadeh et al 2007). These were reported to form epithelia devoid of the stratum corneum, similar to oral epithelia and cost approximately £200 for 12 tissues (4 replicate experiments). Epioral tissues are the most developed buccal models currently available. They are normal human derived epithelial cells grown in serum-free media (Moharamzadeh *et al* 2007). They form highly differentiated cells (8-12 layers thick) expressing normal keratins and naturally occurring antimicrobial peptides found in human tissues. These cost approximately £800 without shipping for 24 tissues (8 replicate experiments). However, the buccal stratification observed in humans (40-50 cell layers) has not been achieved by any presently available cell culture model (Shojaei 1998).

Calcium is a divalent, stable cationic component of bones and teeth that is never found unbound in nature. It is required for an extensive range of cellular processes in the body including enzymatic activities, cell attachment/ adhesion, cell-cell signalling, cell motility and morphology, cell differentiation and even electrochemical responses by the more specialised neural and muscle cells (Coppolino *et al* 1997, Jeyaraju *et al* 2009). In the cell, calcium is primarily stored in the endoplasmic reticulum and plays a role in signalling attachment events from inside the endoplasmic reticulum. Calcium has been implicated in many events that affect the shape or morphology, movement and three-dimensional structure of cells. It also modulates the functions of groups of adhesion molecules including cadherins, selectins and integrins, which are involved in regulation of homologous/ heterologous cell-cell and cell-matrix interactions. Desmosomes are molecular complexes that connect epithelial cells to one another and they attach the cytoskeleton of the keratin intermediate filament to the cell surface (Kelly 1966). These desmosomes comprise various proteins collectively called desmosomal proteins that include members of the cadherins superfamily, which are dependent on Ca^{2+} to function (Presland and Dale 2000). Thus, desmosome formation and assembly in cultured epithelial cells have been reported to occur rapidly in the presence of high extracellular calcium (Trinkaus-Randall and Gipson 1984, Watt *et al* 1984, Garrod and Chidgey 2008). The mechanism of this rapid assembly has been linked to the regulation of desmosomal cadherin by calcium and the specific phosphorylation and de-phosphorylation of desmosomal proteins. Watt et al (1984) reported that extracellular calcium concentrations up to 2.0 mM resulted in rapid cell adhesion and stratification, with the absence of stratification observed below 1.0 mM.

The objective of this work was, therefore, to test the hypothesis that increasing extracellular Ca^{2+} concentration in the specialised culture media for TR146 buccal cell line would enhance stratification of the TR146 buccal cell model; thereafter translating to significant changes in membrane permeability *in vitro*, with the larger aim of achieving higher *in vitro - in vivo* correlations during buccal drug delivery assessment.

4.2 Materials and methods

4.2.1 Materials

Atenolol, recombinant human insulin, propranolol, hydrated calcium chloride, methylthiazolydiphenyl-tetrazolium bromide (MTT) and fluorescein isothiocyanate (FITC)-labelled dextran 4kDa and trifluoroacetic acid (TFA) were purchased from Sigma Aldrich, UK. Fetal bovine serum (FBS), 1% penicillin-streptomycin, 2 mM glutamine and gentamycin were purchased from Bio Sera, UK. Hank's balanced salt solution (HBSS) and Ham's F-12 nutrient mix were purchased from Invitrogen UK. Trypsin-EDTA and Fungizone (amphotericin B) were purchased from Gibco Lab, UK. 4′,6′-diamidino-2-phenylinodole (DAPI) in Vectashield® was purchased from Vector Laboratories, UK. Trypan blue, acetonitrile, absolute ethanol and hydrochloric acid were purchased from Thermo Fisher Scientific, UK. Cell culture plates, microscope coverslips Biofreeze® were purchased from VWR, UK; while transwell inserts with plates were purchased from Appletonwoods, UK. All water used was double-distilled and autoclaved.

4.2.2 Methods

4.2.2.1 TR146 Cell culture procedure

Growing TR146 cells purchased at passage 4+ from Public Health England, were maintained (according to suppliers instructions) on 75 cm^3 T-flasks in Hams-F12 media fortified with 10% FBS, 2mM glutamine, and antibiotics; incubated at 37°C and 98% relative humidity provided by 5% CO_2/ 95% air. Media change occurred every 2-3 days, cells were sub-cultured at 80 - 90% confluence using 0.1% trypsin/EDTA solution in HBSS and passages 10 - 27 were used for experiments.

4.2.2.2 Passaging of cells

At 80 – 90% confluence, the media was decanted and cells washed twice with HBSS, to remove any dead or non-adherent cells. 5 mL of 0.1% trypsin-EDTA solution in HBSS was then added and flasks shaken at 450 rpm and 37°C for 10 minutes, in an orbital plate shaker. Flasks were examined

under light microscopy to ensure that disaggregation had occurred. Care was taken not to leave trypsin solution on for longer than 15 mins to prevent irreversible cell damage. 5 mL of culture media was added to quench trypsin reaction and cell density was measured by haemocytometry (section 4.2.2.5). Cells were then seeded unto continuation flasks, microscope coverslips, well plates or transwells respectively, at the required density.

4.2.2.3 Cell storage and revival

After trypsinising (as described earlier), cell suspensions were centrifuged at 1000 rpm for 5 minutes, the supernatant decanted and withdrawn fully using a pipette. Cells were then resuspended in sufficient volume of cryoprotectant - Biofreeze® to produce $10^6 – 10^7$ cells/mL, and 1 mL each of the resulting cell suspension was transferred into cryovials. After labelling, cryovials were placed in a polystyrene box kept at -20°C for 1 hour which ensures a constant cooling rate of 1°C/ min, then retained overnight at -80°C. The following day, the cryovials were transferred to liquid nitrogen for long-term storage. To ensure cell viability, one cryovial of cells was revived one month later. To revive cells, cryovials containing frozen cells were removed from liquid nitrogen and thawed in the incubator at 37°C, after which contents were immediately emptied into a 25cm^3 T-flask containing 6mL cell culture media. Flasks were incubated at 37° C and, at confluence, passaged into 75 cm^3 T-flasks, and then used as required.

4.2.2.4 Seeding of cells

Microscope coverslips were place in absolute ethanol for 2 minutes, and then transferred singly into the wells of a 12 well plate, and left partially open in the laminar flow hood to dry for two minutes. 1 mL of 0.02% collagen solution in deionised and autoclaved water was added to each well and left partially open in the hood to facilitate collagen coating of coverslips. After 3 hours, collagen solution was removed and wells rinsed twice with 1mL HBSS (to remove residual acetic acid used to solubilise collagen). Upon drying, enough cell suspension to give the required seeding density was added to the wells using an automatic pipette. Seeding density for all supports was maintained at approximately 24,000 cells/ cm^2. Seeding volumes were maintained according to manufacturer recommendations, and are listed in Table 4.1.

Table 4.1 Characteristics of solid supports for cell culture: dimensions and media volumes used

Support	Diameter (mm^2)	Surface area (cm^2)	Total media volume (mL)	Apical media volume (mL)	Basolateral media volume (mL)
T 25 flask	-	25.00	7.00	-	-
T 75 flask	-	75.00	25.00	-	-
6 well plate	34.80	9.50	2.50	-	-
12 well plate	22.10	3.80	1.00	-	-
96 well plate	4.26	0.14	0.31	-	-
6 well transwell	24.00	4.67	4.10	1.50	2.60
12 well transwell	12.00/’;	1.12	2.00	0.50	1.50

4.2.2.5 Cell quantification (haemocytometry)

To calculate cell density, 20 µL each of trypan blue solution and post-trypsinised cell suspension were added to an Eppendorf tube and mixed together. The resulting suspension was placed under a microscope slide cover slip on a haemocytometer, and the number of live cells (cells not stained blue) per square was counted using a TMS-F inverted microscope (Nikon, Japan). Cell density which is the number of live cells per mL of cell suspension was calculated using equation 4.1 below. Subsequently, cell seeding density was achieved by diluting the required number of cells in sufficient culture media.

$$\text{Cell Density} = \frac{\text{Total number of live cells in squares}}{(\text{Number of squares (4)})} \text{ x dilution factor x } 1000 \qquad \text{(Equation 4.1)}$$

4.2.2.6 Effect of extracellular calcium on cell viability, proliferation and stratification

4.2.2.6.1 Preparation of calcium solutions

A 20% w/v stock solution of anhydrous calcium chloride in deionised water was prepared and autoclaved. Sufficient volumes were added to prepare 50 mL of calcified media per concentration

needed, and is shown in Table 4.2. For all experiments, normal media (approx. 0.3 mM Ca) was used as a negative control.

Table 4.2 Volumes of calcium chloride solution required to prepare 50 mL of calcium fortified media

S.N.	Ca^{2+} concentration (mM)	Volume of calcium stock added (µL)
1	0.6	11.0
2	0.9	22.0
3	1.2	33.0
4	1.5	44.0
5	1.8	55.0
6	2.1	66.0
8	4.2	132.0
9	8.4	164.0
10	16.8	528.0
11	33.6	1056.0

4.2.2.6.2 Qualitative analysis

4.2.2.6.2.1 Light microscopy

All cells grown on T-flasks, well plates, microscope coverslips or polyester transwell inserts were viewed using a TMS-F inverted light microscope (Nikon, Japan) at 10x or 40x magnification.

4.2.2.6.2.2 Confocal Laser Scanning Microscopy (CLSM)

Cells grown on microscope coverslips or transwell inserts were rinsed twice with HBSS, and then fixed with 4% paraformaldehyde (PFA) in PBS for 10 minutes. Thereafter, cells were rinsed four times with PBS. For microscope coverslips, a drop of DAPI (4′,6′-diamidino-2-phenylinodole) in vectashield® was placed on a microscope slide and the coverslip placed on the drop, such that the surface with cells contacted the mounting medium, and allowed to air-dry for 10 mins. Transwells were placed on microscope slides and the membrane carefully cut out using a scalpel. Two drops of DAPI in vectashield® were used to mount the specimen, which was immediately covered with

a microscope coverslip and allowed to air-dry for 10 minutes. All prepared samples were then viewed using a Leica confocal microscope (Wetzlar, Germany) at 10x (dry) and/ or 40x (oil) magnifications.

4.2.2.6.3 Quantitative analysis

4.2.2.6.3.1 Cell proliferation using haemocytometry

Cells were seeded unto 25 cm^2 T-flasks in increasing Ca^{2+} concentrations (control, 1.2, 1.5 & 1.8 mM Ca). Cells were trysinised daily and live cells counted by haemocytometry (see section 4.2.2.5 above).

4.2.2.6.3.2 Cell proliferation/ viability by MTT assay

The MTT assay was used to assess proliferation and viability of cells in the presence of increasing Ca^{2+} concentrations over a 7-day period. Cells were seeded equally into 96 well plates at 10,000 cells/well (n=8) in increasing Ca^{2+} concentrations (control, 1.2, 1.5, 1.8, 2.1, & 2.4 mM Ca). For one set of experiments, cells were continuously exposed to calcium fortified media while the second set of cells had an intermittent calcium exposure lasting 24 hours, alternating with normal (control) media for 24 hours, throughout the duration of the test. For the MTT assay, 20 µL MTT solution (5 mg/mL in HBSS) was added to each well containing 200 µL culture media (wells containing media with no cells serving as blank) and the plate incubated for 4 hours at 37°C and 5% CO_2 in air. After 4 hours, wells were emptied and MTT solution was replaced with 100 µL DMSO, then shaken for 15 minutes in an orbital plate shaker at 100 rpm. Finally, the formazan absorbance was read on a Multiskan® spectrum plate reader (Thermo Scientific, UK) at 490 nm. Blank readings were subtracted from the well readings to determine the final absorbance of the cells. The relative enzyme reactivity and therefore cell viability was calculated from equation 4.2.

$$Cell\ viability\ (\%) = \frac{OD_1 - OD_2}{OD_3 - OD_2}\ x\ \frac{100}{1} \quad . \quad . \quad . \quad . \quad . \quad \text{(Equation 4.2)}$$

where OD_1, OD_2 and OD_3 are the optical densities of wells with cells and Ca^{2+} fortified media, blank wells containing normal media with no cells, and wells with cells in normal media (control) respectively.

4.2.2.6.3.3 Transepithelial electrical resistance (TEER)

The ohmic resistance (resistance to current flow via the paracellular pathway) of cells grown on transwell inserts was measured every 2-3 days (30 mins after media change) during the cell culture, as well as before and after each permeability experiment, using an EVOM™ volt ohmmeter (World Precision Instruments, US) with chopstick electrodes. The electrodes were placed erect, such that the longer arm just touched the fluid in the basolateral chamber, while the shorter arm barely touched the apical membrane. The transepithelial electric resistance which reveals the integrity of the cellular layers was calculated using equation 4.3. TEER values were reported as mean ± standard deviation of triple readings from replicate transwells (n=9).

$$TEER = \left(R_{(insert\ with\ cells)} - R_{insert\ without\ cells}\right) * A \qquad \text{(Equation 4.3)}$$

where R is the measured resistance and A is the cross-sectional area of the transwell inserts.

4.2.2.6.3.4 Permeability studies using transport markers

4.2.2.6.3.4.1 Transport studies

The permeability of TR146 cell layers grown in increasing extracellular Ca^{2+} concentrations on 12 well polyester transwell inserts (Appletonwoods, UK) to the transport of paracellular markers (FITC labelled dextran 4kDa, propranolol and atenolol) and insulin was determined over 4 hours as described by Nielsen and Rassing (1999) at 36°C and 140 rpm in an orbital plate shaker. Cells on transwell inserts were rinsed twice with HBSS (37°C) by adding and withdrawing 0.5 mL and 1.5 mL respectively to/ from the apical and basolateral chambers respectively. After incubation for 30mins, TEER readings were taken in triplicate per insert. The basolateral chamber was then replaced with fresh HBSS and the apical chamber with 0.5 mL test solution (0.5mM FITC labelled dextran 4 kDa, 100 mM atenolol or propranolol, or 1 mg/mL insulin solution prepared in HBSS). Immediately, 100 µL of test solution was withdrawn from the apical and basolateral chambers at time 0. Basolateral sampling of 700 µL was done every 30 mins for 4 hours with immediate replacement with pre-warmed HBSS. At the end of the experiment, 100 µL of apical solution was taken. Cells grown in normal (unfortified media) were used as control (Portero *et al* 2002, Xue *et*

al 2012, Sander *et al* 2013). After 4 hours, cells were rinsed twice with 0.5 mL HBSS and equilibrated for 30 minutes after which TEER values were recorded. All FITC-dextran samples were transferred to 96 well plates, protected from light using aluminium foil and immediately read using a fluorescent plate reader at pre-determined excitation and emission wavelengths of 490 nm and 535 nm respectively. All other samples were made up to 700µL (where necessary) using HBSS, and analysed by HPLC (section 4.2.2.6.3.4.2). The resultant data was used to calculate the apparent coefficient of permeability through the insert with cells (P_{app}), the cell-free apparent permeability coefficient (P_{insert}), the cell apparent permeability coefficient (P_{cell}), and the recovery %.

$$P_{app} = \frac{dQ}{dt} \; x \frac{1}{A*C_o} \quad \text{(Equation 4.4)}$$

$$P_{insert} = \frac{dQ}{dt} \; x \; \frac{1}{A* \; C_o} \quad \text{(Equation 4.5)}$$

$$\frac{1}{P_{app}} = \frac{1}{P_{cell}} + \frac{1}{P_{insert}} \quad \text{(Equation 4.6)}$$

$$Recovery \; \% = \frac{X_{apical} + X_{basolateral}}{X_o} \; x \; \frac{100}{1} \quad \text{(Equation 4.7)}$$

where dQ/dt is the rate of drug transport at steady state in µg/s, A is the cross sectional area of cells in cm^2, C_O is the initial apical solution concentration in µg/mL, X_{apical} is the quantity of insulin remaining in the apical chamber after 4 hours, $X_{basolateral}$ is the cumulative amount of insulin sampled from the basolateral chamber after 4 hours and X_o is the initial quantity of insulin in the apical chamber at the start of the experiment (Portero *et al* 2007, Xue *et al* 2012, Sander *et al* 2013).

Drug stability after permeation was monitored by HPLC, where possible, for changes in retention time and/ or appearance of multiple peaks on the HPLC chromatogram.

4.2.2.6.3.4.2 High performance liquid chromatography (HPLC)

A Waters HPLC system (Alliance) with gradient pump and UV/ fluorescent detector employing a reversed phase RP-C18 analytical column (Phenomenex® 110A, 150 x 4.6mm, 5µm), was utilised to quantify the test markers used for transport experiments, as well as monitor stability after permeation through TR146 cell layers. HPLC conditions validated by ICH guidelines for the various test substances are highlighted in Table 4.3.

Table 4.3 HPLC conditions for test substances

S.N.	Marker	Mobile Phase composition	Other conditions
1	Propranolol HCl	0.1% TFA in water and acetonitrile, 67:33	Injection volume 10µL, UV detection at 235nm wavelength.
2	Atenolol	0.1% TFA in water and acetonitrile, 67:33	Injection volume 10µL, fluorescent detection at emission and excitation wavelengths of 350 and 397 nm respectively
3	Insulin	A: 0.1% TFA in water and B:acetonitrile. Gradient elution from 74:26 to 67:33 compositions of A:B over 3 mins, and then maintained at 67:33 for 4 mins.	Injection volume 10µL, UV detection at 214nm wavelength.

4.2.2.7 Statistical analysis

All data generated in replicates were presented as mean ± standard deviation (SD). The data was then analysed for statistical significance using one-way analysis of variance (ANOVA) and Tukey-Kramar multiple comparison post-test from Graphpad Prism® version 6.02 (San Diego, CA, USA). The level of significance was quoted as $p<0.05$ (confidence levels of 95%).

4.3 Results and discussion

4.3.1 Cell proliferation of TR146 cells using light microscopy

Proliferation pattern of TR146 cells on T75 flasks over five days is depicted in Figure 4.1. The cells showed a progression from about 90% confluence on arrival with cells exhibiting distinct intercellular boundaries, to cells which had lost their morphology, become non-adherent and assumed a 'liposome-like' shape upon trypsinisation during sub-culture/ passaging. Trypsin is a proteolytic enzyme that hydrolyses cell membrane proteins required for cell-cell and cell-substrate attachment (Yamada et al 1990). Onward, the cells adhered to the solid support, assumed epithelial morphology and had begun replicating and forming small, then larger colonies by 48 hours post-passage. This process of cell attachment is facilitated by divalent cations (usually Ca^{2+}) and proteins including cell surface glycoproteins, serum derived glycoproteins and conditioning factors secreted by cells (Butler 2003). These factors form an adherent layer between the cells and the substratum.

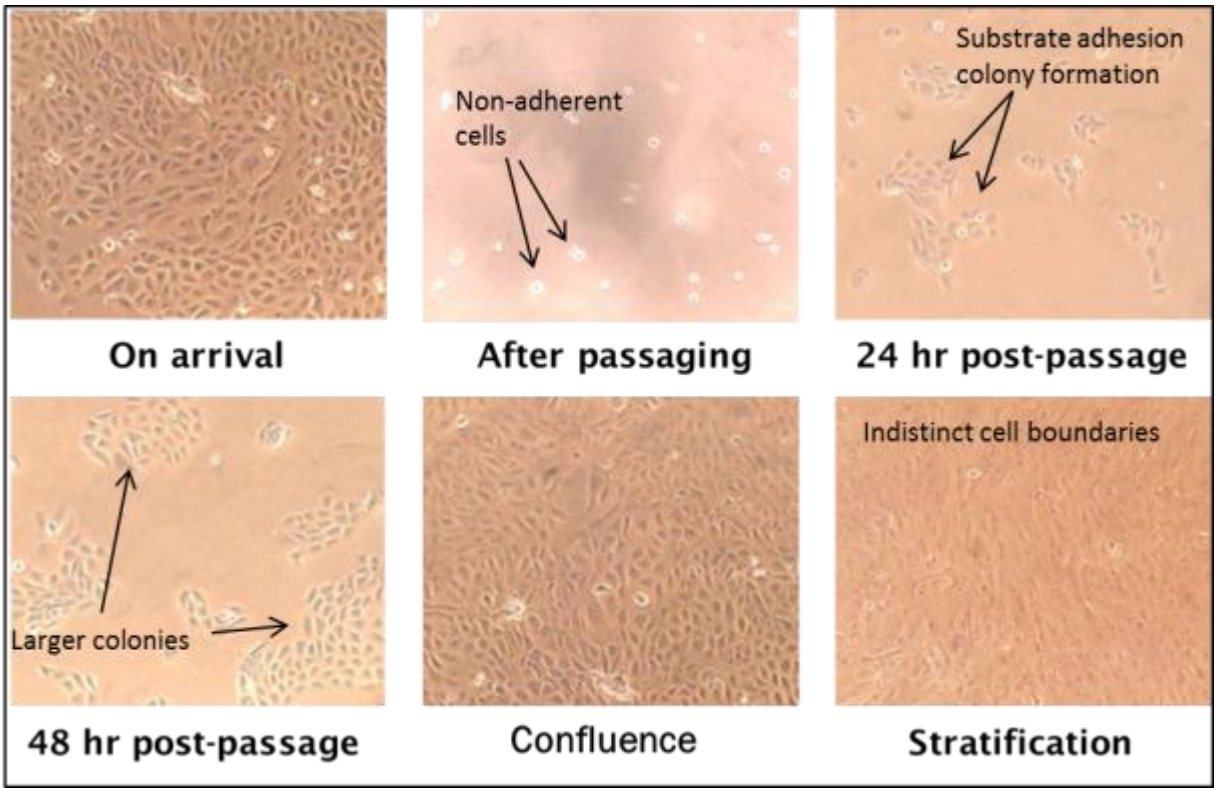

Figure 4.1 Light microscopy (10x magnification) showing proliferation pattern of TR146 cells grown in normal media on 75cm^3 T-flasks from receipt, sub-culture, until confluence and onward stratification.

By 5 days post-passage, monolayer formation was completed and onward stratification initiated, as observed by the indistinct intercellular junctions due to overlapping of stratifying cells. As expected, cells exhibited the stratified squamous epithelial characteristics expected of their buccal origin (Jacobsen et al 1995).

4.3.2 Effect of extracellular Ca^{2+} concentration on cell proliferation, viability, stratification and permeability

4.3.2.1 Light microscopy

Initial qualitative Ca^{2+} toxicity assay was carried out by seeding TR146 cells on 48 well plates in media fortified with increasing Ca^{2+} concentrations (Figure 4.2). Cells were observed to grow faster and appear healthier at concentrations between 1.2 mM and 2.1 mM concentrations. Increasing concentrations to 8.4 mM showed slower growth rates and less healthy cells, while concentrations of 16.8 mM and above resulted in cell lysis.

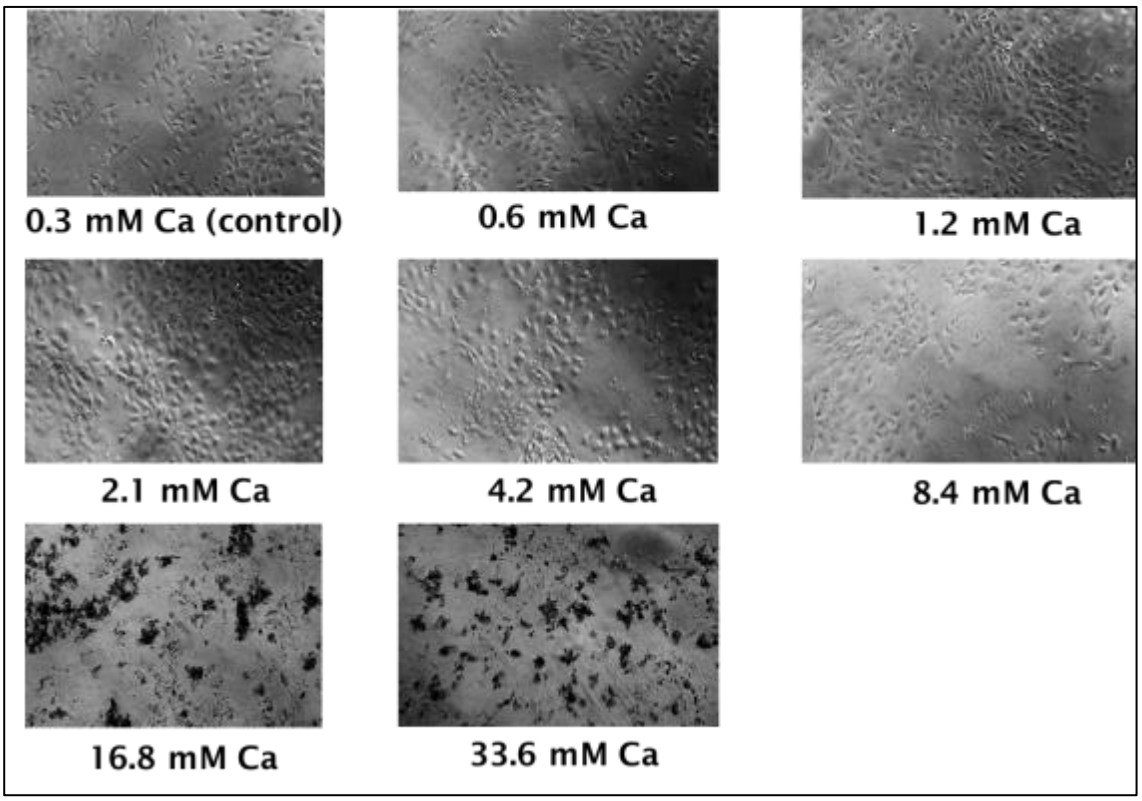

Figure 4.2 Representative light microscopic images (10x magnification) of TR146 cells cultured on 48-well plates for two days in media fortified with increasing calcium chloride concentrations, with normal (uncalcified) media used as control (n=3). Cell lysis was observed to occur at concentrations >8.4mM.

Calcium ion is a mediator for many cell processes including cell adhesion/ attachment; however at high concentrations, it has been implicated in cell death due to initiation of oxidative stress (Zhivotovsky and Orrenius 2011). A large concentration gradient exists between the intracellular and extracellular fluids of healthy cells. This gradient is between 1-3 mM extracellularly and 0.1-0.2 µM in the cytoplasm. An increase of cytoplasmic calcium levels up to 0.5 µM due to leaky membranes caused by lipid peroxidation via oxidative stress results in a cascade of events that destabilises enzyme functions, alters ion and pH balance, as well as interferes with functions of critical organelles like mitochondria (Bers 2008). Thus, to maintain calcium homeostasis, mitochondria remove calcium from the cytoplasm by a process called calcium cycling. Intra-mitochondrial calcium then stimulates release of enzymes of the TCA cycle, resulting in energy production. When cell membranes are damaged (after subculture with trypsin-EDTA or other chelators), influx of calcium into the cytoplasm increases, leading to an imbalance in cellular homeostasis. At extremely high ECF Ca^{2+} concentrations, cytoplasmic calcium cannot be returned to the nanomolar range, placing a burden on calcium cycling via the mitochondria, ultimately

resulting in halting of ATP production, permanent opening of the mitochondrial membrane pores, and triggering of apoptosis-inducing factors that cause cell death (Bers 2008). This would explain the cell death observed at higher extracellular Ca^{2+} concentrations. Maeno et al (2005) reported toxicity to osteoblast cells when exposed to >10mM Ca^{2+} concentrations: 2-4 mM Ca^{2+} was found to induce cell proliferation, while 6-8mM was reported to enhance differentiation and mineralisation. Cao et al (2012) also reported cell death when cells were exposed to media containing 100mM calcium ion concentrations.

A similar trend was seen in cells grown on microscope coverslips (Figure 4.3), with maximal cell proliferation effects observed at 1.5 mM and a slow proliferation observed at 2.1 mM concentration. Figure 4.4 shows a higher magnification of cells cultured on 25cm^2 T-flasks in increasing Ca^{2+} concentrations. Cell density was higher as Ca^{2+} concentration increased to 1.5 and 1.8mM above the control. By day 4, evidence of stratification was observed across all concentrations. Thus, the range of 1.2mM to 1.8mM Ca^{2+} concentration was chosen for further optimisation.

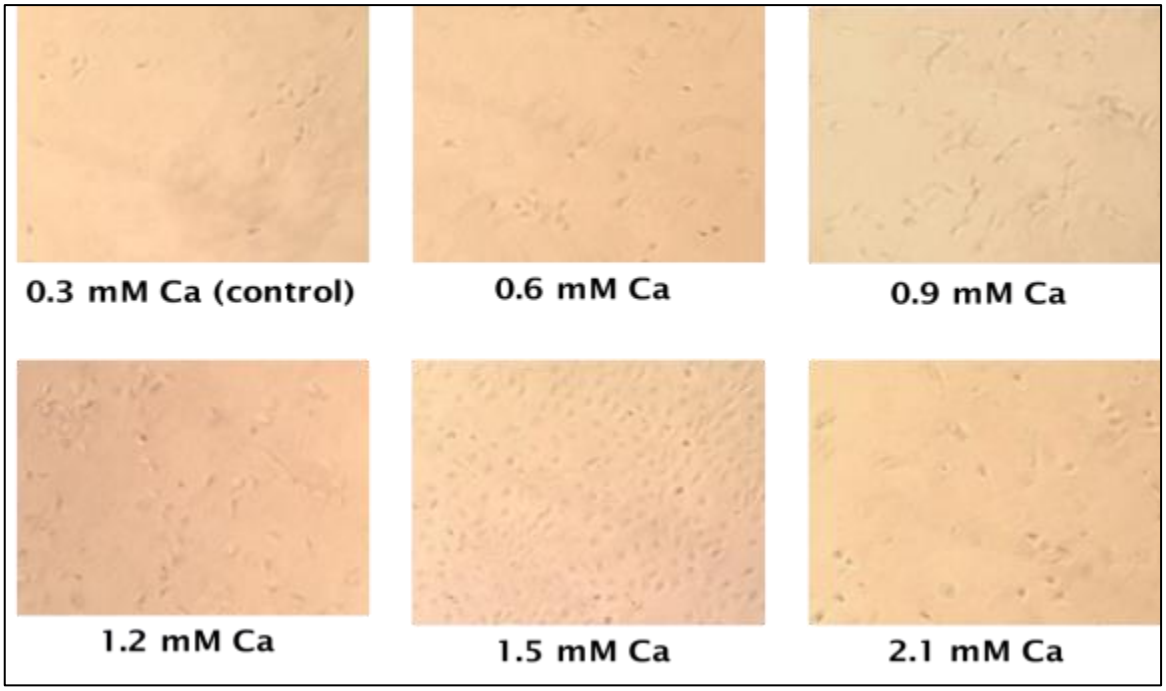

Figure 4.3 Representative light microscopic images (10x magnification) of TR146 cells cultured on collagen-coated microscope coverslips for two days in media fortified with increasing calcium chloride concentrations, with normal (uncalcified) media used as control (n=2). Maximal cell growth was observed at 1.5mM concentrations.

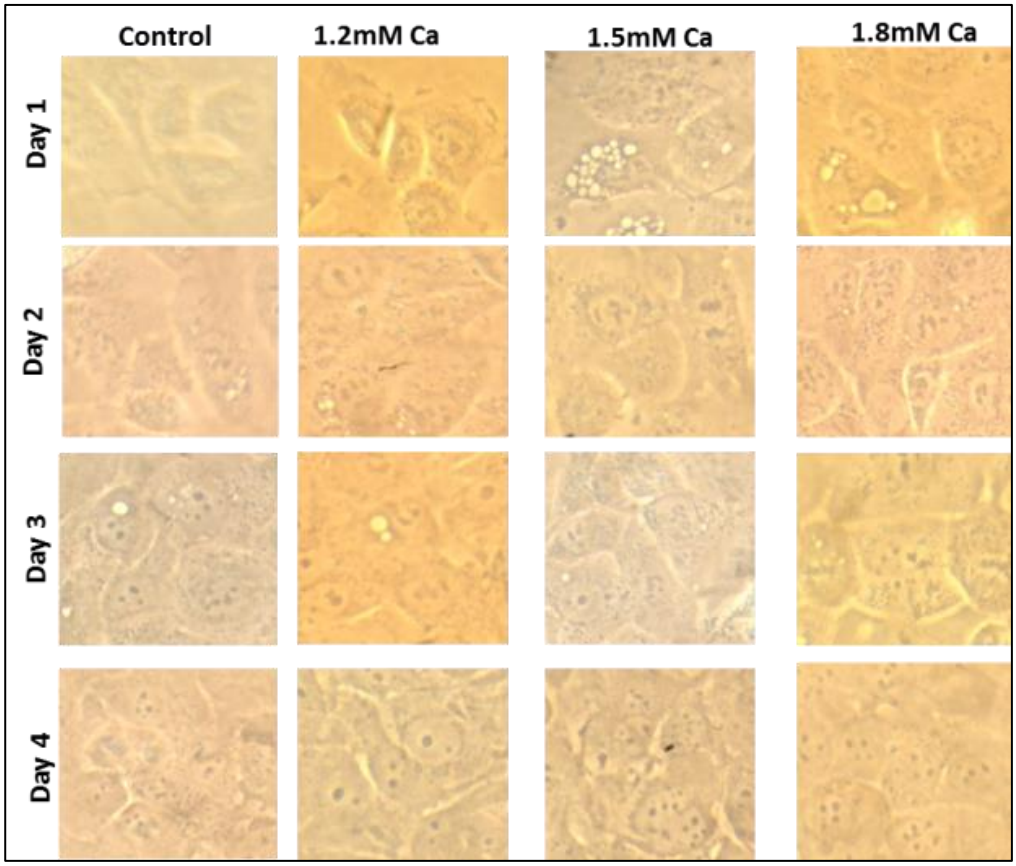

Figure 4.4 Representative light microscopic images (40x magnification) of TR146 cells cultured on 25cm^2 T-flasks in media fortified with increasing calcium chloride concentrations, with normal (uncalcified) media as control (n=3). Cell proliferation increased at concentrations between 1.5-1.8 mM, with stratification observed by day 4.

4.3.2.2 Confocal Laser Scanning Microscopy (CLSM)

To further investigate the role of extracellular calcium, TR146 cells were grown using the optimised Ca^{2+} concentration range (1.2 – 1.8 mM) on microscope coverslips and 6 well polycarbonate or 12 well polyester transwell inserts. Cells were fixed with 4% PFA and stained with DAPI (4',6-diamidino-2-phenylindole) which is a fluorescent dye that binds strongly to double stranded DNA (A-T rich regions) in the nuclei of cells (Manzini et al 1983). Figure 4.5 shows the horizontal plane of DAPI-stained nuclei of cells grown on collagen-coated microscope coverslips. It can be observed that cell density was seen to increase with increasing Ca^{2+} concentration. Also evidence of stratification, inferred from the grouping of nuclei together (highlighted with arrows) was seen with 1.5 mM and 1.8 mM concentrations, when compared to 1.2 mM and control. Calcium has been reported to show paradoxical effects on cell growth. Low concentrations of extracellular calcium have been reported to influence cell proliferation while high

concentrations (1.0mM and above) have been reported to favour stratification and terminal differentiation (Boyce and Ham 1983, Freshney and Freshney 2004).

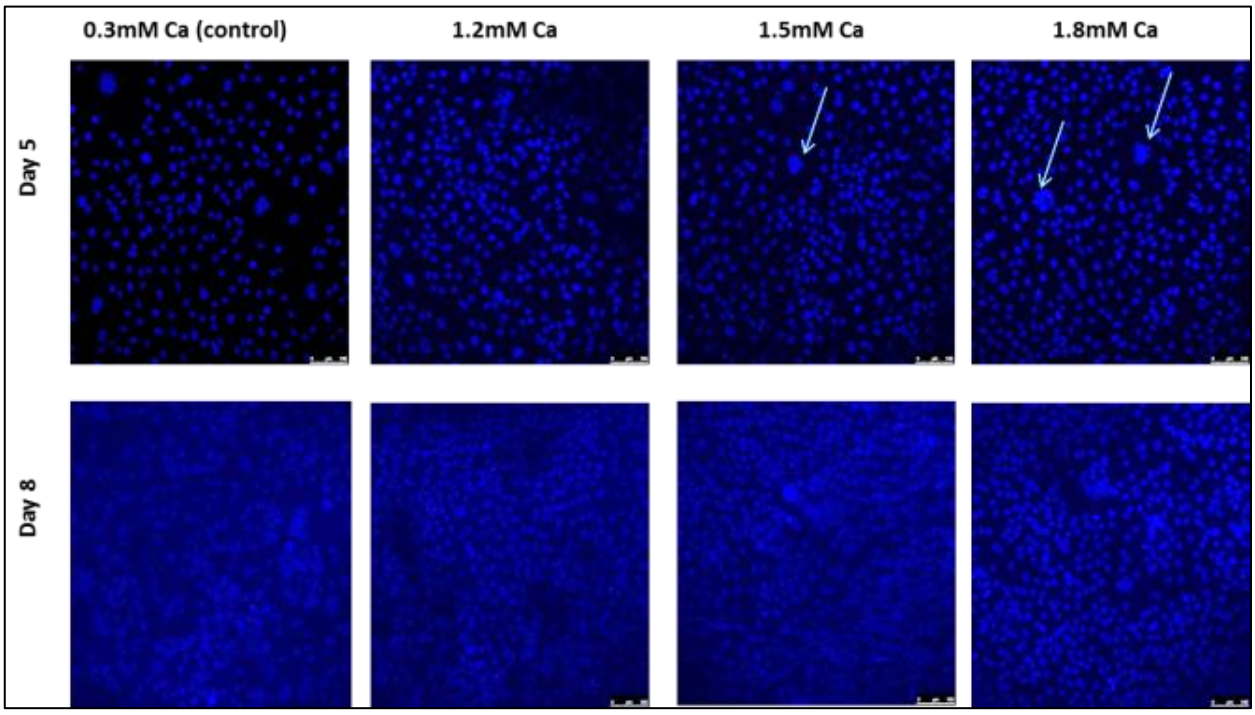

Figure 4.5 Representative confocal microscopic images of TR146 cells grown on collagen coated microscope coverslips in increasing Ca^{2+} fortified media, stained with DAPI (horizontal plane). Arrows indicate areas of stratification; depicted by grouping of nuclei together.

Furthermore, Lechner et al (1982) reported that the effect of calcium was dependent on cell density of clonal cells; where at low cell densities, variations in extracellular Ca^{2+} concentrations between 0.1 and 1.0 mM had no significant effect on cell proliferation, but when cell density increased to greater than 10,000cells/cm^2 there was increased cell differentiation at Ca^{2+} concentrations greater than 0.4mM (Freshney and Freshney 2004). Hennings et al (1980) reported fast cell growth, continuous keratinisation, absence of stratification and no desmosome formation with mouse epidermal cells exposed to low concentrations (0.5 – 1.0mM) of calcium; while at concentrations from 1.2mM and above, desmosome formation and stratification was observed. Evidence from light microscopy (results not presented) revealed that once a colony of cells of reasonable size had been established, stratification could be initiated; even though the solid support was not completely covered by a monolayer of cells. This can be noticed in Figure 4.5. A similar trend was noted from cells grown on transwell permeable supports (Figure 4.6). Cell density on permeable supports was much higher than on coverslips as expected, because cells are maintained in a polarised, more

natural state on permeable supports (Cereijido et al 1978). An increase in cell density was also noted with increasing Ca^{2+} concentration.

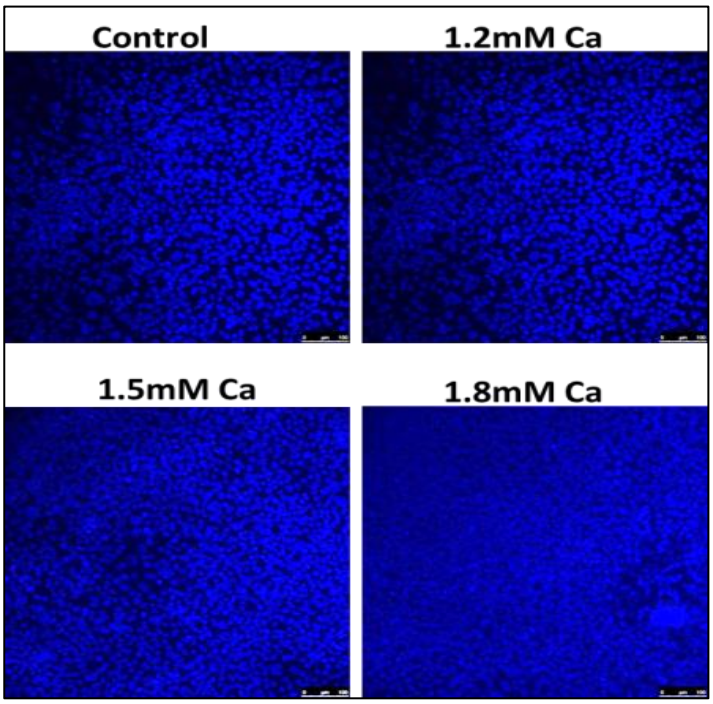

Figure 4.6 Representative confocal microscopic images of TR146 cells grown for 8 days on polycarbonate transwell inserts in increasing Ca^{2+} media, stained with DAPI (horizontal plane). 1.5-1.8 Mm Ca^{2+} enhanced cell proliferation.

Transverse sections of the cells grown on coverslips (Figure 4.7) and permeable supports (Figure 4.8) were able to demonstrate the stratifying nature of the cells, as seen by DAPI-stained nuclei stacked on top of each other. It could be inferred that higher stratification occurred as the concentration of Ca^{2+} increased from the control to 1.8mM. During proliferation of stratifying epithelia, the basal cells divide and push up on cell layers above, causing the topmost layers to flatten (Shojaei 1998). It was, therefore, hypothesised that transverse images revealing clear DAPI stained nuclei were less stratified than those with indistinct nuclear boundaries. Evidence of this can be seen in cells grown on transwell inserts (Figure 4.8), which is a better model than the coverslips for depicting proliferation/ stratification.

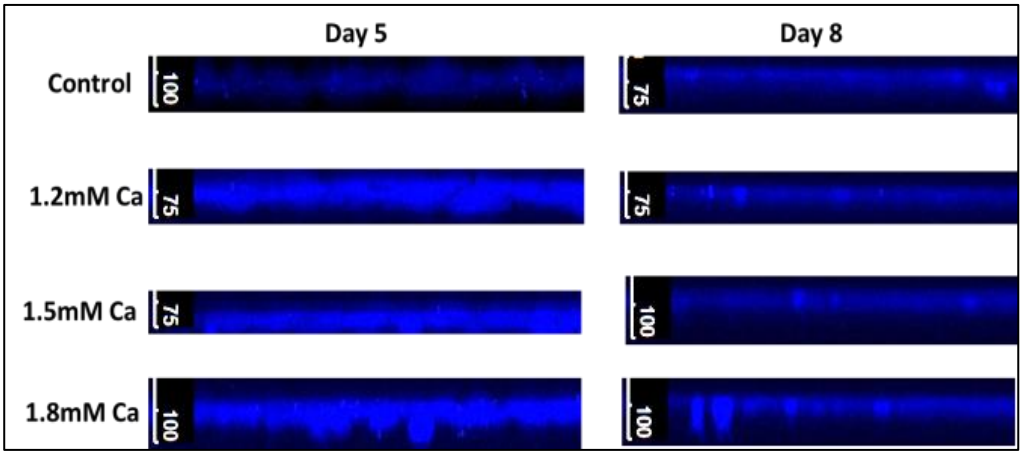

Figure 4.7 Representative confocal microscopic images of TR146 cells grown on collagen coated microscope coverslips in increasing Ca^{2+} fortified media, stained with DAPI (transverse plane). Distinct DAPI-stained nuclei could be seen by day 5, but unclear boundaries were observed as cells begin to flatten out by day 8.

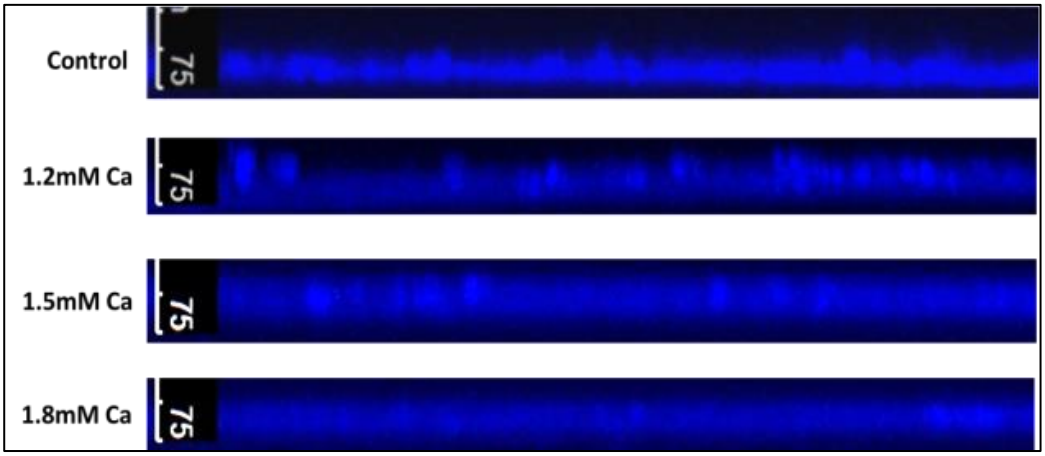

Figure 4.8 Representative confocal microscopic images of TR146 cells grown for 8 days on polycarbonate transwell inserts in increasing Ca^{2+} concentration, stained with DAPI (transverse plane). Indistinct cell boundaries at higher Caa^{2+} may account for higher stratification.

4.3.2.3 MTT assay

The MTT (3-(4,5-dimethylthiazol-2-yl)-2,5-diphenyltetrazolium bromide) assay, which is dependent on the reduction of MTT by NAD(P)H-dependent oxidoreductase enzymes in rapidly metabolising or dividing cells to the purple formazan, was adapted as an indirect method to measure cell proliferation. After subculture, cells were seeded unto 96 well plates in media fortified with increasing Ca^{2+} concentrations. This was slightly different from the normal MTT assay where the test substance is added to already adhered and growing cells. This was done to determine the effect of Ca^{2+} concentration on the adhesion, proliferation and viability of the cells over 7 days. From Figure 4.9 which shows MTT results for cells grown in continuous Ca^{2+} exposure, on day 1, there

was a decrease in proliferation of cells in increasing calcium ion concentrations compared to the control; however, by day 2, all concentrations except 2.8 mM showed higher or equal proliferation as the control. This trend can be explained based on the fact that membrane damage caused by trypsinisation requires maintenance of calcium homeostasis to further promote proliferation.

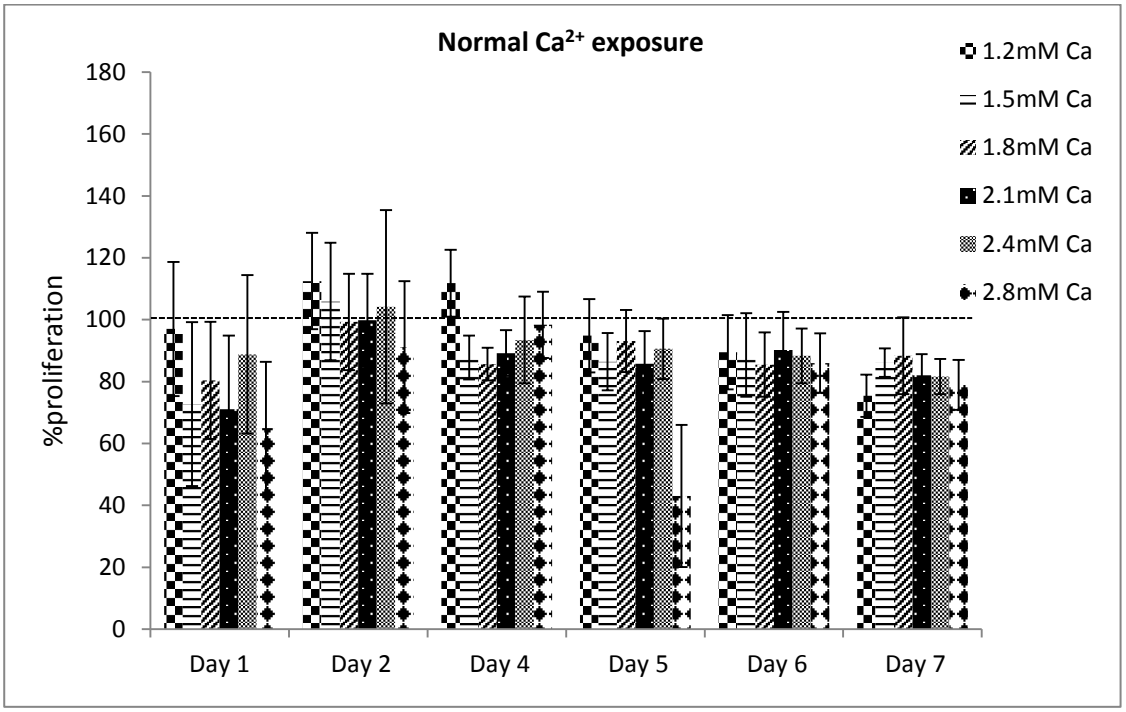

Figure 4.9 Results of MTT proliferation assay of TR146 cells grown in media continuously fortified with increasing calcium chloride concentrations, with respect to cells grown in normal (uncalcified) media used as control (n=24). Cells in 2.8 mM Ca^{2+} concentration showed significantly lower proliferation/ viability than the control.

However, after membrane restoration and cell adhesion had been achieved by day 2, there was an increase seen in cell viability or proliferation, even above that of the control. On the other hand, increased mitochondrial activity due to increased need for calcium cycling could have also prompted this rise in formazan absorbance values; and obscured the results. So this test may not have been as representative as expected. For MTT assay of cells grown in media intermittently fortified (every other 24 hours) with increasing Ca^{2+} alternating with normal control culture media (Figure 4.10), higher cell viability was observed on days where calcium ion was added (days 2, 5 and 7); as compared to days when fortified media was replaced by normal media (days 1, 3 and 5). For both continuous and intermittent exposures tested, cells in 2.8 mM Ca^{2+} concentration showed significantly lower proliferation and viability than the control.

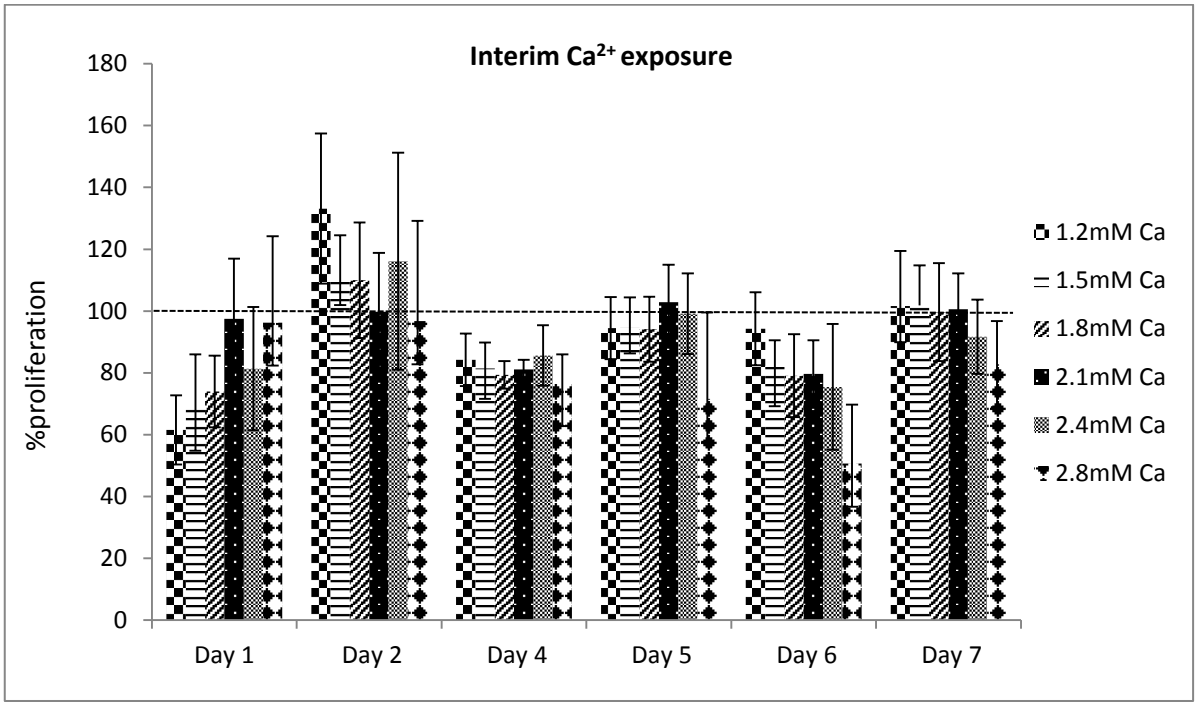

Figure 4.10 Results of MTT proliferation assay of TR146 cells grown in media intermittently fortified (every 24 hours) with increasing calcium chloride concentrations, with normal (uncalcified) media used as control (n=24). Cells in 2.8 mM Ca^{2+} concentration showed significantly lower proliferation/ viability than the control.

4.3.2.4 Haemocytometry

Results of cell count by haemocytometry are shown in Figure 4.11. Results showed that by days 1 and 4, cells in 1.5mM Ca^{2+} media were significantly more than the other concentrations and the control. This result ties in with the light microscopy results seen in Figure 4.3 & Figure **4.4** above. However, by day 7, there was no significant difference in the number of cells between all concentrations tested and the control.

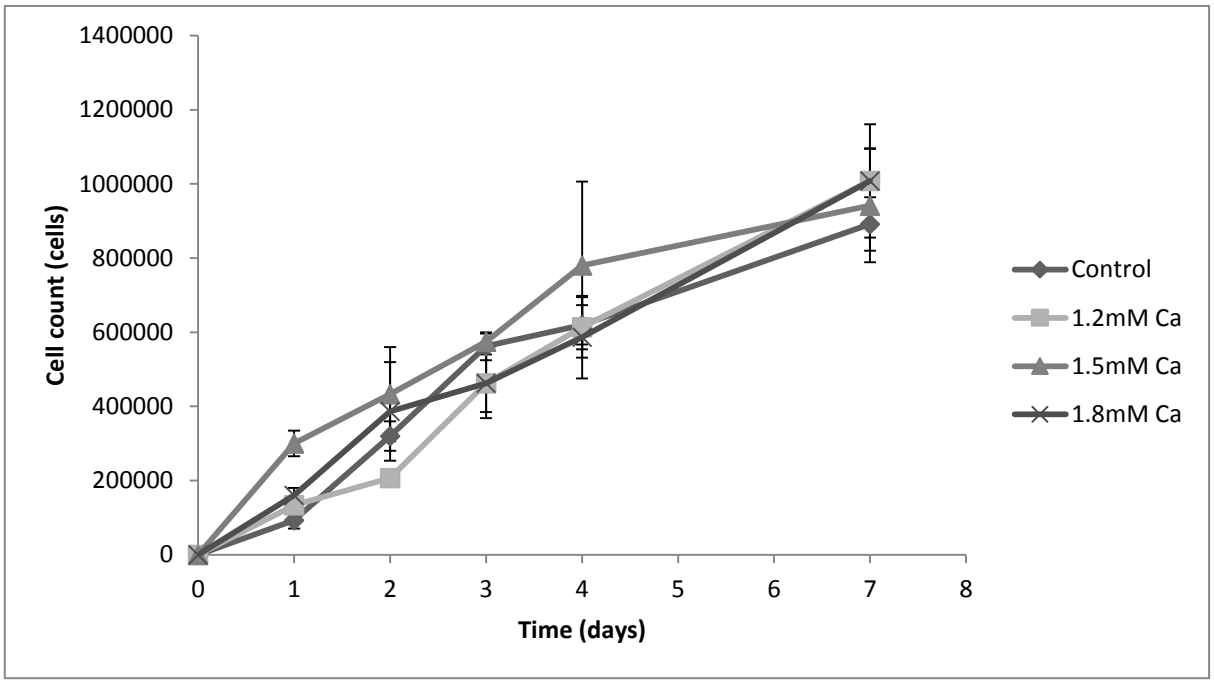

Figure 4.11 Cell count by haemocytometry results for proliferation of cells grown on 25cm2 T-flasks in media fortified with increasing calcium ion concentrations, with normal (uncalcified) media as control (n=12)

4.3.2.5 Transepthelial electrical resistance (TEER)

TEER is a sensitive index used to measure the integrity of intercellular junctions. It is based on Ohm's law and measures the resistance to current flow when a potential difference is applied between the formed cell layer and the culture medium (Benson et al 2013). TEER values in normal media (Figure 4.12) were seen to rise steadily to about 105 Ωcm^2 on day 5, which corresponds to the formation of a monolayer (Figure 4.4), after a slight fall in TEER values on day 7, values rose to 127 Ωcm^2 by day 9. A further fall in TEER values was recorded on day 14, with an increase on day 16 to 150 Ωcm^2. Thereafter, TEER values rose steadily to about 190 Ωcm^2 by day 26 and remained relatively constant until day 29.

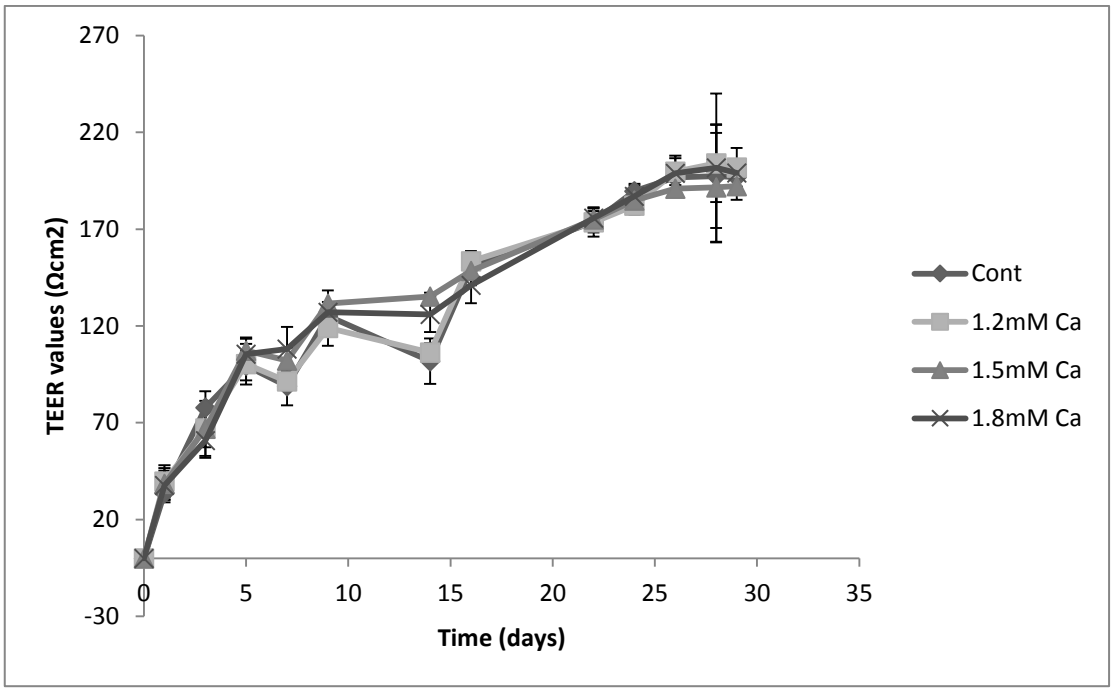

Figure 4.12 TEER measurements for TR146 cells grown on 24 mm transwell inserts in normal media. Results are the mean of single measurements of 6 different transwell inserts (n=6). Proliferation pattern of cells in lower Ca^{2+} concentrations differed from that at higher concentrations of 1.5-1.8 mM, giving indications of the point when a complete monolayer was formed and stratification commenced.

TEER values are expected to increase with age of culture and reach a plateau; with a significant fall in TEER associated with destruction of the cell layer and possible cell death (Gardner et al 1997, Prytherch et al 2011). However, the latter increase in the observed TEER values indicates the formation of tighter layers (Prytherch et al 2011). Such fluctuations have been previously reported in literature (Gardner *et al* 1997, Prytherch *et al* 2011). It has been hypothesised that subsequent increase in TEER values may coincide with completion of stratifying layer formation and expression of desmosomal proteins yielding tighter intercellular junctions. Immunohistlogical and further microscopic assays will be necessary to validate this hypothesis. In calcium fortified media (Figure 4.12) at 1.2 mM Ca^{2+} concentration, cells showed identical proliferation patterns to that of the control media, while fluctuations in TEER values were absent at 1.5 mM and 1.8mM Ca^{2+} concentrations. The addition of calcium to culture media is expected to enhance cell-to cell adhesion and therefore increase TEER values. However, there was no significant difference in TEER values of cells grown at all Ca^{2+} concentrations tested compared with the control; except at on days 7 and 14 when the fall in TEER values was observed for control and 1.2 mM cells.

4.3.2.6 Permeability of paracellular and transcellular markers

In order to verify that the proliferation and stratification enhancement observed from microscopic examination of TR146 cells grown in Ca^{2+} fortified media impacted on the permeation barrier provided by these cells, known paracellular transport markers (FITC dextran 4kDa, atenolol and propranolol HCl) and human insulin were employed for permeation studies. FITC-labelled dextran 4kDa (FD4) has been reported to permeate cell layers via the paracellular route without the need for permeation enhancers, and therefore served as a convenient marker (Nielsen *et al* 1999). Amount of FD4 that permeated the TR146 cell layers from apical to basolateral direction was quantified using fluorescent spectrophotometry, and method validation results are highlighted in the appendix. Table 4.4 displays the permeability parameters for all drugs through the TR146 cell layers. FD4 transport was seen to display a bell shaped curve, with cells grown in 1.2 mM & 1.5 mM Ca^{2+} concentrations exhibiting significantly lower permeation than the control. This result implies that tighter paracellular junctions were formed at these concentrations of extracellular Ca^{2+} and ties in with results observed from microscopic examinations and haemacytometry. However, the highest permeation of FD4 was observed at 1.8 mM Ca^{2+} concentration, and optimal Ca^{2+} concentrations were chosen at 1.2 - 1.5 mM. Furthermore, to confirm that FD4 was transported paracellularly, after permeation experiments, cell layers were washed and stained with DAPI, then viewed by confocal microscopy and representative results are shown in Figure 4.13. It can be observed that FD4 was localised to the cell membrane and was totally absent from the nucleus, as depicted by DAPI staining.

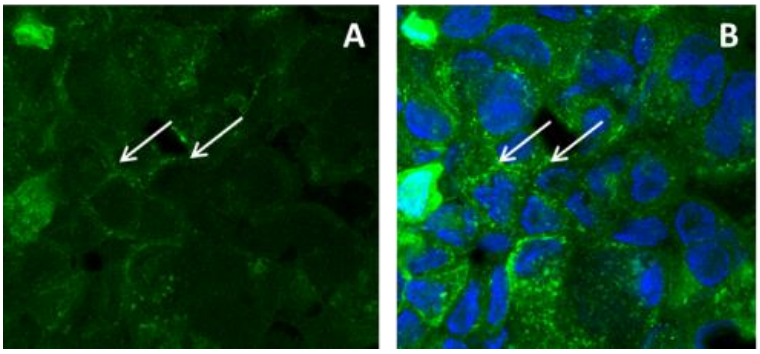

Figure 4.13 Representative confocal microscopic images of FITC-dextran 4kDa localisation (A) in the intercellular spaces of TR146 cells, showing paracellular transport (white arrows). DAPI stained nuclei (blue stain) (B) confirm the absence of the paracellular marker in the cell nucleus.

Table 4.4 Four hour permeability parameters of transport markers through TR146 cells grown in media fortified with increasing Ca^{2+} concentrations, normal media used as control (n=3). (*) represents the level of significant difference from the control ($p<0.05$)

Marker	Sample	% permeated	Papp ($x10^{-6}$)	Pcell ($x10^{-6}$)	% Recovery
FITC dextran 4kDa	Cont	19.10 ± 7.95	5.49 ± 1.72	9.17 ± 3.98	98.23 ± 3.77
0.5 mM	1.2 mM	8.76 ± 1.89**	3.70 ± 2.31	5.71 ± 5.16	98.33 ± 16.68
	1.5 mM	14.22 ± 1.68*	3.59 ± 0.54	4.74 ± 0.96	103.18 ± 4.32
	1.8 mM	23.06 ± 6.02**	6.20 ± 1.77	11.14 ± 5.72	115.48 ± 4.28
Propranolol HCl	Cont	36.25 ± 2.14	10.89 ± 0.43	22.32 ± 1.76	95.97 ± 4.24
0.1mM	1.2 mM	36.38 ± 1.63	10.77 ± 0.93	22.01 ± 4.00	99.77 ± 4.10
	1.5 mM	43.20 ± 2.06**	13.00 ± 0.12	33.32 ± 0.79	109.42 ± 6.32
	1.8 mM	40.66 ± 4.24**	12.53 ± 1.10	30.97 ± 6.67	101.11 ±8.89
Propranolol HCl	Cont	69.99 ± 9.52	13.51 ± 2.04	18.59 ± 3.69	85.21 ± 11.33
0.01mM	1.2 mM	84.05 ± 3.48***	17.45 ± 2.02	26.89 ± 4.89	93.68 ± 4.87
	1.5 mM	77.52 ± 5.07*	14.47 ± 1.53	20.37 ± 2.95	90.42 ± 1.77
	1.8 mM	78.77 ± 1.77*	15.80 ± 0.92	23.06 ± 1.94	92.83 ± 0.90

Atenolol	Cont	43.62 ± 8.39	3.27 ± 0.59	4.87 ± 1.22	110.52 ± 7.90
0.1mM	1.2 mM	52.58 ± 8.21*	3.87 ± 0.61	6.33 ± 1.64	115.70 ± 8.96
	1.5 mM	43.53 ± 4.49	3.49 ± 0.42	5.34 ± 0.96	94.49 ± 4.82
	1.8 mM	53.18 ± 3.42*	4.03 ± 0.32	6.70 ± 0.87	111.08 ± 2.87
Insulin	Cont	1.33 ± 0.26	0.84 ± 0.17	0.84 ± 0.17	74.74 ± 0.58
1mg/mL	1.2 mM	2.01 ± 0.14	1.06 ± 0.23	0.11 ± 0.23	102.26 ± 7.75
	1.5 mM	2.17 ± 0.38	1.22 ± 0.37	1.22 ± 0.37	104.21 ± 1.98
	1.8 mM	2.16 ± 0.10	1.12 ± 0.37	1.12 ± 0.37	103.44 ± 1.23

Propranolol is a highly lipophilic beta receptor blocker that quickly partitions into the lipid bilayer of cell membranes and is transported through the transcellular route (Dressman and Reppas 2010). Use of the hydrochloride salt reduces its lipophilicity, but the drug retained its high permeability with up to 85% drug permeation observed in 1.2mM cells after 4 hours (Table 4.4). There was a significantly lower permeability of propranolol observed in the control and 1.5mM Ca cells, than in the 1.2 and 1.8mM. Penetration of the highly hydrophilic beta-blocker, atenolol was much lower than that of propranolol as expected, with maximum permeation of <55% in all cells tested. The high hydrophilicity of atenolol restricts its transport to the paracellular route, and this is a better model to study paracellular transport than propranolol HCL. However, a similar trend to that seen with propranolol HCl permeation was observed. Control and 1.5mM cells had almost identical permeation profiles, and by 2.5hrs were significantly lower than 1.2 and 1.8mM cells; 1.2mM cells showed the highest permeation of atenolol. As the presence of calcium in the extracellular fluid is expected to enhance intercellular attachment and stratification by alignment and formation of desmosomes, it was expected that a greater barrier to permeability than the control would be seen with increasing Ca^{2+} concentrations; however this was not the case for these small molecules.

Results for permeation of recombinant human insulin are also highlighted in Table 4.4. It was observed that the control showed the highest barrier to insulin permeation than cells in all Ca^{2+} fortified media. However, confocal microscopic results of permeation of FITC labelled insulin through TR146 control cells (Figure 4.14) revealed that insulin permeated the cell layers via the transcellular route, and not the paracellular route. A similar finding was reported by Thompson et al (2011) who investigated the transport of FITC-insulin across Caco-2 cell lines (model for the small intestine) and reported localisation of FITC-insulin in the cell cytoplasm after 30 minutes exposure at 3µg/ mL. These results for insulin suggest that although paracellular integrity of TR146 cells may be enhanced in the presence of 1.5 mM Ca^{2+} added to the specialised culture media for these cells, this effect may not translate to the transcellular pathway, and effect on biochemical composition, protein expression and lipid barrier need to be further investigated for these modified cell lines.

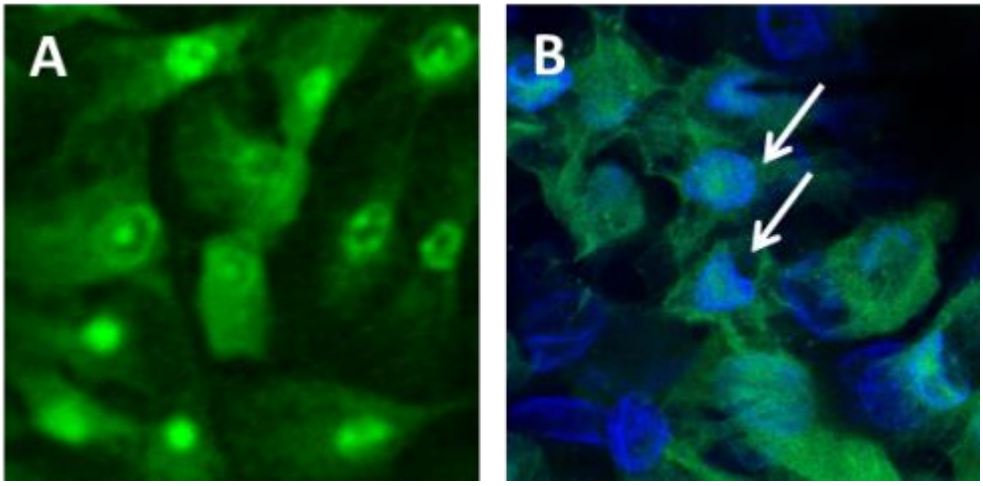

Figure 4.14 Representative confocal microscopic images of FITC-insulin (A) localisation and DAPI nuclear stain (B) on control TR146 cells. DAPI staining confirms localisation of FITC insulin in the nucleus (white arrows)

4.4 Conclusion

Ca^{2+} has been shown to regulate the proliferation and/ or stratification of cells *in vitro*, depending on the concentration employed. Results from microscopic examination revealed that addition of 1.5 mM Ca^{2+} to the specialised media for TR146 cells yielded enhanced proliferation and stratification of cells *in vitro*. Investigation of the effectiveness of this enhancement on the permeation barrier to paracellular transport of large and small molecules revealed a concentration dependent increase in the penetration barrier to large molecules like FITC-labelled dextran 4kDa which was transported via the paracellular route. For small molecules transported via the paracellular route (atenolol and propranolol HCl), and a large peptide transported via the transcellular route (insulin), no positive effect on enhancing the permeation barrier was observed, with 1.5 mM Ca^{2+} showing similar permeation barrier to the control; lower than other concentrations tested. Ca^{2+} enhancement of the barrier to paracellular transport was expected since calcium is a major component of desmosomal proteins that attach cells together. Thus, 1.5mM extracellular Ca^{2+} concentration was the optimal concentration that was able to enhance cell proliferation, cell stratification and enhance the permeation barrier of large paracellularly transported molecules. However, the effect of extracellular Ca^{2+} concentration on the biochemical composition, protein expression and lipid barrier; as well as on desmosome formation and alignment, need to be further investigated for these modified cell lines

Chapter 5

Protein quantification and characterisation

5.1 Introduction

5.1.1 Protein structure and aggregation

Proteins are macromolecules made up of polypeptides which comprise of amino acids linked by peptidic/ amide (-CONH-) bonds. Protein structure is determined by amino acid composition and sequence of the polypeptide chain, and this structure determines the function (or loss of function) of a particular protein (Walsh 2007). The primary protein structure refers to the precise amino acid sequence and location of disulphide linkages. The secondary structure describes the conformation of the polypeptide backbone in space, without taking into cognisance the amino acid sequence. These can be 'twisting' (α –helix) or 'zig-zag/ parallel' (β-Sheets). The tertiary structure of the protein relates to the three-dimensional positioning of all the constituent atoms of the peptide in space, to one another; and tertiary protein structure may be analysed by x-ray diffraction, nuclear magnetic resonance and electron microscopy (Walsh 2007). The quaternary protein structure is obtained when two or more protein molecules associate together to form dimers. Overall, protein structure is stabilised by hydrophobic interactions, electrostatic attractions as well as covalent linkages. Because most polypeptides consists of mainly non-polar amino acid residues, these residues align themselves in a manner that minimises interactions with the polar surrounding aqueous environment, thus causing the proteins to fold. Therefore, hydrophobic interactions contribute the most to stabilising the native structure and functionality of the protein (Walsh 2007). Electrostatic attractions include hydrogen bonding, Van der Waals attractions and ionic interactions, while covalent bonds are generated by the disulphide linkages present in the polypeptides. Protein functionality is closely related to its stability and conformation/ structure, therefore it is important to monitor changes (if any) in protein conformation during processing, manufacture and usage (Walsh 2007).

5.1.2 Insulin

The biologically active and circulating form of human insulin (Figure 5.1) is a polypeptide comprising 2 amino acid chains linked by two di-sulfide linkages afforded by cysteine. It contains

51 amino acids; 21 amino acids make up the A chain and 30 make up the B chain; with molecular weight of 5800 Da. A di-sulphide linkage exists within the A chain (Sarmento et al 2006). Insulin is administered subcutaneously for the management of insulin-dependent diabetes in patients whose pancreas do not produce insulin, or those whose cells have low insulin sensitivity. It is also the most important hormone in the regulation of glucose homeostasis in the body (Xu *et al* 2006).

Figure 5.1 Primary structure of insulin showing A and B polypeptide chains, with inter- and intra-molecular di-sulphide bridges (Snyder *et al* 2012)

Insulin was isolated in 1921 by Frederick Banting and Charles Best in John Macleod's laboratory in Canada. The protein has since been administered by the parenteral route due to stability and bioavailability challenges associated with oral administration. However, attendant complications related to insulin parenteral therapy have driven the on-going search for non-invasive methods of insulin delivery.

5.1.3 Circular dichroism (CD)

Circular dichroism (CD) is a spectrophotometric method that analyses changes in protein secondary structural conformation in the liquid state, using circularly polarised light (Whitmore and Wallace 2004). Plane polarised light comprises two circularly polarised components of equal magnitude - one rotating clockwise (right-handed) and the other anti-clockwise (left-handed). If these components are not absorbed upon passage through a sample, or if they are equally absorbed, the resulting radiation would occur in the same plane (Figure 5.2). If however, the two components are absorbed to different magnitudes, the resulting radiation will be skewed in the direction of the larger component and would be said to exhibit "elliptical polarisation" (Kelly et al 2005).

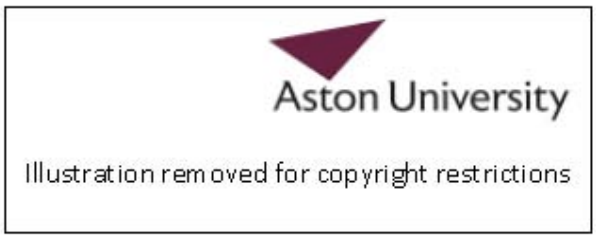

Figure 5.2 The circular dichroism effect. I: Equal absorption of left and right circularly polarised components of plane polarised light resulting in plane polarised radiation. II: Absorption of components to different magnitude resulting in skewed/ elliptical polarisation (Kelly *et al* 2005)

Thus, CD measures the difference in radiation of these two components, or the elliptical polarisation, and can only be applied to materials/ compounds with differential absorption of circularly polarised light. Spectropolarimeters measure the difference in absorbance (ΔA) of left (AL) and right (AR) circularly polarised components, (ΔA = AL – AR). This change is defined in terms of ellipticity, ɵ.

The advancement in production of therapeutic proteins by recombinant technologies has advanced science; but this has also exposed some challenges. Some of these include short serum half-life, immune responses and/ or reduced bioavailability of the protein. These occur mainly because production, purification and storage processes could affect the stereochemical structure of the protein causing unfolding and/ or aggregation (Bertucci et al 2011). Thus, it is important to carry out techniques that monitor these changes whenever they are likely to occur.

Different information may be extracted from CD studies and they include: composition of the secondary structure of the protein, tertiary structure fingerprint, co-factor binding sites integrity, conformational changes in proteins, overall structural features and protein folding (Kelly et al 2005). For the purpose of this work, discussions will be limited to secondary structure and conformational changes. Figure 5.3 shows the CD spectra of different protein secondary structures in the far UV region. Databases comprising information on the structure of various proteins whose

structures have been ascertained by methods such as x-ray crystallography etc. have been developed. When the data from a CD spectrum is inputted into the database, the contribution of each protein molecule is used to elucidate the overall secondary structure of the protein (Whitmore and Wallace 2008).

Figure 5.3 Circular dichroism spectra showing representative secondary structures of some proteins and peptides (Greenfield (2007), data supplied by W. C. Johnson)

Generally for insulin, α-helix shows a maximum at about 193 nm, and two minima at 208 and 222 nm; anti-parallel β-sheets show one maxima at 195 nm, and a minimum at about 216 nm; while disordered proteins are characterised by low ellipticity above 210 nm and negative bands near 195 nm (Chen *et al* 1974, Bouchard *et al* 2000, Greenfield 2007).

5.1.4 High performance liquid chromatography (HPLC)

HPLC is an analytical technique used for the separation, isolation and quantification of components of a sample (Aguilar 2004). HPLC is often employed for the quantitative analysis of pharmaceutical products because chemical methods (such as iodometry or colorimetry) and some spectrophotometric methods commonly employed have limited specificity, with chemical methods showing lower precision; while gas chromatography cannot be effectively utilised because of the

thermolabile nature of many pharmaceuticals (Nachtmann 1979, Roškar and Lušin 2012). HPLC also allows for rapid analysis of different drugs and their metabolites (Chan et al 1986). As a process, HPLC involves the introduction of a small volume of liquid sample into a column packed with minute particles (the stationary phase), and a solvent system (the mobile phase) is used to force the sample through the column under high pressure with the aid of a pump. The components of the liquid sample are then separated from each other by the stationary phase based on physical and/ or chemical interactions of the sample with the stationary phase and/ or the mobile phase (Aguilar 2004). The separated components are transferred at the end of the column through a detector, which measures their signal and produces the results as a liquid chromatogram. The most common detectors used being UV, fluorescence and refractive index detectors.

There are two phases of HPLC; normal phase HPLC utilises a highly polar stationary phase and a non-polar mobile phase, while reverse phase HPLC (more commonly used) employs a non-polar stationary phase and a less polar solvent system as the mobile phase. Two elution techniques are also employed and they include the isocratic elution, in which the composition of the mobile phase remains constant throughout the chromatographic run, and gradient elution where there is a change in mobile phase composition with time, leading to increasing elution, strength throughout the run. Gradient HPLC is preferred because it can effectively separate samples containing mixtures of solutes with various retention capacities (Aguilar 2004). However, isocratic HPLC can be used for analysis of simple solutions conveniently and is less expensive.

HPLC has found increasing applications in the isolation and purification of peptides and proteins in recent years. Proteins like insulin have been quantified using biological assays in the past. These assays, though specific, were limited by their ineffectiveness at detecting very low doses, and could not identify contaminant or decomposition products; hence, the increased use of HPLC (Grego and Hearn 1981). However, the chemical nature and size of proteins makes their HPLC difficult because various factors such as temperature and pH need to be optimised (Rajan et al 2006, Moussa et al 2010). The official monographs (British Pharmacopoeia, United States Pharmacopoeia, European Pharmacopoeia) contain methods for the detection and assay of insulin by HPLC, but

these methods require extended runtimes, or the use of elevated temperatures (Rajan et al 2006, Sarmento et al 2007). Various researchers have also employed HPLC for quantification of insulin in literature (Table 5.1) using buffered (Oliva et al 2000, Rajan et al 2006, Moussa et al 2010, Makhlof et al 2011, Yilmaz et al 2012) and unbuffered mobile phases (Sarmento et al 2006, Amidi et al 2008). However, these methods require either the use of elevated temperatures, specialised detectors or resulted in long run times. More importantly, difficulty in reproducing methods obtained from published literature in different laboratories using different equipment is a constant challenge. The onus, therefore, is on the researcher to develop and validate a suitable reproducible method for quantification of these proteins. The said method should ideally be carried out at room temperature, with as few variables as possible.

The aim of this work, therefore, was to describe our implementation of a literature derived method and step-by-step progression within our laboratory to establish a simple, rapid and effective method for quantification of insulin by HPLC, which would be validated by ICH guidelines (ICH 1996) and can be reproduced in any laboratory using simple UV detectors at room temperature. Furthermore, because changes in protein structure/ conformation that might occur during processing affect protein stability and functionality, the effect of compaction pressure on insulin secondary structures was also investigated.

Table 5.1 Some HPLC methods for insulin quantification in literature

Column	Mobile phase	Detector/ wavelength	Reference
RP-Intersil C18 column (250mm x4.6mm)	Acetonitrile / 0.1M NaH_2PO_4/0.05 M Na_2SO_4 (30:35:35, v/v, pH 2.5).	UV/visible detector 214nm	(Makhlof *et al* 2011)
RP C18 column	Gradient elution with Acetonitrile/ 0.1% trifluoroacetic acid (TFA)	UV detector 214 nm	(Sarmento *et al* 2006)
C18 column (300x7.8mm i.d; 5µm particles with poresize 300Å)	0.2M sodium suphate buffer (pH 2.3) and acetonitrile (74:26).	UV detector 214nm	(Oliva *et al* 2000)
C18 column (150x4.6mm; 5 µm particles)	Solutions A and B (60:40v/v). A: 1mmol Na_2S0_4 and 0.2% triethylamine in water, pH adjusted to 3.2 by phosphoric acid. B:acetonitrile	UV turnable absorption detector 214 nm	(Rajan *et al* 2006)
C-18 (30x4.6, 3µm)	Solutions A and B (48:52v/v) 45-50degC. A: 56.8 Na_2S0 in WFI, adjust pH to 2.3 with o-phosphoric acid and filter. B: 28.5g Na_2S0 in 400mL WFI, adjust pH to 2.3 with o-phosphoric acid; make up to 1L with WFI; and up to 2L with acetonitrile. Flow rate 1mL/min	UV detector 214 nm	(Moussa *et al* 2010)
C18 (5µm, 4.6 x 250mm)	0.2M sodium sulphate/ acetonitrile (pH adjusted to 2.4 with phosphoric acid), 25:75v/v, flow rate 1.2mL/min	Diode array detection 206 nm	(Yilmaz *et al* 2012)

5.2 Materials and methods

5.2.1 Materials

Human recombinant insulin powder, phosphate buffered saline (PBS) tablets, triethylamine and anhydrous sodium sulphate were purchased from Sigma-Aldrich, UK; while o-phosphoric acid and hydrochloric acid were purchased from Fisher Scientific, UK. All water used was double distilled.

5.2.2 Methods

5.2.2.1 High performance liquid chromatography (HPLC) assay

Gradient RP-HPLC was employed for quantitative analysis of insulin in solution and was adapted from Rajan *et al* (2006). A Dionex 1100 autosampler (AS50) system, with gradient pump (GP50), UV detector (UVD 170U) set at 230 nm was used, employing a reversed phase RP-C18 analytical column (Phenomenex 110A, 150x4.6 mm, 5 µm). The mobile phase consisted of solution A: 1mmol sodium sulphate and 0.2% v/v triethylamine in water, pH adjusted to 3.2 with o-phosphoric acid; and solution B: acetonitrile; both filtered under vacuum and sonicated (Rajan et al 2006). A gentle gradient was run from 75:25 v/v to 60:40 v/v compositions of A:B over 5 mins, and then maintained at 60:40 v/v for 2 minutes. Pump flow rate was 1.5 mL/min, with sample injection volume of 20 µL. The maximum wavelength of absorption of insulin had been pre-determined using a Unicam UV-visible spectrophotometer. Finally a rectilinear (Beer-Lamberts) calibration curve was established for insulin within a concentration range of 10-1000 µg/mL dissolved in 0.01N HCl.

5.2.2.2 HPLC assay validation

The HPLC method was validated according to ICH guidelines in terms of specificity, accuracy, precision, linearity, limits of detection/ quantification and stability of insulin solutions (Sarmento et al 2006, Moussa et al 2010).

5.2.2.2.1 Specificity (identification and assay)

20 µL of 200 mg/mL insulin and 0.01N HCl solutions respectively were separately injected into the HPLC system, retention time and resulting chromatograms were recorded. Insulin percentage recovery (the calculated concentration of insulin relative to the actual concentration used) was calculated using the regression equation obtained from linearity experiments below.

5.2.2.2.2 Linearity

A Beer-Lamberts calibration curve was developed by plotting mean peak area against insulin concentration. Linearity was estimated by computing the regression line of the calibration curve for insulin concentration from 10-1000 µg/mL; the correlation coefficient (R^2) was calculated.

5.2.2.2.3 Accuracy

20 µL aliquots of standard solutions were injected into the HPLC system and the protocol described for linearity above followed. The areas under the curve for insulin were recorded and the percentage recovery was calculated using the regression equation.

5.2.2.2.4 Precision

Operator precision was determined by developing the insulin calibration curve in triplicates. The area under the curve was calculated by the HPLC software and relative standard deviation (RSD) was calculated using the equation below:

$$RSD = \frac{standard\ deviation}{mean} \quad . \quad . \quad . \quad . \quad . \quad . \quad \text{(Equation 5.1)}$$

Calibration curves were repeated on different days (n=6 or 9) using freshly prepared mobile phase and the RSD calculated.

5.2.2.2.5 Limit of detection (LOD) & limit of quantification (LOQ)

The LOD and LOQ were determined by the signal-to-noise ratio method (Xu *et al* 2002, Moslemi *et al* 2003). 20 µL of 0.01 N HCl blank was injected into the HPLC system twenty times and the mean peak area recorded. The standard deviation of the recorded peak areas was multiplied by 3

and 10 to calculate the LOD and LOQ respectively. This was repeated twice for two different samples of the blank, in order to validate the obtained results (Moussa et al 2010).

5.2.2.2.6 Inter-laboratory method validation

The validated method was further validated by an independent operator in a different laboratory using a different HPLC system on different days to establish method reproducibility.

5.2.2.3 Stability of insulin solutions

1000 μg/mL insulin solution was freshly prepared in triplicates and immediately analysed on the HPLC system. The solutions were stored in the fridge (2 - 8 °C) and quantified after three days (72 hrs). The peak areas and RSD were recorded.

5.2.2.4 Circular dichroism (CD)

The far UV circular dichroism spectrum of insulin from 290 - 190nm was recorded on a Jasco J-715 spectropolarimeter (Tokyo, Japan). The sample concentration was 1mg/mL insulin in PBS, pH 7.4. The cell path length was 0.01 cm, 2 nm bandwidth, 200 nm/min scan rate, data acquisition interval 0.5 nm and 8 accumulations. To determine the effect (if any) of tablet compaction pressure on insulin conformation, CD data was also collected for neat insulin tablets compressed at 10 and 30 kN compaction pressure respectively, dissolved in sufficient PBS to yield a concentration of 1 mg/mL. Mean residue ellipticities, $[\theta]_\lambda$ were calculated from the equation:

$$[\theta]_\lambda = \theta_\lambda M_0 Cl \quad . \quad . \quad . \quad . \quad . \quad . \quad . \quad \text{(Equation 5.2)}$$

where θ_λ is the observed ellipticity at wavelength λ, M_0 is the residue molecular weight for the protein calculated as 116 for insulin, C is the protein concentration in g/mL and l is the optical path length in cm (Goldman and Carpenter 1974). The composition ratio of the protein secondary structure was computed using CDSSTR algorithm of the online CD analysis software, Dichroweb (Whitmore and Wallace 2004). Statistical analysis of reliability/ validity of CD analysis were carried out using normalised root mean square deviation (NRMSD) and comparison plots of calculated and experimental spectra generated.

5.2.2.5 Fourier transform infra-red (FTIR) spectroscopy

To identify processing effects on the functional groups present in insulin pre- and post-compression, FTIR spectroscopy was carried out on insulin powder and neat tablets compacted at 10 and 30 kN using a Nicolet IS5 FTIR spectrometer equipped with an iD5 attenuated total reflectance (ATR) diamond from Thermo Fisher Scientific (Massachusetts, USA). A small mass of dry powder was lightly sprinkled (or tablet gently placed) on the lens and after measurements the accompanying software identified the available peaks.

5.3 Results and discussion

5.3.1 HPLC method development for quantification of insulin

The HPLC method development began with a method adapted from Rajan et al (2006), employing an isocratic elution using a mobile phase comprising 40 volumes of solution A (1mmol sodium sulphate and 0.2% triethylamine (TEA) in water, pH adjusted to 3.2 with o-phosphoric acid), and 60 volumes of solution B (acetonitrile); UV detection at 214 nm. This method was employed instead of the USP or BP methods, because unlike these official methods that were run at elevated temperatures, the chosen method could be run at room temperature and had less than half the retention time expected from the BP and USP methods. Thus, it minimised the possible variables in the HPLC system. Using this system, insulin eluted almost immediately at about 1 min (Figure 5.4).

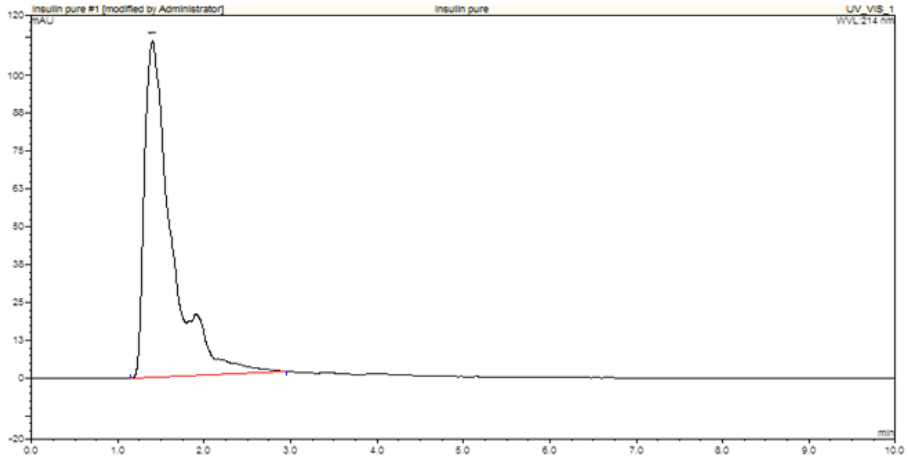

Figure 5.4 Representative chromatogram of 0.5mg/mL insulin in 0.01N HCl at 214nm. Insulin peak was poorly resolved and eluted off the column in about 1 min

The resulting peak was poorly resolved with an accompanying hump. Running a blank solution (containing 0.01N HCl) on the HPLC system showed solvent front coming off the column at about the same retention time as the drug (Figure 5.5). Thus, the hump on the insulin chromatogram resulted from the overlapping of the drug peak with that of the solvent front (Xu et al 2006). RP-HPLC exploits the interactions between the hydrophobic regions of insulin and that of the stationary phase (Moslemi et al 2003). Fast elution of insulin off the column implied very low affinity of insulin for the non-polar column. Generally in reversed phase HPLC, the interaction of hydrophobic analyte with the n-alkyl chain of the column would lead to longer retention of the analyte on the column. But the presence of steric hindrances in large molecules like insulin may restrict access of insulin molecules to the pores of the stationary phase where these interactions take place (Gerber et al 2004). Also, the presence of polar groups (-NH2, COO–) in the insulin moiety would increase the affinity of insulin for the highly aqueous mobile phase, and result in fast elution of insulin. These factors could account for the observed immediate elution of insulin off the column (Aguilar 2004).

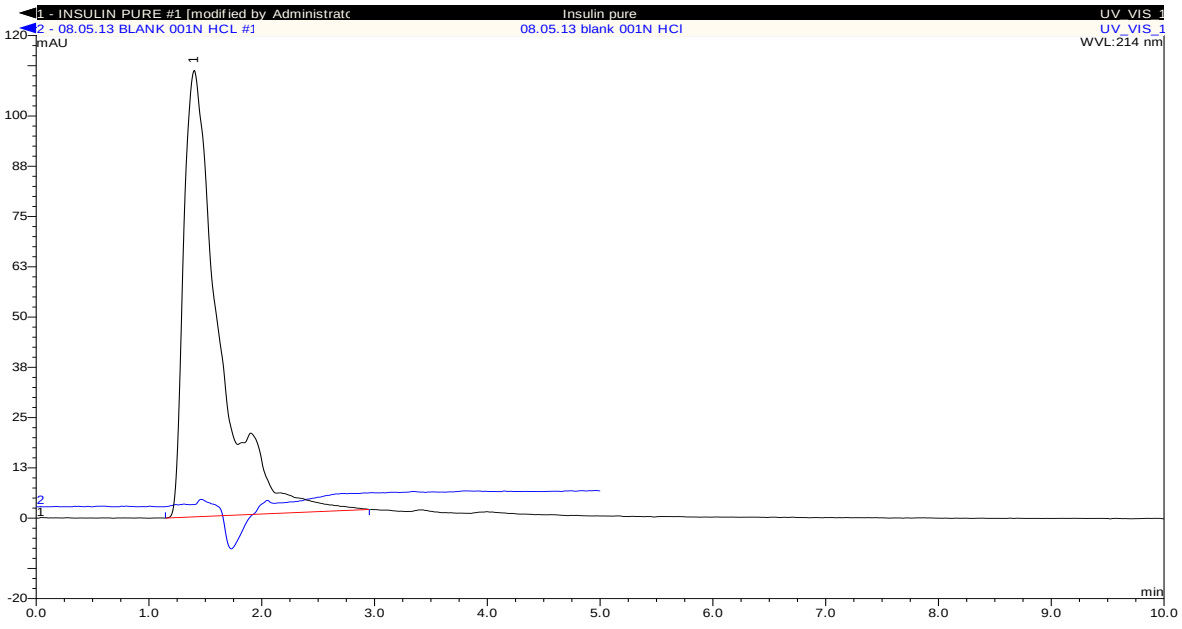

Figure 5.5 Chromatogram showing elution of the solvent front (blue line) at about the same time as insulin (black line), resulting in poor resolution of the insulin peak.

According to the BP 2013, "insulin is practically insoluble in water" (despite the presence of –OH and –NH bonds in the comprising amino acids); however, some authors have reported insulin as

highly water soluble (Xu *et al* 2006). It was expected that hydrophobic insulin would interact with the non-polar column (reverse-phase HPLC) and would, therefore, have a longer retention time on the column (Aguilar 2004). As this was not the case as discussed above, reducing the non-polar organic modifier in the mobile phase would reduce the interaction of insulin with the mobile phase (increased mobile phase polarity), thereby increasing insulin's interaction with the non-polar column; ultimately resulting in an increase in insulin retention time (Lindsay and Kealey 1987). Thus, various mobile phase compositions (from 50:50 to 75:25) were employed in an attempt to increase insulin's retention time, and thereby separate the drug peak from that of the solvent front.

A mobile phase composition of solution A:B 70:30 resulted in an increase in insulin retention time from 1 to 2 minutes. However, this minimal shift was not sufficient to completely separate the insulin peak from that of the solvent front. This minimal shift in insulin retention time despite a 10% change in mobile phase composition could be attributed to the large size of insulin molecules, as large molecules may not easily enter the pores of the column to increase column retention (Gerber et al 2004) .

A further reduction in the amount of the organic modifier used would be expected to further increase the retention time of insulin for reasons discussed above. However, the final composition of the mobile phase would be highly aqueous and would not effect a complete separation of other impurities or degradation products when utilising this method for quantification of insulin from samples. Moreso, highly polar aqueous phases may result in poor retention and separation due to the collapse of the octadecyl alkyl side chains in the stationary column (Olsen 2001). Xu et al (2006) reported an increase in insulin retention time with increasing acetonitrile content of the mobile phase.

At this point, it became necessary to run a blind HPLC to determine the exact mobile phase composition where insulin elutes off the column. Thus, a gradient HPLC was run from 80 – 20% for solution A and 20 – 80% for solution B. From Figure 5.6, it was observed that insulin eluted at about 6 minutes which was equivalent to mobile phase composition of 60:40 for solution A:B. Thus, insulin was eluted off the column immediately the mobile phase composition turned to 60:40,

and using an isocratic system would always produce a poorly resolved peak because of interference from the solvent front. Also the resultant peak caused an upward shift in the baseline, probably due to the changing gradient.

In order to obtain a better resolved insulin peak, we further investigated the role of the mobile phase additives in the HPLC quantification. Triethylamine (TEA) was used in the mobile phase to facilitate end-capping of the free silanol groups on the reversed phase column, resulting in the prevention of band tailing in HPLC (Dolan and Snyder 1989, Li et al 2000). However, TEA is easily degraded and has been implicated to interfere with UV absorption because it has a high UV-cut off above 190 nm. This means that TEA can be picked up by the detector and would interfere with the resolution of obtained peaks. Because the column had been described as endcapped by the manufacturers, it would be irrelevant to retain TEA in the mobile phase if it was interfering with the results.

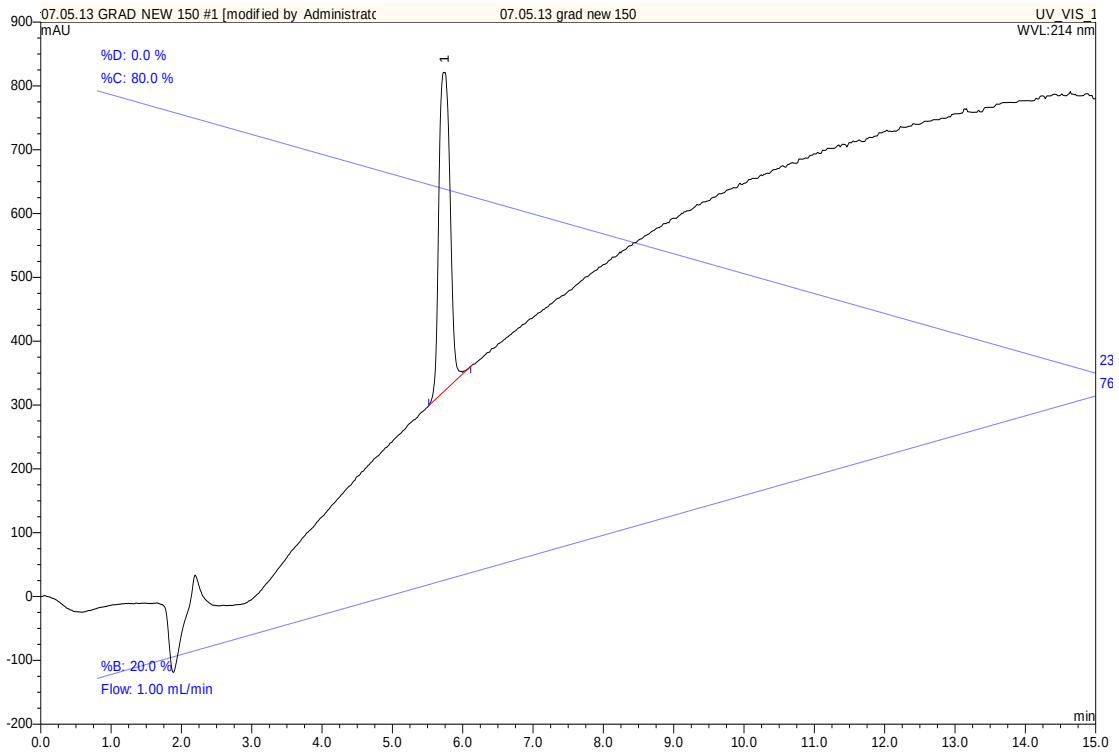

Figure 5.6 HPLC chromatogram showing insulin elution at 6 minute upon gradient elution from solution A:B 80:20 to 20:80. An upward shift in the baseline may be due to the changing gradient.

Thus, TEA was removed from solution A and a gradient HPLC repeated with solution A (1mmol sodium sulphate in water, pH adjusted to 3.2 with o-phosphoric acid) 80 – 20% and solution B (acetonitrile) 20 – 80%. The resulting chromatogram produced no peak for insulin even after 30

minutes, signifying the importance of TEA for insulin elution. Thus, although a column may be claimed to be end capped by the manufacturers, this process might not completely mop up the free silanol groups. This, as well as column use and age, would necessitate the addition of a moiety like TEA to compete with the analyte for the free silanol groups on the column.

Following the unsuccessful reproduction of the HPLC method adapted from the journal article, a return to first principles was necessary, and a UV scan was run for 0.5 mg/mL insulin in 0.01N HCl. The spectrum displayed two maximum wavelength peaks - a major peak at 230 nm and a smaller peak at 275 nm. Thus, a HPLC gradient (80:20 to 20:80) was run at 214, 230 and 275 nm respectively. From Figure 5.7, it can be seen that at 214 nm, there was an upward shift in the baseline, at 275 nm, the insulin peak was highly reduced; while at 230 nm, a well resolved peak with a relatively stable baseline was achieved. Thus, 230 nm was chosen as the wavelength for recombinant insulin detection.

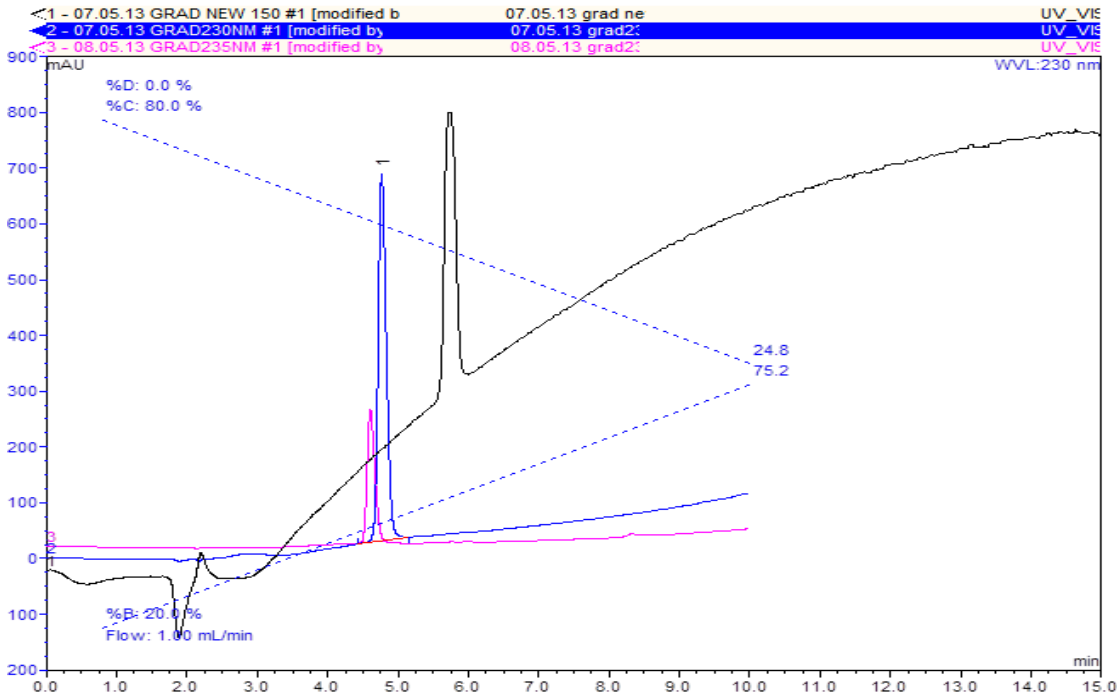

Figure 5.7 Chromatograms showing insulin elution at various wavelengths: 214 nm (black), 230 nm (blue), and 275 nm (pink).

Because insulin eluted off the column immediately when the mobile phase composition was 60:40, and this early elution resulted in a poorly resolved peak due to the concurrent appearance of the solvent front, isocratic HPLC could not be applied to this system. A gradient (80:20 to 20:80 v/v) HPLC for insulin was run at 230 nm and resulted in a well resolved peak with a relatively stable

baseline, and no interference from the solvent front, and elution after about 4 minutes was obtained (Figure 5.8). After it had been established that insulin eluted off the column at 60:40 mobile phase composition, it was not necessary to continue the steep 80:20 to 20:80 gradient, it seemed necessary to employ a gentle gradient. To determine the optimum gradient for separation, the following gradients were run:

Option 1	**Option 2**
0-5 mins: 75:25 - 50:50	0-5 mins: 70:30 - 45:55
5-7 mins: 50:50 - 50:50	5-7 mins: 50:50 - 50:50
7-10 mins: 50:50 - 75:25	7-10 mins: 50:50 - 75:25

The resulting chromatogram for option 1 showed a well resolved peak, completely separated from the solvent front, with a slight shifting of the baseline. Modification of the gradient to option 2 resulted in a poorly resolved peak, which eluted off the column very fast and showed solvent front interference. Thus, the first protocol was maintained.

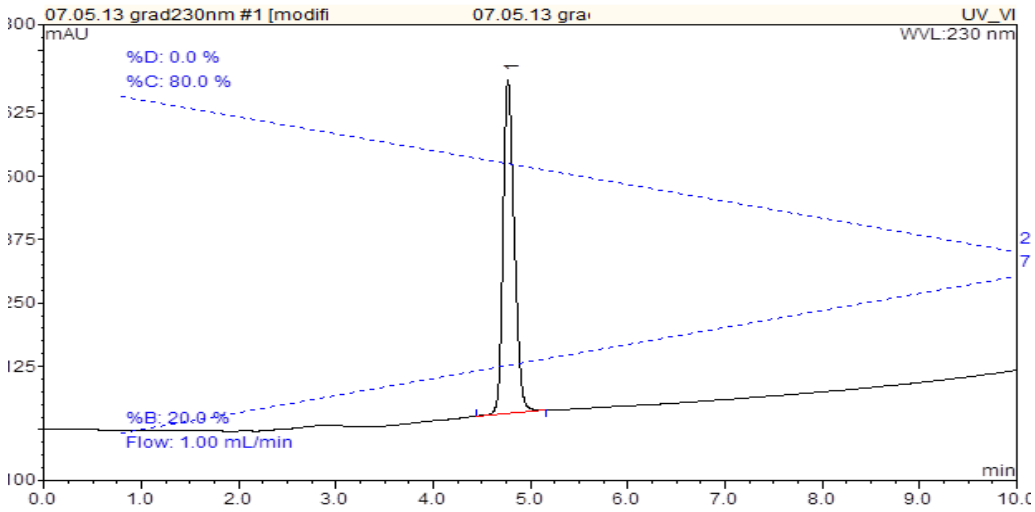

Figure 5.8 Chromatogram showing gradient elution of insulin from mobile phase composition A:B of 80:20 to 20:80 at 230 nm UV detection wavelength

Finally, to achieve a sharper peak, the flow rate was increased to 2 mL/min. A sharper insulin peak was achieved but it eluted off the column at 2 minutes. Gerber *et al* (2004) reported that increased flow rate could reduce retention times, increase baseline noise and produce narrower peaks.

Therefore, flowrate was maintained at an average of 1.5 mL/min. The chromatogram for the final method is shown in Figure 5.9 below:

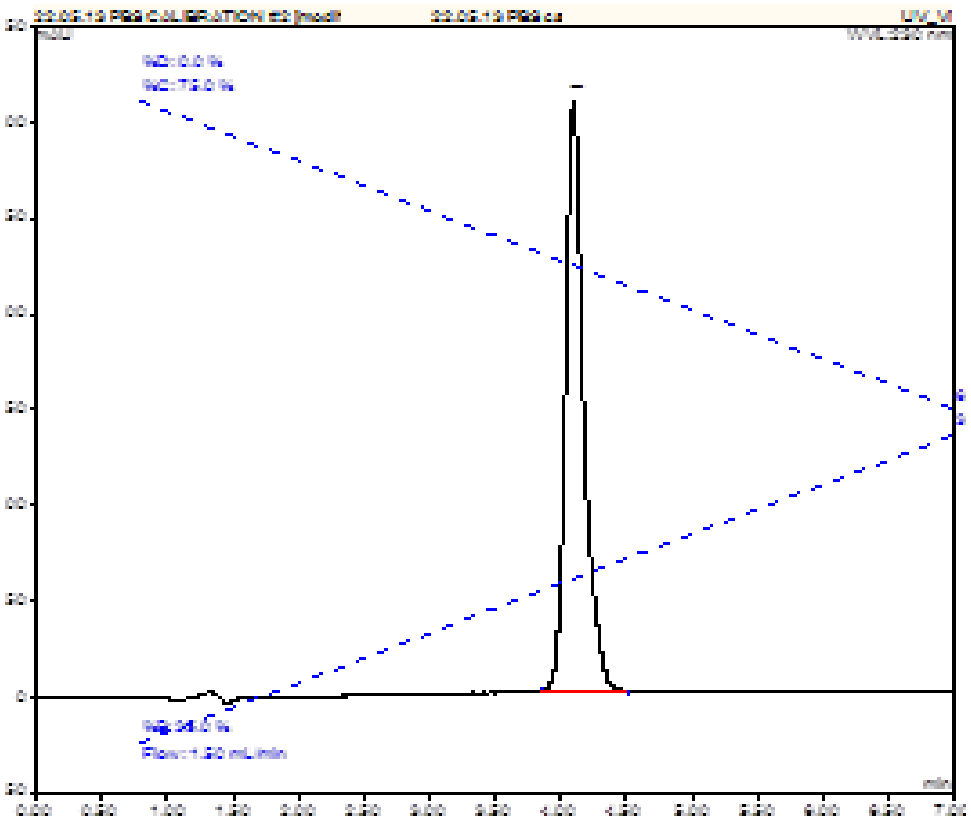

Figure 5.9 Representative chromatogram showing the developed method for insulin elution employing a gentle gradient at 230 nm detection wavelength and 1.5 mL/min flow rate

5.3.2 HPLC assay validation

5.3.2.1 Specificity

To investigate the specificity of the HPLC method, 20 µL each of insulin in 0.01N HCl and the blank (0.01N HCl) were separately injected into the HPLC and chromatograms developed. Figure 5.10 shows the chromatograms of insulin and the blank run in triplicate. From this chromatogram, the insulin peak was well resolved with retention time of 3.84 ± 0.08, there was no interference from the solvent front which eluted at 1.12 ± 0.04 mins (Table 5.2). It would be necessary to test all excipients of the formulated tablets to ensure specificity of the method for insulin in the presence of contaminants.

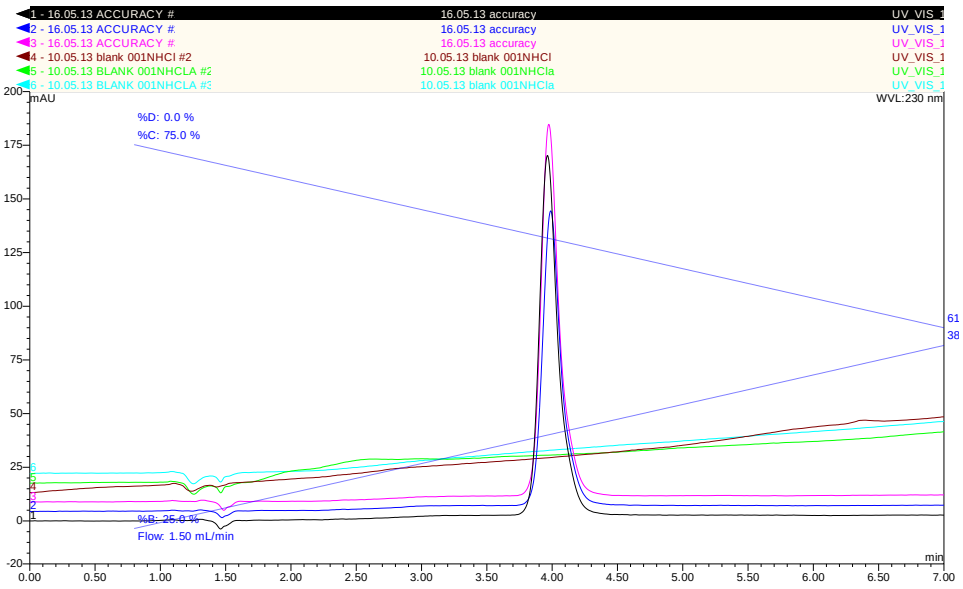

Figure 5.10 Representative chromatograms showing selectivity and instrument precision of HPLC method. Triplicate measurements of 500 µg/ mL insulin solution produced identical peaks that were well resolved from that of the blank.

According to Gupta *et al* (2012), an assay shows specificity when the signal measured from the test compound show no interference with signals from other excipients at the test wavelength. As an evaluation of accuracy, insulin concentrations ranging from 50 – 500 µg/mL were used to calculate the percentage recovery of insulin using the described method. The mean absolute recovery value for insulin was 100.89 ± 1.40% (Table 5.4 below). These results connote that the developed method can quantify insulin effectively. However, the effect of dosage form excipients on the recovery of insulin using this method will need to be investigated (Xu *et al* 2006).

5.3.2.2 Linearity

A Beer-Lamberts calibration curve (Figure 5.11) was established for insulin over a concentration range of 10-1000 µg/mL by plotting the peak area from the chromatograms against the concentration. The regression analysis gave the equation of the line as y = 0.0543x - 1.0026, with R^2 = 0.9993. Parameters of the regression coefficient are presented in Table 5.3. The high correlation coefficient connotes a linear relationship between peak area and insulin concentration within the proposed range (Epshtein 2004, Sarmento et al 2006).

Table 5.2 Specificity of insulin HPLC method

S.N.	Sample	Retention time (min)	% RSD
1	Insulin	3.84 ± 0.08	2.08
2	Blank (0.01N HCl)	1.12 ± 0.04	3.66

Therefore, the concentration of insulin in any sample can be calculated from this curve using this method.

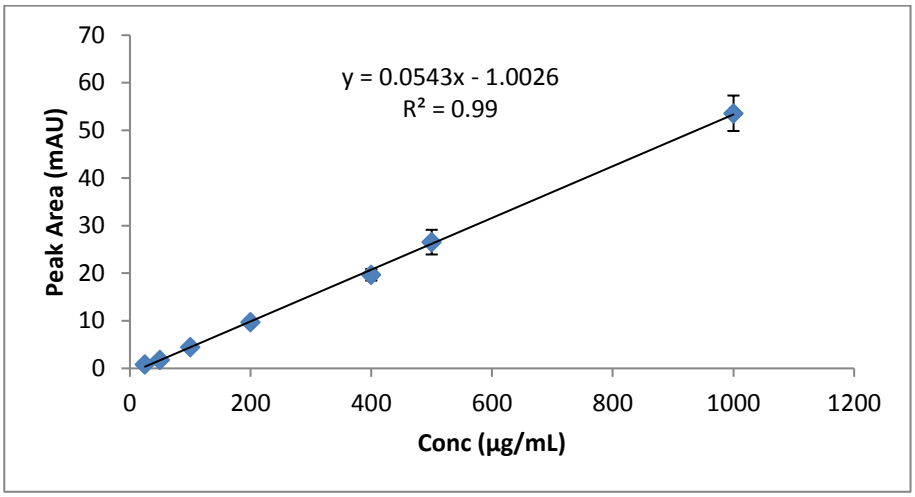

Figure 5.11 Beer-Lamberts calibration curve for insulin.

5.3.2.3 Repeatability (instrument and operator precision)

Instrument precision (accuracy) was determined by injecting the same concentration of insulin solution into the HPLC three times and calculating the %RSD. Figure 5.10 shows the overlapping of the three insulin chromatograms (lines 1-3), indicating precision of the instrument. From Table 5.2, the RSD for insulin and the blank were relatively low at 2.01 and 3.66%, respectively. Similar results were obtained during validation of a HPLC method for insulin reported by Moussa et al (2010). Operator precision was determined by establishing the calibration curve in triplicates. %RSD values calculated ranged from 7.7 – 9.76% (Table 5.4).

Table 5.3 Factors of the regression equation linking insulin concentration to the analytical response (area under the peak)

Parameter	Value
Linearity range, µg/mL	10-1000
LOD, µg /mL	0.63
LOQ, µg /mL	2.00
Slope of regression equation	0.05
Intercept	-1.00
Correlation coefficient	0.99
Standard error	0.81

Table 5.4 Table highlighting intra-day accuracy and precision parameters of the HPLC method due to high %recovery and low RSD (n=3)

Insulin conc. actual (µg/mL)	Peak Area (mAU)	RSD	Insulin conc. calculated (µg/mL)	Recovery (%)
50	1.78 ± 0.14	0.07	51.31 ± 2.55	100.56 ± 2.42
100	4.49 ± 0.43	0.10	101.11 ± 7.85	101.38 ± 4.89
200	9.27 ± 0.06	0.06	197.60 ± 10.14	98.80 ± 4.71
500	26.52 ± 2.59	0.10	506.90 ± 47.67	101.11 ± 3.99
1000	53.60 ± 3.72	0.07	1005.57 ± 68.56	102.63 ± 3.30
Mean % recovery = 100.89 ± 1.40% RSD % Recovery = 0.01 LOD = 0.63 µg /mL LOQ = 2.00 µg /mL				
Correlation coefficient = 0.99				

These values were within the limits for precision as reported by Epshtein (2004). Inter-day precision was determined by establishing calibration curves on different days – results are shown in Table 5.5. The overall %RSD values ranged from 3.3 – 9.3%. These values for %RSD are within the limits for precision. Ephstein (2004) reported that for precision in analysis of pharmaceuticals, %RSD should range between 0-15%.

Table 5.5 Inter-day precision and accuracy parameters for HPLC method (n=6)

Insulin conc. actual (µg/mL)	Amount measured on day 1 (µg/mL)	RSD	Amount measured on day 2 (µg/mL)	RSD	Overall RSD
50	51.31 ± 2.55	0.05	56.03 ± 4.37	0.08	0.08
200	197.60 ± 10.14	0.05	202.43 ± 3.71	0.02	0.04
400	380.55 ± 22.20	0.06	397.27 ± 15.18	0.04	0.05
500	506.90 ± 47.67	0.09	457.48 ± 30.44	0.07	0.09
1000	1005.57 ± 68.56	0.06	1012.82 ± 55.61	0.05	0.06

5.3.2.4 Limit of detection & limit of quantification

The LOD and LOQ were calculated using the signal-to-noise ratio, as well as from the standard deviation of the response and the slope and were found to be 0.63 and 2.00 µg/mL respectively (Table 5.4). Thus, the lowest amount of insulin that can be detected and quantified respectively, within the limits of accuracy and precision, using this method are 0.63 and 2.0 µg/mL (Moslemi et al 2003, Sarmento et al 2006).

5.3.2.5 Inter-laboratory method validation

The HPLC method was validated according to ICH guidelines by an independent operator in a different laboratory and a different HPLC system on three different days, to assess the method's reproducibility. Retention time was 3.70 ± 0.03 mins, with a peak well resolved from the solvent front (Figure 5.12). Regression analysis yielded equation of the line as y = 0.0851x - 1.2928 and R^2 = 0.9998. Intra-day and inter-day results are presented in Table 5.6 and Table 5.7, respectively. From here, it can be seen that the method was reproducible with %RSD of 1-3%. well within the expected limits. Thus, this method could be reproduced in any laboratory and employed for the quantification of insulin from samples.

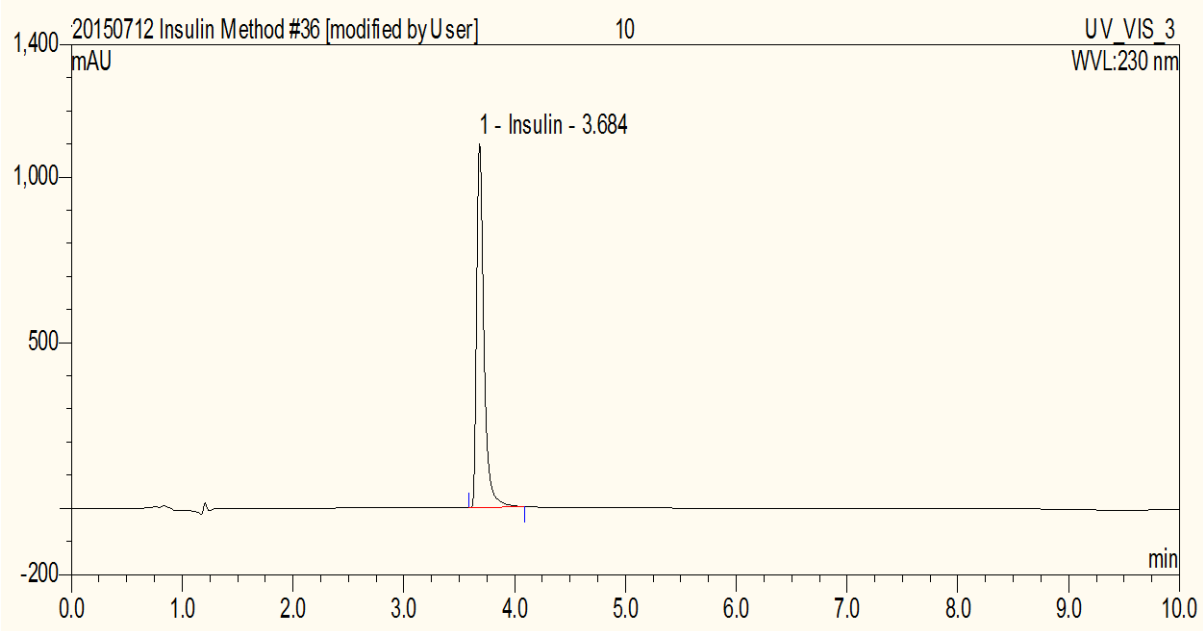

Figure 5.12 Representative chromatogram of insulin elution during inter-laboratory validation of HPLC method at Liverpool John Moores University, UK. A well separated insulin peak with no interference from the mobile phase was seen.

Table 5.6 Intra-day HPLC validation parameters for insulin method carried out in a different laboratory, with a different operator and different HPLC system on the same day, to assess method reproducibility (n=3)

Insulin conc. actual (µg/mL)	Insulin conc. calculated (µg/mL)	RSD	Recovery (%)	RSD
62.5	55.60 ± 1.10	0.02	88.95 ± 1.76	0.02
125.0	120.01 ± 1.30	0.01	96.01 ± 1.04	0.01
250.0	254.47 ± 6.07	0.02	101.83 ± 2.43	0.02
500.0	513.29 ± 13.14	0.03	102.66 ± 2.63	0.03
1000.0	1003.48 ± 23.84	0.03	100.35 ± 2.38	0.02
Mean % recovery = 97.96 ± 5.65 RSD % Recovery = 0.02 LOD = 0.53 µg /mL LOQ = 1.78 µg /mL				
Correlation coefficient = 0.99				

5.3.3 Stability of insulin solutions

Results of stability of 1000 µg/mL insulin solutions stored in the fridge for 72 hours are shown in Table 5.8. The percent recovery was calculated using the regression equation of the calibration curve. ANOVA for the peak areas and amount of insulin measured on both days showed no significant difference ($p > 0.05$). The overall %RSD of 7.94 – 8.07% shows that insulin solutions can be stored in the fridge for up to three days without deterioration.

Table 5.7 Inter-day precision and accuracy parameters carried out in a different laboratory with a different operator and HPLC system on three different days, to assess method reproducibility (n=9)

Insulin conc. actual (µg/mL)	Amount measured on day 1 (µg/mL)	Amount measured on day 2 (µg/mL)	Amount measured on day 3 (µg/mL)	Overall amount measured (µg/mL)	Overall RSD
62.5	55.60 ± 1.10	57.51 ± 2.98	59.43 ± 3.00	57.51 ± 1.91	0.03
125.0	120.01 ± 1.30	123.40 ± 2.79	125.28 ± 6.81	122.90 ± 2.67	0.02
250.0	254.47 ± 6.07	259.08 ± 3.28	257.82 ± 10.57	257.16 ± 2.33	0.01
500.0	513.29 ± 13.14	521.10 ± 4.14	516.62 ± 22.13	517.00 ± 3.92	0.01
1000.0	1003.48 ± 23.84	985.23 ± 10.22	985.94 ± 4.07	991.54± 10.34	0.01
Mean % recovery = 96.06 ± 8.29% RSD % recovery = 0.09					

This is in line with results obtained by Moussa *et al* (2010), who reported that insulin solutions remained stable in the fridge for up to 5 days.

Table 5.8 Stability of 1000 µg/mL insulin solutions after storage at 2 - 8 °C for 72 hours (n=3). Results show that insulin solutions are stable for 3 days when stored in the fridge.

	Day 0	Day 3	Overall RSD
Peak Area	62.32	62.32	0.08
(mAU)	67.80	61.37	
	54.15	56.14	
Amount measured	1054.78	1052.54	0.07
(µg)	1145.52	1036.66	
	919.45	949.26	
Mean % recovery = 102.64 ± 1.85%			
RSD %recovery = 0.08			

5.3.4 Effect of compaction pressure on the secondary structure of insulin

5.3.4.1 Circular dichroism (CD)

5.3.4.1.1 CD data verification

The normalised root mean square deviation (NRMSD) for the CD analysis of the samples is highlighted in Table 5.9. NRMSD values illustrate the 'goodness of fit' or validity of the data and compares "how well the theoretical CD spectrum calculated from the derived secondary structure composition matches the experimental data over the whole wavelength range of interest" (Whitmore and Wallace 2004, Kelly et al 2005). This value ranged from 0.01- 0.012 for all samples tested. Basically, values over 0.25 reflect experimental errors. A value of zero implies a perfect fit. Thus, the CD results obtained were a very good fit. A representative plot comparing the calculated and experimental spectra for the samples are displayed in Figure 5.13 (others appear in the appendix). For all samples, the experimental and reconstructed data points were superimposed on the graph and the difference between them almost a completely straight line. The superimposition of both spectra, and absence of difference, confirms the validity of the data analysis (Whitmore and Wallace 2004).

Table 5.9 Parameters of CD analysis of insulin powder and insulin tablets compacted at 10 and 30 kN respectively (n=3). Normalised root mean square deviation (NRMSD) values close to zero depict the validity of the data generated.

Parameter	Neat insulin	Insulin tablet at 10 kN	Insulin tablet at 30 kN
NRMSD	0.01	0.01	0.01
Helix per 100 residues	5.48	5.69	5.69
Strand segments per 100 residues	2.54	2.52	2.77
Mean helix length per segment	8.25	8.66	8.33
Mean strand length per segment	4.21	4.10	4.08

5.3.4.1.2 CD data interpretation

Figure 5.14 shows the CD spectrum of insulin before, and after compaction at 10 and 30 kN, respectively. On analysis, the neat insulin spectrum exhibited two distinct negative minima at wavelengths of 208 and 222 nm, characteristic of α-helical structure (Goldman and Carpenter 1974, Oak and Singh 2012b). Proteins consisting of only the α-helical secondary structure would be expected to exhibit an ellipticity (ɵ) maximum, about double the ɵ minimum. Because the maximum for the neat insulin appeared at <20mdeg, one would expect the presence of some other secondary structures in the protein. This was confirmed by results of analysis using the Dichroweb software (Table 5.10). As expected, the neat insulin was found to contain about 45% α-helix, 11% β-strands, 13% turns and 31% unordered secondary structures. This is in line with x-ray crystallisation results for insulin reported by Blundell et al (1971) and Bouchard et al (2000). Absorption in the far UV region (below 240 nm) has been attributed to the peptide bond, although in specific cases, the aromatic amino acid side chains of polypeptides may absorb in this region (Kelly et al 2005).

The CD spectra of insulin tablets at 10 and 30 kN compaction pressures were superimposed on that of the neat insulin (Figure 5.14). ANOVA results of the secondary structure quantifications in Table 5.10 showed no significant difference ($p > 0.05$) between the neat and the tableted insulin. The contributions to the secondary structure were almost equal, and there was no shift in the

minimum wavelengths; thus, compaction pressures of 10 and 30 kN were not observed to affect insulin secondary structure.

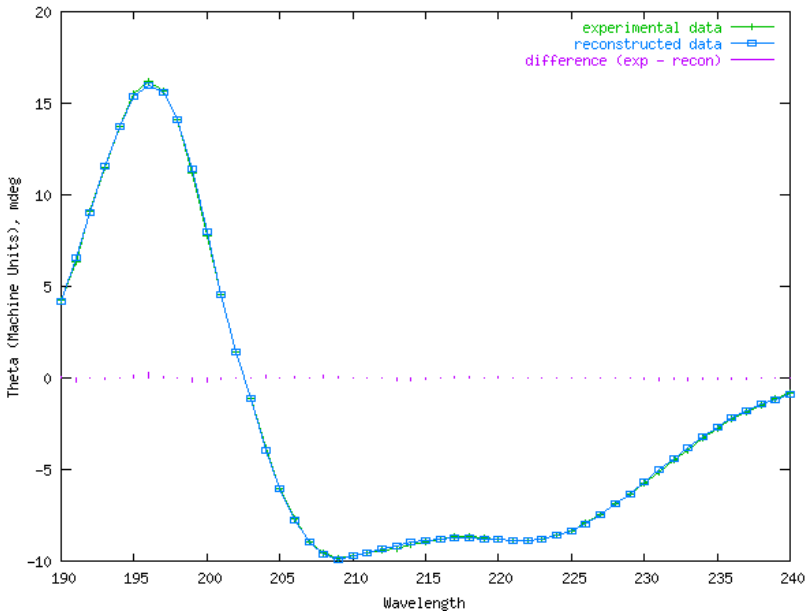

Figure 5.13 Plot of calculated and experimental CD spectra for neat insulin. The difference between the calculated/ reconstructed data and actual experimental data appears as a straight line, depicting the validity of the results generated.

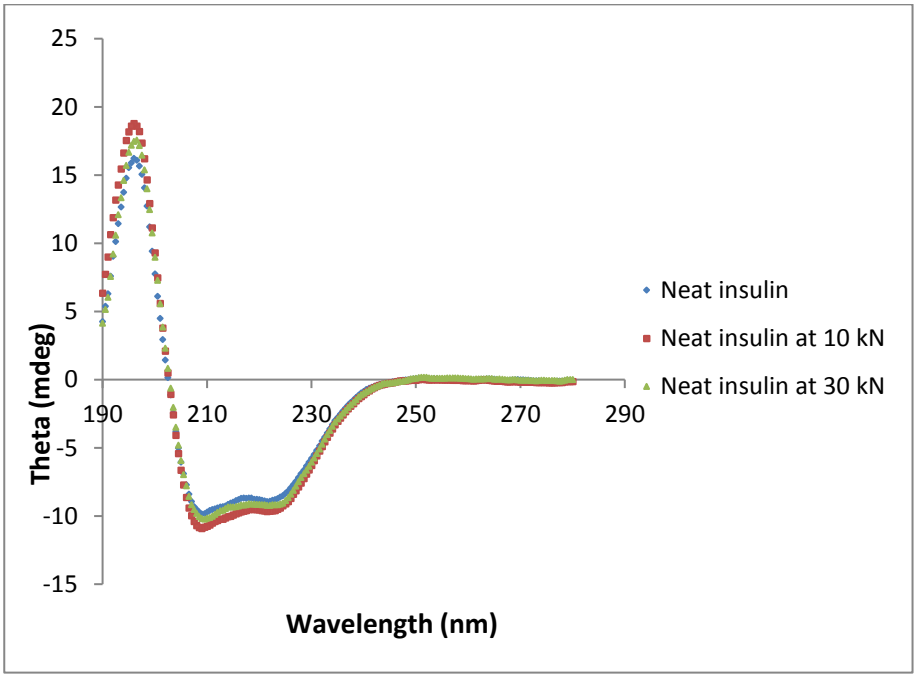

Figure 5.14 Circular dichroism spectrum of insulin powder (neat insulin) and pure insulin tableted at 10 and 30 kN compaction pressures. Each sample was dissolved in sufficient quantities of PBS to prepare a 1 mg/mL solution

Although no scientific papers could be found that compared the CD analysis of insulin before and after compaction into tablets, authors agree that absence of changes in the secondary structure of

the protein would mean that the experimental variable had no significant effect on the secondary structure of the protein (Oak and Singh 2012a). Furthermore, it will be necessary to determine the effect on protein structure, of tablets containing excipients before and after transmucosal delivery.

Table 5.10 Summary of CD data for insulin before and after compaction at 10 and 30 kN respectively (n=3). One-way ANOVA results (P>0.99) showed no significant difference in quantitation of secondary structures in all samples

Sample	Helix 1	Helix 2	Strand 1	Strand 2	Turns	Unordered	Total
Neat insulin	0.23	0.22	0.06	0.05	0.13	0.31	1.00
Insulin tab at 10 kN	0.26	0.23	0.05	0.05	0.13	0.28	1.00
Insulin tab at 30 kN	0.25	0.23	0.06	0.06	0.14	0.27	1.01

5.3.4.2 Fourier-transform infra-red (FTIR)

FTIR spectra for insulin powder (Figure 5.15) was characterised by the presence of absorption bands for amide I (1644 cm^{-1}) and amide II (1514 cm^{-1}) which are due to -C=O stretching characteristic of protein structures. Similar results were obtained by Sarmento et al (2006). The amide I band around 1644 cm^{-1} has been observed in small α-helical peptides in water (Bredenbeck et al 2005). This observation was in line with the high α-helical structure of insulin obtained from CD data. Second derivative FTIR analysis of the amide I region has been reported to separate and identify other secondary structures such as beta-sheets and random coil (Bouchard *et al* 2000, Nielsen *et al* 2001). Analysis of the FTIR data from the tableted drug (Figure 5.15) showed identical spectra to the insulin powder in the amide I and amide II regions. This result was expected, and correlates nicely with results from CD studies indicating that compaction pressure did not significantly affect the secondary structure of the insulin powder.

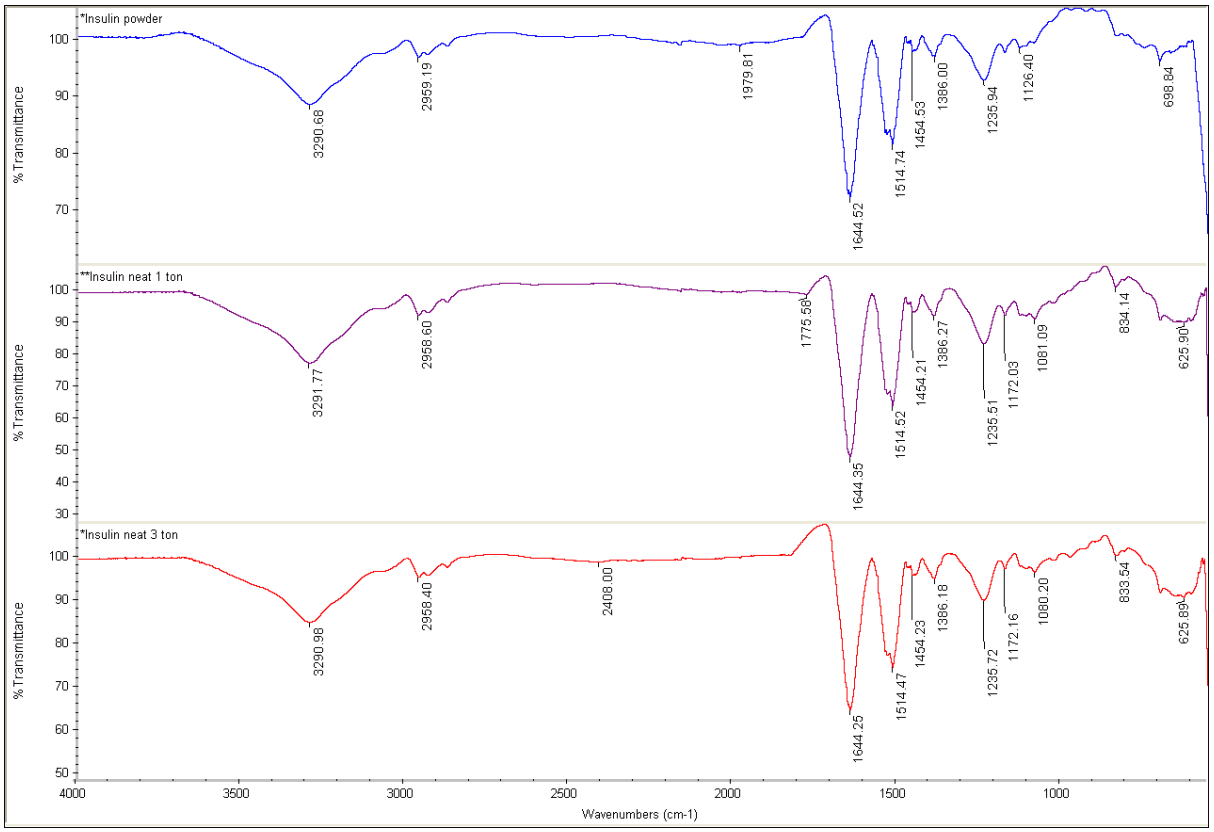

Figure 5.15 FTIR spectra of insulin before and after compaction at 10 and 30 kN, showing the amide I and amide II absorption bands. Identical spectral patterns were obtained pre- and post-compaction, highlighting that compaction did not affect the secondary structure of insulin.

5.4 Conclusion

Considering the complex nature of proteins, the aim of this work was two-fold. Firstly, to describe the steps involved in our optimisation and validation of a simple, rapid and efficient method for insulin quantification by HPLC that could be reproduced in any laboratory at room temperature. And secondly, to characterise our protein using circular dichroism (CD) and FTIR and then investigate the effect that compression into tablets had on its secondary structure, which could affect protein activity *in vivo*. Insulin was effectively eluted at 3.8 mins with no interference from the solvent front. The method was validated in our laboratories and independent operator laboratories with similar results that complied with the ICH guidelines for HPLC method validation. Thus, the developed method is rapid with short runtime, at room temperature with simple UV detectors, and low detection and quantification limits, which can be employed for the HPLC quantification of insulin from any sample with high reproducibility from other laboratories. CD evaluation of insulin secondary structure revealed majorly an α-helical structure, with the

presence of some β sheets, turns and unordered secondary structures. FTIR spectroscopy also identified amide I and II bands, which are characteristic of proteins, with the amide I band specifically found in small α-helical peptides. CD and FTIR results showed that insulin secondary structure was not affected by compaction at elevated pressures. Thus, the developed HPLC method can be employed for the HPLC quantification of insulin from any sample, and compaction pressures up to 30 kN may be used for insulin without affecting its structural integrity. However, the effect of formulation additives on insulin HPLC specificity and on insulin integrity upon transmucosal permeation would need to be studied.

Chapter 6

Pre-formulation and systematic evaluation of amino acid assisted permeability of insulin across buccal cell layers *in vitro*

Publications relating to chapter 6

Iyire, A.; Alayedi, M; Mohammed A.R. (2016) Pre-formulation and systematic evaluation of amino acid assisted permeation of insulin via buccal cell layers. *Nature Scientific Reports* (accepted)

6.1 Introduction

The primary driving factor for investigating non-invasive routes for insulin delivery are built on obtaining stringent blood glucose control (that mimics the situation found in non-diabetics) in diabetic patients, by reducing/removing the need for multiple daily injections of insulin that puts a major strain on patient compliance (Owens *et al* 2003). On the other hand, mucosal delivery of biologicals has been reported to be less effective than parenteral delivery for various reasons, including limited mucosal permeation, as well as absorption site metabolism (Veuillez *et al* 2001). However, high vascularisation and presence of fewer proteolytic enzymes in the buccal mucosa than the gastrointestinal tract (GIT) mucosa promotes buccal delivery as a potential site for protein and peptide delivery. Limitations of buccal delivery of proteins include: large molecular weight and hydrophilicity, leading to low diffusivity; instability, fast metabolism, adsorption, aggregation, biocompatibility and possible immunogenicity (Veuillez *et al* 2001). Thus, factors affecting peptide drug absorption including **structure** (molecular weight/ size, conformation, stereospecificity, immunogenicity and electrostatic charge); **physicochemical properties** (solubility, hydrophilicity/ partition coefficient, aggregation, self-aggregation and hydrogen bonding); **buccal mucosal properties** (structure and biochemistry); **biological environment** (enzyme sensitivity and intracellular metabolism) and **available transport mechanisms** have to be considered during buccal insulin formulation development (Veuillez *et al* 2001).

Strategies such as chemical modification by derivatisation, or prodrug approaches may enhance peptide stability and lipophilicity, and may prevent degradation by proteolytic enzymes at the mucosal surface (Veuillez *et al* 2001). Other strategies that result in the formation of non-covalent complexes between the protein and hydrophilic moieties have been reported to impart a slight reversible unfolding to the peptide molecule, leading to enhanced protein flexibility and lipophilicity (Milstein *et al* 1998, Owens *et al* 2003). This increases passive transcellular diffusion and enhances protein permeability, and is the principle behind the use of ion pairs to enhance drug permeation. An ion pair is formed when a pair of oppositely charged (counter) ions are held together without the formation of a covalent bond, by Coulombic forces forming a neutral molecule

with higher lipophilicity, that can partition into the cell membrane easier than the parent compounds (Samiei *et al* 2013). Most ion pairing agents, such as inorganic surfactants and co-solvents, require high volumes, resulting in high toxicity/ allergenicity and have limited applications in pharmaceutical preparations; thus, the use of biocompatible agents as ion pairs with drug molecules would eliminate this challenge (Miller 2009, Hemenway *et al* 2010, Samiei *et al* 2013). Recently, the use of amino acids as ion pairs to enhance solubility/ permeability of small molecules has been investigated as a biodegradable, low toxicity/ irritant and high stability alternative (Hemenway *et al* 2010). Moreover, the availability of amino acid transport systems across cells may enhance facilitated transport of drug – amino acid complexes (after ion pair formation), leading to enhanced permeation (Elshaer *et al* 2011). Various studies have investigated the use of amino acids as ion pairs to improve solubility/ permeability of small molecules (Chen *et al* 1999, Ivaturi and Kim 2009, Samiei *et al* 2013, Elshaer *et al* 2014, Samiei *et al* 2014). However, the use of amino acids as ion pairs to enhance solubility/ permeability has not been reported for proteins and macromolecules. Usually, with small molecules, molar ratios of the counter ion are used in excess (Miller 2009), but molar ratios cannot be employed for macromolecules like insulin because these would require minute quantities of amino acids with negligible effects observed. Also, the large size, amphiphilic nature, and presence of multiple ionisable sites on proteins further complicate the expected results *in vitro*.

In order to establish the role of ion pairs in the formulation of biologicals, the proposed work is built on insulin as a model compound. Insulin has been classified as a BCS class III molecule with high solubility (depending on solution pH) and low permeability, mostly due to its large molecular weight, low lipophilicity and quick degradation in the presence of proteases (Ohshima and Makino 2014). The insulin monomer (Figure 6.1) consists of six basic groups (two N-terminal amino groups, two histidines, one lysine and one arginine) and six acidic groups (two C-terminal carboxylates and four glutamates) (Matsuura *et al* 1993). Therefore, at pH values around its isoelectric point of 5.35, charges on the monomer balance out providing a neutral molecule, rendering insulin practically insoluble in water (Hames and Hooper 2005, Samiei *et al* 2013).

Figure 6.1 Primary structure (amino acid sequence) of insulin monomer highlighting basic (black arrows) and acidic (blue arrows) groups which provide ionisable sites to the molecule (adapted from http://www.interactive-biology.com/wp-content/uploads/2012/05/Human-Insulin-Protein-Structure-917x1024.pg

Structures of the ionisable sites on the insulin monomer provided by basic and acidic amino acids are presented in Figure 6.2. At acidic pH, the acidic groups on insulin become protonated, and the resulting charge on the molecule is provided by the basic groups (NH_3^+), thus insulin has a positive charge in acidic media. However, in basic media, the acidic groups lose their protons and the charge on the monomer is provided by the acidic groups (COO^-), thus insulin has a negative charge in basic media (Hames and Hooper 2005).

The current work was based on two hypotheses. Firstly, that ionised insulin molecules could form ion pairs with opposite charges provided by basic and acidic amino acids to form an insulin-amino acid neutral complex, with lower hydrophilicity and therefore enhanced lipophilicity, which could then permeate the buccal membrane via transcellular passive diffusion. Secondly, that complexation of insulin with amino acids could possibly trigger alternate transport mechanism of insulin-amino acid complex across buccal membranes, potentially via amino acid nutrient transporters available on the cell membranes (Figure 6.3).

Figure 6.2 Structures of basic and acidic amino acids that provide ionisable sites on the insulin monomer; adapted from Hames and Hooper (2005).

Figure 6.3 Schematic representation of active transport of insulin-amino acid ion pair complex. Where (A) represents amino acids transport via their nutrient carriers, (B) represents amino-acid facilitated insulin transport through amino acid carriers. Adapted from https://www.premedhq.com/passive-active-transport

Thus, the aim of this work was, therefore, to investigate the ion pairing effect of basic and acidic amino acids on the solubility, distribution coefficient, permeability, mechanism and transport route of insulin across TR146 buccal cell layers, in order to highlight safe and effective permeation enhancers for buccal insulin delivery.

6.2 Materials and methods

6.2.1 Materials

The TR146 cell line was purchased from Public Health England, UK. Human recombinant insulin, L-arginine (non-animal source, cell culture tested), L-lysine (≥ 97%), L-histidine (≥ Reagent Plus™ 99%), L-glutamic acid (minimum 99% TLC), L-aspartic acid (99%), sodium deoxycholate, MTT (methylthiazolydiphenyl-tetrazolium bromide; ≥97%; enzymatic), dimethyl sulfoxide (DMSO) and trifluoroacetic acid were purchased from Sigma-Aldrich, UK. Hank's balanced salt solution (HBSS), fetal bovine serum (FBS), Hams F-12 nutrient mix and trypsin-EDTA were obtained from Gibco® Lab., UK. Gentamicin and penicillin/ streptomycin were obtained from Bio Sera, UK. Acetoniltrile and absolute ethanol were purchased from Fisher scientific, UK. 6 well plates, 6 well polycarbonate transwell inserts and 12 well polyester transwell inserts were purchased from Appletonwoods, UK. All the chemicals and reagents were used as obtained. All water used was double-distilled and autoclaved.

6.2.2 Methods

6.2.2.1 High performance liquid chromatography (HPLC) assay

Quantitative analysis of insulin in solution was achieved by gradient RP-HPLC adapted from Sarmento *et al* (2006). A Waters HPLC system (Alliance) with gradient pump and UV/ fluorescent detector was used, employing a reversed phase RP-C18 analytical column (Phenomenex® 110A, 150 x 4.6mm, 5µm). The mobile phase consisted of solution A: 0.1% v/v TFA in water and solution B: absolute acetonitrile, both filtered under vacuum and sonicated prior to use. A gentle gradient was run from 74:26 to 67:33 compositions of A:B over 3 mins, and then maintained at 67:33 for 4

mins. Pump flow rate was 1mL/min, with sample injection volume of 10µL and UV detector wavelength of 214nm. Column and samples were maintained at room temperature. A rectilinear (Beer-Lambert's) calibration curve was established for insulin within a concentration range of 1 – 1000 µg/mL (0.027 – 27 IU/mL) dissolved in 0.01N HCl and linearity calculated. Instrument precision was evaluated by injecting the same concentration of insulin solution (1000µg/mL) into the HPLC three times and calculating the percent relative standard deviation (%RSD) using equation 6.1. Intra-day and inter-day operator precision were evaluated by establishing the calibration curve in triplicates on the same day, and on three different days respectively, and %RSD calculated. Method accuracy was evaluated by calculating the %RSD of percentage recovery (equation 6.2) inter- and intra-day; while limits of detection and quantification (LOD & LOQ) were calculated from the regression line using equations 6.3 & 6.4 respectively (1CH 2005, Sarmento *et al* 2006):

$$\%RSD = \frac{mean}{standard\ deviation}\ x\frac{100}{1} \quad . \quad . \quad . \quad . \quad . \quad \text{(Equation 6.1)}$$

$$\%\ recovery = \frac{actual\ amount\ recovered}{theoretical\ amount\ expected}\ x\frac{100}{1} \quad . \quad . \quad . \quad \text{(Equation 6.2)}$$

$$LOD = \frac{3.3\sigma}{s} \quad . \quad . \quad . \quad . \quad . \quad . \quad . \quad . \quad \text{(Equation 6.3)}$$

$$LOQ = \frac{10\sigma}{s} \quad . \quad . \quad . \quad . \quad . \quad . \quad . \quad . \quad \text{(Equation 6.4)}$$

where σ is the standard deviation of the response and s is the slope of the regression line.

6.2.2.2 Insulin solubility in water & HBSS

To investigate the effect of model basic (L-arginine) and acidic (L-glutamine) amino acids on the solubility of insulin in water, solubility studies were carried out at 25 °C by adding excess amounts of insulin in 5mL of deionised water containing 4, 27 or 50µg/mL concentrations of each amino acid respectively. pH of the solutions was measured using a pHenomenal® pH meter (VWR, USA). The solutions were then allowed to stir on a multi IKA magnetic stirrer overnight (Nicolescu *et al* 2010, Elshaer *et al* 2011). After standing for 2 hours, the supernatant was filtered through 0.45µm filters, and insulin content quantified by the validated HPLC method described above. Similar experiments were carried out using 10, 50, 100, 200, & 400 µg/mL concentrations of basic

(arginine, lysine & histidine) and acidic (glutamic acid & aspartic acid) amino acids, and sodium deoxycholate, using HBSS in place of deionised water; because *in vitro* permeability studies would be carried out in HBSS. Solutions without amino acids were used as control.

6.2.2.3 Insulin distribution coefficient in 1-octanol/ water

To determine the effect of amino acids on the partition behaviour of insulin between polar and non-polar phases, 1 mg insulin was added to 5 mL octanol-saturated deionised water and 5 mL deionised water saturated 1-octanol in the presence of arginine or glutamic acid (4, 27 & 50 µg/ mL) respectively and stirred overnight similar to water solubility experiments described above. The solutions were then separated by allowing to stand in a separating funnel for 4 hours, after which the aqueous fraction was filtered using a 0.45 µm nylon filter and insulin content quantified by HPLC. Solutions without amino acids were used as control.

6.2.2.4 TR146 cell culture procedures

TR146 cells were maintained in $75cm^3$ T-flasks in Ham's F-12 cell culture media fortified with 10% FBS, 2 mM glutamine, 100 IU penicillin/ streptomycin, 10 µg gentamicin; and incubated at 37 °C, 5% CO_2 and 95% air. Media change occurred every 2-3 days and at 90% confluence, cells were passaged using 5mL trypsin-EDTA solution in HBSS, and seeded unto 12 well transwell inserts at a density of 24,000 cells/cm^2 and grown for 28-29 days. Transepithelial electrical resistance was used to monitor cellular layer integrity 30 minutes after each media change (Elshaer *et al* 2014). Passage numbers 30-39 were used for these experiments.

6.2.2.5 Trans-epithelium electric resistance (TEER)

The ohmic resistance (resistance to current flow via the paracellular pathway) of cells grown on transwell inserts was measured every 2-3 days (30 mins after media change) during the cell culture, as well as before and after each permeability experiment, using an EVOM™ volt ohmmeter with chopstick electrodes. The electrodes were placed erect, such that the longer arm just touched the fluid in the basolateral chamber, while the shorter arm barely touched the apical membrane. The transepithelial electric resistance which reveals the integrity of the cellular layers was calculated

using equation 4.5. TEER values were reported as mean ± standard deviation of triple readings from replicate transwells (n=9).

$$TEER = \left(R_{(insert\ with\ cells)} - R_{insert\ without\ cells}\right) * A \quad . \quad . \quad \text{(Equation 6.5)}$$

where R is the measured resistance and A is the cross-sectional area of the cells.

6.2.2.6 Cytotoxicity testing via MTT assay

The methylthiazolyldiphenyl-tetrazolium bromide (MTT) assay was used to assess the cytotoxicity of the enhancers on TR146 cells in their exponential growth phase. Cells were seeded unto 96 well plates at a density of 24,000 cells/cm^2 and incubated for 24 hours. The media was removed and 200µL of increasing concentrations (25, 50, 100, 200, 400 & 800 µg/) of each enhancer in HBSS was added to each well in replicates of 12 per concentration. Cells were incubated for 4 hours (the duration of permeability experiments) after which 20 µL MTT solution (5 mg/mL in HBSS) was added to each well and incubated for a further 4 hours. Finally, wells were emptied and solutions replaced with 100 µL dimethyl sulfoxide (DMSO) and left to shake at 140 rpm and 37 °C for 30 minutes. The absorbance was read at 490nm using a Multiskan® spectrum plate reader (Thermo Scientific, US). The relative enzyme reactivity and therefore cell viability was calculated from equation 6.6.

$$Cell\ viability\ (\%) = \frac{OD_1 - OD_2}{OD_3 - OD_2}\ x\ \frac{100}{1} \quad . \quad . \quad . \quad . \quad \text{(Equation 6.6)}$$

where OD_1, OD_2 and OD_3 are the optical densities of wells with cells and enhancer solution, blank wells without cells or enhancer solution, and wells with cells but no enhancer solution respectively.

6.2.2.7 *In vitro* transbuccal permeation studies

TR146 cells cultured on transwell inserts for 28-29 days with passage numbers 30-39 were used for permeability studies. Permeability studies were conducted as described by Nielsen and Rassing (1999) at 36°C and 140 rpm in an orbital plate shaker. Test solutions containing 1000µg/mL (27 IU/mL) insulin dissolved in HBSS in the presence of increasing concentrations (10, 50, 100, 200, 400 and 600 µg/ mL) of basic and acidic amino acids as well as sodium deoxycholate were prepared

and stirred until a clear solution was observed, and pH of solutions measured. Cells on transwell inserts were rinsed twice with HBSS (37°C) by adding 0.5 mL and 1.5 mL to the apical and basolateral chambers, respectively. After incubation for 30mins, TEER readings were taken in triplicate per insert. The basolateral chamber was then replaced with fresh HBSS and the apical chamber with 0.5mL test solution. Immediately, 100 µL of test solution was withdrawn from the apical and basolateral chambers at time 0. Basolateral sampling of 700 µL was done every 30 mins for 4 hours with immediate replacement with pre-warmed HBSS. At the end of the experiment, 100 µL of apical solution was taken. Test solutions without permeation enhancers were used as control (Portero *et al* 2002, Xue *et al* 2012, Sander *et al* 2013). After 4 hours, cells were rinsed twice with 0.5mL HBSS and equilibrated for 30minutes after which TEER values were recorded. All samples were made up to 700 µL where necessary, using HBSS, and analysed for insulin content by HPLC, and resultant data used to calculate the apparent coefficient of permeability through the insert with cells (P_{app}), the cell-free apparent permeability coefficient (P_{insert}), the cell apparent permeability coefficient (P_{cell}), the percent enhancement ratio (%ER) and the recovery %.

$$P_{app} = \frac{dQ}{dt} \, x \frac{1}{A*C_o} \quad . \quad . \quad . \quad . \quad . \quad . \quad . \quad \text{(Equation 6.7)}$$

$$P_{insert} = \frac{dQ}{dt} \, x \, \frac{1}{A* \, C_o} \quad . \quad . \quad . \quad . \quad . \quad . \quad . \quad \text{(Equation 6.8)}$$

$$\frac{1}{P_{app}} = \frac{1}{P_{cell}} + \frac{1}{P_{ins}} \quad . \quad . \quad . \quad . \quad . \quad . \quad . \quad \text{(Equation 6.9)}$$

$$\%ER = \frac{P_{cell\,(enhancer)}}{P_{cell\,(control)}} \, x \, \frac{100}{1} \quad . \quad . \quad . \quad . \quad . \quad . \quad \text{(Equation 6.10)}$$

$$Recovery\ \% = \frac{X_{apical} + X_{basolateral}}{X_o} \, x \, \frac{100}{1} \quad . \quad . \quad . \quad . \quad \text{(Equation 6.11)}$$

Where dQ/dt is the rate of insulin transport at steady state in µg/s, A is the cross sectional area of cells in cm^2, C_O is the initial apical solution concentration in µg/mL, X_{apical} is the quantity of insulin remaining in the apical chamber after 4 hours, $X_{basolateral}$ is the cumulative amount of insulin sampled from the basolateral chamber after 4 hours and X_o is the initial quantity of insulin in the apical chamber at the start of the experiment (Portero *et al* 2007, Xue *et al* 2012, Sander *et al* 2013).

Insulin stability after permeation was monitored by HPLC for changes in retention time and/ or presence of multiple peaks on the HPLC chromatogram.

6.2.2.8 Route of insulin transport

To investigate the transport route of insulin in the presence of the enhancers, solutions containing FITC-labelled insulin (0.6 mg/mL in HBSS) along with concentrations of enhancers that effectively enhanced insulin permeability, were incubated with TR146 cells grown on transwell inserts for 28 days on an orbital plate shaker equilibrated at 36°C and 140 rpm for 4 hours; as with the transport experiments (Luo *et al* 2006). The transwell inserts with cells were washed three times with warm HBSS before and after the experiment. TEER values in HBSS were also measured before and after the experiment. After washing, transwell inserts were fixed with 4% paraformaldehyde (PFA) in PBS for 10 minutes, and cells were rinsed four times with PBS. Inserts were placed on microscope slides and the membrane carefully cut out using a scalpel. Two drops of DAPI (4'6'-diamidino-2-phenylindole) in Vectashield™ (Vector Laboratories) were used to mount the specimen, which was immediately covered with a microscope cover slip and allowed to air dry for 10 minutes. Samples were then viewed using a Leica® laser confocal scanning microscope (Wetzlar, Germany) at 10x (dry) and 40x (oil) magnifications.

6.2.2.9 Mechanism of insulin transport

To investigate the presence of passive transport, permeability studies described above were carried out using a single concentration of glutamic acid (200 µg/mL) with increasing concentrations of insulin (250, 500, 1000 & 1500 µg/mL = 6.75, 13.5, 27 & 40.5 IU/mL) and all permeability indices calculated. While to investigate the presence of active amino acid-facilitated transport of insulin, permeability studies were repeated at suboptimal temperatures (9°C) with 1000 µg/mL (27 IU/mL) insulin in the presence of increasing concentrations of glutamic acid (100, 200, 400 µg/mL). Transwells were maintained at 9°C for 1 hour prior to commencing studies to ensure a cessation of enzymatic activity, and the resulting insulin transported analysed by HPLC.

6.2.2.10 Statistical analysis

All data generated in replicates were presented as mean ± standard deviation (SD), where n≥3. The data was then analysed for statistical significance using one-way analysis of variance (ANOVA) and Tukey-Kramar multiple comparison post-test from Graphpad Prism® version 6.07 (Graphpad Software, San Diego, CA, USA). The level of significance was quoted as $p<0.05$ (probability values of 95%).

6.3 Results & discussion

6.3.1 Insulin solubility in water

There is a lack of consensus on solubility of insulin in water as various authors have either reported it as soluble/ hydrophilic (Xu *et al* 2006) or insoluble/ hydrophobic (BP 2012). However, the solubility of insulin is determined by the pH of the solution, and its closeness to the isoelectric point of insulin (Lens 1946). Kramer et al (2012) described protein solubility as "a thermodynamic parameter defined as the concentration of protein in a saturated solution that is in equilibrium with a solid phase, either crystalline or amorphous, under a given set of conditions". This solubility depends primarily on intrinsic factors such as the characteristics of its constituent amino acids, as well as extrinsic factors such as temperature, pH, ionic strength and solvent additives (Kramer *et al* 2012). The solubility of insulin in water was tested in the presence and absence of arginine and glutamic acid, as models for basic and acidic amino acids, respectively (Figure 6.4). In the absence of amino acids, insulin remained only slightly soluble in deionised water (<3µg/mL at pH 6.64) (Trevino *et al* 2008). Similar results were obtained by Lens (1946) who measured insulin solubility at pH 6.0. Landreh (2012) also reported low insulin solubility at pH 5 – 6. The insulin monomer comprises six acidic groups (two C-terminal carboxylates and four glutamate residues) and six basic groups (two N-terminal amino groups, two histidine, one lysine and one arginine) (Matsuura *et al* 1993) (Figure 6.1). At the pH of deionised water, the charges on the acidic and basic groups balance out to give a neutral molecule with no net charge, thus being unionised, solubility of the protein is hindered (Hames and Hooper 2005, Samiei *et al* 2013).

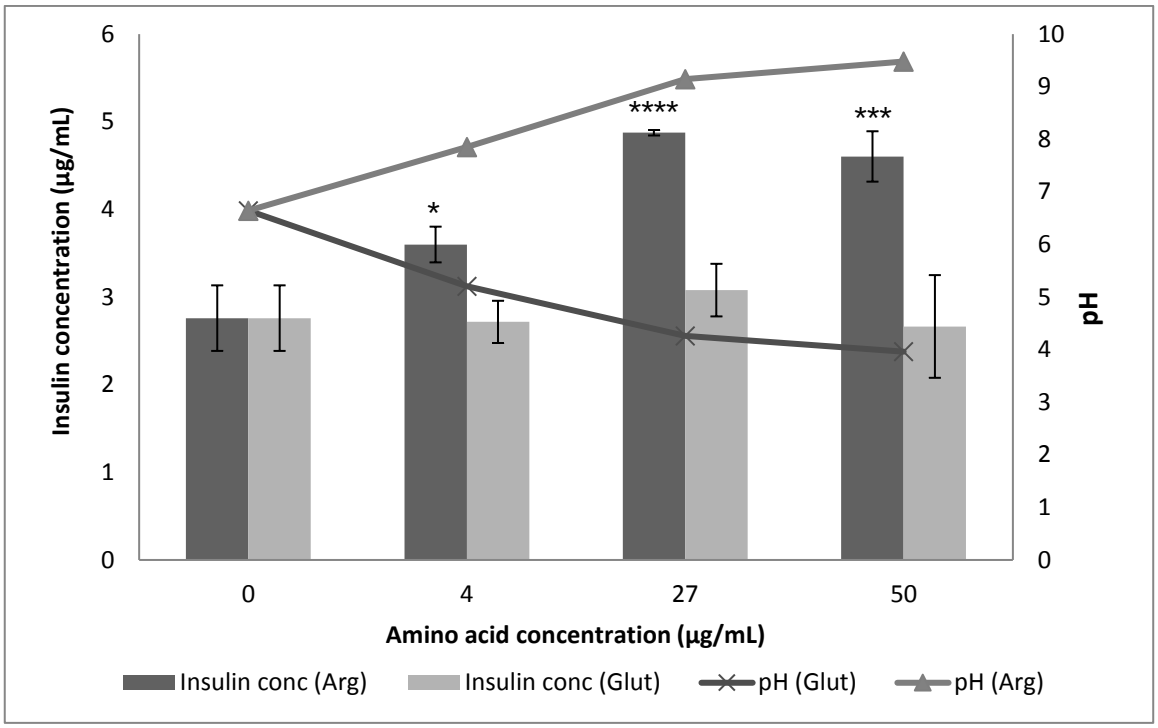

Figure 6.4 Solubility in water at 25 °C and resulting pH of solutions of insulin in the presence/ absence of basic and acidic amino acids (n=3). Horizontal line depicts the isoelectric point of insulin (1 mg insulin = 27 IU).

From Figure 6.2, it can be seen that arginine with a highly basic side chain (pKa = 12.48) was able to increase the pH of the resulting solution to about 9 - over 3 units above the isoelectric point (pI) of insulin (Figure 6.4) (Hames and Hooper 2005). The pI is the pH at which insulin has no net charge across its amino acid groups. The system's basicity was increased to up to pH 9 due to the contribution of the $-NH_2$ group from arginine. Thus, insulin solubility increased significantly with increasing concentrations of arginine. This can be explained using the Henderson-Hasselbalch equation (Leninger *et al* 1993, Wang *et al* 2002):

$$\mathrm{pH} = \mathrm{pKa} + \log\frac{[\mathrm{A}^-]}{[\mathrm{HA}]} \quad . \quad . \quad . \quad . \quad . \quad . \quad \text{(Equation 6.12) or}$$

$$\mathrm{pH} = \mathrm{pKa} + \log\left(\frac{[\text{proton acceptor}]}{[\text{proton donor}]}\right) \quad . \quad . \quad . \quad . \quad \text{(Equation 6.13)}$$

where pH is the negative logarithm of hydrogen ion concentration $[H^+]$, pKa is the negative logarithm of the acid dissociation constant, Ka, and represents the pH at which the acid is halfway dissociated i.e. $[HA] = [A^-]$; $[A^-]$ is the molar concentration of the acid's conjugate base, and [HA] is the molar concentration of the undissociated weak acid (Hames and Hooper 2005). Therefore,

the solubility of a weak acid would increase with increasing pH, while that of a weak base would increase with decreasing pH (Hörter and Dressman 2001). So, for a protein like insulin that is amphoteric in nature, and has the ability to act either as a weak acid or a weak base, solubility of the protein would be expected to increase when pH is at least 2 units below or above its isoelectric point. Thus, the trend seen where increasing concentrations of arginine increased pH, and therefore increased insulin solubility, was expected. At low pH, all acidic groups of insulin become protonated and the resultant charge on the molecule is supplied by the basic groups; while at high pH, all basic groups lose their protons and the resultant charge on the molecule is supplied by the acidic groups (Matsuura *et al* 1993). Thus, insulin remains insoluble at its pI of 5.0-5.35, but solubility increases with change of pH (Matsuura *et al* 1993). In this system, insulin acts as a weak acid to release its proton from the –COOH group to arginine to form $–NH_3^+$, leaving insulin with a negative charge from COO^-. This dissociation of insulin enhanced its solubility since only ionised molecules are soluble (Samiei *et al* 2013). However, because from Figure 6.4, this relationship was not found to be linear, probably due to the presence of various ionisable amino acid groups on the insulin molecule; it could be said that insulin was not fully dissociated in the arginine solution (Elshaer *et al* 2011). However, it should be noted that the ionisation of insulin would be expected to be more complicated than that seen with small molecules due to the presence of multiple ionisable groups on its various component amino acids.

With glutamic acid, there was no significant change in insulin solubility. In the presence of glutamic acid, all acidic groups on the insulin molecule would have been expected to be protonated, leaving a resultant positive charge supplied by its basic groups. However, this was not observed to occur for various reasons. At 4µg/mL glutamic acid, solution pH was 5.26, very close to the isoelectric point of insulin, thus insulin would not be dissociated and solubility would not change. At higher concentrations of glutamic acid, solution pH was 4.2 – 4.3. Although insulin should have been dissociated at this pH, the solution pH was very close to the pKa of glutamic acid 4.07 (Table 6.1). The dissociation of glutamic acid would have been limited, leading to its inability to freely donate protons to insulin, resulting in no change in insulin solubility (Kramer *et al* 2012). Therefore, it is possible that insulin dissociation was not enhanced and its solubility remained

unaffected. These findings are in line with previous reports which have suggested that weak acids exhibit highest buffering capacity within one pH unit of their pKa (Hames and Hooper 2005).

6.3.2 Insulin solubility in HBSS

Insulin solubility in HBSS was determined because it was expected that at pH 7.4, more than 2 units above the isoelectric point of insulin, the protein would be soluble, overcoming precipitation (Trevino *et al* 2008). HBSS also enabled the circumvention of the potential toxicity related to solubilising insulin in 0.01N HCl prior to permeation experiments, as reported by other authors (Yin *et al* 2009, Xue *et al* 2012). For HBSS solubility studies, a range of amino acids were utilised, their physicochemical properties are presented in Table 6.1. The effect of amino acids on insulin solubility was compared to that of sodium deoxycholate, a hydrophobic bile salt that has been widely studied as a permeation enhancer.

Table 6.1 Properties of amino acids used in this study, highlighting the pKa of their ionisable side chains (Silen and Forte 1975, Hames and Hooper 2005).

Enhancer	Molecular weight (g/mol)	Side chain	pKa			pI
			NH_3^+	COOH	Side chain	
L-arginine	174.20	Basic	1.82	8.99	12.48	10.76
L-lysine	146.19	Basic	2.16	9.06	10.54	9.74
L-histidine	155.16	Basic/ neutral	1.80	9.33	6.04	7.59
L-glutamic acid	147.13	Acidic	2.10	9.47	4.07	3.22
L-aspartic acid		Acidic	1.99	9.90	3.90	2.77
Sodium deoxycholate	414.60	-	-	-	-	6.58

This is a surfactant that enhances permeability of biological membranes by dissolution of membrane lipids, thereby interfering with membrane fluidity and integrity (Gandhi and Robinson 1992, Yamamoto *et al* 1992, Uchiyama *et al* 1999, Türker *et al* 2004).

Compared with deionised water, insulin was highly soluble in HBSS even in the absence of amino acids and the bile salt. This can be related to the fact that the pH of HBSS is buffered at 7.4 which is much higher than the pI of insulin and would maintain insulin in its ionised form, thereby

enhancing solubility (Franks et al 2000). Lens (1946) reported complete solubility of insulin in phosphate buffer at pH 7.4, but a solubility of <3 µg/mL in phosphate buffer pH 6.0, with higher solubility of about 5 µg/mL observed at pH 4.95. Figure 6.5 and Figure 6.6 compare the effect of the presence and/ or absence of increasing basic and acidic amino acids and the bile acid salt on insulin solubility and solution pH. Na deoxycholate did not have any significant effect on insulin solubility except at a concentration of 100 µg/mL of the bile salt (Figure 6.5).

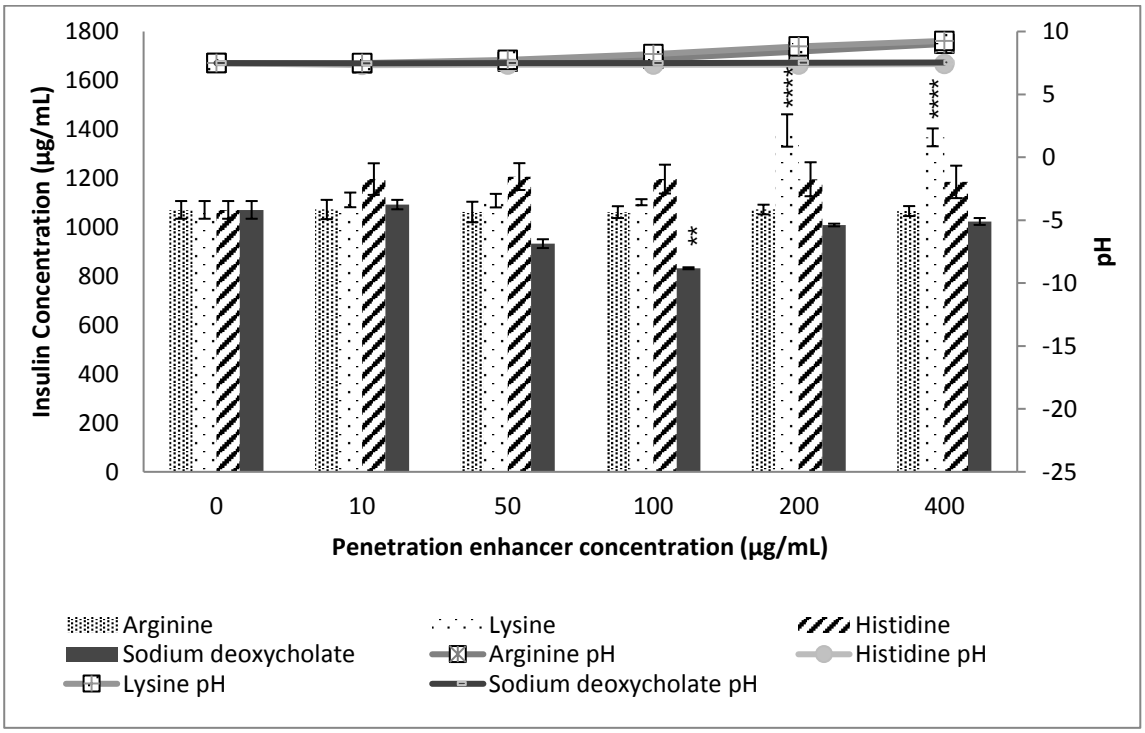

Figure 6.5 Comparing the effect of basic amino acids and the bile salt, Na deoxycholate, on the solubility of insulin in HBSS at 25 °C (n=3). Only lysine was able to alter solution pH and insulin solubility significantly (1 mg insulin = 27 IU).

As a detergent, Na deoxycholate acts as an amphiphile and possesses both polar and non-polar properties and is able to enhance the emulsification of insoluble substances by reducing interfacial surface tension (Rotunda et al 2004). This significant reduction in insulin solubility can be explained as Na deoxycholate has been shown to confer a concentration - dependent hydrophobicity on proteins like insulin, thereby enhancing their lipophilicity, which would reduce aqueous solubility (Sun et al 2011).

At other concentrations tested, no significant change in insulin solubility was observed, although the graph showed a reversed/ inverted bell shaped curve. This was expected as (being a salt of a weak acid with pKa 6.58, which was close to that of HBSS) even at the highest concentrations of the salt used, there was no change in pH of the resulting solution. Therefore, apart from hydrophobic interactions, no counter-ion effects were expected or observed with Na deoxycholate.

Surprisingly, in the presence of arginine, there was no significant change in the solubility of insulin in HBSS even at high concentrations (200-400µg/mL). Data from pH profile in Figure 6.5 also showed that the buffering capacity of HBSS was maintained in the presence of arginine until 200 and 400µg/mL, after which pH increased from 7.4 to about 9 units. Theoretically, an increase in insulin solubility was expected at this pH, following the Henderson-Hasselbalch equation, however this was not evident. A possible reason for this observation could be based on the isoelectric point of arginine (10.76), which is less than two units away from the solution pH, thereby preventing complete ionisation of arginine, to cause the dissociation of insulin. On the other hand, lysine showed similar pH results as that seen for arginine; however, a significant increase in insulin solubility was observed at higher lysine concentrations (200-400 µg/mL) that resulted in an increase in pH from 7.4 to about 9. This difference between solubility enhancement characteristics of arginine and lysine, despite similar effects on pH, can be explained based on the pKa of these amino acids. Because of the high basicity of the arginine side chain, and the presence of other ions contributed by the buffer to the system, ion pairing between arginine and any non-protein ion would be hardly reversible due to high basicity of arginine. Therefore, in the presence of arginine, despite the high pH, insulin might still remain in its non-ionised form and thus have low solubility. However, in the presence of lysine with lower basicity of the side chain, the amino acid would be more available to interact with insulin ions, thereby maintaining its ionised state and enhancing insulin solubility. Elshaer et al (2011) also reported a higher indomethacine solubility in lysine than in arginine solution, despite the higher pKa of the arginine amino acid. This disparity was attributed to the self-association that exists between lysine and the drug, but is absent in the presence of arginine, due to the presence of two proton acceptor and 1 proton donor groups in lysine, but low proton acceptor groups in arginine; resulting in low self-association of arginine. For histidine,

although a slight increase in insulin solubility was observed with the addition of the amino acid, insulin solubility (and solution pH) remained constant irrespective of the concentration of histidine used. Histidine has a side chain pKa of 6.04 and was not able to alter the pH of the system, as expected from the Henderson-Hasselbalch equation. Histidine has slight basic or neutral properties at neutral pH. The low basicity of the histidine side chain means it can gain or lose electrons easily, thereby keeping insulin in both an ionised or non-ionised state. This property of histidine may be of no benefit to insulin solubility, but its usefulness might be enhanced during insulin permeation. Elshaer (2011) reported the inability of histidine to dissociate the acidic drug indomethacin due to its weak basicity, thus ion pairs and salt formation could not be established. Golovanov et al (2004) reported that the presence of arginine or glutamic acid alone was unable to significantly improve the solubility of proteins tested; however, a significant increase in solubility and stability was observed when equimolar ratios of both amino acids were added to the system. Xue et al (2012) also suggested that combinations of permeation enhancers may improve efficacy and further lower the concentrations of each enhancer to be used; resulting in lower toxicity**.**

In the presence of the acidic amino acids (Figure 6.6), insulin solubility in HBSS was slightly increased by glutamic acid, with no observed change in solubility in the presence of aspartic acid from 10-200 µg/mL amino acid concentration. This was not surprising since at these concentrations of both acidic amino acids, no change in pH was observed, due to the buffering capacity of HBSS (Franks *et al* 2000). However, a drastic reduction in insulin solubility was observed at 400 µg/mL amino acid concentrations, with a simultaneous drop in system pH from about 7 to 5.95 and 6.25 for aspartic and glutamic acids, respectively. This reduction in solubility was expected due to the closeness of the system pH to the isoelectric point of insulin, leading to precipitation of the protein from solution. Physical observation showed the formation of a cloudy solution. Wintersteiner and Abramson (1933) reported low solubility of insulin at pH values around its pI. At these pH values (4.6 – 6.5), the solubility of insulin was low and fairly constant (Wintersteiner and Abramson 1933).

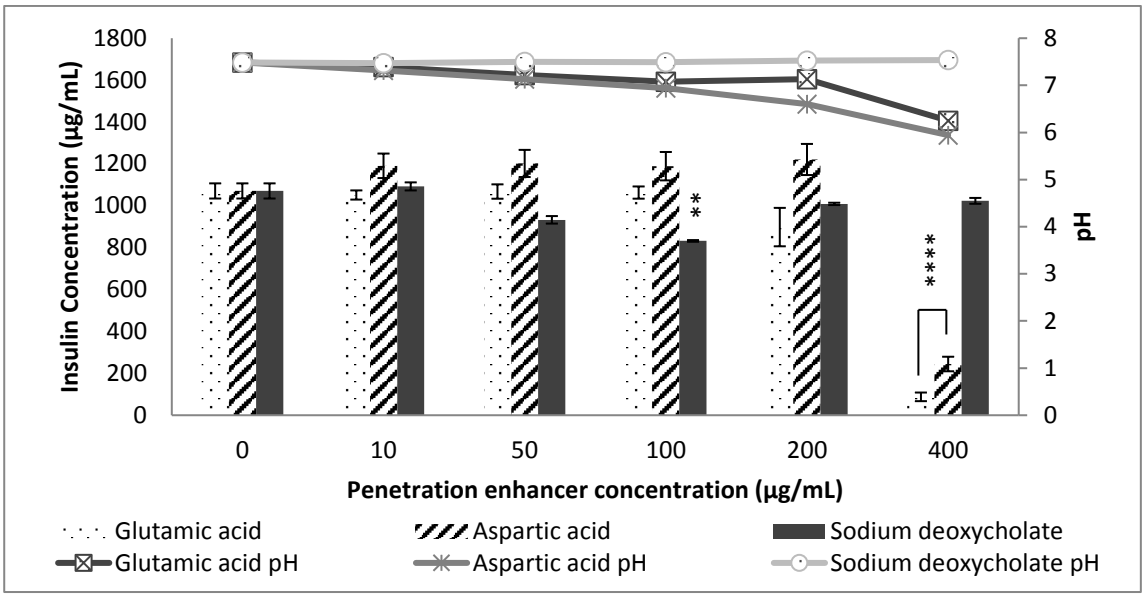

Figure 6.6 Comparing the effect of acidic amino acids and Na deoxycholate on the solubility of insulin in HBSS at 25 ° C, (n=3) (1 mg insulin = 27 IU).

Therefore, it can be concluded that the amino groups of the basic amino acids and the carboxyl groups of the acidic amino acids have the capacity for ionisation, and affect insulin solubility due to the ease of formation of ion pairs and soluble complexes in the presence of counter ions furnished by ionisable sites on the insulin moiety (Elshaer *et al* 2011). This effect was dependent on the resultant system pH, pKa of the amino acids and the differences between these values and the isoelectric points of both insulin and the amino acids/ bile acid salts (Hames and Hooper 2005).

6.3.3 Insulin octanol/ water distribution

Because octanol has been reported to possess similar lipophilicity as the cell membrane, the octanol/ water distribution coefficient (log D) has been employed as a simplistic investigative tool to predict the behaviour of compounds at the cell membrane surface (Elshaer *et al* 2014). The partition behaviour of insulin from the organic phase (deionised water saturated 1-octanol) to the aqueous phase (1-octanol saturated deionised water) was determined, to calculate the log D of insulin, and thereafter determine the ability of basic/ acidic amino acids to modify insulin partition characteristics, as a prediction of *in vivo* behaviour (Camenisch *et al* 1998, Elshaer *et al* 2014).

Figure 6.7 represents the partition behaviour of insulin at equilibrium between aqueous and lipophilic phases in the absence and presence of representative amino acids.

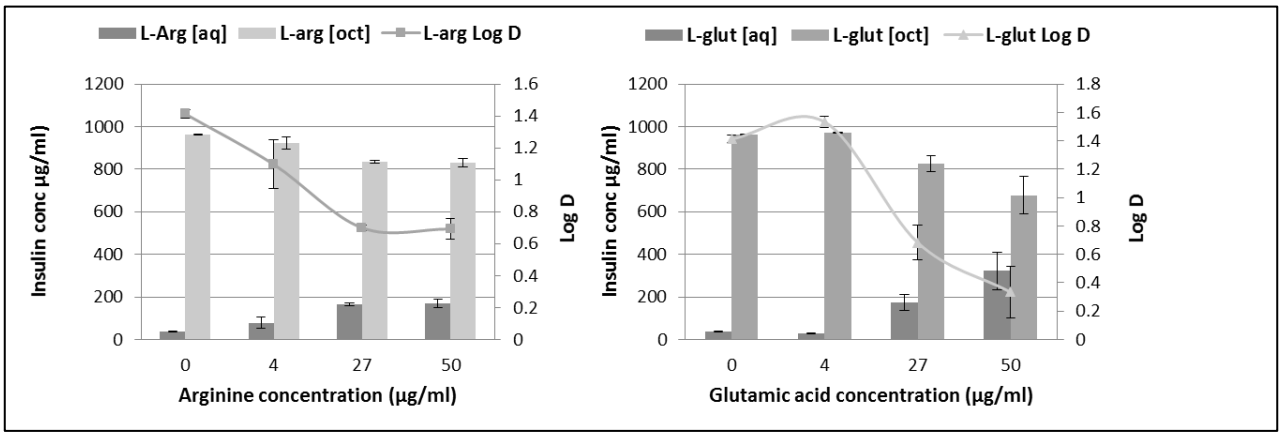

Figure 6.7 Effect of basic and acidic amino acids on octanol/ water distribution of insulin (n=3), as a means of predicting in vivo characteristics (1 mg insulin = 27 IU).

An increase in insulin hydrophilicity was observed with increasing amino acid concentrations, irrespective of either their basic or acidic nature. However, for the basic amino acid arginine, this increase in hydrophilicity was observed to plateau after 27µg/mL, an observation that was not seen with the acidic amino acid, glutamic acid. Arginine was able to reduce the apparent distribution coefficient (log D) of insulin from 1.4 to about 0.7 at 27µg/mL arginine. Similarly, glutamic acid was able to reduce the log D of insulin to about 0.7 at 27µg/mL glutamic acid, with a further reduction to 0.3 at 50µg/mL glutamic acid. Matsuura et al (1993) reported an increase in the apparent distribution coefficient of insulin in 1-octanol in the presence of increasing stoichiometric quantities of sodium dodecyl sulphate resulting in a significant loss in aqueous solubility due to the formation of an insulin-SDS complex with higher lipophilicity than insulin. Thus, it is believed that in this system, the presence of the amino acids impacts on pH, which keeps insulin in the ionised state, and this ionised state of insulin, enhances its solubility in and partitioning into the aqueous phase (Matsuura *et al* 1993, Samiei *et al* 2013). The trend that insulin could not be partitioned from the octanol phase into the aqueous phase beyond 27µg/mL arginine, but was still observed to occur beyond this concentration for glutamic acid, may be explained using the higher free energy required for arginine (12.3 kJ/mol) than glutamic acid (8.2 kJ/mol) to partition into the

octanol phase; since the charged side chains need to be protonated (or deprotonated, respectively) before partitioning can occur. (Engelman *et al.* 1986). Furthermore, it has been reported that at high concentrations of positively charged arginine, promotion of refolding of recombinant proteins is observed; and at higher concentrations, arginine may increase protein destabilisation (Golovanov *et al* 2004).

6.3.4 Insulin permeability across TR146 cell layers

Ion pairs can be formed in the presence of oppositely charged ions in solution. Polypeptides such as insulin with multiple potentially ionisable regions depending on the amino acid sequence and system pH, have the potential of forming ion pairs with reactive amino acid side chains, to increase lipophilicity and thus may enhance permeability (Quintanar-Guerrero *et al* 1997). Quintanar-Guerrero et al (1997) concluded that ion-pairing should be investigated as a potential route for enhancing lipophilicity of compounds to facilitate their absorption across lipophilic membrane barriers. TR146 cells were grown on transwell inserts for 28 – 29 days before use for permeability experiments. Integrity of the stratified layers was monitored using TEER as shown in Figure 6.8. TEER results showed the formation of a stable stratified layer between days 28 to 29 which were used for experiments, as reported by other authors (Xue *et al* 2012).

The permeation of insulin across TR146 cell layers was tested in the absence/ presence of increasing concentrations of the five amino acids and Na deoxycholate. HPLC was used to monitor insulin stability after permeation and there was no significant change in insulin retention time, nor was the appearance of multiple peaks observed. For all the experiments, insulin concentration was held constant at 1000 µg/mL (Xue *et al* 2012). Generally, irrespective of the formulations tested, the amount of insulin permeated increased with time. The maximum amount of insulin that permeated the cells in the absence of enhancers (control) was 4.07 ± 0.82% after 4 hours.

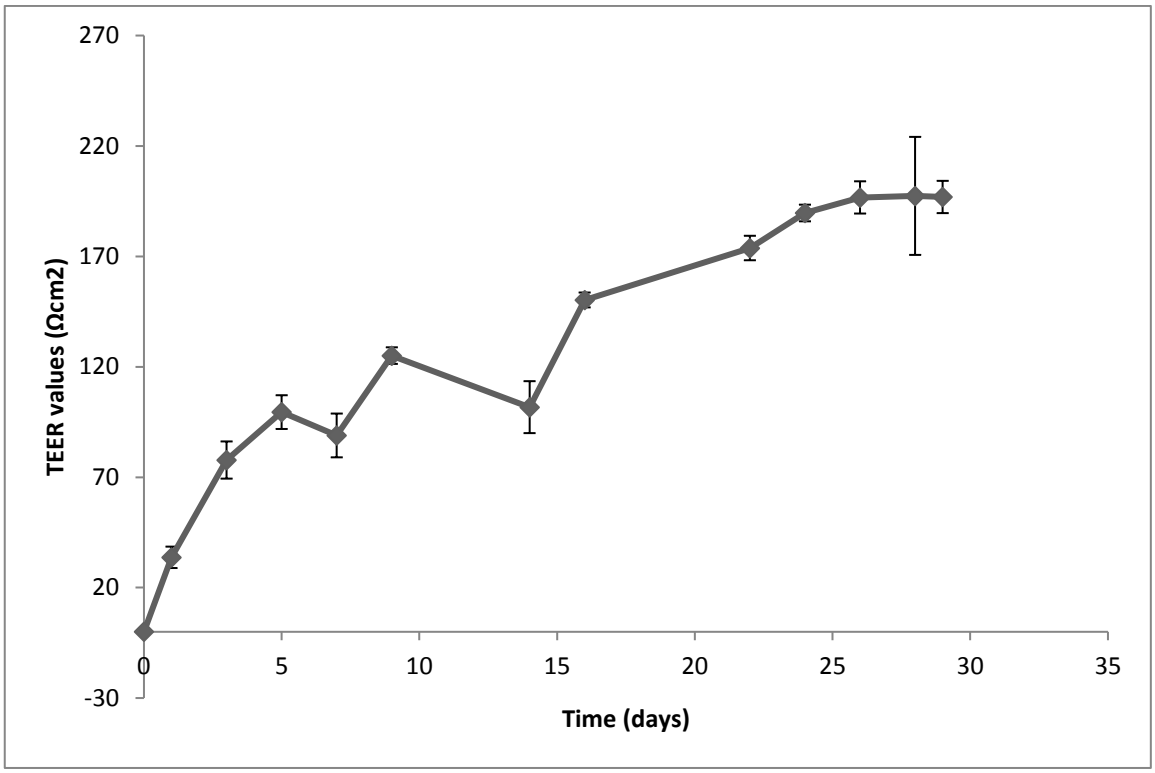

Figure 6.8 Transepithelial electrical resistance results for TR146 cells grown on transwell inserts for 30 days (n=9). Cell layer integrity was found to be maintained over the time period used for the permeability studies.

6.3.4.1 Basic amino acids

6.3.4.1.1 Arginine

For arginine (Arg), the highest percentage permeated was seen with 50µg/mL, at 1.85 ± 0.09% after 30 minutes with a steady increase to 9.86 ± 0.62% after 4 hours (Figure 6.9). The coefficient of apparent permeability of insulin through the actual cell layers, without the interference of the membrane Pcell, was calculated using equation 6.9. As expected, 50 µg/mL Arg solution exhibited the highest Pcell values at 5.65 ± 0.56 x 10-6 cm/s (Table 6.2) and highest enhancement percentage of 184.89 ± 44.83% (Figure 6.10). However, these values were not significant compared to the control.

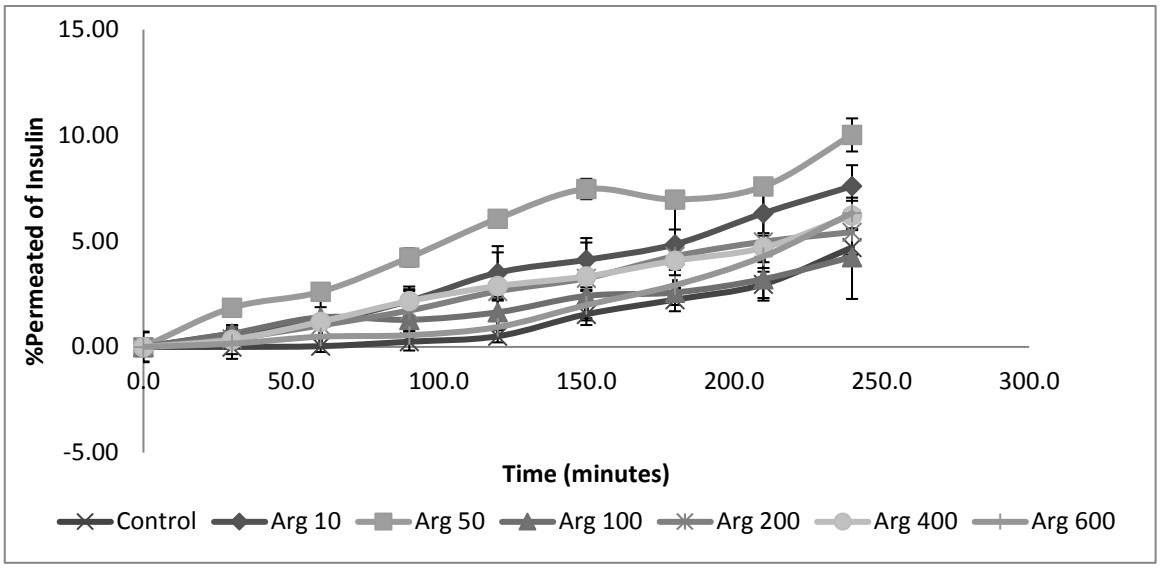

Figure 6.9 Percentage of insulin permeated in the presence of various concentrations of arginine (Arg) (n=3). No significant enhancement in insulin permeability (p>0.05) was observed in the presence of arginine.

Table 6.2 Effect of penetration enhancers on permeability of insulin through TR146 cell layers (n=3)

Formulation	Concentration (μg/mL)	P_{app} ± SD ($x10^{-6}$) (cm/sec)	P_{cell} ± SD ($x10^{-6}$) (cm/sec)	Recovery ± SD (%)
Control	-	2.98 ± 0.40	3.12 ± 0.41	83.94 ± 28.87
Arg	10	3.01 ± 0.38	3.16 ± 0.40	103.03 ± 5.24
	50	5.18 ± 0.40	5.65 ± 0.56	101.72 ± 2.18
	100	2.11 ± 0.39	2.19 ± 0.42	97.56 ± 2.82
	200	2.53 ± 1.48	2.64 ± 1.59	91.75 ± 2.70
	400	3.46 ± 1.40	3.66 ± 1.51	86.63 ± 4.85
	600	3.19 ± 1.75	3.40 ± 1.95	83.55 ± 3.04
Lys	10	7.08 ± 1.82*	7.95 ± 2.12*	81.47 ± 2.13
	50	3.76 ± 1.66	4.02 ± 1.85	82.28 ± 3.03
	100	9.51 ± 0.56***	11.19 ± 0.76***	83.48 ± 0.45
	200	8.92 ± 4.94***	10.56 ± 6.59***	107.14 ± 7.29
	400	3.31 ± 0.65	3.49 ± 0.71	89.83 ± 4.29
	600	0.81 ± 0.80	1.25 ± 0.71	85.96 ± 3.22

His	10	10.7 ± 2.93***	12.9 ± 3.91***	98.76 ± 3.94
	50	3.21 ± 1.19	3.38 ± 1.30	82.22 ± 19.89
	100	2.89 ± 2.30	3.09 ± 2.48	90.57 ± 10.48
	200	4.58 ± 2.96	4.99 ± 4.07	84.05 ± 2.33
	400	3.87 ± 0.62	4.13 ± 0.89	86.16 ± 8.40
	600	2.84 ± 1.12	2.98 ± 1.71	88.18 ± 4.83
Glu	10	6.12± 1.83*	6.77E-06 ± 2.16*	87.83 ± 2.31
	50	5.83 ± 2.53	6.45 ± 2.99	85.43 ± 1.02
	100	7.29 ± 2.77	8.27 ± 3.44*	87.49 ± 0.52
	200	9.05 ± 2.02***	10.61 ± 3.63**	102.32 ± 3.63
	400	5.02 ± 2.64	5.58 ± 3.34	91.28 ± 2.79
	600	0.11 ± 0.01	0.11 ± 0.05	78.39 ± 1.15
Asp	10	7.71 ± 0.92**	8.78 ± 1.19*	95.27 ± 2.60
	50	5.58 ± 2.16	6.13 ± 2.49	89.97 ± 5.76
	100	3.32 ± 0.85	3.51 ± 0.94	96.92 ± 6.27
	200	8.52± 2.61***	9.86 ± 3.32**	85.77 ± 12.40
	400	3.88 ± 0.68	4.14 ± 0.79	77.55 ± 20.39
	600	2.95 ± 0.41	3.09 ± 0.45	63.59 ± 5.53
SDC	10	4.94 ± 0.54	5.12 ± 0.68	109.40 ± 12.72
	50	5.72 ± 0.60	5.96 ± 0.87	104.41 ± 9.39
	100	5.66 ± 0.60	5.90 ± 0.89	108.25 ± 5.63
	200	11.16 ± 0.17***	13.55 ± 0.65***	89.98 ± 2.86
	400	11.00 ± 0.72***	13.26 ± 0.59***	92.55 ± 2.03
	600	11.13 ± 0.68***	13.46 ± 0.55***	95.41 ± 1.35

P_{insert} (no cells) = 65.192 x 10^{-6} cm/s

Solubility data for arginine in HBSS presented in Figure 6.5, showed that arginine did not significantly alter the solubility (and therefore the dissociation) of insulin compared to the control.

Thus, it was not surprising that arginine could not significantly alter the permeation of insulin, although a slight increase was observed at 50µg/ mL compared with the control.

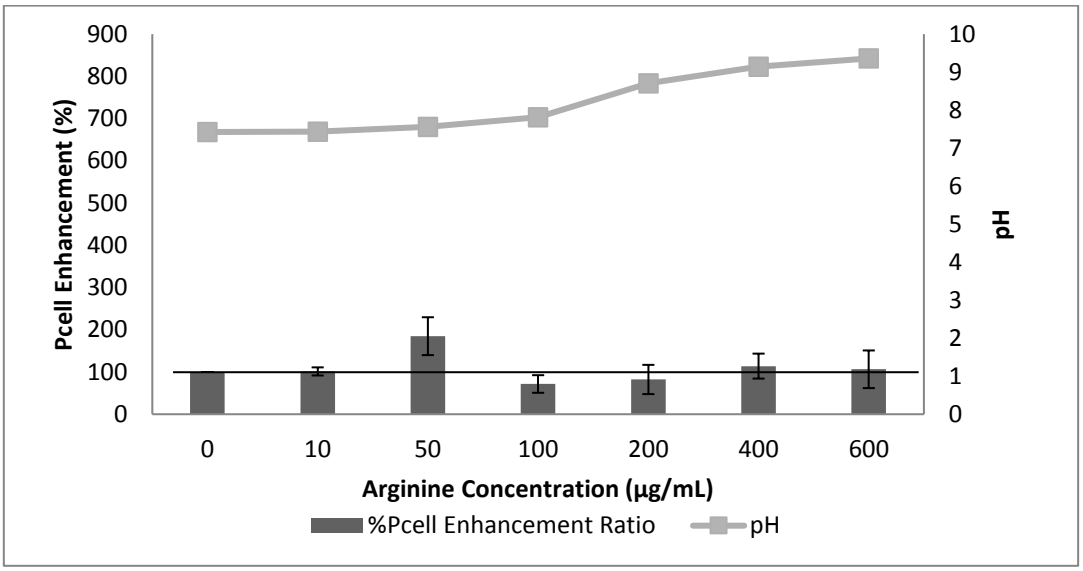

Figure 6.10 Comparing the percent enhancement of insulin permeability through TR146 cell layers in the presence of various concentrations of arginine and solution pH (n=3).

This was expatiated in Figure 6.11 that compares the solubility of insulin in the presence of the amino acids to the permeation observed at these concentrations. Arginine has a basic side chain with pKa 12.48 and at lower arginine concentrations of 10 – 100 µg/mL (pH 7.4 – 7.8), both insulin and arginine would be expected to be ionised and able to form stable unionised ion pairs that would enhance insulin permeability (Elshaer *et al* 2014). Significant increase in permeability at these lower concentrations of arginine was not observed, possibly due to the presence of limited concentration of ionised arginine molecules to pair with the ionised insulin moieties. However, as arginine concentration increased, solution pH increased steadily to a maximum of 9.36 at 600µg/mL arginine. Since this pH is close to the isoelectric point of arginine (10.71), it is possible that although insulin molecules were ionised, less ionisation of the arginine molecule occurred, with the presence of less counter ions available to form neutral insulin-arginine moieties, and the final result of insignificant difference in insulin permeation was observed (Samiei *et al* 2013, Samiei *et al* 2014). It would seem that for the concentrations of arginine tested, the 50µg/mL concentration gave the best balance of insulin-arginine unionised molecules to enhance

permeability, since only the non-ionised form of a drug would permeate the cell membrane (Ivaturi and Kim 2009, Dahan and Miller 2012).

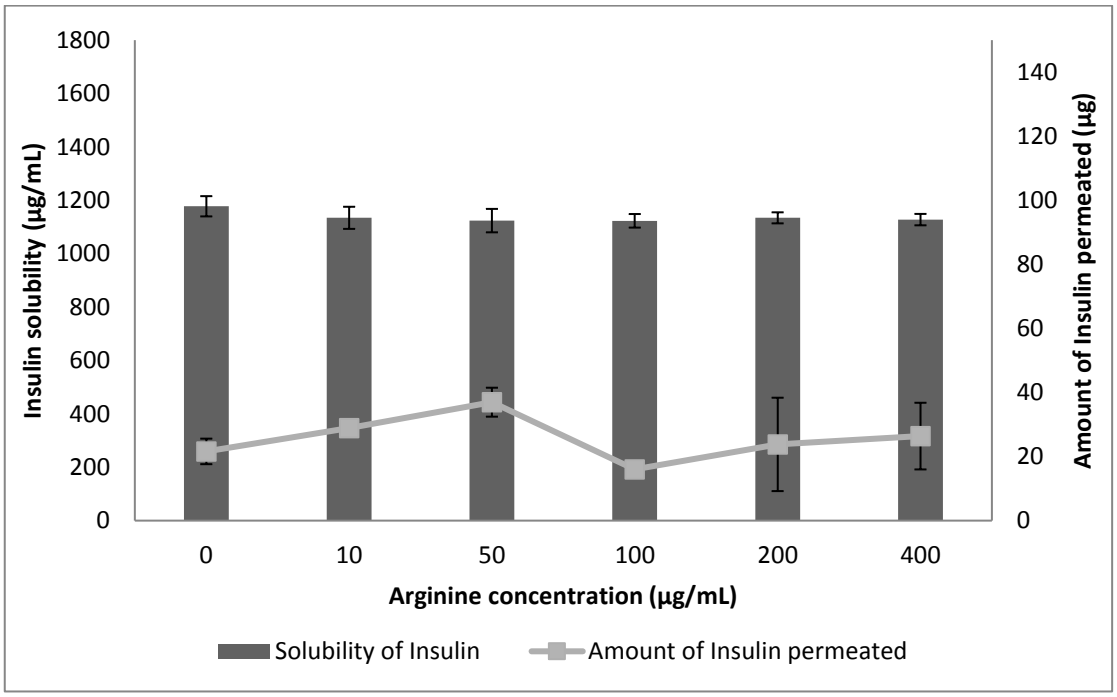

Figure 6.11 Comparing the solubility in HBSS at 25°C and permeability of insulin through TR146 cells layers, in the presence of various concentrations of arginine (n=3) (1 mg insulin = 27 IU).

Since an aim of this study was to identify effective and safe penetration enhancers for insulin through buccal cells, transepithelial electrical resistance (TEER) of the cell layers and the MTT assay were conducted to assess the toxicity of amino acids to the cells, to determine if any observed permeation enhancement was due to destruction of cell layers or increase in cellular toxicity. The TEER results for arginine represented in Table 6.3 exhibited no significant reduction in TEER values across all concentrations of arginine used. Thus, cell layer integrity can be said to have been maintained throughout the 4 hours of the permeability experiment (Nielsen and Rassing 2002, Xue *et al* 2012, Elshaer *et al* 2014). Elshaer (2014) reported similar findings where high concentrations of arginine did not significantly affect the TEER measurements before and after permeability studies using Caco-2 cells. This was an expected result since MTT results (Figure 6.12) revealed a reduction in cell viability from arginine concentrations 500µg/mL and above. Thus, although arginine was safe, it did not significantly enhance the permeation of insulin through TR146 cells (Van Meerloo *et al* 2011). These MTT results for arginine were in conflict with findings reported by Xue et al (2012), where 10 - 50µg/mL arginine solutions were found to be toxic to TR146 cells

using the MTT assay. This conflict could be explained on the basis that in the current study, TR146 cells were exposed to amino acids for 4 hours - duration of a permeability study, adapted from Jacobsen *et al* (1996); while in the earlier study, exposure times ranged from 24 – 48 hours. However, because the TR146 cells used for permeability studies formed multiple layers of stratified squamous epithelial cells, while MTT assays were carried out on single cells in active exponential growth phase, low toxicity is to be expected from the permeability studies (Xue *et al* 2012).

Table 6.3 Transepithelial electrical resistance (TEER) measurements for enhancers before and after permeability experiments through TR146 cell layers (n=9).

Formulation	Concentration (µg/mL)	TEER measurements before ± SD (Ω/cm^2)	TEER measurements after ± SD (Ω/cm^2)	Recovery (%)
Control	-	254.99 ± 75.45	254.12 ± 83.06	99.66
Arg	10	255.73 ± 60.48	266.56 ± 83.77	104.23
	50	223.25 ± 25.88	281.49 ± 60.83	126.09
	100	215.16 ± 46.03	238.68 ± 48.21	110.93
	200	265.19 ± 98.54	275.40 ± 53.04	103.85
	400	255.11 ± 72.29	281.74 ± 80.82	110.44
	600	324.43 ± 112.63	260.09 ± 90.12	80.17
Lys	10	275.27 ± 58.57	299.91 ± 97.82	108.95
	50	317.21 ± 54.83	294.44 ± 53.03	107.18
	100	447.00 ± 69.32	274.4 ± 41.58****	61.39
	200	337.37 ± 86.83	299.91 ± 54.94	88.90
	400	296.55 ± 70.94	283.86 ± 65.75	95.72
	600	279.63 ± 38.03	304.27 ± 69.22	108.81

His	10	284.60 ± 69.65	338.99 ± 71.12	119.11
	50	283.61 ± 102.74	271.04 ± 70.50	95.57
	100	366.86 ± 85.50	298.54 ± 62.06	81.38
	200	394.24 ± 69.75	283.86 ± 48.88**	72.00
	400	348.82 ± 52.10	273.53 ± 78.09	78.42
	600	308.25 ± 50.88	362.76 ± 58.50	117.68
Glu	10	370.60 ± 97.80	336 ± 147.11	90.66
	50	381.42 ± 96.48	320.57 ± 59.24	84.05
	100	459.2 ± 102.68	286.72 ± 43.37	62.44
	200	343.96 ± 86.82	252.37 ± 52.52	73.37
	400	350.93 ± 102.59	283.11 ± 38.77	80.67
	600	303.77 ± 87.62	337 ± 72.72	110.94
Asp	10	295.06 ± 25.06	295.56 ± 98.81	100.17
	50	275.27 ± 27.47	292.44 ± 64.82	106.24
	100	289.71 ± 80.61	258.84 ± 46.01	89.35
	200	349.44 ± 104.69	243.66 ± 50.88	69.73
	400	379.80 ± 114.17	251.25 ± 85.45	66.15
	600	558.51 ± 67.52	283.61 ± 108.87***	50.78
SDC	10	211.33 ± 38.58	222.22 ± 40.91	105.15
	50	234.56 ± 48.87	195 ± 37.08	83.14
	100	179.67 ± 48.87	199.89 ± 44.80	111.26
	200	252.78 ± 45.86	188.89 ± 39.91*	74.73
	400	244.56 ± 87.71	172 ± 61.47*	70.33
	600	224.22 ± 25.82	155.33 ± 57.05**	67.05

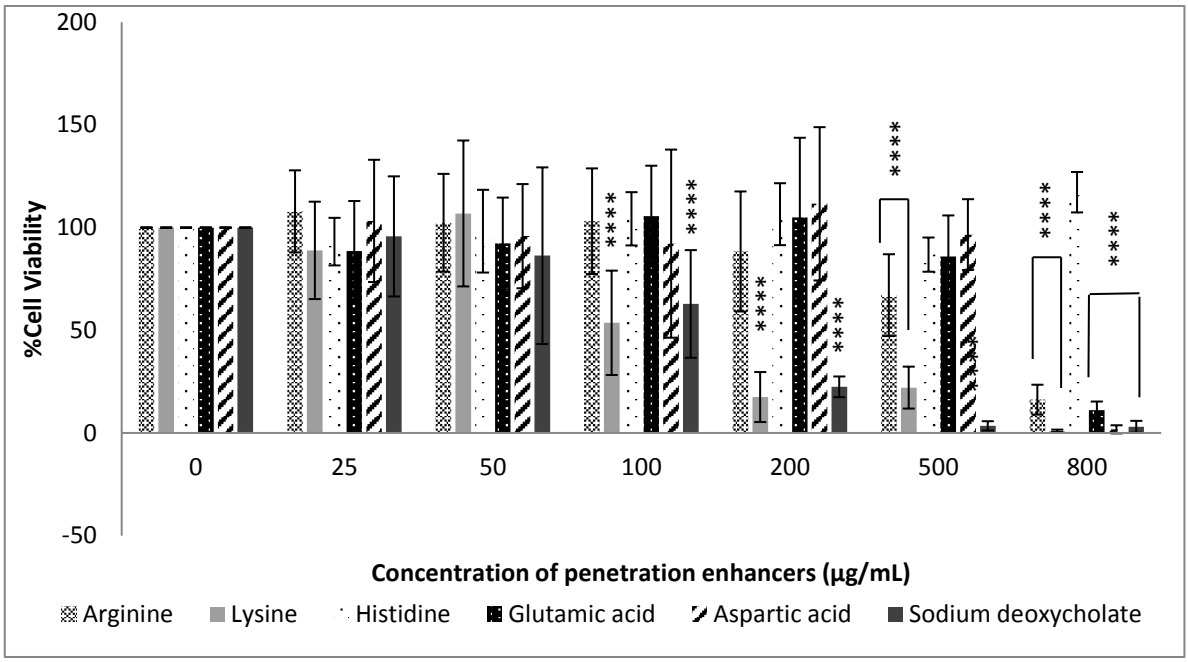

Figure 6.12 Effect of penetration enhancers on the viability of TR146 cells in the presence of increasing concentrations of amino acids and Na deoxycholate, utilising the MTT assay (n=12). Na deoxycholate and lysine exhibited the highest toxicity to cells, while histidine, glutamic acid and aspartic acid exhibited the highest safety potential.

6.3.4.1.2 Lysine

Lysine is a basic amino acid with side chain pKa of 10.54 and isoelectric point 9.74 (Table 6.1). Similar to arginine, the increase in insulin permeability in the presence of increasing lysine concentrations was concentration-dependent; with maximum percentage permeated observed at 100 µg/mL lysine (Figure 6.13). Results showed that 4.69 ± 0.42% insulin permeated after 30 minutes, with a significant steady increase after 2 hours to 13.28 ± 1.78% and 27.11 ± 0.88% at the end of the experiment (4 hours). At 600 µg/mL lysine, maximum percentage of insulin permeated was observed to be lower than the control. Overall, 100, 200 and 10 µg/mL lysine significantly increased the Pcell with values of 11.19 ± 0.76 x 10-6, 10.56 ± 6.59 x 10-6 and 7.95 ± 2.12 x 10-6 cm/s, respectively (Table 6.2). High enhancement percentages were also recorded as 363.01 ± 64.22%, 328.01 ±175.85% and 251.43 ± 37.94%, respectively, as highlighted in Figure 6.14. From solubility results in HBSS in the presence of increasing lysine concentrations (Figure 6.5), insulin solubility (and therefore insulin ionisation) was observed to significantly increase from 200 µg/mL lysine concentration, with resultant increase in pH from 7 to 9.

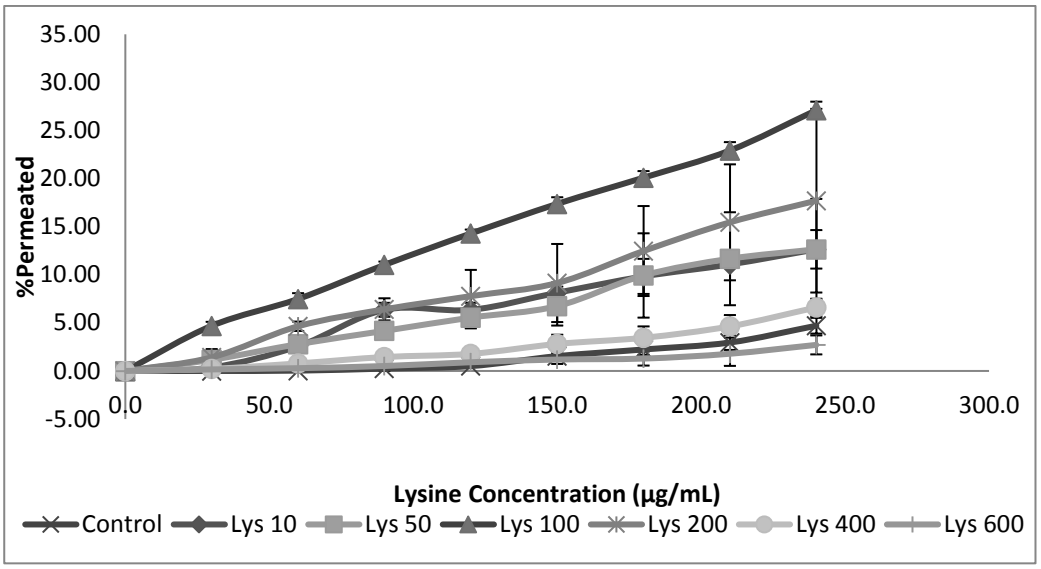

Figure 6.13 Percentage of insulin permeated in the presence of various concentrations of lysine (n=3). 10, 100 and 200 µg/mL significantly enhanced insulin permeation above the control.

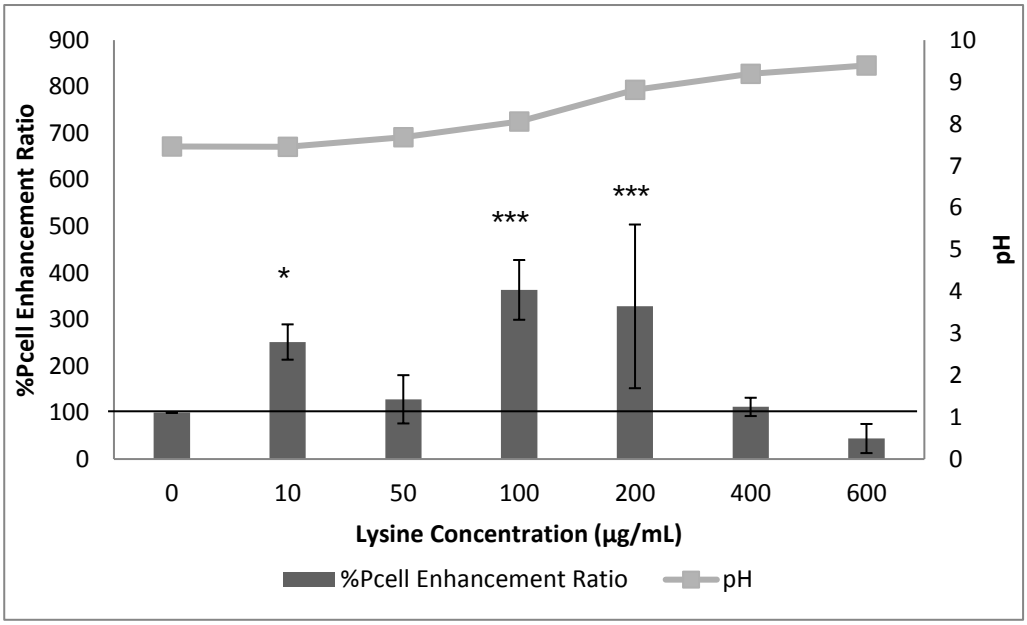

Figure 6.14 Comparing the %enhancement of insulin permeability through TR146 cell layers in the presence of various concentrations of lysine and solution pH (n=3). At higher pH permeation was hindered due to partial dissociation of lysine, and therefore reduced potential for counter-ion formation with insulin.

At 100µg/mL lysine with pH of 7, both lysine and insulin molecules would be ionised, the potential for formation of insulin-lysine neutral molecules would be enhanced with a further increase in permeability. As discussed for arginine earlier, at increasing concentrations of lysine above 200 µg/mL, pH of the solution moved closer to the isoelectric point of lysine (9.74), causing a reduction in lysine ionisation, a fall in the concentration of lysine counter ions available for neutral complex formation with insulin, and a resultant fall in permeability as shown in Figure 6.15. However at 50

µg/mL lysine, a fall in insulin permeability was observed, probably due to the low concentrations of lysine counter ions available for complexation with ionised insulin moieties. Surprisingly, 10 µg/mL lysine significantly enhanced insulin permeability above the control. This observation could be related to the high ionisation of lysine and insulin expected at pH 7. Moreso, insulin permeability could have been facilitated in the presence of lysine through amino acid membrane transporters, which could have been saturated at higher concentrations (Bröer 2008, Elshaer *et al* 2014). Insulin permeability results with lysine as permeation enhancer reinforced the fact that for permeation enhancement to occur in dynamic systems, a stringent balance between ionised and non-ionised species must be maintained (Samiei *et al* 2013, Elshaer *et al* 2014, Samiei *et al* 2014).

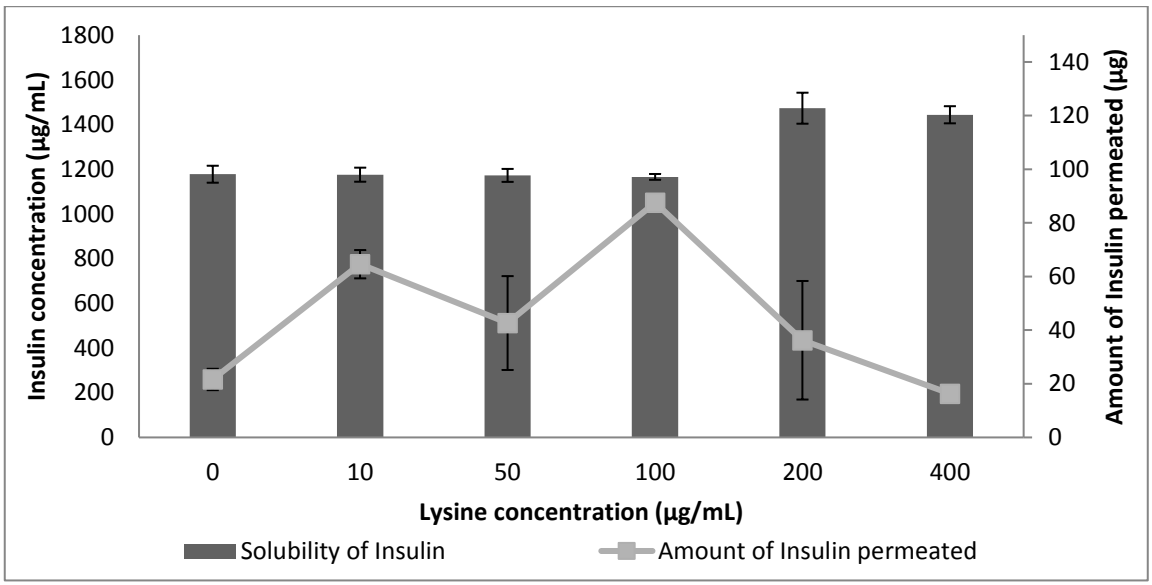

Figure 6.15 Comparing the solubility at 25 °C and permeability of insulin through TR146 cells layers, of insulin in the presence of various concentrations of lysine (n=3). Maximum amount of insulin permeated correlated with the lower ionisation of insulin molecules, enabling the permeability of non-ionised moieties (1 mg insulin = 27 IU).

TEER results presented in Table 6.3 revealed that 100 µg/mL lysine significantly reduced TEER values post permeability assay, thus the enhancement recorded for this concentration could have been produced by leakage through disrupted cellular layers (Xue et al 2012). MTT assay results in Figure 6.12 further revealed a significant concentration-dependent decrease in TR146 cell viability with lysine concentrations ≥100 µg/mL and this could affect cell integrity (Van Meerloo et al 2011). Furthermore, above 100 µg/mL lysine, pH values increased beyond physiologically accepted pH (Figure 6.15); thus, 10 µg/mL lysine was chosen as the optimal concentration of lysine

that effectively enhanced permeation of insulin without affecting cell viability or causing membrane disruption (Khafagy El et al 2007, Kumria and Goomber 2011, Patel et al 2011).

6.3.4.1.3 Histidine

Histidine has a side chain with pKa of 6.04 and isoelectric point of 7.59 (Table 6.1) which may render it neutral or basic at neutral pH. From Figure 6.16, 10µg/mL histidine was found to significantly enhance insulin permeation above the control with 1.69 ± 0.90% permeated after 1 hour, and a steady increase to 8.20 ± 3.50% after 3 hours and a further 16.71 ± 7.65 % after 4 hours. Maximum Pcell (Table 6.2) and percent enhancement (Figure 6.17) values achieved at 10 µg/mL were 12.9 ± 3.91 x 10^{-6} cm/s and 409.44 ± 95.14%, respectively. All concentrations of histidine above 10 µg/mL showed no significant effect on insulin permeation. As highlighted in Figure 6.5, increasing histidine concentration above 10 µg/mL had no significant effect on insulin solubility in HBSS, with no change in solution pH at all concentrations tested. It was expected that histidine and insulin were ionised at this pH, the availability of counter ions facilitated the formation of insulin-histidine neutral complexes that could enhance insulin permeability significantly. Figure 6.18 compares the solubility and permeability of insulin at different concentrations of histidine. From here, it can be seen that no advantage was produced for both insulin solubility and permeability when histidine concentration was increased above 10 µg/mL. Thus, similar to results obtained from lysine, 10 µg/mL histidine was able to produce the optimal balance between ionised and non-ionised insulin molecules in solution, as well as possibly effectively triggering peptide transport proteins to enhance the permeation of insulin across TR146 buccal cells; with higher concentration saturating the transporters.

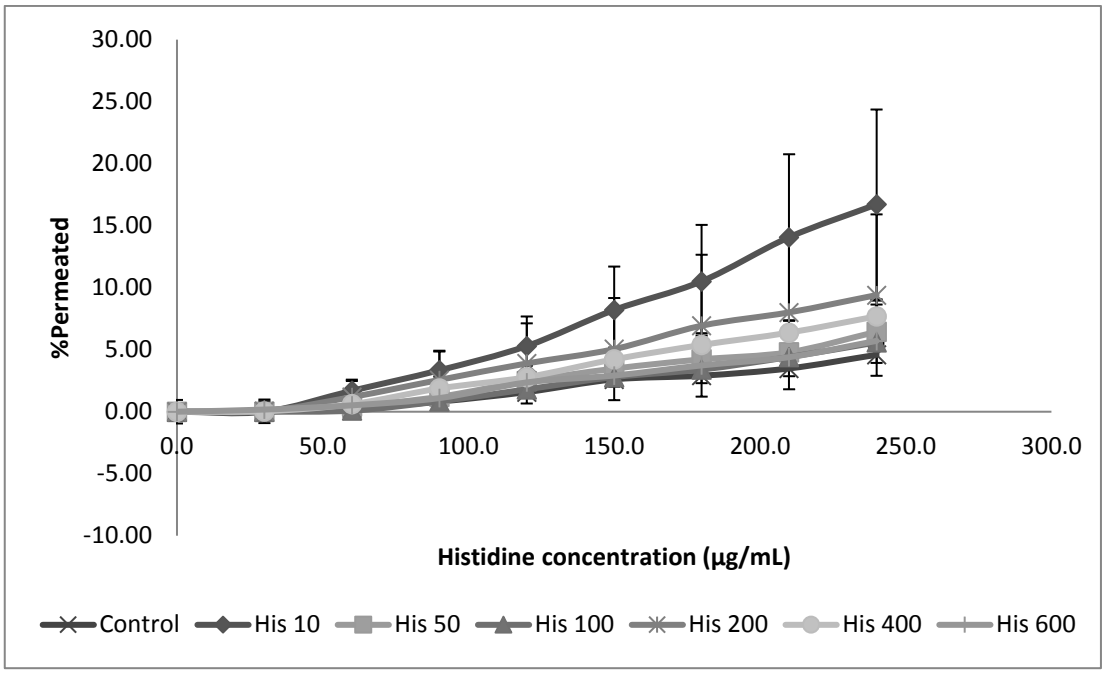

Figure 6.16 Cumulative percentage of insulin permeated in the presence of various concentrations of histidine (n=3). 10 µg/ mL histidine significantly enhanced insulin permeation above the control.

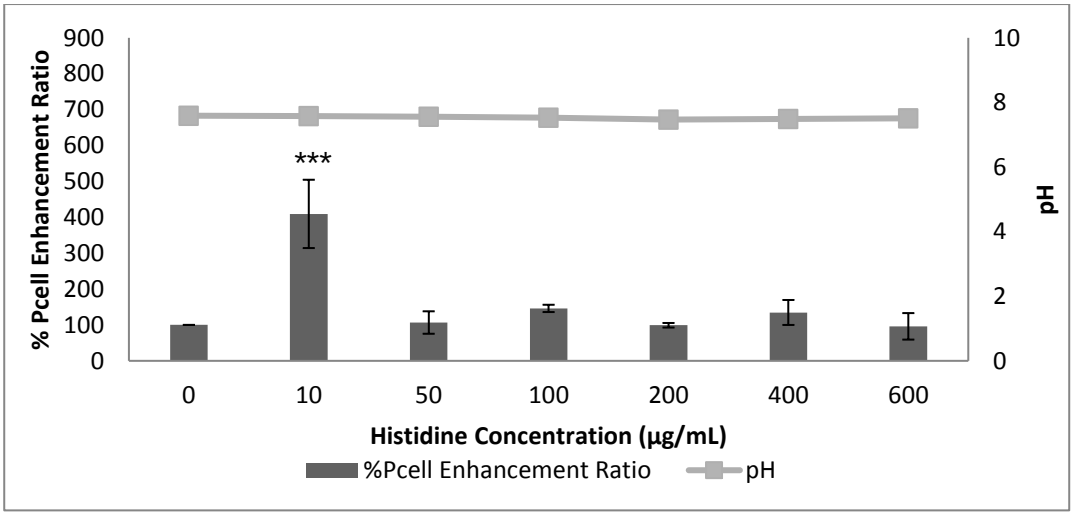

Figure 6.17 Comparing the percent enhancement of insulin permeability through TR146 cell layers in the presence of various concentrations of histidine and solution pH (n=3). Enhanced insulin transport in the presence of histidine occurred with no change in solution pH.

This was further supported by TEER results (Table 6.3) where only 100 µg/mL histidine significantly disrupted cellular integrity, and results from MTT assay (Figure 6.12) revealed that histidine was non-toxic to TR146 cells even at the highest concentration (800 µg/mL) tested. Therefore for the basic amino acids, 10, 100 and 200 µg/mL lysine and 10µg/mL histidine were effective as permeation enhancers for insulin, but only 10 µg/mL of each amino acid was both

effective and non-toxic to TR146 cells (Figure 6.19). 10 µg/mL histidine showed significantly higher permeation enhancement than 10µg/mL lysine.

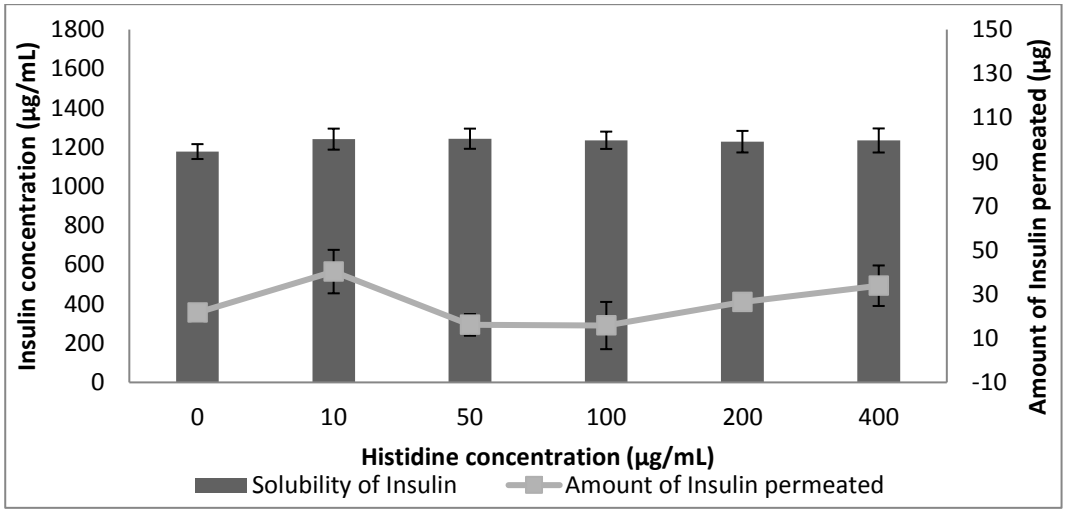

Figure 6.18 Comparing the solubility at 25 °C and permeability of insulin through TR146 cells layers, of insulin in the presence of various concentrations of histidine (n=3). Significant enhancement observed at 10 µg/ mL due to a balance between ionised and non-ionised states of insulin, and the possible triggering of amino acid transporters (1 mg insulin = 27 IU).

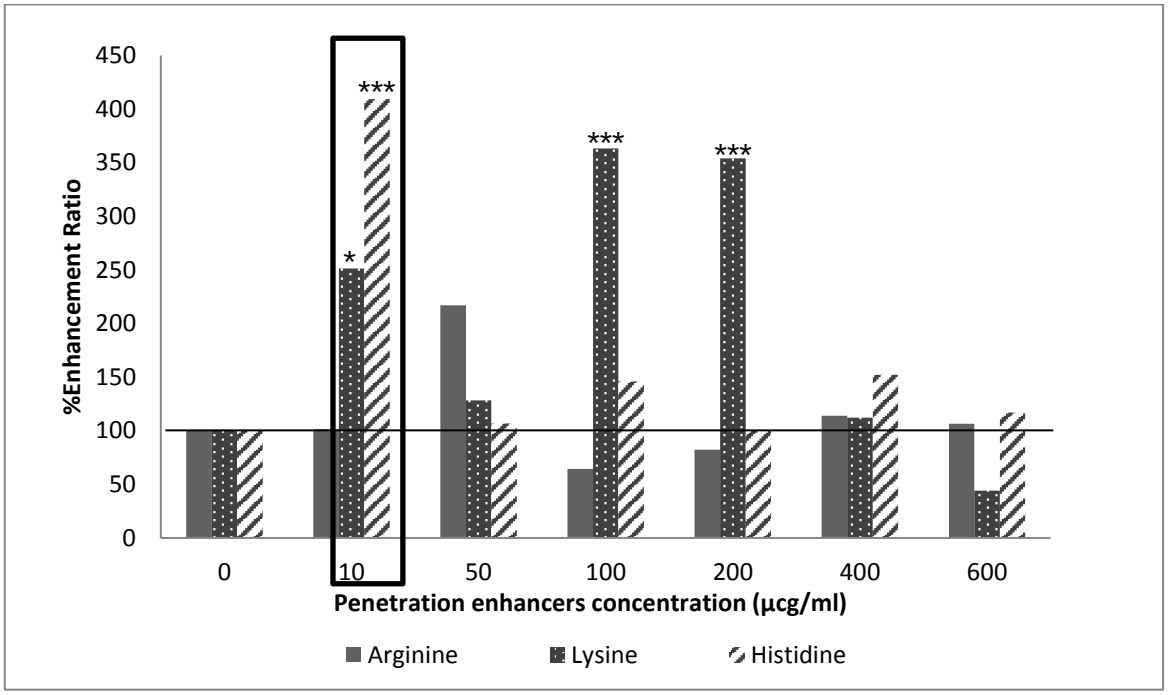

Figure 6.19 Graph highlighting concentrations of basic amino acids that significantly enhanced insulin permeability with no toxicity to TR146 cells (n=3). 10µg/ mL of both lysine and histidine were effective and safe permeation enhancers.

6.3.4.2 Acidic amino acids

6.3.4.2.1 Glutamic acid

Glutamic acid has an acidic side chain with pKa 4.07 and isoelectric point 3.22 (Table 6.1). From Figure 6.20, 10 and 100 µg/mL glutamic acid concentrations were able to significantly increase insulin permeability to 13.97 ± 3.01% and 16.98 ± 9.30% after 4 hours. 200 µg/mL increased permeability to 13.66 ± 4.77% after 3 hours. However, at concentrations above 200 µg/mL, no significant improvement in insulin permeation was observed; with no permeation occurring at 600 µg/mL. Maximum Pcell values were achieved for 200 µg/mL at 10.61 ± 3.63 x 10-6 cm/s (Table 6.2). Maximum enhancement percent for 200, 100 and 10 µg/mL were 307.82 ± 79.23%, 260.36 ± 88.40% and 215.70 ± 53.10%, respectively (Figure 6.21).

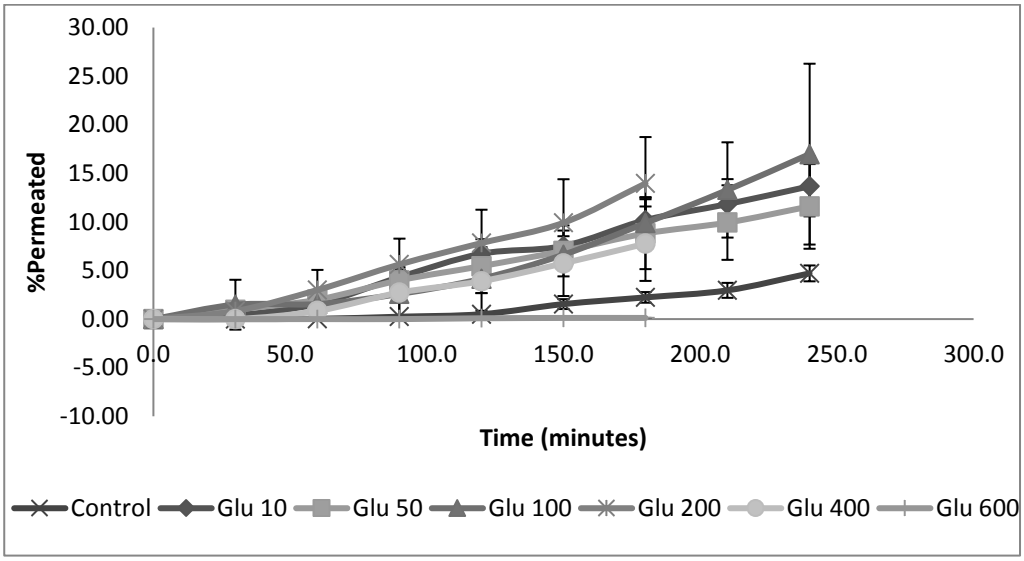

Figure 6.20 Cumulative percentage of insulin permeated in the presence of various concentrations of glutamic acid (n=3). 10, 100 and 200 µg/mL glutamic acid showed significantly higher insulin permeation than the control. Glu 200 and Control were discontinued after 3 hours following a mishap.

These observations for glutamic acid can be directly related to the solubility profile presented in Figure 6.6 and were expected based on the discussions in sections above. No significant difference in insulin solubility and solution pH was observed with increasing glutamic acid concentrations up to 200 µg/mL, however, at 400 µg/mL, insulin solubility reduced drastically with a solution pH of 6.09 at 600 µg/mL (Figure 6.21).

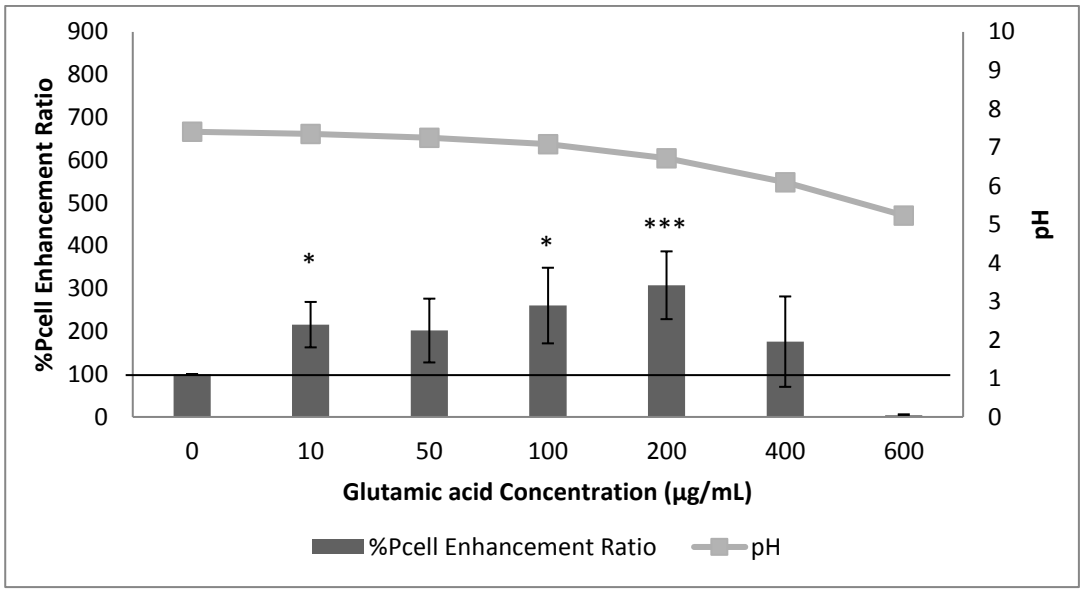

Figure 6.21 Comparing the percent enhancement of insulin permeability through TR146 cell layers in the presence of various concentrations of glutamic acid and solution pH (n=3). No permeation of insulin was observed at 600 µg/ mL glutamic acid due to the low solubility of insulin at this pH.

As these pH values were close to the pI of insulin, less insulin was found in solution with outright precipitation of insulin expected at 600 µg/mL. Thus, no insulin was observed to permeate the cells at this high glutamic acid concentration (Figure 6.22), because only the soluble form of a drug is available to permeate cells and be absorbed into the bloodstream (Dahan and Miller 2012, Samiei *et al* 2013, Samiei *et al* 2014).

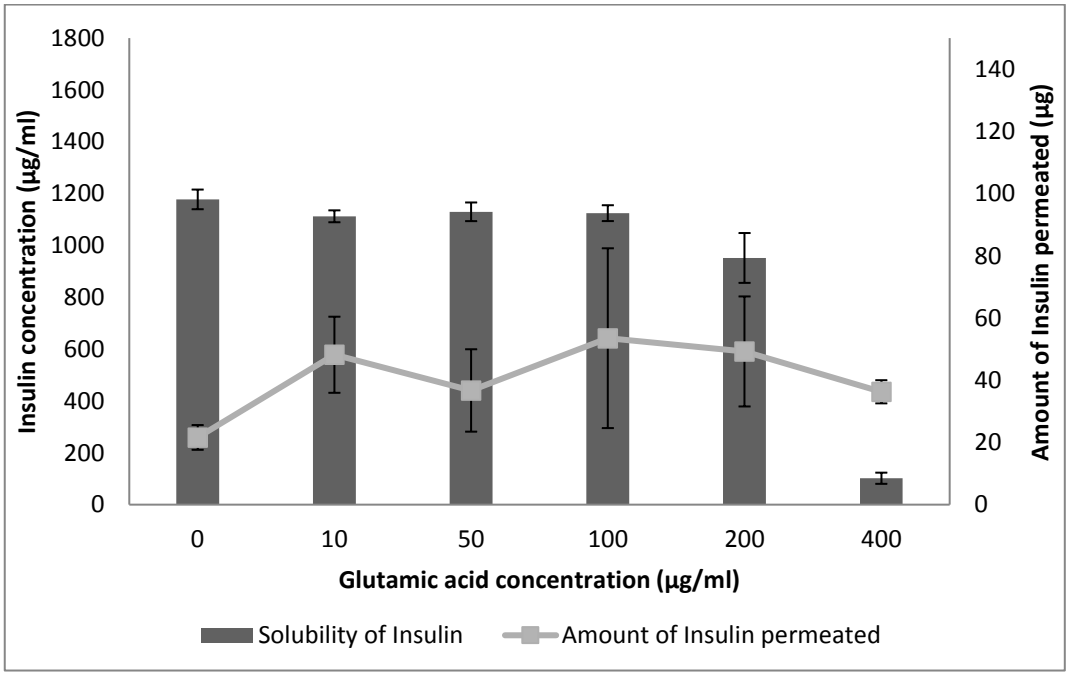

Figure 6.22 Comparing the solubility at 25 °C and permeability of insulin through TR146 cells layers, in the presence of various concentrations of glutamic acid (n=3) (1 mg insulin = 27 IU).

TEER results for glutamic acid (Table 6.3) showed no significant reduction in TEER values at all concentrations tested, while MTT assay results (Figure 6.12) revealed toxicity of cells only at 800 µg/mL glutamic acid, which was outside the concentration range tested. Therefore, glutamic acid was found to be safe and non-toxic to cells across all tested concentrations. Thus, the enhancement in insulin permeability by 10, 100 and 200 µg/mL glutamic acid could be attributed solely to the amino acid facilitation of permeation through the formation of neutral ion pairs with insulin, and/ or through the use of membrane peptide transporter mechanisms, rather than disruption of cell layers or reduced cellular integrity (Elshaer *et al* 2014, Samiei *et al* 2014).

6.3.4.2.2 Aspartic acid

Aspartic acid has an acidic side chain with pKa of 3.9 and isoelectric point of 2.77 (Table 6.1). For aspartic acid, 10 and 200 µg/mL concentrations significantly enhanced the cumulative percentage of insulin permeated with respect to the control (Figure 6.23). The percentages of insulin permeated were 2.03 ± 0.37% and 2.73 ± 0.96% after 1 hour, and increased steadily to 16.20 ± 2.81 and 17.78 ± 4.79% after 4 hours, respectively. As expected, 200 µg/mL gave maximum Pcell values (Table 6.2) at 9.86 ± 4.25 x 10^{-6} cm/s and maximum enhancement percentage (Figure 6.24) of 314.50 ± 85.46%, while 10 µg/mL produced values of 8.78 ± 1.19 x 10^{-6} cm/s and 285.56 ± 62.45%, respectively. Increasing aspartic acid concentration above 400µg/mL did not enhance insulin absorption. Similar to results observed for glutamic acid, increasing aspartic acid concentrations up to 200 µg/mL did not significantly change the solubility of insulin or solution pH, as seen in Figure 6.6. Moreover, for concentrations above 200 µg/mL, insulin permeability drastically declined, with a significant drop in solution pH. However, at all concentrations tested, insulin solubility was higher for aspartic acid than for glutamic acid.

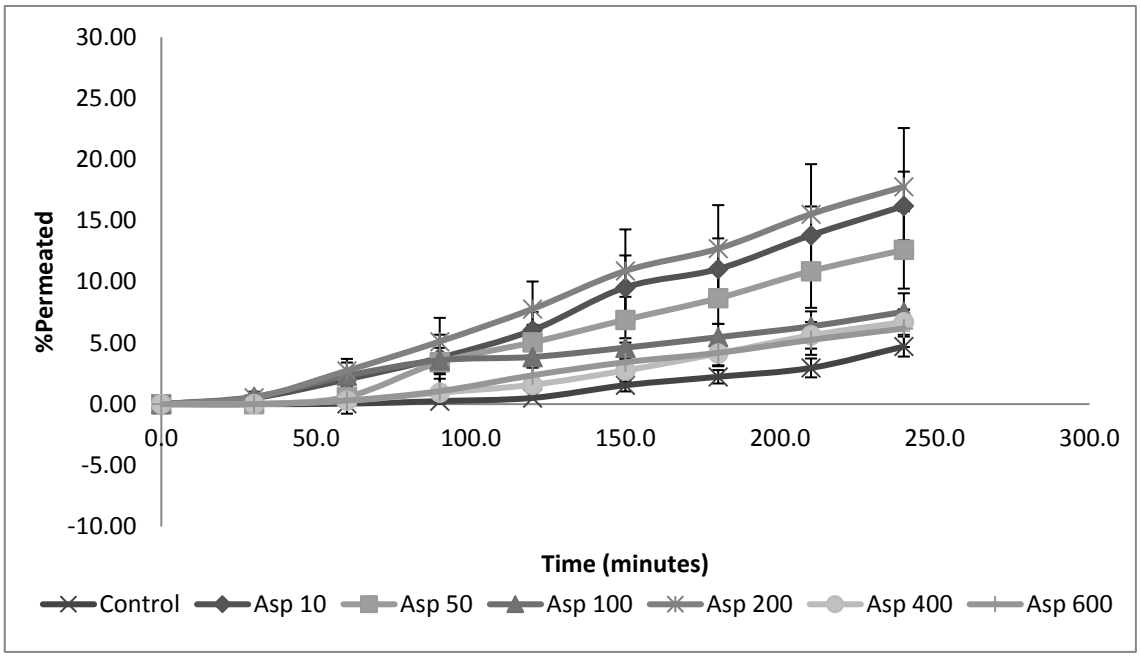

Figure 6.23 Cumulative percentage of insulin permeated in the presence of various concentrations of aspartic acid (n=3). 10 and 200 µg/ mL significantly enhanced insulin permeation above the control.

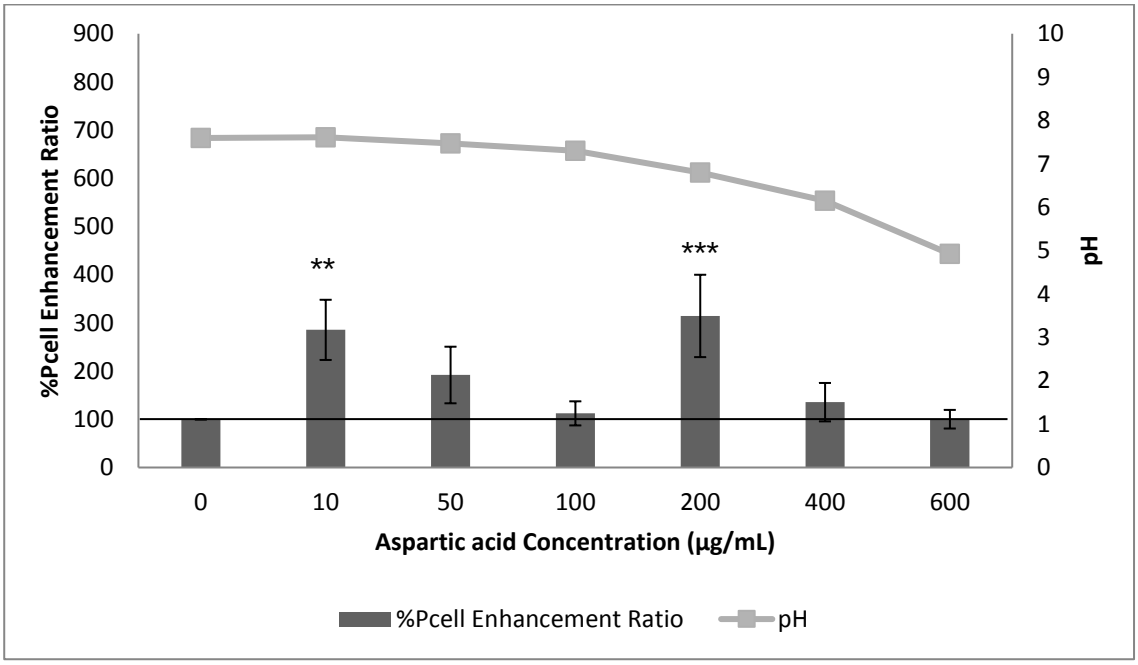

Figure 6.24 Comparing the percent enhancement of insulin permeability through TR146 cell layers in the presence of various concentrations of aspartic acid and solution pH (n=3).

This could be attributed to the fact that the pKa of aspartic acid is lower than that of glutamic acid, and thus there was a larger difference in pKa between insulin and aspartic acid, than insulin and glutamic acid, to enable dissociation and onward ion-pair formation. Elshaer et al (2011) suggested

that for candidates to sufficiently ionise to produce counter ions that could form non-ionised complexes that enhance permeability, the difference in pKa should be up to 3 units.

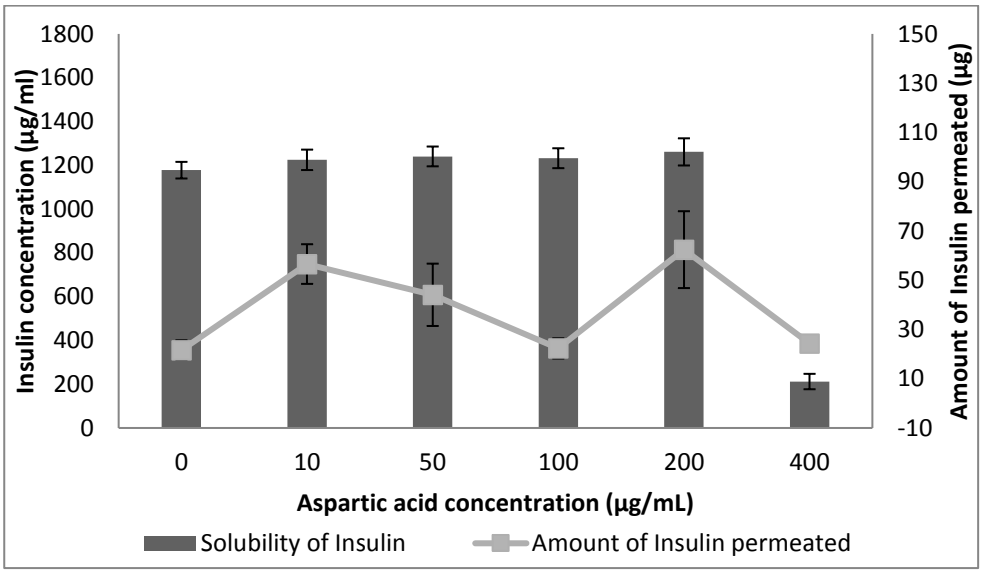

Figure 6.25 Comparing the solubility at 25 °C and permeability of insulin through TR146 cells layers, in the presence of various concentrations of aspartic acid (n=3). Low insulin concentration permeated at 400 µg/ mL due to low insulin solubility at pH of this solution (1 mg insulin = 27 IU).

An investigation of TEER results for aspartic acid (Table 6.3) revealed that only 600 µg/mL concentration significantly reduced TEER values during the course of the 4 hour experiment. Similar to glutamic acid results, MTT assay results in Figure 6.12 showed that aspartic acid was non-toxic to cells within the concentration range of the permeation experiments, as only 800 µg/mL significantly decreased cell viability. Thus, the permeation enhancement recorded was not due to leakage from the disrupted cell membranes or compromised cellular integrity. Therefore, for aspartic acid, 10 and 200 µg/mL were observed to effectively and safely enhance permeability due to its ability to effectively create an optimal balance between ionised insulin to enhance solubility, and the formation of neutral insulin-aspartic acid ion paired molecules with higher lipophilicity; and/ or the use of membrane peptide/ amino acid transporters to enhance permeation, as discussed in earlier sections (Elshaer *et al* 2014, Samiei *et al* 2014). Therefore, for the acidic amino acids, 10, 100 and 200 µg/mL glutamic acid and 10 and 200 µg/mL aspartic acid were able to effectively and safely enhance insulin permeation without any toxicity to TR146 cells, as highlighted in Figure 6.26.

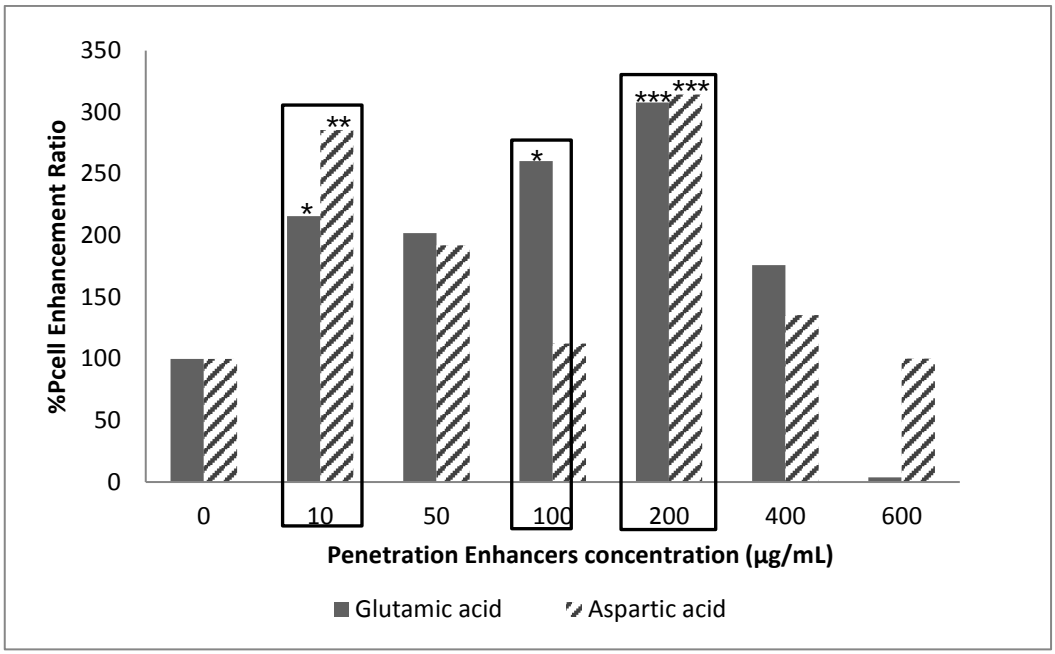

Figure 6.26 Highlighting concentrations of acidic amino acids that significantly enhanced insulin permeability with no toxicity to TR146 cells (n=3). 10, 100 & 200 µg/ mL glutamic acid and 10 & 200 µg/ mL aspartic acid significantly enhanced insulin permeation without causing toxicity to cells.

6.3.4.3 Sodium deoxycholate

Sodium deoxycholate (SDC) is a bile acid salt with pKa 6.58 (Table 6.1), which has been widely investigated for its role in enhancing permeation of drugs across cell membranes (Shojaei 1998, Junginger *et al* 1999, Şenel and Hıncal 2001, Nicolazzo *et al* 2005). In this study, the effectiveness and safety of the amino acids as permeation enhancers was compared against that obtained with sodium deoxycholate, to verify if amino acids could serve as less toxic and safer alternative permeation enhancers for insulin than bile salts. From Figure 6.27, 200, 400 and 600 µg/mL sodium deoxycholate were able to significantly enhance insulin permeability at 26.61 ± 0.24%, 23.10 ± 1.21% and 23.04 ± 1.075%, respectively. These three concentrations were observed to exhibit significantly higher Pcell values than the control at about 13.5 cm/s respectively and maximum percentage enhancement was 440.82 ± 83.92%, 428.21 ± 45.06% and 434.84 ± 49.26%, respectively (Figure 6.28). The high enhancement observed in insulin permeability with sodium deoxycholate was an expected finding based on the ability of surfactants to fluidise the lipid membranes of the cells and impact on their integrity and barrier forming properties (Şenel and Hıncal 2001).

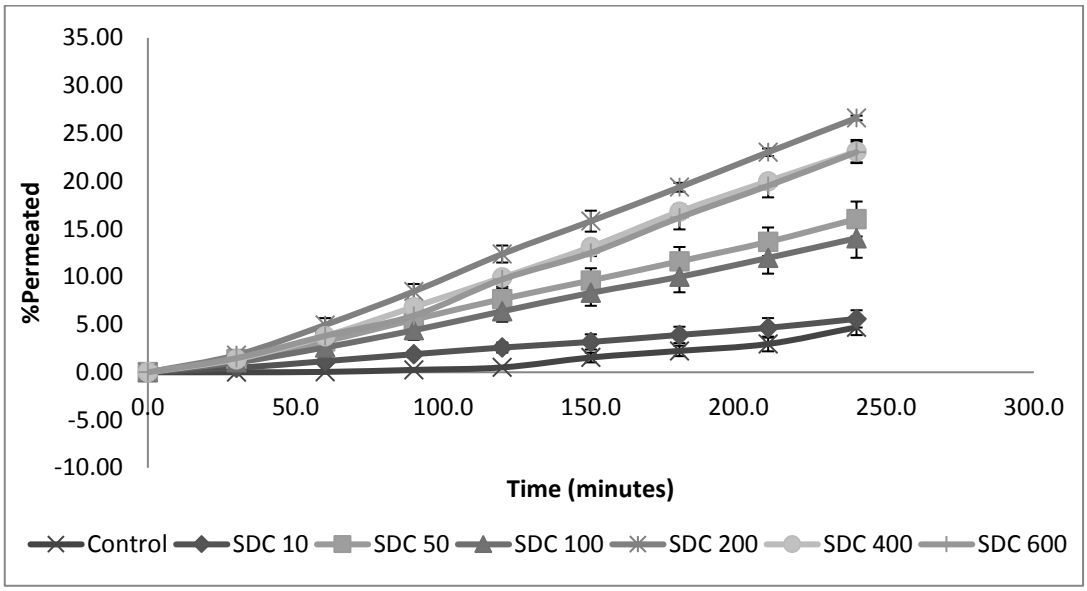

Figure 6.27 Cumulative percentage of insulin permeated in the presence of various concentrations of sodium deoxycholate (SDC) (n=3). All concentrations ≥ 200 µg/ mL significantly enhanced insulin permeation above the control. SDC showed higher permeation enhancement than all the amino acids tested.

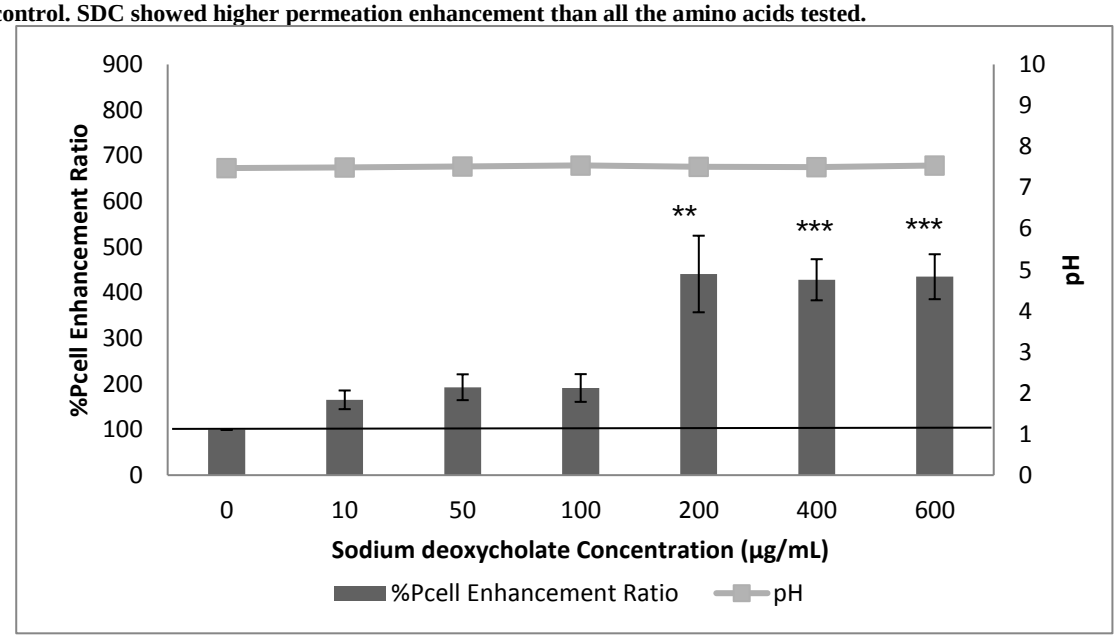

Figure 6.28 Comparing the percent enhancement of insulin permeability through TR146 cell layers in the presence of various concentrations of sodium deoxycholate and solution pH (n=3)

This effect was seen with TEER results, where a significant and linear drop in TEER values signifying a reduction in cell layer integrity was recorded at concentrations of SDC >100 µg/mL (Table 6.3). Cell viability results (Figure 6.12) further confirmed increased toxicity of cells exposed to 100 µg/mL SDC and above. Xue et al (2012) reported no significant change in TEER results in

the presence of 10 and 50 µg/mL Na deoxycholate, however 10 – 50 µg/mL reduced the viability of TR146 cells after 24 – 48 hour exposure using the MTT assay.

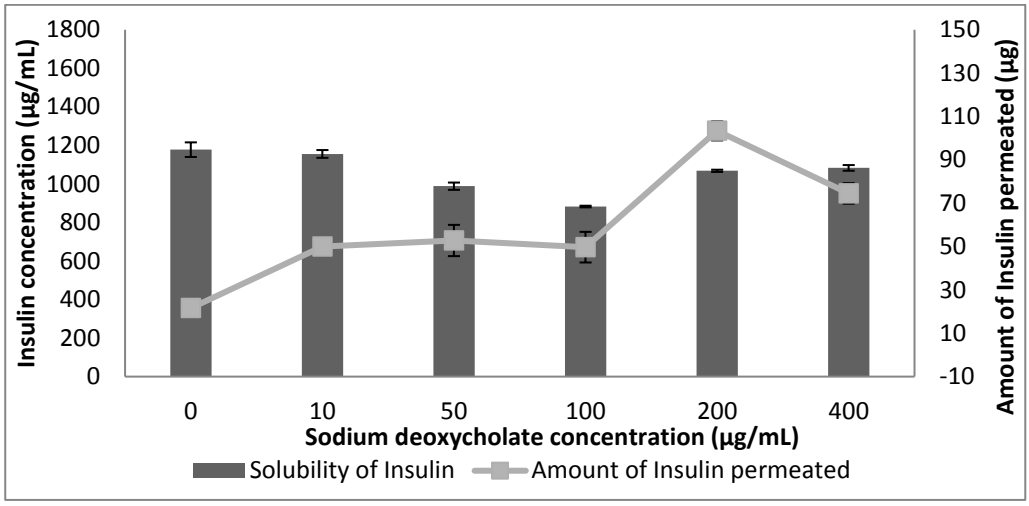

Figure 6.29 Comparing the solubility at 25 °C and permeability of insulin through TR146 cells layers, in the presence of various concentrations of sodium deoxycholate (n=3). Insulin enhancement observed for SDC found to be via disruption of cellular membranes lowering cell integrity (1 mg insulin = 27 IU).

Because the increase in insulin permeability afforded by SDC showed a linear trend (Figure 6.28), while that of the amino acids showed a somewhat "zig-zag trend", it is possible that for the amino acids, a further mechanism (such as triggering of amino acid/ peptide transporters) outside disruption of cell membranes, came into play. Surfactants such as SDC enhance drug permeation paracellularly by binding to calcium ions or disruption of hemi desmosomes between cells which might enhance both paracellular and transcellular transport (Buchert *et al* 2012, Moghimipour *et al* 2015). Thus, because of the toxicity exhibited by SDC, none of the tested concentrations yielded effective and safe permeation enhancement.

Figure 6.30 compares the concentrations of enhancers that effectively and safely improved insulin permeation across TR146 cell layers in vivo. It can be noted that apart from arginine which showed no significant improvement in the coefficient of apparent permeability through the cell layers (P_{cell}), at 10 µg/mL all amino acids were safe and effective; SDC was safe but ineffective. At high concentrations of 200 µg/mL, the acidic amino acids were both safe and effective while lysine and SDC were effective but unsafe; and at 100 µg/mL, only glutamic acid was safe and effective; lysine

was effective but unsafe, while SDC was ineffective and toxic. Thus, we have been able to demonstrate that acidic and basic amino acids act as effective penetration enhancers which circumvent the toxicity issues related with the use of surfactants such as SDC.

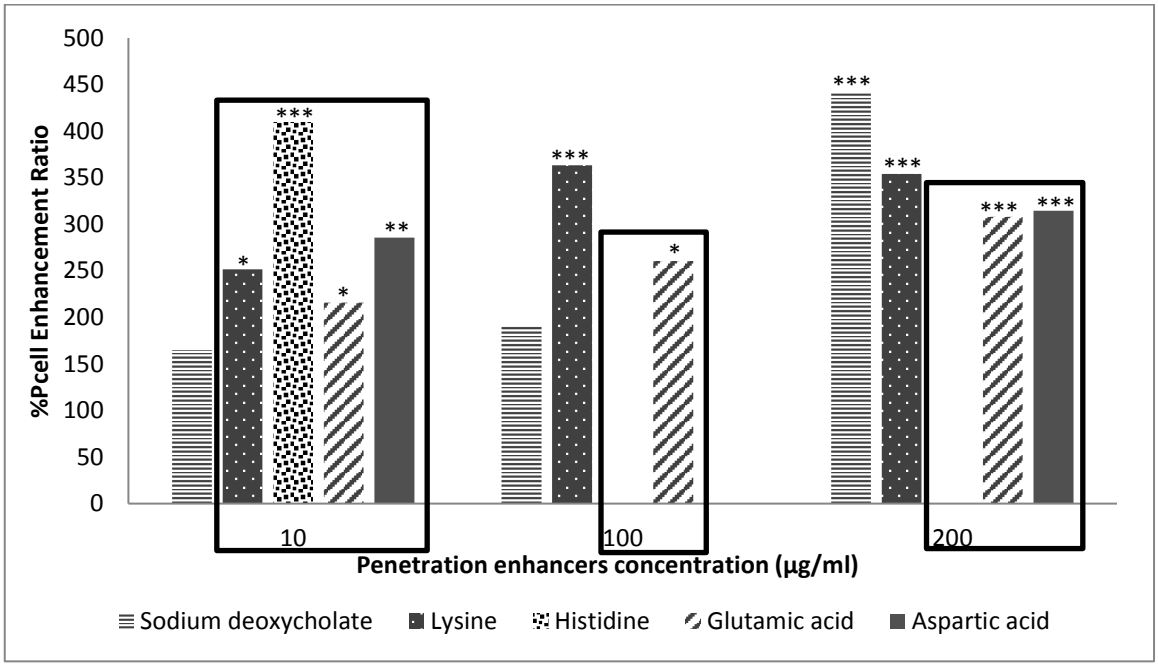

Figure 6.30 Graph highlighting concentrations of tested penetration enhancers that significantly enhanced insulin permeability with no toxicity to TR146 cells (n=3). Black rectangles signify concentrations that were both effective and safe.

6.3.5 Route of insulin transport

After identifying safe and effective amino acid permeation enhancers for insulin, the next priority was to determine the route of insulin transport (whether paracellular or transcellular) across the buccal cell layers. In order to test our first hypothesis that formation of neutral insulin-amino acid ion pairs with higher lipophilicity would enhance transcellular insulin transport by passive diffusion, FITC-labelled insulin (6 µg/mL) was transported for 4 hours across TR146 cells grown on transwell inserts and cells analysed by confocal microscopy. Results revealed localisation of FITC-insulin molecules in the cell cytoplasm (not paracellularly), both in the presence and absence of amino acids and bile salts. Figure 6.31 presents the localisation of FITC insulin on TR146 cells in the presence of the amino acid concentrations that enhanced insulin permeation, cells without amino acids used as control. Figure 6.32 are DAPI-stained images confirming that FITC-insulin

localisation occurred close to the nucleus. These findings were in contrast to investigations for FITC-labelled dextran 4kDa as a marker for paracellular transport via TR146 cell layers (data from chapter 4). FITC-dextran was seen to traverse the buccal cells via the paracellular route with no localisation at all in the nucleus or cytoplasm (Figure 6.33). These results confirmed our hypothesis that insulin transport did not occur paracellularly but was through the transcellular facilitated transport system. The paracellular route has been reported to transport small hydrophilic molecules (≤300 Da) by passive diffusion. The absence of paracellular transport for insulin could be due to its large molecular weight (5,800 Da) and the fact that the intercellular spaces of the buccal cavity are highly lipophilic due to the extrusion of the lipid content of the membrane coating granules that occur in the upper one-thirds of the buccal epithelium into the intercellular spaces, thereby inhibiting buccal paracellular transport (Shojaei 1998, Şenel and Hıncal 2001). The transcellular transport observed in the absence of amino acids (control) indicates that insulin transport possibly occurred via insulin receptors. Insulin has been reported to adsorb to apical membranes of cells and permeate the cell via endocytosic processes (Agarwal and Khan 2001, Muheem *et al* 2014). Similar findings were recorded by Thompson et al (2011) who investigated the transport of FITC-insulin across Caco-2 cell lines (model for small intestine) and reported localisation of FITC-insulin in the cell cytoplasm after 30 minutes exposure at 3 µg/mL. This uptake of insulin was reported to be mediated by interactions with insulin receptors (Thompson *et al* 2011). Xu (2002) reported that confocal microscopic imaging of FITC-labelled insulin showed that insulin could be transported via both the transcellular and paracellular routes in rabbit buccal mucosa.

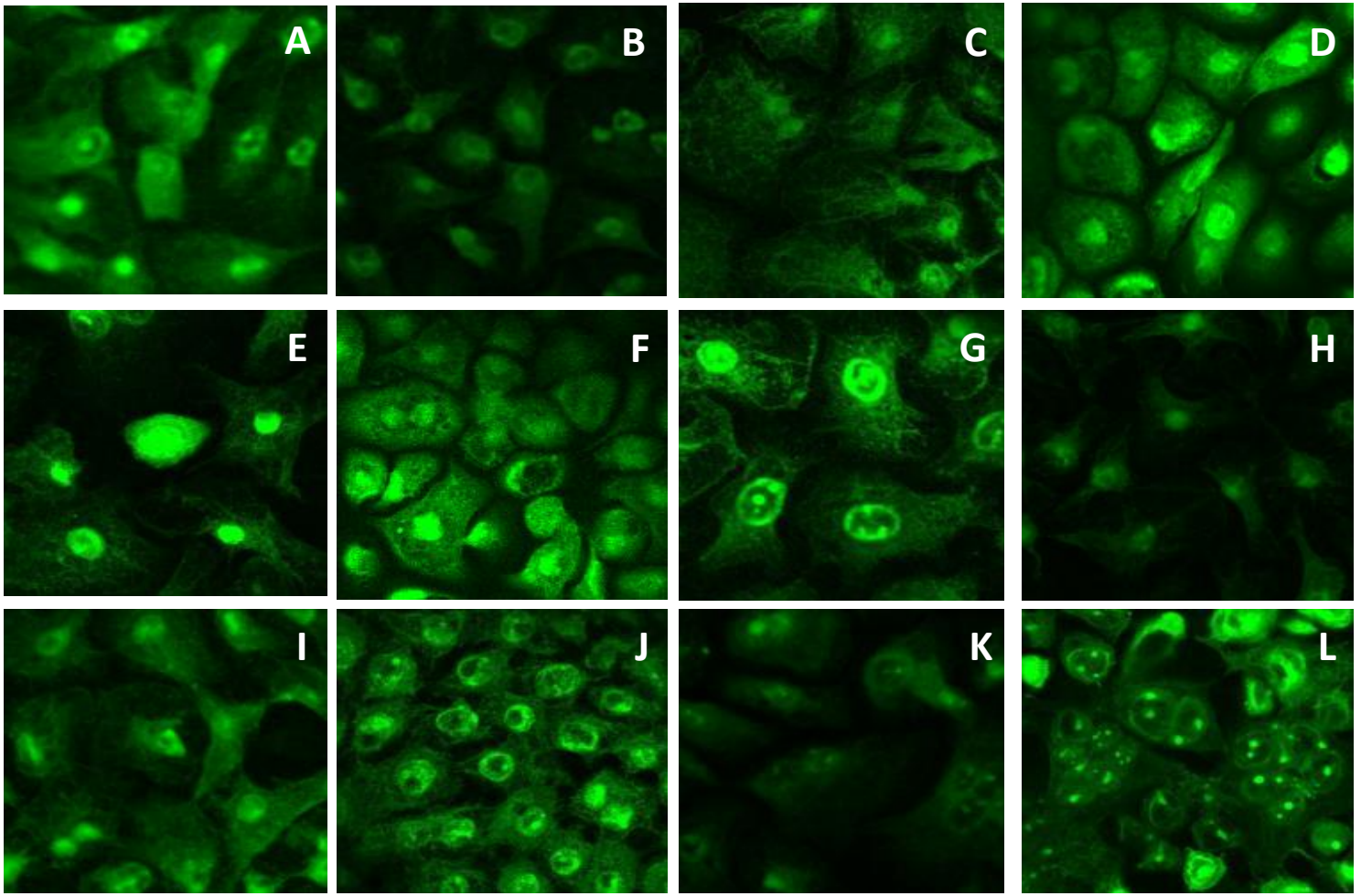

Figure 6.31 Confocal microscopic images x40, showing transport pathway of FITC-labelled insulin through TR146 buccal cell layers in the presence of amino acid concentrations that effectively enhanced insulin permeability Insulin observed to traverse transcellularly with localisation in the nucleus. Control (A), Arg 50µg/mL (B), Asp10µg/mL (C), Asp 200 µg/mL (D), Glu 10 µg/mL (E), Glu 100 µg/mL (F), Glu 200 µg/mL (G), Hist 10 µg/mL (H), Lys 10 µg/mL (I), Lys 100 µg/mL (J), Lys 200 µg/mL (K), SDC 200 µg/mL (L).

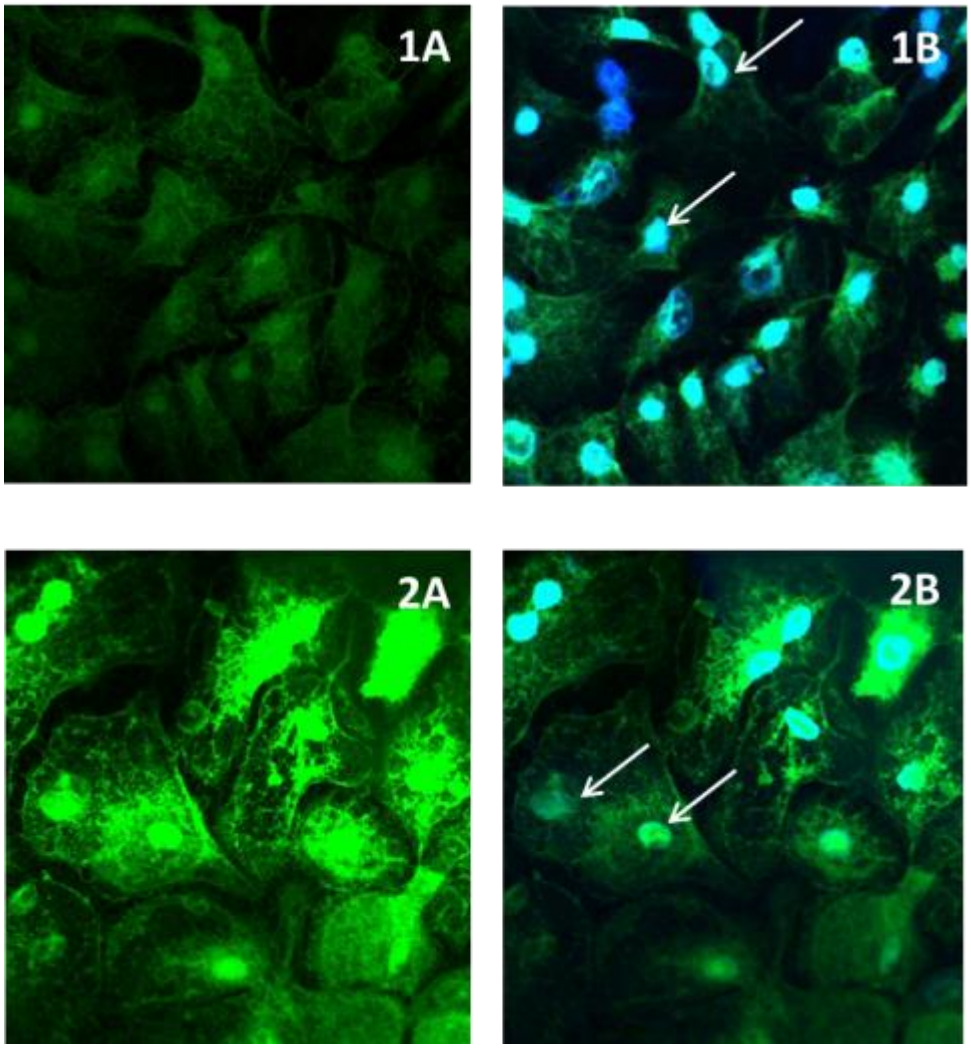

Figure 6.32 Representative confocal microscopic images of FITC-insulin, x40 (A) localisation and DAPI nuclear stain (B) on TR146 cells for control (1) and in the presence of Glu 10µg/mL (2). DAPI staining confirms localisation of FITC insulin in the nucleus (white arrows), with no paracellular transport.

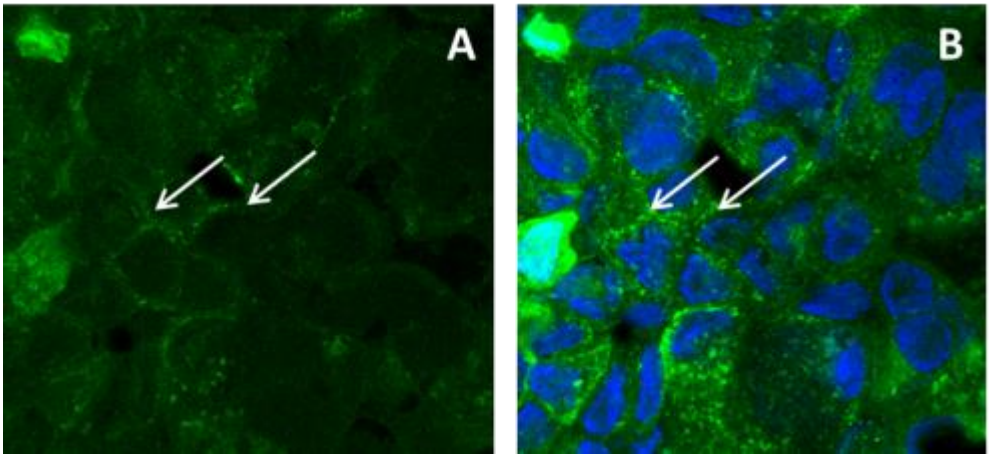

Figure 6.33 Representative confocal microscopic images of FITC-dextran 4kDa localisation, x40 (A) in the intercellular spaces of TR146 cells, showing paracellular transport (white arrows). DAPI stained nuclei (blue stain) (B) confirm the absence of the paracellular marker in the nucleus.

6.3.6 Mechanism of insulin transport through TR146 cell culture model

Upon confirming that insulin traversed the buccal cell layers via the transcellular and not the paracellular route, we needed to test our second hypothesis that this transport was by active transporter facilitated mechanisms. Glutamic acid was chosen as a representative amino acid since it showed enhanced permeation and overall safety over the widest range of concentrations tested. Sauberlich (1961) reported that of all the 20 amino acids fed in excess of recommended doses to weanling rats, L-glutamic acid showed the least toxicity expressed as inhibition of growth, and showed the least absorption into the plasma.

To investigate the presence of active transport, the concentration of insulin was kept constant at 1 mg/mL (27 IU/mL), while glutamic acid concentration was varied at 0, 100, 200 and 400 µg/mL. Transport experiments were carried out in a cold room at 9 °C. Results depicted in Figure 6.34 revealed a significant reduction in insulin permeation at 9 °C compared with 36 °C. Furthermore, at 9 °C the amount of insulin permeated decreased with increasing amino acid concentration.

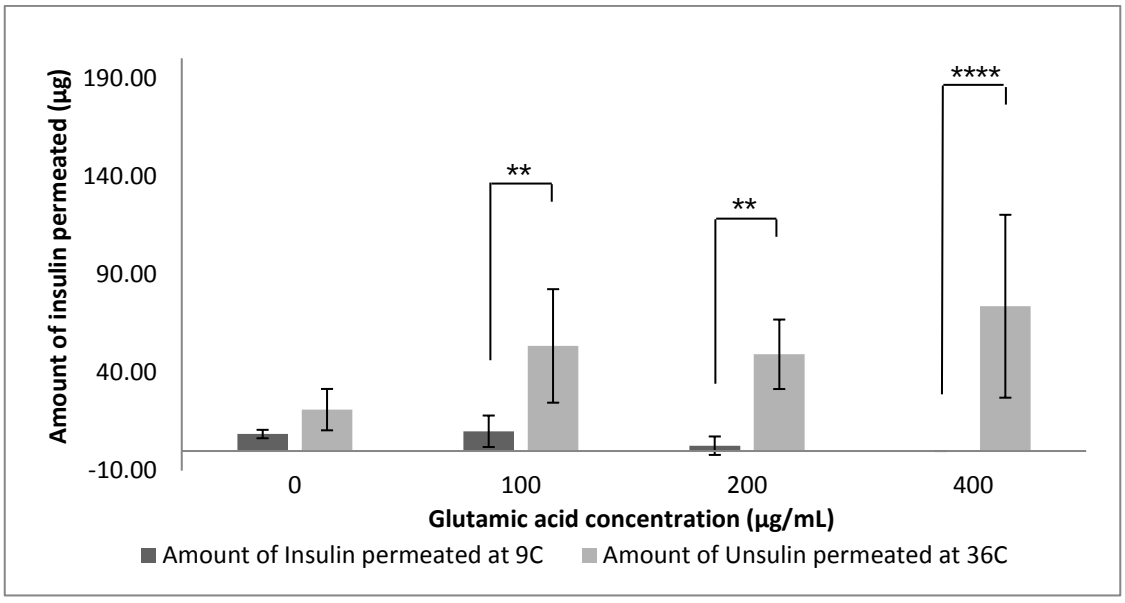

Figure 6.34 To investigate active insulin transport in the presence of amino acids. Insulin concentration was fixed at 1mg/mL while amino acid concentration was varied, and permeation experiments carried out at 9 °C for 4 hours (n=3). Note: Results for 200µg/mL at 36 °C, permeated for only 3 hours. Temperature and concentration dependent fall in insulin permeation at suboptimal temperatures confirm the presence of active transport of insulin due to enzyme inactivation that occurs at low temperatures, and early saturation of transporters (1 mg insulin = 27 IU).

These results point to the presence of active transport of insulin-glutamic acid neutral complexes formed by ion-pairing, possibly via amino acid/ peptide transporters in the cell membranes (Lehr 2003). Membrane transporters are membrane bound proteins that selectively facilitate the transport of substances across biological membranes (Lin *et al* 2015). This facilitated transport is depicted in Figure 6.3 above. Inactivation of enzymatic activity at suboptimal temperatures results in reduced function of these transporters, thereby inhibiting insulin permeation across the cell layer. Furthermore, as transporter activity had already been compromised by the low temperature, increasing amino acid concentrations above 100 µg/mL caused a further reduction and ultimate cessation of insulin transportation probably through early saturation of the transporters (Elshaer *et al* 2014). It is possible that the low transport recorded at 400 µg/mL glutamic acid could be related to the low solubility of insulin at this concentration (Figure 6.6), however this concentration showed insulin permeation at 36 $^{\circ}$C (Figure 6.34), thereby suggesting that the change was due to saturation of the transporter proteins (Artursson *et al* 2012, Elshaer *et al* 2014).

To further establish the presence of active transport in this system, glutamic acid concentration was maintained at 200µg/mL while insulin concentration was varied at 250, 500, 1000 and 1500 µg/mL (Figure 6.35). It was observed that increasing insulin concentrations above 500µg/mL showed no significant increase in permeation. Biochemical reports on the buccal epithelium reveals the extrusion of lipid components of the epithelium into the paracellular spaces, thereby increasing its lipophilicity and causing an added permeation barrier (Patel *et al* 2011), Thus, passive paracellular diffusion would not be expected for a macro molecule such as insulin (5,800 Da), since this route favours the transport of hydrophilic molecules $\leq$ 300 Da (Lehr 2003). Passive diffusion relies on the concentration gradients between the extracellular and intracellular compartments, while active transport can occur against a concentration gradient; therefore, no increase in permeation would be observed with increasing drug concentration if the molecule was solely transported actively (Lehr 2003). The rate of transport in passive diffusion is governed by Fick's law and is, therefore, directly dependent on the initial concentration; with active transport, this relationship is only relevant at low concentrations, and with increasing concentrations, carrier saturation occurs and no increase

in uptake is observed with increasing concentrations (Lehr 2003). Thus, results from Figure 6.35 point to the presence of passive and active transport mechanisms for insulin.

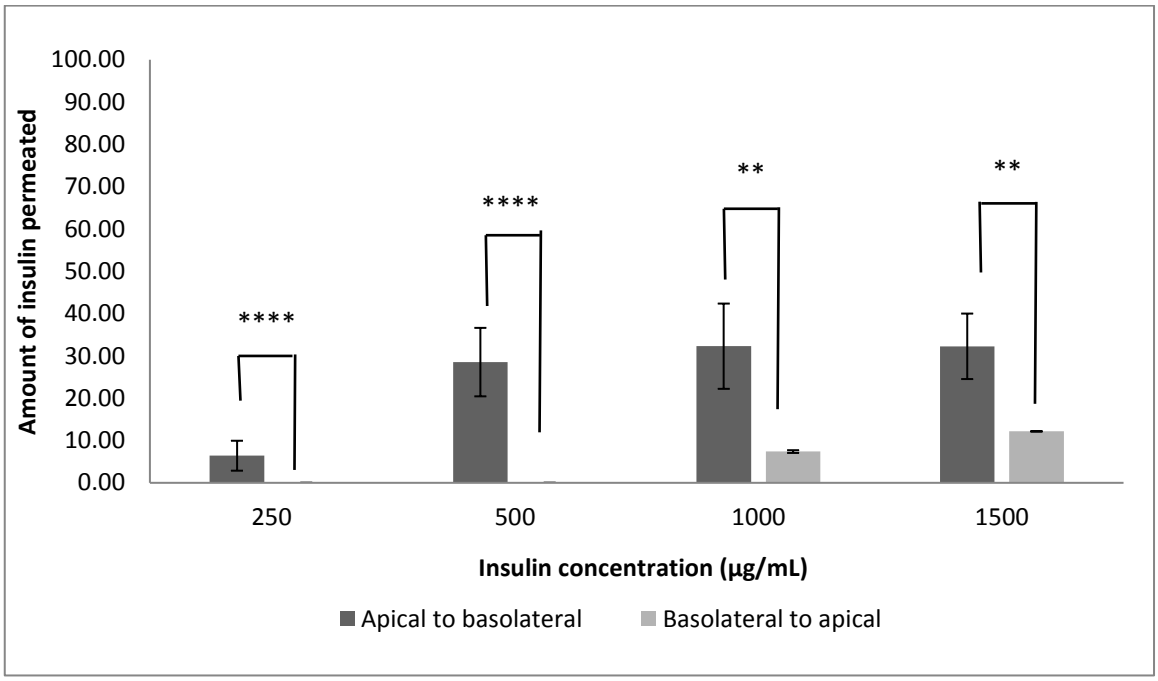

Figure 6.35 Investigating active and passive transport of insulin-amino acid ion pairs across TR146 buccal cell layers (n=3). Glutamic acid concentration was fixed at 200 µg/mL, and insulin concentration varied. Vectoral transport was investigated by reversing the transport direction from basolateral-to-apical. Results highlight a dependence on initial concentration and direction of transport, pointing to active transport mechanisms (1 mg insulin = 27 IU).

We further investigated vectoral transport of insulin across the cell layers. Reversal of transport direction from apical-basolateral, to basolateral-apical revealed a concentration dependent increase in insulin permeation, with no permeation recorded at 250 and 500 µg/mL insulin. According to Biopharmaceutical Classification System (BCS) guidelines, to confirm the presence of passive transport *in vitro*, there should be a lack of dependence on initial concentration and directional transport (Lehr 2003). Thus, results from Figure 6.35 further confirm the presence of active transcellular transport for insulin, since the concentration of nutrient transporter proteins are higher at the apical surface than at the basolateral surface. Artusson et al (2012) agreed that highly potent hydrophilic compounds such as peptide antigens, with similar structures as food nutrients could be transported across cell layers by a combination of active facilitated transport as well as passive transport. However, these results obtained for insulin was the first indication of a possible amino

acid mediated transport of insulin via formation of insulin-amino acid neutral complexes by the ion pairing mechanism.

6.4 Conclusion

The aim of this work was to investigate the effect of basic and acidic amino acids on the physicochemical and biological properties of insulin, in order to provide alternative safe and effective excipients that enhance buccal insulin delivery. Basic amino acids were able to significantly improve insulin solubility in water, while 200 and 400 µg/mL lysine significantly increased insulin solubility in HBSS. The presence of amino acids was able to increase the hydrophilicity of insulin and lower its log D by 0.7 units. However, despite this reduced lipophilicity, amino acids were able to effectively and safely enhance permeation of insulin across TR146 cell layers significantly, pointing to the presence of an active carrier transport system. It was hypothesised that at buccal cavity pH, both amino acids and insulin were ionised and able to form stable ion pairs which penetrated through the cells as one entity. Permeability data showed a significant improvement in insulin permeation, especially for 10 µg/mL of lysine ($p < 0.05$) and histidine 10 µg/mL ($p < 0.001$), 100 µg/mL of glutamic acid ($p < 0.05$) and 200 µg/mL of glutamic acid and aspartic acid ($p < 0.001$) without affecting cell integrity; in contrast to sodium deoxycholate which enhanced insulin permeability but was toxic to the cells. The results of these studies demonstrated a "bell-shaped" impact on insulin permeability upon increasing the concentration of amino acid counter ions, and suggest that the concentration of the counter ion requires optimisation to provide a stringent control of insulin dissociation to enhance both protein solubility and permeation. Interestingly, investigating the mechanism and route of insulin permeation using increasing concentrations of insulin at suboptimal temperatures, reversed transport direction and confocal microscopy revealed that insulin was transported by both active and passive transcellular processes, with active processes afforded by the presence of insulin receptors and amino acid nutrient transporters on the cell membrane. Therefore, amino acids were established as safer, effective and novel penetration enhancers than the commonly used surfactant for insulin using the ion-pairing mechanism.

Chapter 7

Characterisation of insulin buccal tablets

7.1 Introduction

Buccal drug delivery has received increasing attention as a potential site for delivery of proteins that are inactivated in the GIT due to its high lymphatic drainage, lower drug metabolism and ease of patient acceptance (Khafagy *et al* 2007, Patel *et al* 2011). A major setback for ODTs is the saliva scavenging and accidental swallowing that occurs upon tablet placement into the mouth (Behra *et al* 2012). Thus, an ODT placebo base was formulated (chapter 3) containing various viscosity grades of the mucoadhesive polymer polyethylene oxide (Polyox™), that would allow for fast disaggregation of the tablet upon placement in the mouth, but continued adhesion of the produced slurry to the buccal mucosa until drug release and permeation is completed. Such a tablet would be expected to exhibit enough mechanical strength to withstand stress during packaging and transport, but also be able to imbibe water into its bulk to facilitate fast disintegration/ disaggregation and onward release of the contained drug (Al-Khattawi *et al* 2014).

Various kinetic models have been employed to describe the rate of drug release from dissolving tablet matrices. Zero order kinetics (equation 7.1) can be used to describe the slow release of a poorly soluble drug from non-disintegrating dosage forms, with release rate that is independent of initial concentration (Dash *et al* 2010). This is applicable to coated systems and osmotic systems (Dash *et al* 2010). The first order model (equation 7.2) has been used to describe the dissolution soluble drugs from porous polymer matrices, where the rate is dependent on initial concentration. Higuchi kinetics (equation 7.3) describes a release that follows a Fickian diffusion from an insoluble matrix that is dependent on the square root of time. The Higuchi model has been to several modified release dosage forms containing water soluble drugs. While the Hixson-Crowell cube root law (equation 7.4) describes a dissolution-controlled drug release from or tablets that takes into account the change in surface area as the dissolution process proceeds (Shoaib *et al* 2006, Tamilvanan and Sa 2006, Dash *et al* 2010). The Korsmeyer-peppas model (equation 7.5) derived by Korsmeyer *et al* (1983) is used to determine the overall mechanism of drug release from polymer containing systems such as tablets, estimated when ≤60% of the drug

has been released (Shoaib *et al* 2006). The 'n' values depict the actual release mechanism, and interpretations of this value for a cylindrical system such as a tablet are given in

Table **7.1** below.

$$Q_t = Q_0 + K_0 t \quad . \quad . \quad . \quad . \quad . \quad . \quad . \quad \text{(Equation 7.1)}$$

$$lnQ_t = lnQ_0 + Kt \quad . \quad . \quad . \quad . \quad . \quad . \quad . \quad \text{(Equation 7.2)}$$

$$\sqrt[3]{Q_0} - \sqrt[3]{Q_t} = K_{HC} t \quad . \quad . \quad . \quad . \quad . \quad . \quad . \quad \text{(Equation 7.3)}$$

$$Q = K_H \sqrt{t} \quad . \quad . \quad . \quad . \quad . \quad . \quad . \quad . \quad \text{(Equation 7.4)}$$

$$\frac{M_t}{M_\infty} = K_{KP} t^n \quad . \quad . \quad . \quad . \quad . \quad . \quad . \quad . \quad \text{(Equation 7.5)}$$

Where Q_0 is the initial amount of insulin, Q_t is the cumulative amount of insulin released at time, t; M_t/M_∞ is the fraction of drug released, n is the release exponent that gives an indication of the release mechanism involved and K_0, K, K_{HC}, K_H and K_{KP} are the zero order, first order, Hixson-Crowell, Higuchi and Korsmeyer-peppas rate constants respectively.

Table 7.1 Table highlighting the overall mechanism of drug release from cylindrically shaped systems such as tablets derived from the release exponent of the Korsmeyer-peppas model (Jacques *et al* 1974, Shoaib *et al* 2006, Dash *et al* 2010)

Release exponent (n)	Overall release mechanism	Details	Rate as a function of time
≤ 0.45	Fickian diffusion	Molecular drug diffusion via a chemical gradient	$t^{-1/2}$
0.45 < n < 0.89	Anomalous (non-Fickian) diffusion	Diffusion does not obey Fick's law	t^{n-1}
0.89	Case-II transport	Relaxational drug release through stress and state transition in hydrophilic glassy polymer that swell in water	Zero order release
>0.89	Super case-II transport	Cannot be described by the K-P model	t^{n-1}

The aim of this work was to bring together the design parameters generated from the QbD study in chapter 3 and results from insulin transport in chapter 6, to formulate buccal tablets incorporating insulin and glutamic acid into the placebo tablet base; and thereafter characterise disintegration time, mechanical strength and release characteristics, to serve as a basis for the onward assessment of *in vitro* and *in vivo* effectiveness in buccal insulin delivery.

7.2 Materials and methods

7.2.1 Materials

Sentry Polyox® (polyethylene oxide) WSR N10 (MW 100,000 Da), 1105 (MW 900kDa), N-60K (MW 2000 kDa) and Coagulant (MW 5000 kDa) were a gift from Colorcon (Kent, UK). L-HPC grade NBD-022 was a gift from Shin-Etsu (Tokyo, Japan). D-Mannitol, magnesium stearate, human recombinant insulin powder, L-glutamic acid (minimum 99% TLC) and TFA were purchased from Sigma Aldrich Chemicals (Poole, UK). All materials were of pharmaceutical grade and used as received.

7.2.2 Methods

7.2.2.1 Preparation of insulin buccal tablets

The critical process parameters (CPP) generated by the MODDE software optimiser for the various polyox polymer blend formulations (ODT base) from chapter 3 were used to prepare 50 mg buccal tablets containing 1mg insulin and 200 µg glutamic acid each (information from chapter 6). Formulation compositions are shown in Table 7.2 below. The ingredients were weighed, geometrically mixed, and 50 mg each of the powder blends was singly weighed and compacted at 30 kN (3 tons) using a semi-automatic bench-top tablet press (Sympatec, UK), equipped with 5 mm flat faced dies.

Table 7.2 Composition of insulin buccal tablets developed from the critical process parameters (CPP) determined from results from chapters 3 and 6.

Formulation	Quantities					
	Mannitol	**LHPC**	**Polyox**	**Insulin**	**Glutamic acid**	**Mg stearate**
N10	to 50mg	7%	1.32%	1.0 mg	0.2 mg	0.50%
1105	to 50mg	7%	1.32%	1.0 mg	0.2 mg	0.50%
N60K	to 50mg	7%	1.36%	1.0 mg	0.2 mg	0.50%
Coag	to 50mg	7%	1.36%	1.0 mg	0.2 mg	0.50%

7.2.2.2 Tablet disintegration/ disaggregation

The disintegration/ disaggregation time was determined by placing a tablet in a well of a 12 well cell culture plate containing 1.5 mL of HBSS rotated at 30 rpm and 37°C in an orbital shaker. This adapted method was used due to the small size of the tablets, and the limited saliva volume present in the buccal cavity for tablet disintegration, compared with the USP apparatus II test employed in earlier sections of the work. For these experiments, disintegration/ disaggregation time was taken as the time for the tablet to crumble into a slurry still held together by the mucoadhesive polymer.

7.2.2.3 Tablet friability

The ability of the tablets to withstand mechanical stress, known as friability was measured using a rotating drum friabilator (J. Engelsmann AG, Ludwigshafen, Germany). 6 tablets were utilised at 25 rpm for 100 revolutions or 4 minutes. Tablets were carefully dusted before and after the test, and friability expressed as the percentage loss in weight.

$$Friability = \frac{initial\ weight - final\ weight}{initial\ weight}\ x\frac{100}{1} \quad . \quad . \quad . \quad . \quad \text{(Equation 7.6)}$$

7.2.2.4 Tablet hardness

The hardness (crushing strength) of the tablets was measured using a 4M hardness tester (Schleuniger, Thun-Switzerland). Tensile strength, σ was calculated from the equation:

$$Tensile\ strength\ (\sigma) = \frac{2\ x\ Hardness}{\pi d\mathrm{h}} \quad . \quad . \quad . \quad . \quad . \quad \text{(Equation 7.7)}$$

Where d = tablet diameter and h = tablet thickness; measured using a digital Vernier calliper.

7.2.2.5 Drug release from buccal tablets

The release of insulin from the buccal tablets was studied using 12 well cell culture plates (similar to drug transport studies from chapter 6, but without cells) adapted from Heikkilä *et al* (2007). Each tablet was placed in a well of a 12 well plate containing 1.5 mL HBSS, pH 7.4 and rotated on an orbital plate shaker at 140 rpm. The release studies were carried out using a similar method to the permeability studies from chapter 6, to provide a basis for comparison when carrying our permeability studies of insulin from buccal tablets. 700 µL samples were withdrawn at specific intervals and immediately replaced with equal volume of HBSS, to maintain sink conditions where drug concentration was <10% saturation solubility of the drug at all times. Samples were assayed for insulin content using the validated HPLC method from chapter 6. The amount of insulin released per time was calculated from equation 7.8 and percentage drug release calculated from equation 7.9 below:

$$M_t[n] = \frac{V_r * C[n] + V_S \sum_{m=1}^{n-1} C[m]}{1000} \quad . \quad . \quad . \quad . \quad . \quad \text{(Equation 7.8)}$$

Where M_t is total drug released at time, t in mg; n is the number of samples taken, V_r is the dissolution volume in mL, V_s is the sampling volume, C[n] is the current concentration in the dissolution medium in mg/L, ΣC[m] is the summed total of previous concentrations.

$$\%\ Drug\ released = \frac{Actual\ calculated\ amount}{Theoretical\ amount}\ x\ \frac{100}{1} \quad . \quad . \quad \text{(Equation 7.9)}$$

7.2.2.6 Determination of insulin release mechanism from buccal tablets

Five kinetic models namely zero order, first order, Hixson-Crowell cube root, Higuchi and Korsmeyer-peppas kinetics (equations 7.1, 7.2, 7.3, 7.4 and 7.5, respectively) were applied to the collated data, to determine the model that best fit the release pattern of insulin from the formulations; based on the highest correlation coefficients (R^2) obtained (Shoaib *et al* 2006, Tamilvanan and Sa 2006). From here, five graphs were plotted as follows: cumulative % insulin released vs time (zero order kinetics), log cumulative % drug remaining vs time (first order

kinetics), cumulative % drug release vs square root of time (Higuchi kinetics), cube root of % insulin remaining vs time (Hixson-Crowell cube root kinetics) and log cumulative % insulin released vs log time (Korsmeyer-peppas kinetics) (Shoaib *et al* 2006).

7.2.2.6 Statistical analysis

All data generated in replicates were presented as mean ± standard deviation (s.d.), where n=3. The data was then analysed for statistical significance using one-way analysis of variance (ANOVA) and Tukey-Kramar multiple comparison post-test from Graphpad Prism® version 6.07 (Graphpad Software, San Diego, CA, USA). The level of significance was quoted as $p<0.05$ (probability values of 95%).

7.3 Results and discussion

7.3.1 Insulin buccal tablet characteristics

Results of tested tablet characteristics are shown in Table 7.3. Porosity of the tablets could not be determined due to the small size of the tablets in relation to the size of the pycnometer cell. From Table 7.3 it can be seen that tablet disintegration time increased with increasing polymer viscosity from Polyox N10 to Polyox coagulant. These results are in line with that obtained for similar formulations of 500 mg placebo tablets (without insulin or glutamic acid) discussed in chapter 3 of this work. These results also reveal the predictive power of our model and the fact that critical process parameters (CPPs) could be extrapolated to smaller sized tablets containing similar formulation compositions. All tablets disintegrated in <60 seconds except those containing the highest viscosity of polyox. This was an expected result from our model and can be explained, as high viscosity polymers form a matrix that impedes the imbibing of water into the tablet and therefore hinder disintegration (Royce 1993, Lee *et al* 1999, Efentakis and Vlachou 2000, Streubel *et al* 2003, Alhusban *et al* 2011). However, the low concentrations of polyox polymers used in this study allowed for fast disintegration/ disaggregation of all the tablets in line with the BP specification of <3 mins.

Table 7.3 Results of tablet characteristics and drug release parameters for insulin buccal tablets (n=3)

Polymer viscosity grade	Disintegration time (s)	Friability (%)	Hardness (N)	Tensile strength (MPa)	% Drug Release
Polyox N10	25.67 ± 3.51	1.68	37.53 ± 5.15	3.65 ± 0.44	86.89 ± 8.28
Polyox 1105	48.67 ± 3.06	0.96	52.03 ± 3.71	4.60 ± 0.26	102.66 ± 13.43
Polyox N60K	50.33 ± 1.53	1.29	54.57 ± 1.17	4.49 ± 0.26	106.37 ± 3.22
Polyox Coag	66.67 ± 2.08	0.85	53.3 ± 1.25	4.35 ± 0.09	87.92 ± 4.90

Similar disintegration times were recorded for the 50 mg tablets and the 500 mg placebo tablets tested in chapter 3, despite the smaller volume of disintegration medium utilised in the former case. This could be due to the presence of water soluble glutamic acid in the formulation of the insulin tablets. Water soluble excipients/ carriers have been reported to enhance the disintegration and/ or dissolution of poorly water soluble drugs due to their ability to attract water molecules and enhance wettability (Vasconcelos *et al* 2007, Sareen *et al* 2012)

As with our model results from chapter 3, tablet hardness did not follow a linear pattern with regards polymer viscosity. Only the formulation containing the lowest viscosity polyox (N10) showed a significantly lower hardness; there was no significant difference in the hardness of the other formulations tested. Hardness for all tablets was less than our minimum limit of 60N, but higher than 50 N for all formulations except N10. This value for hardness is not of concern because tablet hardness is dependent on tablet dimensions (shape, size and thickness) and the cross sectional area of load application (Razavi *et al* 2015, Gamlen 2016). Therefore, tablet tensile strength, which is more representative of mechanical strength, was calculated, as it takes into account the size and dimensions of the tested tablet and relates to the crushing strength. The calculated tensile strength was above 3 MPa for all formulations and, therefore, within acceptable limits. Amidon *et al* (2009) reported that tablet tensile strengths of >1 MPa are suitable to maintain mechanical strength throughout the lifetime of a tablet (Gumaste *et al* 2013).

For tablet friability, the lowest viscosity polyox formulation (N10) exhibited the highest friability and this was expected due to its low hardness. Polyox 1105 and Polyox coagulant formulations

were able to significantly lower the friability of the tablets within the acceptable limits of <1% respectively. From our model in chapter 3, 1105 placebo tablets exhibited the lowest friability compared to other formulations. The friability of tablets containing polyox is dependent on the elastic recovery exhibited by the polymer under compaction, and this in turn affects the tablet's porosity (data from chapter 3). However, tablet porosity was not measured in this study. The observed reduction in friability by 1105 and Coagulant was an achievement that was not obtained with all the previously tested placebo tablets. It should be noted that for all the critical quality attributes (CQAs) tested, a linear relationship was not expected, except for disintegration time due to polymer viscosity. This is because the MODDE optimiser selected levels of the critical process parameters (CPPs) that would yield optimal CQAs (Table 7.2), and these CPP levels differed for the various polyox polymers utilised.

7.3.2 *In vitro* insulin release from buccal tablets

From Figure 7.1 it can be seen that the formulation containing the lowest viscosity grade of polyox (N10) had the fastest release rate of insulin, with maximum release occurring within 30 mins; closely followed by N1105 and N60K with intermediate viscosities. Conversely, as expected, the highest viscosity grade polyox (coagulant) showed a slower release of the drug, with maximum drug release after 1 hour. This observation is possibly related to the matrix-forming ability of high viscosity polymers (Lee *et al* 1999). Thus, even at the low polymer concentrations employed (<1.5%), polyox polymers were able to modify the release of insulin from the formulations depending on their viscosity.

Fitting the release data into the available kinetic models showed that the release kinetics for all the formulations could be described by the Higuchi kinetic model, having the highest correlation coefficient (R^2) as seen in Table 7.4. This result implies that the release of insulin from the LHPC/ polyox containing formulation was determined by a diffusion controlled mechanism (Tamilvanan and Sa 2006).

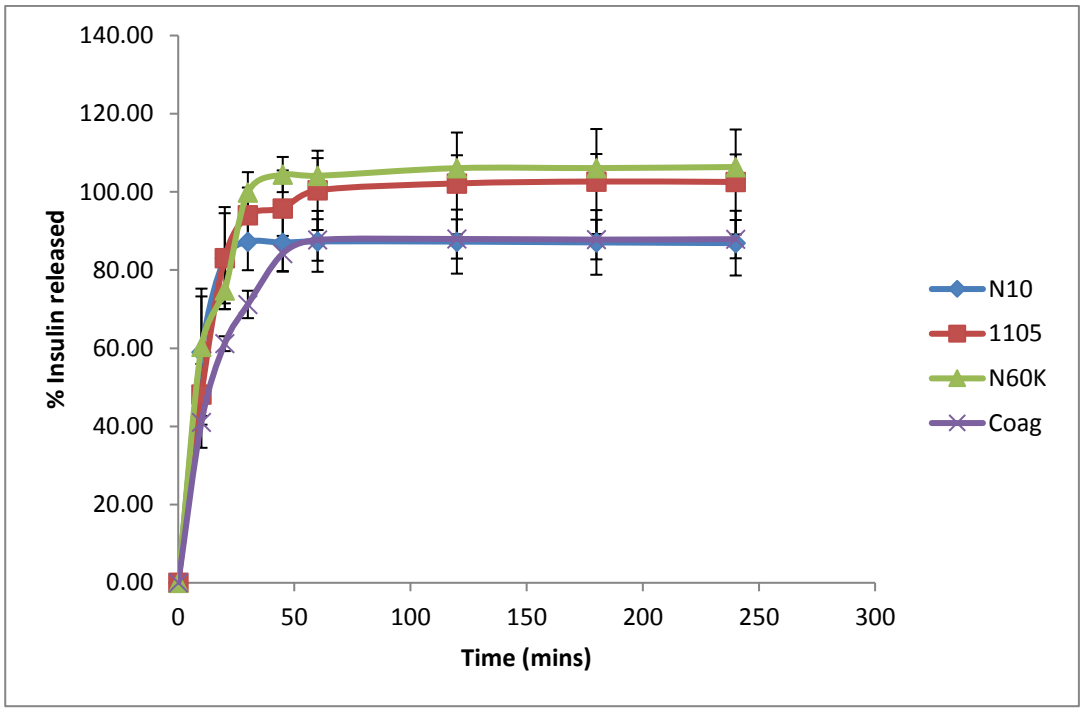

Figure 7.1 Results highlighting insulin release from buccal tablets formulated from compositions generated by the MODDE software optimiser from chapters 3 and 6 (n=3). High viscosity polyox (coagulant) formulation exhibited some modified release of insulin from tablets.

From Table 7.4, Polyox Coag formulation exhibited the highest R^2 for the Higuchi model compared to the other formulations, and this was in line with visual observations of the formulation which disintegrated into a slurry that was held within a sticky matrix, thereby impeding direct contact of drug with the dissolution media and thus producing a diffusion controlled release. It had been expected that the formulations containing lower viscosity grade polyox would exhibit release kinetics described by the Hixson-Crowell cube root law, which describes a dissolution controlled release of drug due to direct drug contact with the dissolution medium, as expected for conventional tablets (Tamilvanan and Sa 2006). However, our data showed that the presence of polyox (irrespective of the polymer grade) was able to impede direct contact of insulin with the dissolution media and produce diffusion-controlled release kinetics. The first order kinetics had the next highest R^2 value to the Higuchi kinetics, for all the formulations and indicated that drug release was dependent on initial concentration. The Korsmeyer-peppas equation is used to fit the portion of the curve where ≤60% of drug release has occurred (Dash *et al* 2010). Because >60% of the drug had been released by 20mins of the dissolution process, estimation of release mechanism using this equation was not carried out due to a limited number of time points.

Table 7.4 Release parameters for insulin buccal tablets containing LHPC (7%) and various viscosity grades of polyox polymer (n=3)

Formulation	Zero order kinetics		First order kinetics		Hixson-Crowell kinetics		Higuchi kinetics	
	R^2	K_0 (hr^{-1})	R^2	K (hr^{-1})	R^2	K_{HC} ($hr^{-1/2}$)	R^2	K_H ($hr^{-1/3}$)
N10	0.84	171.55	0.80	2.75	0.68	307.41	0.98	129.38
1105	0.72	89.42	0.95	4.54	0.79	321.60	0.92	105.57
N60K	0.82	131.15	0.96	4.14	0.92	511.91	0.92	125.23
Coag	0.83	80.21	0.98	2.10	0.82	209.49	0.98	91.11

7.4 Conclusion

Applying the design parameters obtained from the QbD study in chapter 3 with results obtained from insulin permeability studies (from chapter 6) enabled the formulation of buccal tablets containing insulin and glutamic acid. Despite difference in the amount of polyox polymers in the various formulations, disintegration time of the tablets was still dependent on polymer viscosity, rather than polymer concentration, in line with results from our model in chapter 3. A reduction in friability to values within the acceptable limits of <1% was achieved for tablets containing polyox 1105 and polyox coagulant; this was not possible from any of the previous placebo tablet formulations and could be related to the smaller tablet size or presence of insulin and/ or glutamic acid in the formulation. Drug release from the formulations was shown to be dependent on polymer viscosity with a decrease in release rate observed with increase in polymer viscosity. Fitting data into the various kinetic models of drug release highlighted insulin release to follow Higuchi kinetics for all the formulations (highest R^2 value); revealing that drug release was diffusion-controlled.

Chapter 8

General discussion

8.1 General discussion

Advancements in biotechnology have enabled the large scale production of therapeutic proteins – insulin being the first of such biotechnologically engineered molecules to be produced in large scale. However, this has only solved one of the problems associated with protein therapy. The major challenge of the unavailability of non-invasive routes of administration for these molecules still remains. To date, proteins are primarily administered via the parenteral route, raising such concerns as psychological trauma, pain at injection site, need for daily injections, risk of infection and side effects such as angiopathy from parenteral insulin administration; which culminates in poor patient compliance and the risk of therapeutic failure. ODTs have been identified in recent years as a highly attractive dosage form that enhances patient compliance, especially for children and the elderly. The saliva scavenging and accidental swallowing that occurs after ODT administration, however, reduces its potential for epigastric absorption which is one of the advantages of this dosage form. Thus, the incorporation of mucoadhesive polymers into ODT formulations could prolong drug residence time and enhance drug absorption from the oral cavity.

The high lymphatic supply, easy accessibility and low peptide degradation characteristics of the buccal mucosa has highlighted the buccal route as an emerging site for delivery of GI-sensitive proteins. A major setback to buccal delivery is the low drug permeation observed due to the stratifying nature of the epithelium, an effect which becomes more pronounced during delivery of large molecules such as insulin. This has necessitated the incorporation of permeation enhancers within buccal formulations, generating the need for naturally occurring, biodegradable enhancers that reduce systemic toxicity and lower the risk of immunogenicity; with the possibility of elucidating transport routes and mechanisms for these macromolecules in the presence of various enhancers. A further shortcoming during development of buccal dosage forms is the unavailability of standardised, highly reproducible, cost-effective pre-clinical methods for assessing buccal drug delivery. *In vivo* methods in humans and animals being cumbersome and non-standardised, *in vitro* methods using animal tissues having low reproducibility, while *in vitro* cell culture based assays are either not representative of *in vivo* nomenclature, or are expensive for continuous testing. The aim of this thesis was, thus, to offer solutions to, and fill existing gaps in the knowledge about

buccal delivery of therapeutic proteins using insulin as a model drug. Results of these will be highlighted in the following sections.

To facilitate the development of a placebo ODT base, HPC and LHPC were individually characterised and assessed for their role(s) in ODT development in order to identify multi-functionality within the polymers, which would be applied to develop ODTs with these qualities intelligently built into them. The characteristics of LHPC and HPC were found to be controlled by the degree of hydroxypropyl substitution of these polymers, which impacted on the appearance of crystallinity upon compaction (as seen from XRD results), functional groups available for intermolecular interactions (as seen from FTIR results) that further impacted on their water solubility. Thus, HPC produced tablets with good binding properties that eroded on contact with water, while LHPC produced good binder and disintegrant properties in tablets that broke up into smaller pieces (flaking off) in contact with water. A formulation containing 7% LHPC with mannitol as filler and magnesium stearate as lubricant gave the optimal balance of good mechanical and disintegrating properties with regards ODT acceptance criteria, and was therefore chosen as the optimised formulation.

A QbD study incorporating design of experiments (DoE) was then carried out to identify factors that would enhance the incorporation of different viscosity grades of the mucoadhesive multi-functional polymer, Polyox™ (polyethyleneoxide), into our previously formulated ODT base. This study exposed an interesting feature of polyox that allowed an enhancement in disintegration of tablets with increasing compaction pressure due to the elastic recovery of polyox at elevated compaction pressures that resulted in higher porosity, thereby facilitating drug disintegration. Therefore, it was possible to formulate mucoadhesive placebo ODTs containing polyox at high compaction pressures that reduced the tablet friability produced by the filler mannitol, without compromising the disintegration/ disaggregation time of the tablets.

The ability of extracellular Ca^{2+} concentration to alter the stratification and proliferation of the TR146 buccal cell line was investigated in an attempt to produce buccal cell cultures with similar stratification properties as human buccal mucosa, which would increase the drug permeation

barrier of these cells and, therefore, serve as a reproducible, cost effective and reliable method for *in vitro* buccal drug delivery assessment. Addition of 1.5 mM Ca^{2+} to the specialised culture media for TR146 cells yielded enhanced proliferation and stratification of cells as captured using light/ confocal microscopy and haemocytometry. This enhancement was further seen to improve the penetration barrier of the cells to the paracellular transport marker FIT-C labelled dextran 4kDa. This was because calcium is a component of desmosomal proteins that line the intercellular spaces between cells. However, the effect of extracellular Ca^{2+} on the biochemical properties of these cells requires elucidation.

Characterisation of our model drug was carried out by the development of a simple, rapid method for insulin quantification at ambient temperature by UV detection which was validated in our laboratory using ICH guidelines, as well as in a separate laboratory employing a different operator, a different HPLC system and on different days. The effect of high compaction pressure (from formulation of the ODT base) on the secondary structure and bonds available for intermolecular interactions of insulin was investigated by circular dichroism (CD) and FTIR respectively. Insulin was observed to withstand compaction pressures of 3 tons without significant changes to its secondary structure (as assessed by CD) or changes to the appearance and magnitude of functional groups as seen from the location and magnitude of FTIR bands; indicating that a compaction pressure of 3 tons could be used in the formulation of insulin buccal tablets.

Furthermore, basic and acidic amino acids were investigated for their effects on the solubility, distribution coefficient (log D) and permeability of insulin through TR146 buccal cell layers as novel, alternative, safe and effective buccal penetration enhancers for peptides; as well as to highlight their effect on the route and mechanism of insulin transport. Basic amino acids were able to significantly improve insulin solubility in water, while only lysine significantly increased insulin solubility in HBSS. The presence of amino acids was able to increase the hydrophilicity of insulin and lower its log D value by 0.7 units. However, despite this reduced lipophilicity, amino acids were able to effectively and safely enhance permeation of insulin across TR146 cell layers significantly, pointing to the presence of an active carrier transport system. Permeability data

showed a significant concentration-dependent improvement in insulin permeation (above 400% enhancement) without affecting cell integrity; in contrast to the bile salt sodium deoxycholate, which enhanced insulin permeability but was toxic to the cells. Glutamic acid exhibited the highest enhancement that was both effective and safe across a wide range of amino acid concentrations tested. It was hypothesised that at buccal cavity pH, both amino acids and insulin were ionised and able to form stable ion pairs which penetrated through the cells as one entity. Interestingly, investigating the mechanism and route of insulin permeation using increasing concentrations of insulin at suboptimal temperatures, reversed transport direction and confocal microscopy revealed that insulin was transported by active transcellular processes, probably provided by the presence of insulin receptors and amino acid nutrient transporters on the cell membrane. This result obtained for insulin is the first indication of a possible amino acid mediated transport of insulin via formation of insulin-amino acid neutral complexes by the ion pairing mechanism. Amino acids were, therefore, established as safer, effective and novel penetration enhancers than the commonly used surfactant for insulin using the ion-pairing mechanism.

Finally, insulin and the amino acid glutamic acid were incorporated into the optimised placebo base to produce insulin buccal tablets exhibiting sufficient mechanical characteristics to withstand handling during packaging and transport (tensile strength >1 MPa, friability <1%) but with fast disintegration/ disaggregation of < 3 mins. Drug release from these tablets was found to follow Higuchi kinetics, which describes drug release that is diffusion-controlled. Thus, buccal insulin tablets incorporating glutamic acid were successfully fabricated from an ODT placebo base. These can then be taken forward to investigate the *in vitro* and *in* vivo effect of insulin delivered from buccal tablets.

Future work

- Elucidation of the effect of extracellular Ca^{2+} concentration on the biochemical composition, protein expression and lipid barrier of TR146 cell lines; and its effect on desmosome formation employing techniques such as transmission emission microscopy (TEM) and immunohistological assays.

- Investigation of the effect of transmucosal permeation on the secondary structure of insulin, employing techniques such as circular dichroism and x-ray crystallography.
- *In vitro* and *in vivo* studies highlighting the release of insulin from the formulated buccal tablets and the formulation efficacy in glycaemic control.
- Stability studies on developed insulin buccal tablets.

List of References

Adolfsson, Å., Caramella, C. and Nyström, C. (1998) The effect of milling and addition of dry binder on the interparticulate bonding mechanisms in sodium chloride tablets. *International Journal of Pharmaceutics* **160**(2): 187-195.

Adrian, C. L., Olin, H. B. D., Dalhoff, K. and Jacobsen, J. (2006) *In vivo* human buccal permeability of nicotine. *International Journal of Pharmaceutics* **311**(1–2): 196-202.

Agarwal, V., Habib, W. and Moe, D. (2005) Effervescent mediated transmucosal enhancement of fentanyl permeability: Comparison across *ex vivo* porcine buccal mucosa and *in vitro* cultured human buccal epithelium test. *American Association of Pharmaceutical Sciences, Abstract* **2126**.

Agarwal, V. and Khan, M. A. (2001) Current status of the oral delivery of insulin. *Pharmaceutical Technology* **10**: 76-90.

Aguilar, M. -I. (2004) HPLC of peptides and proteins: Methods and Protocols, Springer.

Al-Khattawi, A., Iyire, A., Dennison, T., Dahmash, E., Bailey, C., Smith, J., *et al* (2014) Systematic screening of compressed ODT excipients: Cellulosic versus non-cellulosic. *Current Drug Delivery* **11**(4):486-500

Al-Khattawi, A. and Mohammed, A. (2014). Excipients in medicines for children: Scientific and regulatory paradigms. *European Pharmaceutical Review* **19:** 67-70.

Al-Khattawi, A. and Mohammed, A. R. (2013) Compressed orally disintegrating tablets: Excipients evolution and formulation strategies. *Expert Opinion on Drug Delivery* **10**(5): 651-663.

Alderborn, G. and Nystrom, C. (1995) Pharmaceutical powder compaction technology. New York: Marcel Dekker.

Alhusban, F., Elshaer, A. M., Kansara, J. H., Smith, A. M., Grover, L. M., Perrie, Y., *et al* (2010) Investigation of formulation and process of lyophilised orally disintegrating tablet (ODT) using novel amino acid combination. *Pharmaceutics* **2**(1): 1-17.

Alhusban, F., Perrie, Y. and Mohammed, A. R. (2011) Formulation of multiparticulate systems as lyophilised orally disintegrating tablets. *European Journal of Pharmaceutics and Biopharmaceutics* **79**(3): 627-634.

Alvarez-Lorenzo, C., Gómez-Amoza, J. L., MartíNez-Pacheco, R., Souto, C. and Concheiro, A. (2000) Evaluation of low-substituted hydroxypropylcelluloses (L-HPCs) as filler-binders for direct compression. *International Journal of Pharmaceutics* **197**(1–2): 107-116.

Amidi, M., Pellikaan, H. C., De Boer, A. H., Crommelin, D. J. A., Hennink, W. E. and Jiskoot, W. (2008) Preparation and physicochemical characterization of supercritically dried insulin-loaded microparticles for pulmonary delivery. *European Journal of Pharmaceutics and Biopharmaceutics* **68**(2): 191-200.

Amidon, G. E., Secreast, P. J. and Mudie, D. (2009) Particle, powder, and compact characterization in Oiu Y, Chen Y, Zhang G. (eds) Developing solid oral dosage forms: Pharmaceutical theory and practice. Massachusettes: Academic Press, pp 163-170.

Anderson, M. J. and Whitcomb, P. J. (1974) Design of experiments, Wiley Online Library.

Arbab, A. and Turner, P. (1971) Influence of pH on absorption of thymoxamine through buccal mucosa in man. *British Journal of Pharmacology* **43**(2): 479.

Artursson, P., Palm, K. and Luthman, K. (2012) Caco-2 monolayers in experimental and theoretical predictions of drug transport. *Advanced Drug Delivery Reviews* **64, Supplement**(0): 280-289.

Aungst, B. J. (1994) Site-dependence and structure-effect relationships for alkylglycosides as transmucosal absorption promoters for insulin. *International Journal of Pharmaceutics* **105**(3): 219-225.

Aungst, B. J. (2000) Intestinal permeation enhancers. *Journal of pharmaceutical sciences* **89**(4): 429-442.

Aungst, B. J. (2012) Absorption enhancers: Applications and advances. *The AAPS Journal* **14**(1): 10-18.

Aungst, B. J. and Rogers, N. J. (1988) Site dependence of absorption-promoting actions of laureth-9, Na salicylate, Na2EDTA, and aprotinin on rectal, nasal, and buccal insulin delivery. *Pharmaceutical Research* **5**(5): 305-308.

Aungst, B. J. and Rogers, N. J. (1989) Comparison of the effects of various transmucosal absorption promoters on buccal insulin delivery. *International Journal of Pharmaceutics* **53**(3): 227-235.

Aurora, J. and Pathak, V. (2005) Oral disintegrating technologies: Oral disintegrating dosage forms: An overview. *Drug Delivery Technology* **5**(3): 50-54.

Balimane, P. V., Chong, S. and Morrison, R. A. (2000) Current methodologies used for evaluation of intestinal permeability and absorption. *Journal of Pharmacological and Toxicological Methods* **44**(1): 301-312.

Banga, A. K. and Chien, Y. W. (1988) Systemic delivery of therapeutic peptides and proteins. *International Journal of Pharmaceutics* **48**(1): 15-50.

Bansal, M., Bansal, S. and Kumria, R. (2014). The rapidmist™ system for buccal delivery of insulin in Mucosal delivery of biopharmaceuticals, Springer**,** pp 423-436.

Beckett, A. and Triggs, E. (1967) Buccal absorption of basic drugs and its application as an *in vivo* model of passive drug transfer through lipid membranes. *The Journal of Pharmacy and Pharmacology* **19**: Suppl: 31S-41S.

Behra, A., Giri, T. K., Tripathi, D. K., Alexander, A. and A., A. (2012) An exhaustive review on recent advancement in pharmaceutical bioadhesive used for systemic drug delivery through oral mucosa for achieving maximum pharmacological response and effect. *International Journal of Pharmacology* **8**(5): 283-305.

Benson, K., Cramer, S. and Galla, H.-J. (2013) Impedance-based cell monitoring: Barrier properties and beyond. *Fluids and Barriers of the CNS* **10**(5).

Bernkop-Schnürch, A. and Kast, C. E. (2001) Chemically modified chitosans as enzyme inhibitors. *Advanced Drug Delivery Reviews* **52**(2): 127-137.

Bers, D. M. (2008) Calcium cycling and signaling in cardiac myocytes. *Annual Review of Physiology*. **70**: 23-49.

Bertucci, C., Pistolozzi, M. and De Simone, A. (2011) Structural characterization of recombinant therapeutic proteins by circular dichroism. *Current Pharmaceutical Biotechnology* **12**(10): 1508-1516.

Bi, Y., Sunada, H., Yonezawa, Y. and Danjo, K. (1999) Evaluation of rapidly disintegrating tablets prepared by a direct compression method. *Drug Development and Industrial Pharmacy* **25**(5): 571-581.

Bi, Y., Sunada, H., Yonezawa, Y., Danjo, K., Otsuka, A. and Iida, K. (1996) Preparation and evaluation of a compressed tablet rapidly disintegrating in the oral cavity. *Chemical & Pharmaceutical Bulletin* **44**(11): 2121.

Bird, A. P., Faltinek, J. R. and Shojaei, A. H. (2001) Transbuccal peptide delivery: Stability and *in vitro* permeation studies on endomorphin-1. *Journal of Controlled Release* **73**(1): 31-36.

Blundell, T., Cutfield, J. F., Cutfield, S. M., Dodson, E., Dodson, G., Hogkin, D., *et al* (1971) Atomic positions in rhombohedral 2-zinc insulin crystals. *Nature* **231**(5304): 506-511.

Boddupalli, B. M. M., Z N K; Nath, R a; Banji, D. (2010) Mucoadhesive drug delivery systems: A review. *Journal of Advanced Pharmaceutical Technology & Research* **1**(4): 381-387.

Bondos, S. E. (2006) Methods for measuring protein aggregation. *Current Analytical Chemistry* **2**(2): 157-170.

Bouchard, M., Zurdo, J., Nettleton, E. J., Dobson, C. M. and Robinson, C. V. (2000) Formation of insulin amyloid fibrils followed by FTIR simultaneously with CD and electron microscopy. *Protein Science* **9**(10): 1960-1967.

Boyce, S. T. and Ham, R. G. (1983) Calcium-regulated differentiation of normal human epidermal keratinocytes in chemically defined clonal culture and serum-free serial culture. *Journal of Investigative Dermatology* **81**: 33s-40s.

British Pharmacopoeia Commission (2012). British pharmacopoeia, London : Stationery Office.

Bredenbeck, J., Helbing, J., Kumita, J. R., Woolley, G. A. and Hamm, P. (2005) A-helix formation in a photoswitchable peptide tracked from picoseconds to microseconds by time-resolved ir spectroscopy. *Proceedings of the National Academy of Sciences of the United States of America* **102**(7): 2379-2384.

Bredenberg, S., Duberg, M., Lennernäs, B., Lennernäs, H., Pettersson, A., Westerberg, M., *et al* (2003) *In vitro* and *in vivo* evaluation of a new sublingual tablet system for rapid oromucosal absorption using fentanyl citrate as the active substance. *European Journal of Pharmaceutical Sciences* **20**(3): 327-334.

Bröer, S. (2008) Amino acid transport across mammalian intestinal and renal epithelia. *Physiological Reviews* **88**(1): 249-286.

Buchert, M., Turksen, K. and Hollande, F. (2012) Methods to examine tight junction physiology in cancer stem cells: TEER, paracellular permeability, and dilution potential measurements. *Stem Cell Reviews and Reports* **8**(3): 1030-1034.

Bundgaard, H. and Møss, J. (1990) Prodrugs of peptides. 6. Bioreversible derivatives of thyrotropin-releasing hormone (TRH) with increased lipophilicity and resistance to cleavage by the TRH-specific serum enzyme. *Pharmaceutical Research* **7**(9): 885-892.

Butler, M. (2003). Animal cell culture and technology, Taylor & Francis.

Camenisch, G., Alsenz, J., Van De Waterbeemd, H. and Folkers, G. (1998) Estimation of permeability by passive diffusion through caco-2 cell monolayers using the drugs' lipophilicity and molecular weight. *European Journal of Pharmaceutical Sciences* **6**(4): 313-319.

Cao, N., Chen, X. and Schreyer, D. (2012) Influence of calcium ions on cell survival and proliferation in the context of an alginate hydrogel. *ISRN Chemical Engineering* **2012**.

Caon, T., Jin, L., Simões, C. M., Norton, R. S. and Nicolazzo, J. A. (2014) Enhancing the buccal mucosal delivery of peptide and protein therapeutics. *Pharmaceutical Research* **32**(1): 1-21.

Cappello, B., De Rosa, G., Giannini, L., La Rotonda, M. I., Mensitieri, G., Miro, A., *et al* (2006) Cyclodextrin-containing poly (ethyleneoxide) tablets for the delivery of poorly soluble drugs: Potential as buccal delivery system. *International Journal of Pharmaceutics* **319**(1): 63-70.

Carino, G. P. and Mathiowitz, E. (1999) Oral insulin delivery1. *Advanced Drug Delivery Reviews* **35**(2–3): 249-257.

Cereijido, M., Robbins, E., Dolan, W., Rotunno, C. and Sabatini, D. (1978) Polarized monolayers formed by epithelial cells on a permeable and translucent support. *The Journal of Cell Biology* **77**(3): 853-880.

Chan, C., Chan, K. and French, G. (1986) Rapid high performance liquid chromatographic assay of cephalosporins in biological fluids. *Journal of Antimicrobial Chemotherapy* **18**(4): 537-545.

Chen, B. L., Wu, X., Babuka, S. J. and Hora, M. (1999) Solubility of recombinant human tissue factor pathway inhibitor. *Journal of Pharmaceutical Sciences* **88**(9): 881-888.

Chen, Y.-H., Yang, J. T. and Chau, K. H. (1974) Determination of the helix and β form of proteins in aqueous solution by circular dichroism. *Biochemistry* **13**(16): 3350-3359.

Cilurzo, F., Selmin, F., Minghetti, P., Rimoldi, I., Demartin, F. and Montanari, L. (2005) Fast-dissolving mucoadhesive microparticulate delivery system containing piroxicam. *European Journal of Pharmaceutical Sciences* **24**(4): 355-361.

Collins, L. and Dawes, C. (1987) The surface area of the adult human mouth and thickness of the salivary film covering the teeth and oral mucosa. *Journal of Dental Research* **66**(8): 1300-1302.

Coppolino, M. G., Woodside, M. J., Demaurex, N., Grinstein, S., St-Arnaud, R. and Dedhar, S. (1997) Calreticulin is essential for integrin-mediated calcium signalling and cell adhesion. *Nature* **386:** 843-847.

Dahan, A. and Miller, J. M. (2012) The solubility–permeability interplay and its implications in formulation design and development for poorly soluble drugs. *The AAPS Journal* **14**(2): 244-251.

Dash, S., Murthy, P. N., Nath, L. and Chowdhury, P. (2010) Kinetic modeling on drug release from controlled drug delivery systems. *Acta Poloniae Pharmaceutica* **67**(3): 217-223.

Davis, S. (1986). Advanced delivery systems for peptides and proteins—pharmaceutical considerations. Delivery systems for peptide drugs, Springer**:** 1-21.

Davoudi, B., Lindenmaier, A., Standish, B. A., Allo, G., Bizheva, K. and Vitkin, A. (2012) Noninvasive *in vivo* structural and vascular imaging of human oral tissues with spectral domain optical coherence tomography. *Biomedical Optics Express* **3**(5): 826-839.

Deshpande, O. and Yadav, V. (2009) Improvement in physicochemical properties of indomethacin by melt granulation technique. *International Journal of Chemical Technology Research* **1**: 1312-1317.

Di Colo, G., Burgalassi, S., Chetoni, P., Fiaschi, M., Zambito, Y. and Saettone, M. (2001) Relevance of polymer molecular weight to the *in vitro/in vivo* performances of ocular inserts based on poly (ethylene oxide). *International Journal of Pharmaceutics* **220**(1): 169-177.

Dimitrov, M. and Lambov, N. (1999) Study of verapamil hydrochloride release from compressed hydrophilic polyox-wsr tablets. *International Journal of Pharmaceutics* **189**(1): 105-111.

Dixit, R. and Puthli, S. (2009) Oral strip technology: Overview and future potential. *Journal of Controlled Release* **139**(2): 94-107.

Dolan, J. W. and Snyder, L. R. (1989). Troubleshooting LC systems: A comprehensive approach to troubleshooting LC equipment and separations, Springer Science & Business Media.

Dowty, M. E., Knuth, K. E., Irons, B. K. and Robinson, J. R. (1992) Transport of thyrotropin releasing hormone in rabbit buccal mucosa *in vitro*. *Pharmaceutical Research* **9**(9): 1113-1122.

Dressman, J. B. and Reppas, C. (2010). Oral drug absorption: Prediction and assessment. Florida: CRC Press.

Efentakis, M. and Vlachou, M. (2000) Evaluation of high molecular weight poly (oxyethylene)(polyox) polymer: Studies of flow properties and release rates of furosemide and captopril from controlled-release hard gelatin capsules. *Pharmaceutical Development and Technology* **5**(3): 339-346.

Ek, R., Wormald, P., Iversen, T. and Nyström, C. (1995) Crystallinity index of microcrystalline cellulose particles compressed into tablets. *International Journal of Pharmaceutics* **125**(2): 257-264.

Elshaer, A., Hanson, P. and Mohammed, A. R. (2013) A systematic and mechanistic evaluation of aspartic acid as filler for directly compressed tablets containing trimethoprim and trimethoprim aspartate. *European Journal of Pharmaceutics and Biopharmaceutics* **83**(3): 468-476.

Elshaer, A., Hanson, P. and Mohammed, A. R. (2014) A novel concentration dependent amino acid ion pair strategy to mediate drug permeation using indomethacin as a model insoluble drug. *European journal of pharmaceutical sciences* **62**: 124-131.

Elshaer, A., Kaialy, W., Akhtar, N., Iyire, A., Hussain, T., Alany, R., *et al* (2015) A methodological evaluation and predictive *in silico* investigation into the multi-functionality of arginine in directly compressed tablets. *European Journal of Pharmaceutics and Biopharmaceutics* **96**: 272-281.

Elshaer, A., Khan, S., Perumal, D., Hanson, P. and R Mohammed, A. (2011) Use of amino acids as counterions improves the solubility of the BCS II model drug, indomethacin. *Current Drug Delivery* **8**(4): 363-372.

Engelman, D. M., Steitz, T.A. and Goldman, A. (1986) Identifying nonpolar transbilayer helices in amino acid sequences of membrane proteins. *Annual Reviews of Biophysical Chemistry* **15**(1):321-353

Epshtein, N. (2004) Validation of hplc techniques for pharmaceutical analysis. *Pharmaceutical Chemistry Journal* **38**(4): 212-228.

Eriksson, L. (2008). Design of experiments: Principles and applications, MKS Umetrics AB.

Eriksson, M. and Alderborn, G. (1995) The effect of particle fragmentation and deformation on the interparticulate bond formation process during powder compaction. *Pharmaceutical Research* **12**(7): 1031-1039.

Fahmy, R. H. and Kassem, M. A. (2008) Enhancement of famotidine dissolution rate through liquisolid tablets formulation: *in vitro* and *in vivo* evaluation. *European Journal of Pharmaceutics and Biopharmaceutics* **69**(3): 993-1003.

Francis, M. F., Piredda, M. and Winnik, F. M. (2003) Solubilization of poorly water soluble drugs in micelles of hydrophobically modified hydroxypropylcellulose copolymers. *Journal of Controlled Release* **93**(1): 59-68.

Franks, K., Abrahams, I. and Knowles, J. (2000) Development of soluble glasses for biomedical use part i: *In vitro* solubility measurement. *Journal of Materials Science: Materials in Medicine* **11**(10): 609-614.

Freshney, R. I. and Freshney, M. G. (2004). Culture of epithelial cells, John Wiley & Sons.

Fukami, J., Yonemochi, E., Yoshihashi, Y. and Terada, K. (2006) Evaluation of rapidly disintegrating tablets containing glycine and carboxymethylcellulose. *International Journal of Pharmaceutics* **310**(1): 101-109.

Gamlen, T. L. (2016). "The importance of normalisation when comparing tablet properties." Retrieved 17/03/2016, 2016, from http://gamlentableting.com/images/The%20importance%20of%20normalization%20when%20analysing%20tablet%20hardness.pdf.

Gandhi, R. and Robinson, J. (1992) Mechanisms of penetration enhancement for transbuccal delivery of salicylic acid. *International Journal of Pharmaceutics* **85**(1): 129-140.

Gandhi, R. B. and Robinson, J. R. (1991) Permselective characteristics of rabbit buccal mucosa. *Pharmaceutical Research* **8**(9): 1199-1202.

Gandhi, R. B. and Robinson, J. R. (1994) Oral cavity as a site for bioadhesive drug delivery. *Advanced Drug Delivery Reviews* **13**(1): 43-74.

Gardner, T. W., Lieth, E., Khin, S. A., Barber, A., Bonsall, D. J., Lesher, T., *et al* (1997) Astrocytes increase barrier properties and ZO-1 expression in retinal vascular endothelial cells. *Investigative Ophthalmology & Visual Science* **38**(11): 2423-2427.

Garrod, D. and Chidgey, M. (2008) Desmosome structure, composition and function. *Biochimica et Biophysica Acta (BBA) - Biomembranes* **1778**(3): 572-587.

Gerber, F., Krummen, M., Potgeter, H., Roth, A., Siffrin, C. and Spoendlin, C. (2004) Practical aspects of fast reversed-phase high-performance liquid chromatography using 3µm particle packed columns and monolithic columns in pharmaceutical development and production working under current good manufacturing practice. *Journal of Chromatography A* **1036**(2): 127-133.

Giri, T., Tripathi, D. and Majumdar, R. (2010) Formulation aspects in the development of orodispersible tablets: An overview. *International Journal of Pharmacy and Pharmaceutical Sciences* **2**(3): 38-42.

Goel, H., Rai, P., Rana, V. and Tiwary, A. K. (2008) Orally disintegrating systems: Innovations in formulation and technology. *Recent Patents on Drug Delivery & Formulation* **2**(3): 258-274.

Gohel, M., Patel, M., Amin, A., Agrawal, R., Dave, R. and Bariya, N. (2004) Formulation design and optimization of mouth dissolve tablets of nimesulide using vacuum drying technique. *AAPS Pharmaceutical Science and Technology* **5**(3): 10-15.

Goldman, J. and Carpenter, F. H. (1974) Zinc binding, circular dichroism, and equilibrium sedimentation studies on insulin (bovine) and several of its derivatives. *Biochemistry* **13**(22): 4566-4574.

Golovanov, A. P., Hautbergue, G. M., Wilson, S. A. and Lian, L.-Y. (2004) A simple method for improving protein solubility and long-term stability. *Journal of the American Chemical Society* **126**(29): 8933-8939.

Gómez-Carracedo, A., Alvarez-Lorenzo, C., Gómez-Amoza, J. and Concheiro, A. (2003) Chemical structure and glass transition temperature of non-ionic cellulose ethers. *Journal of Thermal Analysis and Calorimetry* **73**(2): 587-596.

Gong, G. L., Li, H. and Li, X. Y. (2011) Studies on swelling kinetics for HPC/PAN thermo-sensitive blending films. *Polymers for Advanced Technologies* **22**(10): 1422-1426.

Gosai, A. R., Patil, S. B. and Sawant, K. K. (2008) Formulation and evaluation of oro dispersible tablets of ondansetron hydrochloride by direct compression using superdisintegrants. *International Journal of Pharmaceutical Sciences and Nanotechnology* **1**(1): 106-111.

Gracias, D. and Somorjai, G. (1998) Continuum force microscopy study of the elastic modulus, hardness and friction of polyethylene and polypropylene surfaces. *Macromolecules* **31**(4): 1269-1276.

Greenfield, N. J. (2007) Using circular dichroism spectra to estimate protein secondary structure. *Nature Protocols* **1**(6): 2876-2890.

Grego, B. and Hearn, M. (1981) Role of the organic solvent modifier in the reversed phase high-performance liquid chromatography of polypeptides. *Chromatographia* **14**(10): 589-592.

Guariguata, L., Whiting, D., Hambleton, I., Beagley, J., Linnenkamp, U. and Shaw, J. (2014) Global estimates of diabetes prevalence for 2013 and projections for 2035. *Diabetes Research and Clinical Practice* **103**(2): 137-149.

ICH (1996) *ICH Q1B,* Photostability testing of new drug substances and products, Geneva, Switzerland.

ICH (2005) International Conference on Harmonisation for validation of analytical procedures: Text and methodology. *Q2 (R1)* **1**.

ICH (2009) International conference on harmonisation of technical requirements for registration of pharmaceuticlas for human use, pharmaceutical development Q8 (R2). *ICH Steering Committee, Step* **4**.

Gumaste, S. G., Pawlak, S. A., Dalrymple, D. M., Nider, C. J., Trombetta, L. D. and Serajuddin, A. T. (2013) Development of solid sedds, IV: Effect of adsorbed lipid and surfactant on tableting properties and surface structures of different silicates. *Pharmaceutical Research* **30**(12): 3170-3185.

Gupta, V., Jain, A. D. K., Gill, N. and Gupta, K. (2012) Development and validation of HPLC method-a review. *International Research Journal of Pharmaceutical and Applied Sciences* **2**(4): 17-25.

Hames, D. and Hooper, N. (2005) Biochemistry, 3 th. New York: Taylor and Francis.

Hancock, B. C., Carlson, G. T., Ladipo, D. D., Langdon, B. A. and Mullarney, M. P. (2001) The powder flow and compact mechanical properties of two recently developed matrix-forming polymers. *Journal of Pharmacy and Pharmacology* **53**(9): 1193-1199.

Hancock, B. C., Colvin, J. T., Mullarney, M. P. and Zinchuk, A. V. (2003) Pharmaceutical powders, blends, dry granulations, and immediate-release tablets. *Pharmaceutical Technology* from http://images.alfresco.advanstar.com/alfresco_images/pharma/2014/08/22/1bb0fa3e-fc52-47bd-b20e-39b55d9063e1/article-52997.pdf. Accessed 13/07/2013

Hao, J. and Heng, P. W. (2003) Buccal delivery systems. *Drug Development and Industrial pharmacy* **29**(8): 821-832.

Harris, D. and Robinson, J. R. (1992) Drug delivery via the mucous membranes of the oral cavity. *Journal of Pharmaceutical Sciences* **81**(1): 1-10.

Hassan, N., Ahad, A., Ali, M. and Ali, J. (2010) Chemical permeation enhancers for transbuccal drug delivery. *Expert Opinion on Drug Delivery* **7**(1): 97-112.

Hayward, A. (1979) Membrane-coating granules. *International Review of Cytology* **59**: 97-127.

He, X., Secreast, P. J. and Amidon, G. E. (2007) Mechanistic study of the effect of roller compaction and lubricant on tablet mechanical strength. *Journal of Pharmaceutical Sciences* **96**(5): 1342-1355.

Heikkilä, T., Salonen, J., Tuura, J., Hamdy, M. S., Mul, G., Kumar, N., *et al* (2007) Mesoporous silica material TUD-1 as a drug delivery system. *International Journal of Pharmaceutics* **331**(1): 133-138.

Heinemann, L. (2008) The failure of exubera: Are we beating a dead horse? *Journal of Diabetes Science and Technology* **2**(3): 518-529.

Heinemann, L. and Jacques, Y. (2009) Oral insulin and buccal insulin: A critical reappraisal. *Journal of Diabetes Science and Technology* **3**(3): 568-584.

Hemenway, J. N., Jarho, P., Henri, J. T., Nair, S. K., Vandervelde, D., Georg, G. I., *et al* (2010) Preparation and physicochemical characterization of a novel water-soluble prodrug of carbamazepine. *Journal of Pharmaceutical Sciences* **99**(4): 1810-1825.

Hennings, H., Michael, D., Cheng, C., Steinert, P., Holbrook, K. and Yuspa, S. H. (1980) Calcium regulation of growth and differentiation of mouse epidermal cells in culture. *Cell* **19**(1): 245-254.

Hiestand, E. N. (1997) Principles, tenets and notions of tablet bonding and measurements of strength. *European Journal of Pharmaceutics and Biopharmaceutics* **44**(3): 229-242.

Hirani, J. J., Rathod, D. A. and Vadalia, K. R. (2009) Orally disintegrating tablets: A review. *Tropical Journal of Pharmaceutical Research* **8**(2).

Ho, N., Day, J., Barsuhn, C., Burton, P. and Raub, T. (1990) Biophysical model approaches to mechanistic transepithelial studies of peptides. *Journal of Controlled Release* **11**(1): 3-24.

Hoogstraate, A., Senel, S., Cullander, C., Verhoef, J., Junginger, H. and Bodde, H. (1996a) Effects of bile salts on transport rates and routes of fitc-labelled compounds across porcine buccal epithelium *in vitro*. *Journal of Controlled Release* **40**(3): 211-221.

Hoogstraate, A., Verhoef, J., Tuk, B., Pijpers, A., Van Leengoed, L., Verheijden, J., *et al* (1996b) *In-vivo* buccal delivery of fluorescein isothiocyanate–dextran 4400 with glycodeoxycholate as an absorption enhancer in pigs. *Journal of Pharmaceutical Sciences* **85**(5): 457-460.

Hoogstraate, A. J. and Boddé, H. E. (1993) Methods for assessing the buccal mucosa as a route of drug delivery. *Advanced Drug Delivery Reviews* **12**(1): 99-125.

Hörter, D. and Dressman, J. (2001) Influence of physicochemical properties on dissolution of drugs in the gastrointestinal tract. *Advanced Drug Delivery Reviews* **46**(1): 75-87.

Hosny, E. A., Elkheshen, S. A. and Saleh, S. I. (2002) Buccoadhesive tablets for insulin delivery: *In-vitro* and *in-vivo* studies. *Bollettino Chimico Farmaceutico* **141**(3): 210-217.

Hunjan, M. K. and Evered, D. F. (1985) Absorption of glutathione from the gastro-intestinal tract. *Biochimica et Biophysica Acta (BBA) - Biomembranes* **815**(2): 184-188.

Ishikawa, T., Mukai, B., Shiraishi, S., Utoguchi, N., Fuji, M., Matsumoto, M., *et al* (2001) Preparation of rapidly disintegrating tablet using new types of microcrystalline cellulose (ph-m series) and low substituted-hydroxypropylcellulose or spherical sugar granules by direct compression method. *Chemical and Pharmaceutical Bulletin* **49**(2): 134-139.

Ivaturi, V. D. and Kim, S. K. (2009) Enhanced permeation of methotrexate *in vitro* by ion pair formation with L-arginine. *Journal of Pharmaceutical Sciences* **98**(10): 3633-3639.

Jacobsen, J., Pedersen, M. and Rassing, M. R. (1996) TR146 cells as a model for human buccal epithelium: II. Optimisation and use of a cellular sensitivity MTS/PMS assay. *International Journal of Pharmaceutics* **141**(1): 217-225.

Jacobsen, J., Van Deurs, B., Pedersen, M. and Rassing, M. R. (1995) Tr146 cells grown on filters as a model for human buccal epithelium: I. Morphology, growth, barrier properties, and permeability. *International Journal of Pharmaceutics* **125**(2): 165-184.

Jacques, C. H. M., Hopfenberg, H. B. and Stannett, V. (1974). Super case II transport of organic vapors in glassy polymers. Permeability of plastic films and coatings: To gases, vapors, and liquids. Hopfenberg, H. B. Boston, MA, Springer US**:** 73-86.

Jacques, Y. and Buri, P. (1998) La muqueuse buccale en tant que barriere d'absorption des médicaments: Caractéristiques structurales et dynamique de perméabilité. *Muqueuse Buccale et Systemes Thérapeutiques Bioadhésifs. Médecine et Hygiene, Geneve*: 9-45.

Janůšová, B., Školová, B., Tükörová, K., Wojnarová, L., Šimůnek, T., Mladěnka, P., *et al* (2013) Amino acid derivatives as transdermal permeation enhancers. *Journal of Controlled Release* **165**(2): 91-100.

Jayatilake, J., Samaranayake, Y. and Samaranayake, L. (2005) An ultrastructural and a cytochemical study of candidal invasion of reconstituted human oral epithelium. *Journal of Oral Pathology & Medicine* **34**(4): 240-246.

Jeyaraju, D. V., Cisbani, G. and Pellegrini, L. (2009) Calcium regulation of mitochondria motility and morphology. *Biochimica et Biophysica Acta (BBA) - Bioenergetics* **1787**(11): 1363-1373.

Jiménez-Castellanos, M. R., Zia, H. and Rhodes, C. (1993) Mucoadhesive drug delivery systems. *Drug Development and Industrial Pharmacy* **19**(1-2): 143-194.

Johnston, T. P., Rahman, A., Alur, H., Shah, D. and Mitra, A. K. (1998) Permeation of unfolded basic fibroblast growth factor (bFGF) across rabbit buccal mucosa—does unfolding of bFGF enhance transport? *Pharmaceutical Research* **15**(2): 246-253.

Junginger, H. E., Hoogstraate, J. A. and Verhoef, J. C. (1999) Recent advances in buccal drug delivery and absorption — *in vitro* and *in vivo* studies. *Journal of Controlled Release* **62**(1–2): 149-159.

Kashi, S. D. and Lee, V. H. (1986) Enkephalin hydrolysis in homogenates of various absorptive mucosae of the albino rabbit: Similarities in rates and involvement of aminopeptidases. *Life Sciences* **38**(22): 2019-2028.

Kelly, D. E. (1966) Fine structure of desmosomes, hemidesmosomes, and an adepidermal globular layer in developing newt epidermis. *The Journal of Cell Biology* **28**(1): 51-72.

Kelly, S. M., Jess, T. J. and Price, N. C. (2005) How to study proteins by circular dichroism. *Biochimica et Biophysica Acta (BBA)-Proteins and Proteomics* **1751**(2): 119-139.

Khafagy, E.-S., Morishita, M., Onuki, Y. and Takayama, K. (2007) Current challenges in non-invasive insulin delivery systems: A comparative review. *Advanced Drug Delivery Reviews* **59**(15): 1521-1546.

Khafagy El, S., Morishita, M., Onuki, Y. and Takayama, K. (2007) Current challenges in non-invasive insulin delivery systems: A comparative review. *Advanced Drug Delivery Reviews* **59**(15): 1521-1546.

Khan, S., Kataria, P., Nakhat, P. and Yeole, P. (2007) Taste masking of ondansetron hydrochloride by polymer carrier system and formulation of rapid-disintegrating tablets. *AAPS Pharmaceutical Science and Technology* **8**(2): E127-E133.

Khossravi, D. and Morehead, W. T. (1997) Consolidation mechanisms of pharmaceutical solids: A multi-compression cycle approach. *Pharmaceutical r***14**(8): 1039-1045.

Kim, K.-S. and Park, S.-J. (2011) Influence of glyceryl palmitostearate on release behaviors of hydroxypropyl cellulose microcapsules containing indomethacin by w/o emulsion. *Macromolecular Research* **19**(11): 1121-1126.

Kleinebudde, P. (2004) Roll compaction/dry granulation: Pharmaceutical applications. *European Journal of Pharmaceutics and Biopharmaceutics* **58**(2): 317-326.

Korhonen, O., Pohja, S., Peltonen, S., Suihko, E., Vidgren, M., Paronen, P., *et al* (2002) Effects of physical properties for starch acetate powders on tableting. *AAPS Pharmaceutical Science and Technology* **3**(4): 68-76.

Korsmeyer, R. W., Gurny, R., Doelker, E., Buri, P. and Peppas, N. A. (1983) Mechanisms of solute release from porous hydrophilic polymers. *International Journal of Pharmaceutics* **15**(1): 25-35.

Kramer, R. M., Shende, V. R., Motl, N., Pace, C. N. and Scholtz, J. M. (2012) Toward a molecular understanding of protein solubility: Increased negative surface charge correlates with increased solubility. *Biophysical Journal* **102**(8): 1907-1915.

Kumria, R. and Goomber, G. (2011) Emerging trends in insulin delivery: Buccal route. *Journal of Diabetology* **2**(1): 1-9.

Kurosaki, Y., Vano, K. and Kimura, T. (1997) Perfusion cells for studying regional variation in oral-mucosal permeability in humans. I: Kinetic aspects in oral-mucosal absorption of alkylparabens. *Pharmaceutical Research* **14**(9): 1241-1245.

Kurosaki, Y., Yano, K. and Kimura, T. (1998) Perfusion cells for studying regional variation in oral mucosal permeability in humans. 2. A specialized transport mechanism in d-glucose absorption exists in dorsum of tongue. *Journal of Pharmaceutical Sciences* **87**(5): 613-615.

L'hote-Gaston, J., Schmitt, R., Levina, M., Wen, G. and Rajabi-Siahboomi, A. (2009) The use of polyethylene oxide mixtures to study formulation robustness in hydrophilic extended release matrix tablets from https://www.colorcon.com/literature/Corporate/eNewsletter/2010/DOW-198-02205%20AAPS%202009%20Technical%20Poster%20L'Hote-Gaston%20Robustness.pdf. Accessed 14/03/2014.

Landreh, M., Alvelius, G., Willander, H., Stukenborg, J. B., Söder, O., Johansson, J., *et al* (2012) Insulin solubility transitions by ph-dependent interactions with proinsulin C-peptide. *FEBS Journal* **279**(24): 4589-4597.

Lane, M. E., O'driscoll, C. M. and Corrigan, O. I. (2005) Quantitative estimation of the effects of bile salt surfactant systems on insulin stability and permeability in the rat intestine using a mass balance model. *Journal of Pharmacy and Pharmacology* **57**(2): 169-175.

Lawrence, X. Y. (2008) Pharmaceutical quality by design: Product and process development, understanding, and control. *Pharmaceutical research* **25**(4): 781-791.

Lechner, J. F., Haugen, A., Mcclendon, I. A. and Pettis, E. W. (1982) Clonal growth of normal adult human bronchial epithelial cells in a serum-free medium. *In vitro* **18**(7): 633-642.

Lee, B.-J., Ryu, S.-G. and Cui, J.-H. (1999) Formulation and release characteristics of hydroxypropyl methylcellulose matrix tablet containing melatonin. *Drug development and Industrial Pharmacy* **25**(4): 493-501.

Lee, V. H. and Yamamoto, A. (1989) Penetration and enzymatic barriers to peptide and protein absorption. *Advanced Drug Delivery Reviews* **4**(2): 171-207.

Lehr, C.-M. (2003). Cell culture models of biological barriers: *In vitro* test systems for drug absorption and delivery, CRC Press.

Leninger, A., Nelson, D. L. and Cox, M. M. (1993) Principles of biochemistry. New York: Worth Publishers.

Lens, J. (1946) The solubility curve and the purity of insulin. *Journal of Biological Chemistry* **164**(1): 223-231.

Leone-Bay, A., Paton, D. R., Freeman, J., Lercara, C., O'toole, D., Gschneidner, D., *et al* (1998) Synthesis and evaluation of compounds that facilitate the gastrointestinal absorption of heparin. *Journal of Medicinal Chemistry* **41**(7): 1163-1171.

Leone-Bay, A., Santiago, N., Achan, D., Chaudhary, K., Demorin, F., Falzarano, L., *et al* (1995) N-acylated. Alpha.-amino acids as novel oral delivery agents for proteins. *Journal of Medicinal Chemistry* **38**(21): 4263-4269.

Lesch, C., Squier, C., Cruchley, A., Williams, D. and Speight, P. (1989) The permeability of human oral mucosa and skin to water. *Journal of Dental Research* **68**(9): 1345-1349.

Li, B. and Robinson, J. R. (2005) Preclinical assessment of oral mucosal drug delivery systems. *Drugs and the Pharmaceutical Sciences* **145**: 41.

Li, H., Krieger, R. I. and Li, Q. X. (2000) Improved HPLC method for analysis of 1-hydroxypyrene in human urine specimens of cigarette smokers. *Science of the Total Environment* **257**(2–3): 147-153.

Lin, L., Yee, S. W., Kim, R. B. and Giacomini, K. M. (2015) SLC transporters as therapeutic targets: Emerging opportunities. *Nature Reviews Drug Discovery* 14(8):543-60.

Lindsay, S. and Kealey, D. (1987) High performance liquid chromatography.

Lionberger, R. A., Lee, S. L., Lee, L., Raw, A. and Lawrence, X. Y. (2008) Quality by design: Concepts for ANDAs. *The AAPS Journal* **10**(2): 268-276.

Lu, Q., Jayatilake, J. A., Samaranayake, L. P. and Jin, L. (2006) Hyphal invasion of candida albicans inhibits the expression of human β-defensins in experimental oral candidiasis. *Journal of Investigative Dermatology* **126**(9): 2049-2056.

Luo, Y., Xu, H., Huang, K., Zhang, Z., Luo, Q. and Liu, Q. (2006). Imaging on the binding of fitc-insulin with insulin receptors in cortical neurons of rat. Engineering in Medicine and Biology Society, 2005. IEEE-EMBS 2005. *27th Annual International Conference of the IEEE*.

Machida, Y. N., T. (1974) Directly compressed tablets containing hydroxypropyl cellulose in addition to starch or lactose. *Chemical and Pharmaceutical Bulletin (Tokyo)* **22**: 2346-2351.

Maeno, S., Niki, Y., Matsumoto, H., Morioka, H., Yatabe, T., Funayama, A., *et al* (2005) The effect of calcium ion concentration on osteoblast viability, proliferation and differentiation in monolayer and 3D culture. *Biomaterials* **26**(23): 4847-4855.

Maggi, L., Segale, L., Torre, M., Ochoa Machiste, E. and Conte, U. (2002) Dissolution behaviour of hydrophilic matrix tablets containing two different polyethylene oxides (peos) for the controlled release of a water-soluble drug. Dimensionality study. *Biomaterials* **23**(4): 1113-1119.

Mahato, R. I., Narang, A. S., Thoma, L. and Miller, D. D. (2003) Emerging trends in oral delivery of peptide and protein drugs. *Critical Reviews™ in Therapeutic Drug Carrier Systems* **20**(2&3).

Makhlof, A., Tozuka, Y. and Takeuchi, H. (2011) Design and evaluation of novel pH-sensitive chitosan nanoparticles for oral insulin delivery. *European Journal of Pharmaceutical Sciences* **42**(5): 445-451.

Manly, R. (2012). Adhesion in biological systems, Elsevier.

Manzini, G., Barcellona, M., Avitabile, M. and Quadrifoglio, F. (1983) Interaction of diamidino-2-phenylindole (DAPI) with natural and synthetic nucleic acids. *Nucleic Acids Research* **11**(24): 8861-8876.

Mashru, R., Sutariya, V., Sankalia, M. and Sankalia, J. (2005) Transbuccal delivery of lamotrigine across porcine buccal mucosa: *In vitro* determination of routes of buccal transport. *J Pharmacology and Pharmaceutical Sciences* **8**(1): 54-62.

Mather, J. P. and Roberts, P. E. (1998). Introduction to cell and tissue culture: Theory and technique, Springer Science & Business Media.

Mathias, N. R. and Hussain, M. A. (2010) Non-invasive systemic drug delivery: Developability considerations for alternate routes of administration. *Journal of pharmaceutical sciences* **99**(1): 1-20.

Matsuura, J., Powers, M. E., Manning, M. C. and Shefter, E. (1993) Structure and stability of insulin dissolved in 1-octanol. *Journal of the American Chemical Society* **115**(4): 1261-1264.

Maximilien, J. (2013) Polyethylene oxide. Medicines Complete.

Miller, J. M. (2009). The impact of molecular complexation on intestinal membrane permeation, Pharmaceutical Science, The University of Michigan.

Milstein, S. J., Leipold, H., Sarubbi, D., Leone-Bay, A., Mlynek, G. M., Robinson, J. R., *et al* (1998) Partially unfolded proteins efficiently penetrate cell membranes—implications for oral drug delivery. *Journal of Controlled Release* **53**(1): 259-267.

Modi, P. (2002). Pharmaceutical compositions for buccal and pulmonary administration comprising an alkali metal alkyl sulfate and at least three micelle-forming compounds, Google Patents.

Modi, P. (2010). Method for administering insulin to the buccal region, Google Patents.

Moghimipour, E., Ameri, A. and Handali, S. (2015) Absorption-enhancing effects of bile salts. *Molecules* **20**(8): 14451-14473.

Moharamzadeh, K., Brook, I., Van Noort, R., Scutt, A. and Thornhill, M. (2007) Tissue-engineered oral mucosa: A review of the scientific literature. *Journal of Dental Research* **86**(2): 115-124.

Montgomery, D. C. (2004). Design and analysis of experiments, New York ; Chichester : Wiley, 2005. 6th ed.

Morishita, M., Barichello, J. M., Takayama, K., Chiba, Y., Tokiwa, S. and Nagai, T. (2001) Pluronic F-127 gels incorporating highly purified unsaturated fatty acids for buccal delivery of insulin. *International Journal of Pharmaceutics* **212**(2): 289-293.

Morishita, M., Kajita, M., Suzuki, A., Takayama, K., Chiba, Y., Tokiwa, S., *et al* (2000) The dose-related hypoglycemic effects of insulin emulsions incorporating highly purified EPA and DHA. *International Journal of Pharmaceutics* **201**(2): 175-185.

Moslemi, P., Najafabadi, A. R. and Tajerzadeh, H. (2003) A rapid and sensitive method for simultaneous determination of insulin and a21-desamido insulin by high-performance liquid chromatography. *Journal of Pharmaceutical and Biomedical Analysis* **33**(1): 45-51.

Moussa, B., Farouk, F. and Azzazy, H. (2010) A validated RP-HPLC method for the determination of recombinant human insulin in bulk and pharmaceutical dosage form. *Journal of Chemistry* **7**(S1): S449-S457.

Muheem, A., Shakeel, F., Jahangir, M. A., Anwar, M., Mallick, N., Jain, G. K., *et al* (2014) A review on the strategies for oral delivery of proteins and peptides and their clinical perspectives. *Saudi Pharmaceutical Journal*.

Nachtmann, F. (1979) Automated high-performance liquid chromatography as a means of monitoring the production of penicillins and 6-aminopenicillanic acid. *Chromatographia* **12**(6): 380-385.

Nerurkar, J., Jun, H., Price, J. and Park, M. (2005) Controlled-release matrix tablets of ibuprofen using cellulose ethers and carrageenans: Effect of formulation factors on dissolution rates. *European Journal of Pharmaceutics and Biopharmaceutics* **61**(1): 56-68.

Nicolazzo, J. A., Reed, B. L. and Finnin, B. C. (2005) Buccal penetration enhancers—how do they really work? *Journal of Controlled Release* **105**(1): 1-15.

Nicolescu, C., Aramă, C., Nedelcu, A. and Monciu, C.-M. (2010) Phase solubility studies of the inclusion complexes of repaglinide with β-cyclodextrin and β-cyclodextrin derivatives. *Farmacia* **58**(5): 620-628.

Nielsen, H. M. and Rassing, M. R. (1999) TR146 cells grown on filters as a model of human buccal epithelium: III. Permeability enhancement by different pH values, different osmolality values, and bile salts. *International Journal of Pharmaceutics* **185**(2): 215-225.

Nielsen, H. M. and Rassing, M. R. (2000a) TR146 cells grown on filters as a model of human buccal epithelium: IV. Permeability of water, mannitol, testosterone and β-adrenoceptor antagonists. Comparison to human, monkey and porcine buccal mucosa. *International Journal of Pharmaceutics* **194**(2): 155-167.

Nielsen, H. M. and Rassing, M. R. (2000b) TR146 cells grown on filters as a model of human buccal epithelium: V. Enzyme activity of the TR146 cell culture model, human buccal epithelium and porcine buccal epithelium, and permeability of leu-enkephalin. *International Journal of Pharmaceutics* **200**(2): 261-270.

Nielsen, H. M. and Rassing, M. R. (2002) Nicotine permeability across the buccal TR146 cell culture model and porcine buccal mucosa in vitro: Effect of ph and concentration. *European journal of pharmaceutical sciences* **16**(3): 151-157.

Nielsen, H. M., Verhoef, J., Ponec, M. and Rassing, M. R. (1999) TR146 cells grown on filters as a model of human buccal epithelium: Permeability of fluorescein isothiocyanate-labelled

dextrans in the presence of sodium glycocholate. *Journal of Controlled Release* **60**(2): 223-233.

Nielsen, L., Frokjaer, S., Carpenter, J. F. and Brange, J. (2001) Studies of the structure of insulin fibrils by fourier transform infrared (FTIR) spectroscopy and electron microscopy. *Journal of Pharmaceutical Sciences* **90**(1): 29-37.

Nokhodchi, A., Ford, J. L., Rowe, P. H. and Rubinstein, M. H. (1996) The effects of compression rate and force on the compaction properties of different viscosity grades of hydroxypropylmethylcellulose 2208. *International Journal of Pharmaceutics* **129**(1): 21-31.

Nyström, C., Alderborn, G., Duberg, M. and Karehill, P.-G. (1993) Bonding surface area and bonding mechanism-two important factors fir the understanding of powder comparability. *Drug Development and Industrial Pharmacy* **19**(17-18): 2143-2196.

Oak, M. and Singh, J. (2012a) Chitosan-zinc-insulin complex incorporated thermosensitive polymer for controlled delivery of basal insulin in vivo. *Journal of Controlled Release* **163**(2): 145-153.

Oak, M. and Singh, J. (2012b) Controlled delivery of basal level of insulin from chitosan-zinc-insulin-complex-loaded thermosensitive copolymer. *Journal of Pharmaceutical Sciences* **101**(3): 1079-1096.

Odeku, O., Awe, O., Popoola, B., Odeniyi, M. and Itiola, O. (2005) Compression and mechanical properties of tablet formulations: Containing corn, sweet potato, and cocoyam starches as binders. *Pharmaceutical Technology* **29**(4): 82-90.

Oh, C. K. and Ritschel, W. (1990) Biopharmaceutic aspects of buccal absorption of insulin. *Methods and Findings in Experimental and Clinical Pharmacology* **12**(3): 205-212.

Oh, D.-H., Chun, K.-H., Jeon, S.-O., Kang, J.-W. and Lee, S. (2011) Enhanced transbuccal salmon calcitonin (sct) delivery: Effect of chemical enhancers and electrical assistance on *in vitro* sCT buccal permeation. *European Journal of Pharmaceutics and Biopharmaceutics* **79**(2): 357-363.

Ohshima, H. and Makino, K. (2014). Colloid and interface science in pharmaceutical research and development, Elsevier.

Okuda, T., Kadotsuji, K., Takayama, C., Hanada, K., Mukaizawa, F., Ogawara, K. I., *et al* (2006) Involvement of intracellular Ca^{2+} dynamics in cytoprotective action by amino acids and cytotoxicity by sodium laurate, an absorption enhancer. *Journal of Pharmaceutical Sciences* **95**(10): 2256-2265.

Oliva, A., Fariña, J. and Llabrés, M. A. (2000) Development of two high-performance liquid chromatographic methods for the analysis and characterization of insulin and its degradation products in pharmaceutical preparations. *Journal of Chromatography B: Biomedical Sciences and Applications* **749**(1): 25-34.

Olsen, B. A. (2001) Hydrophilic interaction chromatography using amino and silica columns for the determination of polar pharmaceuticals and impurities. *Journal of Chromatography A* **913**(1–2): 113-122.

Owens, D. R., Zinman, B. and Bolli, G. (2003) Alternative routes of insulin delivery. *Diabetic Medicine* **20**(11): 886-898.

Pan, Y., Li, Y.-J., Zhao, H.-Y., Zheng, J.-M., Xu, H., Wei, G., *et al* (2002) Bioadhesive polysaccharide in protein delivery system: Chitosan nanoparticles improve the intestinal absorption of insulin *in vivo*. *International Journal of Pharmaceutics* **249**(1): 139-147.

Park, K., Kwon, I. C. and Park, K. (2011) Oral protein delivery: Current status and future prospect. *Reactive and Functional Polymers* **71**(3): 280-287.

Paronen, T. P. (1986) Using the heckel equation in the compression studies of pharmaceuticals. *Pharmaceutical Technology: 4th International Conference: Papers* **1986**: 301-307.

Patel, V. F., Liu, F. and Brown, M. B. (2011) Advances in oral transmucosal drug delivery. *Journal of Controlled Release* **153**(2): 106-116.

Patel, V. F., Liu, F. and Brown, M. B. (2012) Modeling the oral cavity: *In vitro* and *in vivo* evaluations of buccal drug delivery systems. *Journal of Controlled Release* **161**(3): 746-756.

Pfister, W. R. and Ghosh, T. K. (2005) Orally disintegrating tablets: Products, technologies, and development issues. *Pharmaceutical Technology* **29**(10): 136-150.

Picker-Freyer, K. M. and Dürig, T. (2007) Physical mechanical and tablet formation properties of hydroxypropylcellulose: In pure form and in mixtures. *AAPS Pharmaceutical Science and Technology* **8**(4): 82-90.

Picker, K. M. (2004) "Soft tableting": A new concept to tablet pressure sensitive materials. *Pharmaceutical Development and Technology* **9**(1): 107-121.

Pinto, J. F., Wunder, K. F. and Okoloekwe, A. (2004) Evaluation of the potential use of poly (ethylene oxide) as tablet-and extrudate-forming material. *AAPS Pharmaceutical Science* **6**(2): 17-26.

Portero, A., Remuñán-López, C. and Nielsen, H. M. (2002) The potential of chitosan in enhancing peptide and protein absorption across the TR146 cell culture model—an *in vitro* model of the buccal epithelium. *Pharmaceutical Research* **19**(2): 169-174.

Portero, A., Teijeiro-Osorio, D., Alonso, M. J. and Remuñán-López, C. (2007) Development of chitosan sponges for buccal administration of insulin. *Carbohydrate Polymers* **68**(4): 617-625.

Presland, R. B. and Dale, B. A. (2000) Epithelial structural proteins of the skin and oral cavity: Function in health and disease. *Critical Reviews in Oral Biology & Medicine* **11**(4): 383-408.

Prytherch, Z., Job, C., Marshall, H., Oreffo, V., Foster, M. and Bérubé, K. (2011) Tissue-specific stem cell differentiation in an *in vitro* airway model. *Macromolecular Bioscience* **11**(11): 1467-1477.

Quintanar-Guerrero, D., Allémann, E., Fessi, H. and Doelker, E. (1997) Applications of the ion-pair concept to hydrophilic substances with special emphasis on peptides. *Pharmaceutical Research* **14**(2): 119-127.

Rajan, D. S., Gowda, K. V., Mandal, U., Ganesan, M., Bose, A., Sarkar, A., *et al* (2006) Development of RP-HPLC for analysis of human insulin. *Indian Journal of Pharmaceutical Sciences* **68**(5): 662.

Rajeswari, T. (2011) Non invasive insulins: Advanced insulin therapy over this decade. *Journal of Applied Pharmaceutical Science* **1**(08): 12-20.

Rathbone, M. J., Drummond, B. K. and Tucker, I. G. (1994) The oral cavity as a site for systemic drug delivery. *Advanced Drug Delivery Reviews* **13**(1): 1-22.

Rathbone, M. J. and Hadgraft, J. (1991) Absorption of drugs from the human oral cavity. *International Journal of Pharmaceutics* **74**(1): 9-24.

Razavi, S. M., Gonzalez, M. and Cuitino, A. M. (2015) General and mechanistic optimal relationships for tensile strength of doubly convex tablets under diametrical compression. *International Journal of Pharmaceutics* **484**(1): 29-37.

Reichl, S., Bednarz, J. and Müller-Goymann, C. (2004) Human corneal equivalent as cell culture model for *in vitro* drug permeation studies. *British Journal of Ophthalmology* **88**(4): 560-565.

Roškar, R. and Lušin, T. T. (2012). Analytical methods for quantification of drug metabolites in biological samples, INTECH Open Access Publisher.

Rossi, S., Sandri, G. and Caramella, C. M. (2005) Buccal drug delivery: A challenge already won? *Drug Discovery Today: Technologies* **2**(1): 59-65.

Rotunda, A. M., Suzuki, H., Moy, R. L. and Kolodney, M. S. (2004) Detergent effects of sodium deoxycholate are a major feature of an injectable phosphatidylcholine formulation used for localized fat dissolution. *Dermatologic Surgery* **30**(7): 1001-1008.

Roy, D., Semsarilar, M., Guthrie, J. T. and Perrier, S. (2009a) Cellulose modification by polymer grafting: A review. *Chemical Society Reviews* **38**(7): 2046-2064.

Roy, S., Pal, K., Anis, A., Pramanik, K. and Prabhakar, B. (2009b) Polymers in mucoadhesive drug-delivery systems: A brief note. *Designed monomers and polymers* **12**(6): 483-495.

Royce, A. E. (1993). Directly compressible polyethylene oxide vehicle for preparing therapeutic dosage forms, Google Patents.

Rupniak, H. T., Rowlatt, C., Lane, E. B., Steele, J. G., Trejdosiewicz, L. K., Laskiewicz, B., *et al* (1985) Characteristics of four new human cell lines derived from squamous cell carcinomas of the head and neck. *Journal of the National Cancer Institute* **75**(4): 621-635.

Sakagami, M., Sakon, K., Kinoshita, W. and Makino, Y. (2001) Enhanced pulmonary absorption following aerosol administration of mucoadhesive powder microspheres. *Journal of controlled release* **77**(1): 117-129.

Salamat-Miller, N., Chittchang, M. and Johnston, T. P. (2005) The use of mucoadhesive polymers in buccal drug delivery. *Advanced Drug Delivery Reviews* **57**(11): 1666-1691.

Samiei, N., Mangas-Sanjuan, V., González-Álvarez, I., Foroutan, M., Shafaati, A., Zarghi, A., *et al* (2013) Ion-pair strategy for enabling amifostine oral absorption: Rat *in situ* and *in vivo* experiments. *European Journal of Pharmaceutical Sciences* **49**(4): 499-504.

Samiei, N., Shafaati, A., Zarghi, A., Moghimi, H. and Foroutan, S. (2014) Enhancement and in vitro evaluation of amifostine permeation through artificial membrane (PAMPA) via ion pairing approach and mechanistic selection of its optimal counter ion. *European Journal of Pharmaceutical Sciences* **51**: 218-223.

Samuels, R. J. (1969) Solid-state characterization of the structure and deformation behavior of water-soluble hydroxypropylcellulose. *Journal of Polymer Science Part A-2: Polymer Physics* **7**(7): 1197-1258.

Sander, C., Nielsen, H. M. and Jacobsen, J. (2013) Buccal delivery of metformin: TR146 cell culture model evaluating the use of bioadhesive chitosan discs for drug permeability enhancement. *International Journal of Pharmaceutics* **458**(2): 254-261.

Sareen, S., Mathew, G. and Joseph, L. (2012) Improvement in solubility of poor water-soluble drugs by solid dispersion. *International Journal of Pharmaceutical Investigation* **2**(1): 12.

Sarmento, B., Ribeiro, A., Veiga, F. and Ferreira, D. (2006) Development and validation of a rapid reversed-phase hplc method for the determination of insulin from nanoparticulate systems. *Biomedical Chromatography* **20**(9): 898-903.

Sarmento, B., Ribeiro, A., Veiga, F., Sampaio, P., Neufeld, R. and Ferreira, D. (2007) Alginate/chitosan nanoparticles are effective for oral insulin delivery. *Pharmaceutical Research* **24**(12): 2198-2206.

Sarpotdar, P. P., Gaskill, J. L., Giannini, R. P. and Daniels, C. R. (1988). L-α-amino acids as transdermal penetration enhancers, Google Patents.

Sauberlich, H. (1961) Studies on the toxicity and antagonism of amino acids for weanling rats. *The Journal of Nutrition* **75**(1): 61-72.

Selvaratnam, L., Cruchley, A., Navsaria, H., Wertz, P., Hagi-Pavli, E., Leigh, I., *et al* (2001) Permeability barrier properties of oral keratinocyte cultures: A model of intact human oral mucosa. *Oral Diseases* **7**(4): 252-258.

Şenel, S. and Hıncal, A. A. (2001) Drug permeation enhancement via buccal route: Possibilities and limitations. *Journal of Controlled Release* **72**(1–3): 133-144.

Shah, A. P. and Bhandary, S. R. (2010) Polyox (polyethylene oxide)-applications in pharma industry from http://www.pharmainfo.net/reviews/polyox-polyethylene-oxide-applications-pharma-industry. Accessed 09/06/2013.

Shah, K. R., Chaudhary, S. A. and Mehta, T. A. (2014) Polyox (polyethylene oxide) multifunctional polymer in novel drug delivery system. *International Journal of Pharmaceutical Sciences and Drug Research* **6**: 95-101.

Shahi, S., Sonawane, A., Vanamore, S. and Zadbuke, N. (2013) Formulation and *in-vitro* characterization of acyclovir floating matrix tablets: A factorial design study. *Journal of Applied Pharmaceutical Sciences* **3**(5): 65.

Sharma, R., Varshney, V., Chauhan, G. S., Naithani, S. and Soni, P. (2009) Hydroxypropylation of cellulose isolated from bamboo (dendrocalamus strictus) with respect to hydroxypropoxyl content and rheological behavior of the hydroxypropyl cellulose. *Journal of Applied Polymer Science* **113**(4): 2450-2455.

Shirai, Y., Sogo, K., Yamamoto, K., Kojima, K., Fujioka, H., Makita, H., *et al* (1993) A novel fine granule system for masking bitter taste. *Biological & Pharmaceutical Bulletin* **16**(2): 172.

Shoaib, M. H., Tazeen, J., Merchant, H. A. and Yousuf, R. I. (2006) Evaluation of drug release kinetics from ibuprofen matrix tablets using HPMC. *Pakistan Journal of Pharmaceutical Sciences* **19**(2): 119-124.

Shojaei, A. H. (1998) Buccal mucosa as a route for systemic drug delivery: A review. *Journal of Pharmacology and Pharmaceutical Sciences* **1**(1): 15-30.

Shukla, D., Chakraborty, S., Singh, S. and Mishra, B. (2009) Fabrication and evaluation of taste masked resinate of risperidone and its orally disintegrating tablets. *Chemical and Pharmaceutical Bulletin* **57**(4): 337-345.

Siegel, I. (1984) Permeability of the rat oral mucosa to organic solutes measured *in vivo*. *Archives of Oral Biology* **29**(1): 13-16.

Siegel, I., Izutsu, K. and Watson, E. (1981) Mechanisms of non-electrolyte penetration across dog and rabbit oral mucosa *in vitro*. *Archives of Oral Biology* **26**(5): 357-361.

Silen, W. and Forte, J. (1975) Effects of bile salts on amphibian gastric mucosa. *American Journal of Physiology--Legacy Content* **228**(2): 637-644.

Sinko, Ed. (2011). Martin's physical pharmacy and pharmaceutical sciences. London, Lippincott Williams & Wilkinson.

Smart, J. D. (1993) Drug delivery using buccal-adhesive systems. *Advanced Drug Delivery Reviews* **11**(3): 253-270.

Snyder, L. R., Kirkland, J. J. and Glajch, J. L. (2012). Practical HPLC method development, Wiley-Interscience.

Sohi, H., Ahuja, A., Ahmad, F. J. and Khar, R. K. (2010) Critical evaluation of permeation enhancers for oral mucosal drug delivery. *Drug Development and Industrial Pharmacy* **36**(3): 254-282.

Sonnergaard, J. (1999) A critical evaluation of the heckel equation. *International Journal of Pharmaceutics* **193**(1): 63-71.

Squier, C. A. and Kremer, M. J. (2000) Biology of oral mucosa and esophagus. *Journal of the National Cancer Institute. Monographs*(29): 7-15.

Starokadomskyy, P. L. and Dubey, I. Y. (2006) New absorption promoter for the buccal delivery: Preparation and characterization of lysalbinic acid. *International Journal of Pharmaceutics* **308**(1-2): 149-154.

Streubel, A., Siepmann, J. and Bodmeier, R. (2003) Floating matrix tablets based on low density foam powder: Effects of formulation and processing parameters on drug release. *European journal of pharmaceutical sciences* **18**(1): 37-45.

Sudhakar, Y., Kuotsu, K. and Bandyopadhyay, A. K. (2006) Buccal bioadhesive drug delivery — a promising option for orally less efficient drugs. *Journal of Controlled Release* **114**(1): 15-40.

Sun, S., Liang, N., Kawashima, Y., Xia, D. and Cui, F. (2011) Hydrophobic ion pairing of an insulin-sodium deoxycholate complex for oral delivery of insulin. *International Journal of Nanomedicine* **6**: 3049.

Sung, K., Nixon, P. R., Skoug, J. W., Ju, T. R., Gao, P., Topp, E., *et al* (1996) Effect of formulation variables on drug and polymer release from HPMC-based matrix tablets. *International Journal of Pharmaceutics* **142**(1): 53-60.

Suzuki, T. and Nakagami, H. (1999) Effect of crystallinity of microcrystalline cellulose on the compactability and dissolution of tablets. *European Journal of Pharmaceutics and Biopharmaceutics* **47**(3): 225-230.

Tadokoro, H., Chatani, Y., Yoshihara, T., Tahara, S. and Murahashi, S. (1964) Structural studies on polyethers,$[-(CH_2)_m-O-]_n$. II. Molecular structure of polyethylene oxide. *Die Makromolekulare Chemie* **73**(1): 109-127.

Tamilvanan, S. and Sa, B. (2006) *In vitro* and *in vivo* evaluation of single-unit commercial conventional tablet and sustained-release capsules compared with multiple-unit polystyrene microparticle dosage forms of ibuprofen. *AAPS Pharmaceutical Science and Technology* **7**(3): E126-E134.

Tavakoli-Saberi, M. R. and Audus, K. L. (1989) Cultured buccal epithelium: An *in vitro* model derived from the hamster pouch for studying drug transport and metabolism. *Pharmaceutical Research* **6**(2): 160-166.

Thanou, M., Verhoef, J. and Junginger, H. (2001) Oral drug absorption enhancement by chitosan and its derivatives. *Advanced Drug Delivery Reviews* **52**(2): 117-126.

Thompson, C., Cheng, W. P., Gadad, P., Skene, K., Smith, M., Smith, G., *et al* (2011) Uptake and transport of novel amphiphilic polyelectrolyte-insulin nanocomplexes by Caco-2 cells—towards oral insulin. *Pharmaceutical Research* **28**(4): 886-896.

Torchilin, V. P. and Lukyanov, A. N. (2003) Peptide and protein drug delivery to and into tumors: Challenges and solutions. *Drug Discovery Today* **8**(6): 259-266.

Trevino, S. R., Scholtz, J. M. and Pace, C. N. (2008) Measuring and increasing protein solubility. *Journal of Pharmaceutical Sciences* **97**(10): 4155-4166.

Trinkaus-Randall, V. and Gipson, I. (1984) Role of calcium and calmodulin in hemidesmosome formation *in vitro*. *The Journal of Cell Biology* **98**(4): 1565-1571.

Tucker, I. G. (1988) A method to study the kinetics of oral mucosal drug absorption from solutions. *Journal of Pharmacy and Pharmacology* **40**(10): 679-683.

Türker, S., Onur, E. and Ózer, Y. (2004) Nasal route and drug delivery systems. *Pharmacy world and Science* **26**(3): 137-142.

Tye, C. K., Sun, C. C. and Amidon, G. E. (2005) Evaluation of the effects of tableting speed on the relationships between compaction pressure, tablet tensile strength, and tablet solid fraction. *Journal of Pharmaceutical Sciences* **94**(3): 465-472.

Uchiyama, T., Sugiyama, T., Quan, Y. S., Kotani, A., Okada, N., Fujita, T., *et al* (1999) Enhanced permeability of insulin across the rat intestinal membrane by various absorption enhancers: Their intestinal mucosal toxicity and absorption-enhancing mechanism of n-lauryl-β-d-maltopyranoside. *Journal of Pharmacy and Pharmacology* **51**(11): 1241-1250.

Ugwoke, M. I., Agu, R. U., Verbeke, N. and Kinget, R. (2005) Nasal mucoadhesive drug delivery: Background, applications, trends and future perspectives. *Advanced Drug Delivery Reviews* **57**(11): 1640-1665.

Utoguchi, N., Watanabe, Y., Suzuki, T., Maehara, J., Matsumoto, Y. and Matsumoto, M. (1997) Carrier-mediated transport of monocarboxylic acids in primary cultured epithelial cells from rabbit oral mucosa. *Pharmaceutical Research* **14**(3): 320-324.

Van Meerloo, J., Kaspers, G. J. and Cloos, J. (2011). Cell sensitivity assays: The MTT assay. Cancer cell culture, Springer**:** 237-245.

Vasconcelos, T., Sarmento, B. and Costa, P. (2007) Solid dispersions as strategy to improve oral bioavailability of poor water soluble drugs. *Drug Discovery Today* **12**(23): 1068-1075.

Vávrová, K., Hrabálek, A., Doležal, P., Holas, T. and Zbytovská, J. (2003) L-serine and glycine based ceramide analogues as transdermal permeation enhancers: Polar head size and hydrogen bonding. *Bioorganic & Medicinal Chemistry Letters* **13**(14): 2351-2353.

Verma, A., Kumar, N., Malviya, R. and Sharma, P. K. (2014) Emerging trends in noninvasive insulin delivery. *Journal of Pharmaceutics* **2014**.

Veuillez, F., Deshusses, J. and Buri, P. (1999) Synthesis and characterization of an acylated di-peptide (myr-trp-leu) with modified transmucosal transport properties. *European Journal of Pharmaceutics and Biopharmaceutics* **48**(1): 21-26.

Veuillez, F., Kalia, Y. N., Jacques, Y., Deshusses, J. and Buri, P. (2001) Factors and strategies for improving buccal absorption of peptides. *European Journal of Pharmaceutics and Biopharmaceutics* **51**(2): 93-109.

Veuillez, F., Rieg, F. F., Guy, R. H., Deshusses, J. and Buri, P. (2002) Permeation of a myristoylated dipeptide across the buccal mucosa: Topological distribution and evaluation of tissue integrity. *International Journal of Pharmaceutics* **231**(1): 1-9.

Wagh, M. A., Kothawade, D. P., Salunkhe, K. S., Chavan, N. V. and Daga, V. R. (2011) Techniques used in orally disintegrating drug delivery system. *International Journal of Drug Delivery* **2**(2).

Walker, G. F., Langoth, N. and Bernkop-Schnurch, A. (2002) Peptidase activity on the surface of the porcine buccal mucosa. *International Journal of Pharmaceutics* **233**(1-2): 141-147.

Walsh, G. (2007). Pharmaceutical biotechnology: Concepts and applications, John Wiley & Sons.

Wang, C., Dong, Y. and Tan, H. (2003) Study on lyotropic liquid-crystalline properties of trimethylsilyl hydroxypropylcellulose. *Carbohydrate Research* **338**(6): 535-540.

Wang, X.-L., Ying, A.-L. and Wang, W.-N. (2002) Nanofiltration of l-phenylalanine and l-aspartic acid aqueous solutions. *Journal of Membrane Science* **196**(1): 59-67.

Watanabe, Y., Koizumi, K.-I., Zama, Y., Kiriyama, M., Matsumoto, Y. and Matsumoto, M. (1995) New compressed tablet rapidly disintegrating in saliva in the mouth using crystalline cellulose and a disintegrant. *Biological and Pharmaceutical Bulletin* **18**(9): 1308.

Watt, F. M., Mattey, D. L. and Garrod, D. R. (1984) Calcium-induced reorganization of desmosomal components in cultured human keratinocytes. *The Journal of Cell Biology* **99**(6): 2211-2215.

Werbowyj, R. S. and Gray, D. G. (1980) Ordered phase formation in concentrated hydroxpropylcellulose solutions. *Macromolecules* **13**(1): 69-73.

Whitmore, L. and Wallace, B. (2004) Dichroweb, an online server for protein secondary structure analyses from circular dichroism spectroscopic data. *Nucleic Acids Research* **32**(suppl 2): W668-W673.

Whitmore, L. and Wallace, B. A. (2008) Protein secondary structure analyses from circular dichroism spectroscopy: Methods and reference databases. *Biopolymers* **89**(5): 392-400.

Wilcox, G. (2005) Insulin and insulin resistance. *Clinical Biochemistry Reviews* **26**(2): 19.

Wintersteiner, O. and Abramson, H. A. (1933) The isoelectric point of insulin electrical properties of adsorbed and crystalline insulin. *Journal of Biological Chemistry* **99**(3): 741-753.

Xu, H.-B., Huang, K.-X., Zhu, Y.-S., Gao, Q.-H., Wu, Q.-Z., Tian, W.-Q., *et al* (2002) Hypoglycaemic effect of a novel insulin buccal formulation on rabbits. *Pharmacological Research* **46**(5): 459-467.

Xu, X., Fu, Y., Hu, H., Duan, Y. and Zhang, Z. (2006) Quantitative determination of insulin entrapment efficiency in triblock copolymeric nanoparticles by high-performance liquid chromatography. *Journal of Pharmaceutical and Biomedical Analysis* **41**(1): 266-273.

Xue, X.-Y., Zhou, Y., Chen, Y.-Y., Meng, J.-R., Jia, M., Hou, Z., *et al* (2012) Promoting effects of chemical permeation enhancers on insulin permeation across TR146 cell model of buccal epithelium *in vitro*. *Drug and chemical toxicology* **35**(2): 199-207.

Yamada, N., Okano, T., Sakai, H., Karikusa, F., Sawasaki, Y. and Sakurai, Y. (1990) Thermo-responsive polymeric surfaces; control of attachment and detachment of cultured cells. *Die Makromolekulare Chemie, Rapid Communications* **11**(11): 571-576.

Yamada, T., Saito, N., Imai, T. and Otagiri, M. (1999) Effect of grinding with hydroxypropyl cellulose on the dissolution and particle size of a poorly water-soluble drug. *Chemical And Pharmaceutical Bulletin-Tokyo-* **47**: 1311-1313.

Yamamoto, A., Hayakawa, E., Kato, Y., Nishiura, A. and Lee, V. (1992) A mechanistic study on enhancement of rectal permeability to insulin in the albino rabbit. *Journal of Pharmacology and Experimental Therapeutics* **263**(1): 25-31.

Yamamoto, A., Hayakawa, E. and Lee, V. H. (1990) Insulin and proinsulin proteolysis in mucosal homogenates of the albino rabbit: Implications in peptide delivery from nonoral routes. *Life Sciences* **47**(26): 2465-2474.

Yamamoto, A., Taniguchi, T., Rikyuu, K., Tsuji, T., Fujita, T., Murakami, M., *et al* (1994) Effects of various protease inhibitors on the intestinal absorption and degradation of insulin in rats. *Pharmaceutical Research* **11**(10): 1496-1500.

Yang, L., Venkatesh, G. and Fassihi, R. (1996) Characterization of compressibility and compactibility of poly (ethylene oxide) polymers for modified release application by compaction simulator. *Journal of Pharmaceutical Sciences* **85**(10): 1085-1090.

Yang, S., Fu, Y., Jeong, S. H. and Park, K. (2004) Application of poly (acrylic acid) superporous hydrogel microparticles as a super-disintegrant in fast-disintegrating tablets. *Journal of Pharmacy and Pharmacology* **56**(4): 429-436.

Yang, T.-Z., Wang, X.-T., Yan, X.-Y. and Zhang, Q. (2002) Phospholipid deformable vesicles for buccal delivery of insulin. *Chemical and Pharmaceutical Bulletin* **50**(6): 749-753.

Yilmaz, B., Kadioglu, Y. and Capoglu, I. (2012) Determination of insulin in humans with insulin-dependent diabetes mellitus patients by HPLC with diode array detection. *Journal of Chromatographic Science* **50**(7): 586-590.

Yin, L., Ding, J., He, C., Cui, L., Tang, C. and Yin, C. (2009) Drug permeability and mucoadhesion properties of thiolated trimethyl chitosan nanoparticles in oral insulin delivery. *Biomaterials* **30**(29): 5691-5700.

Yoshinari, T., Forbes, R. T., York, P. and Kawashima, Y. (2003) The improved compaction properties of mannitol after a moisture-induced polymorphic transition. *International Journal of Pharmaceutics* **258**(1): 121-131.

Zhang, J., Niu, S., Ebert, C. and Stanley, T. H. (1994) An *in vivo* dog model for studying recovery kinetics of the buccal mucosa permeation barrier after exposure to permeation enhancers: Apparent evidence of effective enhancement without tissue damage. *International Journal of Pharmaceutics* **101**(1): 15-22.

Zhivotovsky, B. and Orrenius, S. (2011) Calcium and cell death mechanisms: A perspective from the cell death community. *Cell Calcium* **50**(3): 211-221.

Zhou, X. and Po, A. L. W. (1990) Comparison of enzymic activities of tissues lining portals of drug absorption, using the rat as a model. *International Journal of Pharmaceutics* **62**(2): 259-267.

Appendices

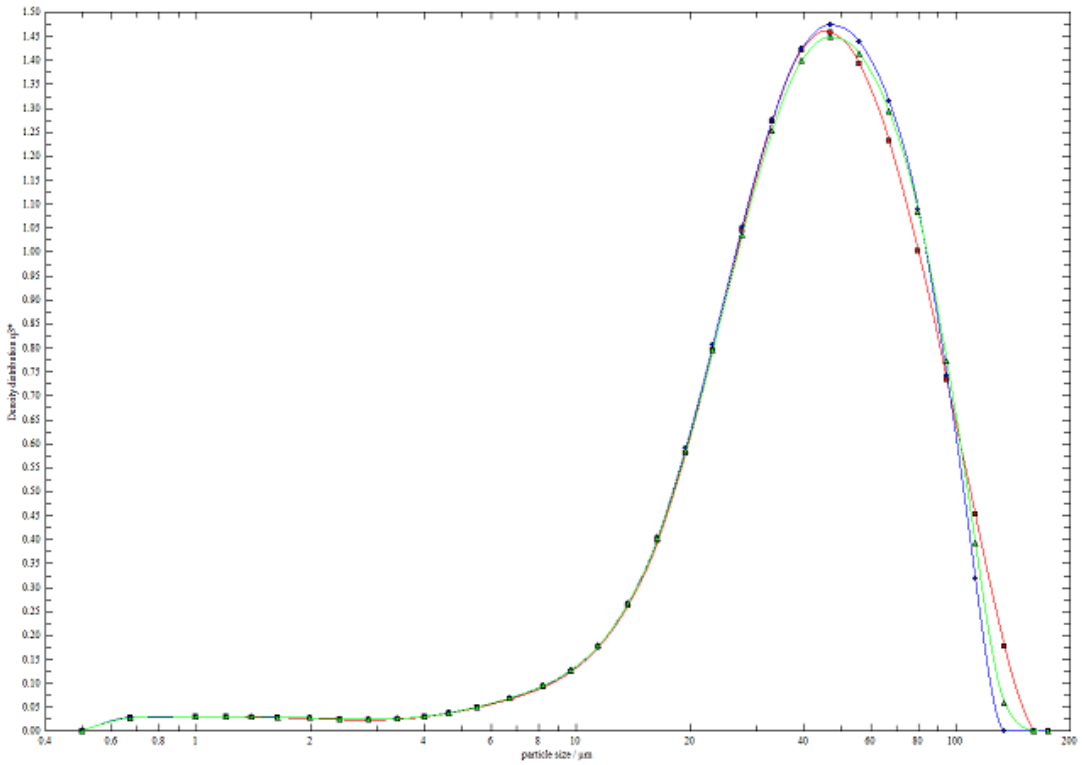

Figure A-1. Representative graph showing particle size distribution of LHPC powder using laser diffractometry (n=3)

Table A-1. MODDE worksheet showing experimental run order, factors, observed responses and included/ excluded data sets. All responses are reported as means of triplicate runs. (Incl = included, Excl = excluded)

Exp Name	Run Order	Incl/Excl	Polymer viscosity	Polymer concentration	Compaction pressure	Disintegration time (s)	Friability (%)	Hardness (N)	Porosity
N1	14	Incl	-1	0.5	1	59	1.75	89.5	0.3034
N2	6	Incl	1	0.5	1	93.67	1.76	89.2	0.3379
N3	11	Incl	-1	2.5	1	75.67	2.5	52	0.2694
N4	13	Incl	1	2.5	1	223.33	2.88	52.87	0.2891
N5	9	Incl	-1	0.5	3	38.33	1.11	154.1	0.201

N6	7	Incl	1	0.5	3	77.33	1.02	151.3	0.2306
N7	17	Incl	-1	2.5	3	51	1.06	128.3	0.3004
N8	15	Incl	1	2.5	3	83	1.09	138.27	0.2863
N9	3	Incl	-1	1.5	2	63	1.53	98.47	0.2679
N10	5	Excl	1	1.5	2	189.67	1.35	123.8	0.2718
N11	2	Incl	0	0.5	2	53	1.49	97.3	0.2621
N12	8	Incl	0	2.5	2	142.33	1.52	92.3	0.2686

N13	4	Excl	0	1.5	1	122.67	2.92	48.03	0.3036
N14	12	Excl	0	1.5	3	65.33	1.11	131.67	0.2345
N15	1	Incl	0	1.5	2	89.67	1.06	124.5	0.2994
N16	10	Incl	0	1.5	2	66	1.33	104.83	0.2813
N17	16	Incl	0	1.5	2	77.67	1.32	100.4	0.2696

Polymer viscosity: Polyox N10 (-1), Polyox 1105 (0), Polyox coagulant (1)

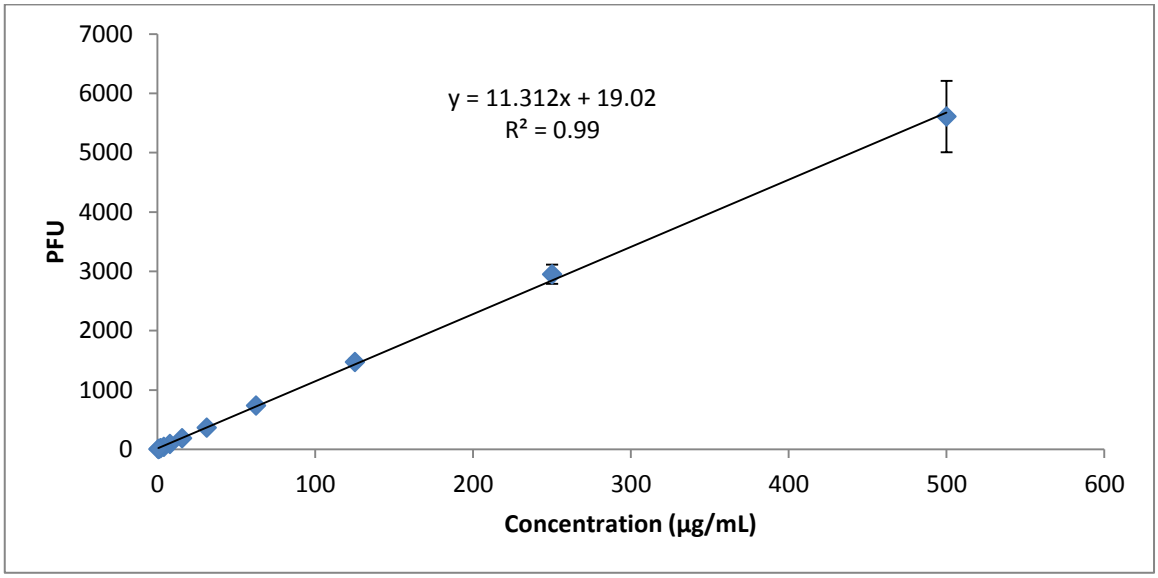

Figure A-2. Beer-Lambert's calibration curve for fluorescent spectroscopic method for assay of FD4, from chapter 4 (n=16).

Table A-2. Table highlighting intra-day validation parameters of the fluorescent spectrophotometric method for FD4 analysis showing high recovery % and low RSD, including linearity factors of the regression equation linking FD4 concentration to the analytical response (area under the peak) (n=8)

FD4 conc. actual (µg/mL)	Peak Area (RFU)	RSD	FD4 conc. calculated (µg/mL)	Recovery (%)
0.49	5.21 ± 0.44	0.08	0.46 ± 0.04	95.57 ± 8.05
3.91	44.55 ± 1.07	0.02	3.99 ± 0.1	102.01 ± 3.7
31.25	371.13 ± 15.30	0.04	33.22 ± 1.37	106.3 ± 4.39
62.5	748.12 ± 16.07	0.02	66.96 ± 1.43	107.14 ± 2.3
250	2896.61 ± 127.73	0.04	259.27 ± 0.04	103.71 ± 4.57
Mean % recovery = 102.96 ± 4.60% RSD % Recovery = 0.05 LOD = 0.27 µg /mL LOQ = 0.89 µg /mL				
Regression equation		y = 11.172x		
Correlation coefficient		0.99		
Linearity range		0.4 – 500 µg/ mL		

Table A-3. Inter-day precision and accuracy parameters for fluorescent spectrophotometric method for FITC-labelled dextran (FD4) analysis (n=24)

FD4 conc. actual (µg/mL)	Amount measured on day 1 (µg/mL)	RSD	Amount measured on day 2 (µg/mL)	RSD	Amount measured on day 3 (µg/mL)	RSD	Overall RSD
0.49	0.48 ± 0.02	0.05	0.48 ± 0.06	0.11	0.46 ± 0.03	0.06	0.07
3.91	3.99 ± 0.10	0.02	4.01 ± 0.39	0.10	4.04 ± 0.35	0.09	0.09
31.25	33.22 ± 1.37	0.04	33.24 ± 2.62	0.05	32.34 ± 1.62	0.07	0.06
62.5	66.96 ± 1.43	0.05	67.53 ± 1.84	0.03	63.54 ± 4.01	0.06	0.04
250	259.27 ± 0.04	0.04	272.6 ± 7.79	0.03	260.06 ± 15.68	0.06	0.04

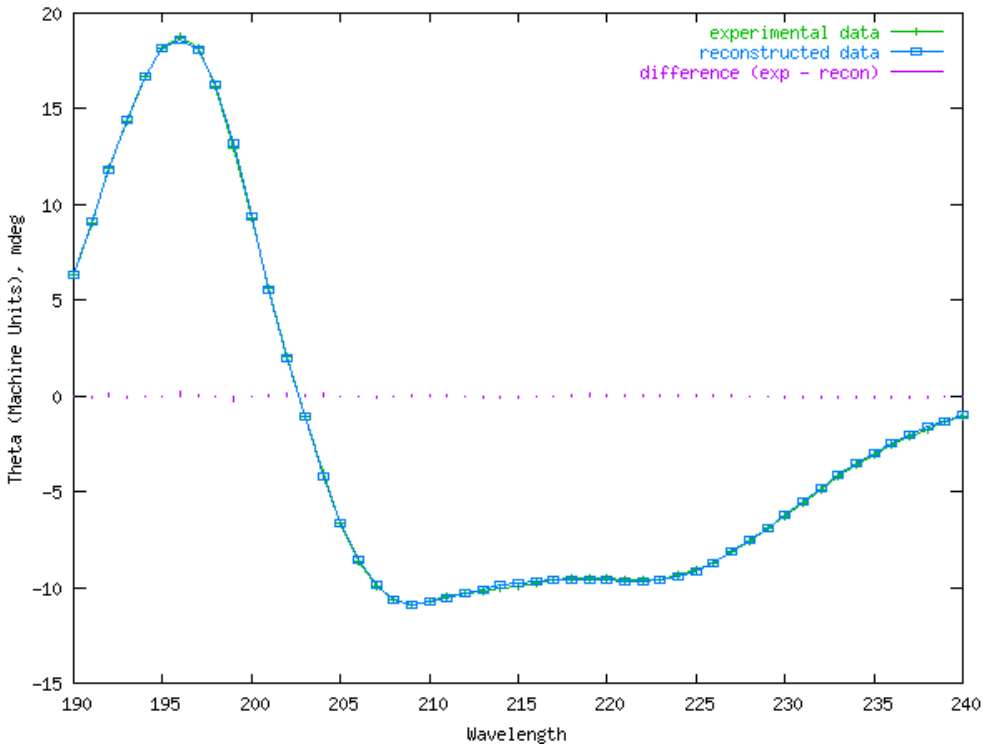

Figure A-3. Calculated and experimental CD spectra for insulin tablet compacted at 10 kN

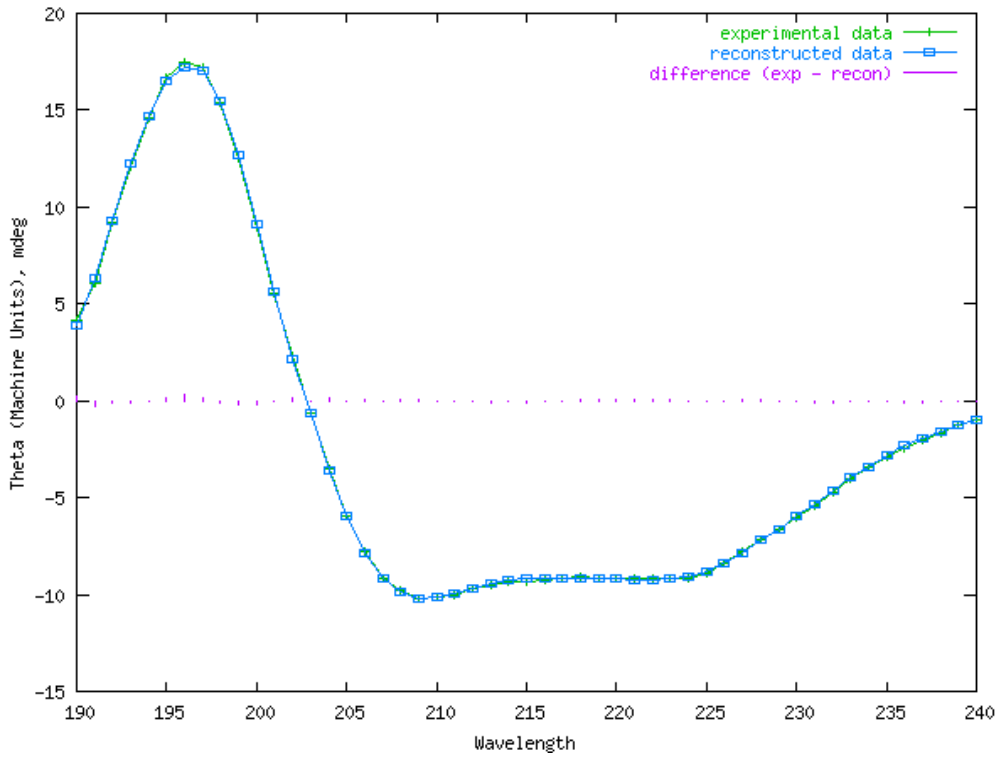

Figure A-4. Calculated and experimental CD spectra for insulin tablet compacted at 30 kN

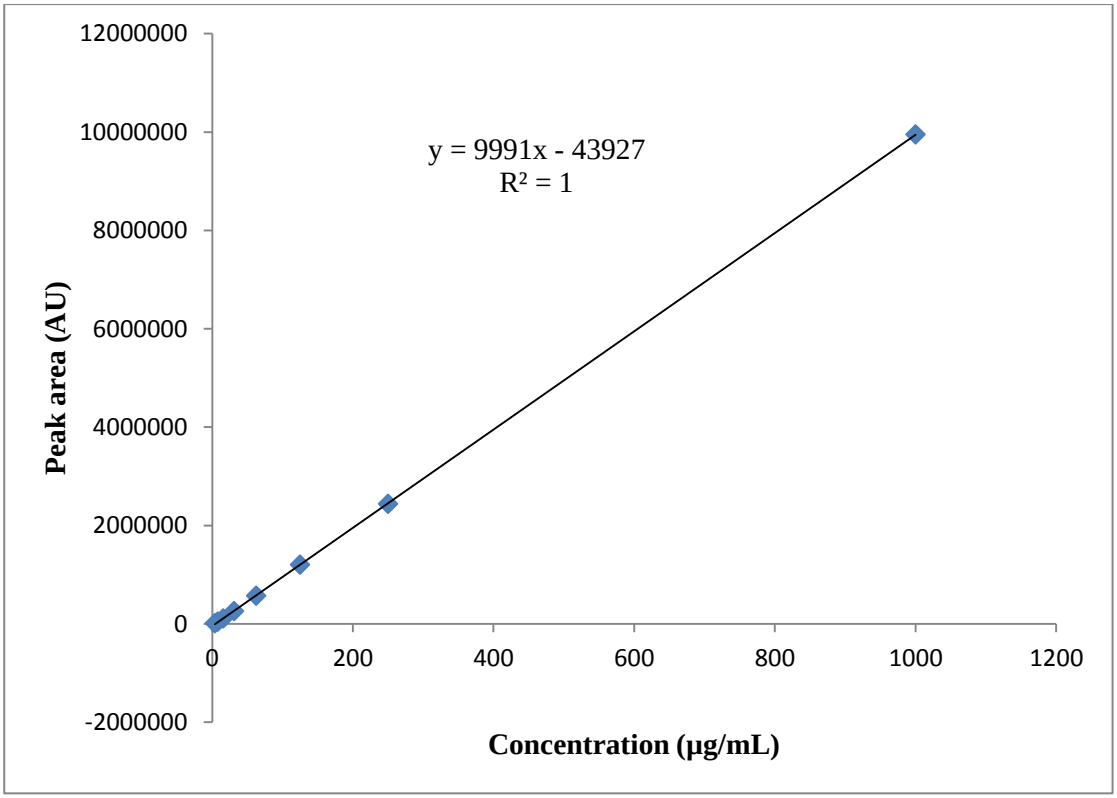

Figure A-5. Beer-Lambert's calibration curve for insulin method employed for insulin permeation studies in chapter 6 (n=3)

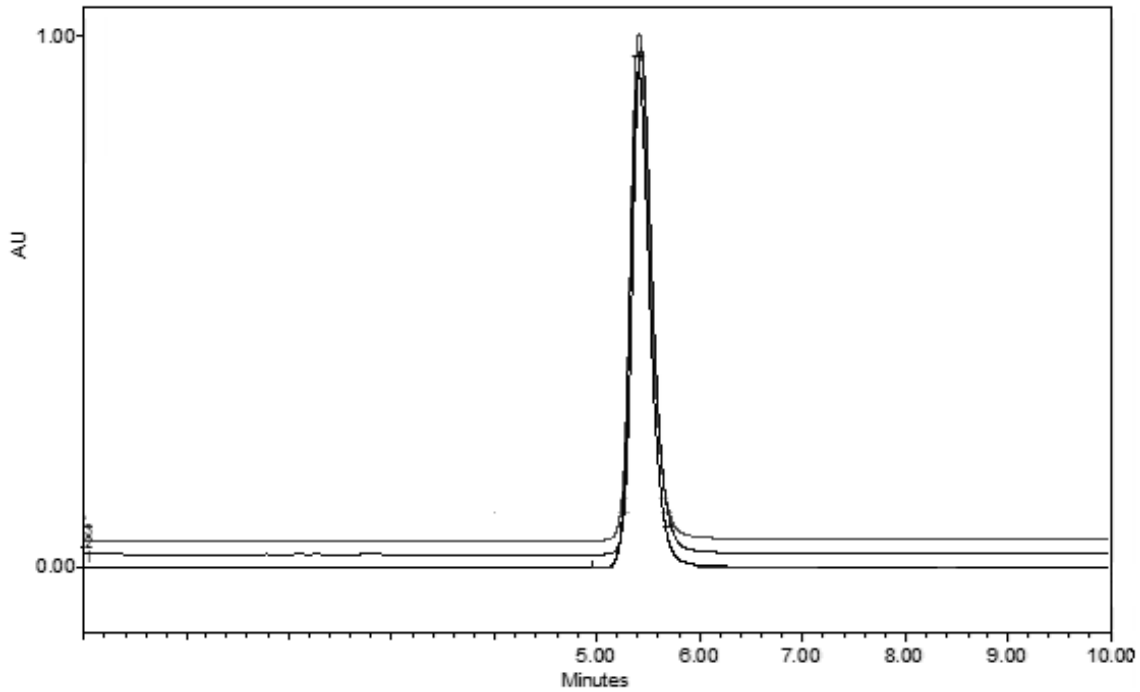

Figure A-6. Precision parameters of insulin analysis by HPLC method from chapter 6, superimposition of the three chromatograms depict instrument precision. 1mg/mL insulin solution was injected three times into the HPLC.

Table A-4. Table highlighting intra-day validation parameters of the HPLC method for insulin analysis (chapter 6) showing high recovery % and low RSD, including linearity factors of the regression equation linking insulin concentration to the analytical response (area under the peak) (n=3)

Insulin conc. actual (µg/mL)	Peak Area (AU)	RSD	Insulin conc. calculated (µg/mL)	Recovery (%)
7.81	42756.3 ± 1513.3	0.04	8.61 ± 0.15	110.21 ± 1.94
15.63	108581.7 ± 485500.5	0.02	15.20 ± 0.55	97.28 ± 3.52
31.25	261868.3 ± 4884.6	0.02	30.54 ± 0.49	97.74 ± 1.56
62.50	575054.3 ± 17882.2	0.03	61.89 ± 1.79	99.70 ± 1.96
Mean % recovery = 101.06 ± 6.14% RSD % Recovery = 0.06 LOD = 0.46 µg /mL LOQ = 1.55 µg /mL				
Regression equation		y = 9991x – 43927		
Correlation coefficient		1		
Linearity range		3.9 - 1000 µg/ mL		

Table A-5. Inter-day precision and accuracy parameters of the HPLC method for insulin analysis from chapter 6 (n=24)

Insulin conc. actual (µg/mL)	Amount measured on day 1 (µg/mL)	RSD	Amount measured on day 2 (µg/mL)	RSD	Amount measured on day 3 (µg/mL)	RSD	Overall RSD
7.81	7.98 ± 0.67	0.05	8.08 ± 0.20	0.03	8.61 ± 0.15	0.02	0.03
15.63	15.59 ± 0.43	0.02	15.30 ± 0.49	0.03	15.20 ± 0.55	0.04	0.03
31.25	31.15 ± 1.14	0.04	30.37 ± 0.23	0.01	30.54 ± 0.49	0.02	0.02
62.50	62.54 ± 1.41	0.05	62.96 ± 1.49	0.02	61.89 ± 1.79	0.03	0.03